Interannual Variability in Cloudiness, Sea Surface Temperature, and Atmospheric Circulation over the Midlatitude North Pacific during Summer

by

Joel R. Norris

Ph.D. Dissertation

Department of Atmospheric Sciences
University of Washington

1997

In presenting this dissertation in partial fulfillment of the requirements for the Doctoral degree at the University of Washington, I agree that the Library shall make its copies freely available for inspection. I further agree that extensive copying of this dissertation is allowable only for scholarly purposes, consistent with “fair use” as prescribed in the U.S. Copyright Law. Requests for copying or reproduction of this dissertation may be referred to University Microfilms, 1490 Eisenhower Place, P.O. Box 975, Ann Arbor, MI 48106, to whom the author has granted “the right to reproduce and sell (a) copies of the manuscript in microform and/or (b) printed copies of the manuscript made from mircoform.”

Signature _____

Date _____

ABSTRACT

Large-scale interannual and interdecadal variability in surface-observed marine stratiform cloud (MSC) amount and sea surface temperature (SST) are closely coupled over the central North Pacific during summer. Increased (decreased) MSC amount occurs with decreased (increased) SST, resulting from coincident meridional shifts in the regions of strong SST gradient and cloud gradient between subtropics and midlatitudes. Investigation of variability in low cloud types indicates that a shift in the SST gradient region produces corresponding shifts in the transition from subtropical cumulus to midlatitude stratus and the transition from midlatitude stratocumulus to subtropical cumulus. Since MSC reduces the amount of radiation absorbed by the ocean, these processes create the potential for a positive MSC feedback on SST; however, estimated MSC radiative anomalies are observed to have little net impact on SST, probably due to the tendency for compensation by latent heat flux anomalies.

Large-scale interannual and interdecadal variability in nimbostratus and SST are also coupled over the central North Pacific during summer, suggesting coincident meridional shifts in the storm track and region of strong SST gradient. This suggests synoptic activity also plays a role in MSC variability.

TABLE OF CONTENTS

LIST OF FIGURES

LIST OF TABLES

GLOSSARY

ASTEX	Atlantic Stratocumulus Transition Experiment (Albrecht et al. 1995a)
AWP	amount-when-present
c	specific heat of liquid water
CAPE	convective available potential energy
Cb	cumulonimbus
CCN	cloud condensation nuclei
C_E	evaporation exchange coefficient
C_L	synoptic low cloud type code (Table 3.2) (WMO 1975)
COADS	Comprehensive Atmosphere–Ocean Dataset (Woodruff et al. 1987)
CRF	cloud radiative forcing
Cu	cumulus
d	depth of the oceanic mixed layer
DJF	December–January–February
ECMWF	European Center for Medium-Range Weather Forecasts
EECRA	Extended Edited Cloud Report Archive
EOF	empirical orthogonal function (see Kutzbach 1967)
ENSO	El Niño / Southern Oscillation
ERBE	Earth Radiation Budget Experiment (Barkstrom et al. 1989)
f	Coriolis parameter
FIRE	First ISCCP Regional Experiment (Albrecht et al. 1988)
FQ	frequency-of-occurrence
Fs	fractostratus (bad-weather stratus)
g	asymmetry factor
GCM	general circulation model or global climate model
GOSTA	Global Ocean Surface Temperature Atlas (Bottomley et al. 1990)

IPCC	Intergovernmental Panel on Climate Change
ISCCP	International Satellite Cloud Climatology Project (Rossow and Schiffer 1991)
JJA	June–July–August (summer season for the North Pacific)
L	latent heat flux of vaporization
LW	longwave
LWC	liquid water content
MBL	marine boundary layer
MSC	marine stratiform cloudiness (stratus, stratocumulus, and sky-obscuring fog)
N	synoptic code for total cloud cover (WMO 1974)
N_h	synoptic code for cloud cover of the lowest layer (WMO 1974)
NC	normalized root-mean-squared covariance (defined in Zhang et al. 1997)
NCAR	National Center for Atmospheric Research
NCDC	National Climatic Data Center
NCEP	National Centers for Environmental Prediction
NH	Northern Hemisphere
NL	Norris and Leovy (1994)
Ns	nimbostratus
NZW	Norris et al. (1997)
OWS	Ocean Weather Station
PC	principal component
PNA	Pacific/North America pattern (Wallace and Gutzler 1981)
q	water vapor mixing ratio
q_s	saturation water vapor mixing ratio
q_{SST}	SST saturation water vapor mixing ratio
r	correlation coefficient between left and right SVD expansion coefficient time series
r_{PC}	correlation coefficient between the EOF time series (PCs)
S	lower tropospheric static stability, $S \equiv \theta(700\ \mathrm{mb}) - \theta(\mathrm{SST,SLP})$
Sc	stratocumulus

SCF	squared covariance fraction
SH	Southern Hemisphere
SLP	sea level pressure
SST	sea surface temperature
St	stratus (fair-weather stratus)
SVD	singular value decomposition (see Bretherton et al. 1992)
SW	shortwave
T_{air}	surface air temperature
t	transmittance through a cloud
TOA	top-of-atmosphere
u	zonal wind component
$u_?$	friction velocity
UTC	universal time coordinated (Greenwich time)
v	meridional wind component
V	seasonal-mean meridional wind
$\boldsymbol{V}$	vector wind
VOS	Volunteer Observing Ship
VV	seasonal variance of daily meridional wind
W88	Warren et al. (1988)
WMO	World Meteorological Organization
ww	synoptic present-weather code (WMO 1974)
x	distance in the zonal direction
ΔX_0	anomalous zonal wind stress
y	distance in the meridional direction
z_i	MBL height
δq	decoupling parameter, $\delta q \equiv q(z/z_i = 0.2) - q(z/z_i = 0.9)$
Δt	time period over which radiative anomalies act
ΔT	air-sea temperature difference, $\Delta T \equiv T_{air} - \mathrm{SST}$

ρ	density of air
ρ_w	density of water
θ_e	equivalent potential temperature
θ_v	virtual potential temperature
τ	cloud optical thickness

ACKNOWLEDGMENTS

I wish to express my greatest appreciation for the encouragement, support, and guidance my advisor, Conway Leovy, has graciously provided to me during my seven years of graduate study. Further appreciation is extended to David Battisti, Chris Bretherton, Mike Wallace, and Steve Warren for their willingness to engage in many fruitful discussions about my research. I would also like to thank Steve Klein for his help with data, stimulating ideas, and affirming friendship.

Along more technical lines, I must acknowledge that I am greatly indebted to Marc Michelsen for his computer advice in general and his plotting programs in particular. Further acknowledgment must also be given to Bart Brashers for his very useful sounding plotting program, and to Carole Hahn for her programs, computer time, and advice which allowed me to process the EECRA dataset.

I would also like to thank all those in and out of the department who have not been mentioned by name but nonetheless gave me valuable research assistance and even more valued friendship.

Finally, I am grateful for the love that has been given to me by my brothers and sisters in Christ in the InterVarsity Christian Fellowship grad group and at Green Lake Presbyterian Church.

All of these things have been God's blessing to me.

This work was supported by a NASA Global Change Fellowship, NASA Grant NGT-30092 and Earth Observing System Grant, NASA Grant NAGW-2633.

DEDICATION

The heavens declare the glory of God
The skies proclaim the work of his hands
Day after day they pour forth speech
Night after night they display knowledge
There is no speech or language
where their voice is not heard
Their voice goes out into all the earth
Their words to the ends of the world. . . .

Psalm 19

CHAPTER 1

Introduction

1.1 Cloudiness and the Earth's radiation budget

Clouds are one of the most important variables influencing the Earth's radiation budget and play a key role in the global climate system (Arking 1991). Although intimately associated with latent heating, precipitation, and the transport of water, cloudiness directly affects the transfer of energy in the atmosphere by scattering, absorbing, and emitting radiation. With the increasing potential for significant global warming due to perturbation of the Earth's radiation budget by anthropogenic increases in greenhouse gases, it has become essential to understand processes responsible for both natural climate variability and possible future climate change. However, there are many uncertainties in our present knowledge, particularly regarding interaction between variability in cloud amount, cloud radiative properties, and the climate system.

The radiative effectiveness of cloudiness is commonly measured by cloud radiative forcing (CRF), conventionally defined as the difference in net radiation flux between cloudy and clear conditions and generally calculated separately for shortwave (SW) and longwave (LW) parts of the spectrum (Ramanathan et al. 1989). Top-of-atmosphere (TOA) LW CRF results when clouds absorb and re-emit outgoing terrestrial radiation to space at a temperature different from that where clear-sky emission primarily occurs; hence, TOA LW CRF strongly depends on cloud amount and cloud top temperature (and therefore height). Because clouds are typically colder than the effective emission level of the clear-sky atmosphere, they emit less radiation and TOA LW CRF is accordingly positive (the climate system gains energy). On the other hand, surface LW CRF depends on cloud base temperature and is also usually positive (the surface gains energy), but may be small if the specific humidity (and therefore emissivity) of the lower troposphere is large. TOA SW CRF results primarily from the reflection of solar radiation back to space

by clouds and strongly depends on cloud amount and cloud optical thickness. Because clouds typically have a greater albedo than that of the surface, TOA SW CRF is usually negative (the climate system loses energy). SW CRF at the surface is also usually negative (the surface loses energy), but may have greater magnitude than the SW CRF at the TOA if a significant amount of radiation is absorbed in the clouds. Recent studies indicate that SW cloud absorption may be much larger than previously thought (Cess et al. 1995; Pilewskie and Valero 1995; Ramanathan et al. 1995), although this is disputed (Arking 1996; Imre et al. 1996).

Instruments in space, such as those used in the Earth Radiation Budget Experiment (ERBE) (Barkstrom et al. 1989), can measure TOA CRF directly, but surface CRF must be estimated. Observational studies show that SW and LW effects tend to compensate for each other, but SW CRF outweighs LW CRF on the global scale (Table 1.1). Although clouds produce a net cooling effect on the surface and the Earth as a whole, Table 1.1 suggests that this is largely the result of strong SW CRF in the summer hemisphere produced by the much greater summer insolation. Seasonal changes in the amount and vertical distribution of cloudiness alone actually produce warming in the summer hemisphere relative to the annual mean (Cess et al. 1992), but this is small compared to the relative cooling produced by the change in insolation. The strong role of the seasonal cycle of insolation suggests the climate system may be most sensitive to changes in cloudiness during summer.

Intra-hemispheric variations in net CRF are substantial as well. The top panel of Fig. 1.1 shows TOA net CRF over the globe during the season of June–July–August (JJA) using ERBE data previously displayed in Fig. 15a of Hartman et al. (1992). TOA net CRF is most negative over middle and high latitude oceans during summer with significant negative CRF also occurring in eastern subtropical oceans. TOA net CRF is slightly positive at middle and high latitudes during winter when LW CRF becomes stronger than SW CRF due to the lesser insolation. TOA net CRF is generally close to zero at low latitudes. The distribution of surface net CRF displayed by Plate 4 of Gupta et al. (1993) is generally similar to that of the top panel of Fig. 1.1 except surface net CRF is more

negative during summer and more positive during winter at middle and high latitudes (not shown, but hemispheric mean values are provided in Table 1.1). The most notable difference is the strongly negative surface net CRF which occurs in regions of convection at low latitudes. The fact that seasonal and geographical variations in net CRF are very large compared to the 2.45 W m^{-2} radiative forcing estimated to result from the increase in greenhouse gases between pre-industrial times and the present (IPCC 1996) suggests that variability in cloudiness must be evaluated to assess and attribute changes in the climate system to increased greenhouse gases.

Geographical variations in CRF are closely related to geographical variations in cloud amount and type. The bottom panel of Fig. 1.1 shows the average amount of low and midlevel clouds (defined by cloud top at pressures greater than 440 mb) seen by satellite during JJA of the years 1986 and 1990–92 using D2 data from the International Satellite Cloud Climatology Project (ISCCP) (Rossow and Schiffer 1991) obtained from B. Soden (Geophysical Fluid Dynamics Laboratory, Princeton University). This is actually an underestimate of the true amount since no correction was made for obscuration of low and midlevel clouds by high clouds, but high cloud amount is minimal in the regions of interest. Comparing the top and bottom panels of Fig. 1.1 demonstrates that large negative TOA net CRF over summertime midlatitude and eastern subtropical oceans results from low and midlevel cloudiness (also verified by Hartmann et al. 1992), which is primarily stratiform in these regions (Warren et al. 1988). Because stratiform clouds are optically thick but occur relatively low in the atmosphere, TOA SW CRF is much stronger than TOA LW CRF during summer (Harrison et al. 1990; Hartmann and Doelling 1991). TOA net CRF is more negative over the ocean than over land because cloud amount is greater and surface albedo is lower over ocean than over land. Low and midlevel clouds are observed less often at low latitudes (this is due in part to obscuring higher clouds that frequently occur in convective regions) and TOA net CRF is generally close to zero, either because there is less cloud cover or because SW CRF and LW CRF largely cancel in tall tropical convective cloud towers.

These results and those of others (e.g. Slingo 1990) suggest that the global TOA

energy budget may be more sensitive to changes in low stratiform cloudiness (hereafter called marine stratiform cloudiness, comprising of stratus, stratocumulus, and sky-obscuring fog) and midlevel stratiform cloudiness over the ocean than any other cloud types, and more sensitive to changes during summer than any other season. Furthermore, variability in marine stratiform cloudiness (MSC) and midlevel stratiform cloudiness over the midlatitude ocean is likely to have a strong influence on the surface energy budget during summer as well.

1.2 Difficulties in estimating cloud radiative forcing from cloud amount

In order to quantitatively understand the influence of cloudiness on other parameters of the climate system, particularly sea surface temperature (SST), it is necessary to know how variability in measured cloud properties relates to variability in CRF. The simplest procedure would be to use satellite radiances to directly calculate cloud properties (e.g. ISCCP), directly calculate TOA SW and LW CRF (e.g. ERBE), estimate surface SW CRF (e.g. Bishop and Rossow 1991; Chertock et al. 1991; Gupta et al. 1993; Laszlo and Pinker 1993; Li and Leighton 1993; Whitlock et al. 1995; Bishop et al. 1997; Li et al. 1997) and, with lesser accuracy, estimate LW CRF (e.g. Gupta et al. 1993; Zhi and Harshvardhan 1993). Unfortunately, satellite datasets have records too short to observe variability over time periods longer than a decade. On the other hand, surface-based cloud datasets have time records several decades long, but provide no quantitative radiative information. Therefore, any study of variability in cloudiness on timescales longer than a few years will be unable to determine the associated variability in CRF with precision (i.e. with direct measurements).

Bulk models have been developed to calculate surface SW and LW radiation flux from observed cloud amount using empirically-obtained relationships. The use of a bulk model assumes the location where the bulk model is applied has a similar cloud, temperature, and humidity regime to the location where the bulk model was developed. SW models based on total cloud amount (e.g. Reed 1977, Atwater and Ball 1981) are simplest to implement, but may have substantial inaccuracy in regions where many

different cloud types occur. Other SW bulk models have several categories for various cloud conditions (e.g. Lumb 1964, updated in Lind and Katsaros 1986), but are difficult to implement because cloud type and amount reported by the synoptic code is not easily translated into the categories. For surface LW radiation, Katsaros (1990) suggests Lind and Katsaros (1982) is best. Bulk models can have considerable errors at hourly (~80 W m^{-2}) and daily (~30 W m^{-2}) timescales, but this is reduced at monthly and seasonal timescales (~10 W m^{-2}) (Dobson and Smith 1988). However, significant long-term biases can occur if the bulk model is not valid at the location where it is applied. Furthermore, bulk SW models cannot provide information on variability in CRF resulting from variability in cloud optical thickness, except perhaps variability in cloud optical thickness due to changes in cloud type.

For these reasons, less-detailed but more easily implemented methods may provide CRF at equivalent accuracy and precision. The present study will adopt values from Norris and Leovy (1994), who used a combination of satellite observations, aircraft observations, and radiative transfer model results to estimate that a 1% increase in MSC amount during summer was associated with a 1 W m^{-2} decrease in surface downward radiation. This value was obtained for both midlatitude and eastern subtropical oceans, suggesting that variability in CRF associated with variability in MSC amount during summer may not be particularly sensitive to location. The presence of overlying midlevel stratiform clouds at midlatitudes may make an additional contribution to decreased surface downward radiation.

1.3 Examining the role of cloudiness in the climate system

In order to understand the role of clouds in climate variability and climate change, it is necessary to determine not only the present distribution of cloudiness and CRF, but also how cloudiness and CRF respond to changes in the climate and how the climate in turn responds to the changes in CRF. One common approach is to examine the sensitivity of the climate system to cloud feedbacks; that is, to determine how the magnitude of climate response to forcing depends on processes involving cloudiness. A positive cloud

feedback acts to increase the surface climate response to the original forcing while a negative cloud feedback acts to decrease the surface climate response. The distinction between cloud forcing and cloud feedback is important because the fact that cloudiness presently has a cooling effect on the Earth does not mean cloudiness will necessarily respond in such a way to mitigate an increase in global mean temperature. For example, a hypothetical decrease in MSC and midlevel stratiform cloud amount over the midlatitude ocean during summer in response to increasing global mean temperature would cause a reduction in global mean SW CRF which would act to augment the increasing temperature (a positive feedback). On the other hand, a hypothetical increase in MSC and midlevel stratiform cloud amount in response to increasing global mean temperature would act to retard the increasing temperature (a negative feedback). Hence, it is important to identify and measure cloud feedbacks as well as the climatological distributions of cloudiness and CRF. However, the magnitude and even the sign of the net cloud feedback on the climate system is presently uncertain (Arking 1991).

Net cloud feedback is difficult to determine because it is the sum of many, sometimes compensating, individual feedbacks, corresponding to many types of cloudiness, each with different radiative properties. Furthermore, the separate processes responsible for variability in different types of cloudiness and cloud radiative properties are not well-understood. Therefore, a primary goal of cloud–climate studies should be determining the direct dependence of cloud properties on other climate parameters. This can be done through observational or modeling studies.

Modeling studies have several advantages over observational studies: (1) the state of the (model) climate system is exactly known everywhere, (2) many realizations of the climate system are possible, and, most importantly, (3) other parameters can be held constant to focus on the relationship between a cloud property and a specific climate parameter. General circulation models (GCMs) are the best modeling tools for studying the global climate system, but they do not consistently and correctly simulate cloudiness (Cess et al. 1989; Cess et al. 1990; Weare et al. 1995; Cess et al. 1996; Weare et al. 1996) and give different values for cloud feedback depending on the parameterization used

(Senior and Mitchell 1993). This is a consequence of both the lack of knowledge about processes affecting cloudiness and the impracticality of modeling processes with sufficient detail when they are understood. For example, eddy-resolving models of the marine boundary layer (MBL) are now reaching the point where they simulate the transition from stratocumulus to trade cumulus in the subtropics well (e.g. Wyant et al. 1997), but such resolution cannot be incorporated into GCMs. In fact, cloud amount and CRF simulated by GCMs can significantly change when only the grid resolution (e.g. Kiehl and Williamson 1991; Tiedtke 1993) or assumed subgrid vertical cloud structure (e.g. Stubenrauch et al. 1997) is changed.

MBL cloudiness in particular is generally poorly simulated by GCMs (e.g. Randall et al. 1985; Kiehl and Ramanathan 1990; Slingo and Slingo 1991; Smith and Vonder Haar 1991; Soden 1992; Kiehl et al. 1994; Haskins et al. 1995; Mannoji 1995; Ward 1995; Del Genio et al. 1996). This produces large errors in the surface energy budget which cause other aspects of the climate system to be poorly simulated, such as the distribution of SST and convection in the eastern tropical Pacific (Ma et al. 1996; Philander et al. 1996). Thus, observational studies are currently necessary to both investigate cloud–climate relationships and improve model parameterizations.

In contrast to modeling simulations, observations of important cloud properties and climate parameters are often not available, and when available, often suffer from significant noise and biases. In order to obtain statistical significance in studies of interannual and interdecadal variations in cloudiness, it is necessary to have a long time record of data for a large part of the Earth, preferably several decades of data over the entire globe. Satellite data provide global coverage, but a single dataset such as ISCCP spans little more than a decade. Moreover, although CRF, cloud top temperature, and cloud optical thickness can be calculated from satellite observations, lack of calibration between satellites at the present time introduces overwhelming spurious variability at interannual timescales (Klein and Hartmann 1993a). On the other hand, data based on synoptic surface cloud observations have a longer time record, but unfortunately lack quantitative radiative information.

Similar problems exist in other climate parameters besides cloudiness. Information on temperature, moisture, and circulation above the surface over the ocean is limited, particularly prior to the decade of the 1980s, although this situation may improve when data from the National Centers for Environmental Prediction (NCEP) / National Center for Atmospheric Research (NCAR) Reanalysis Project becomes available (Kalnay et al. 1996). Other important information, such as the depth of the MBL, is not available at all over most of the global ocean, even at the present time.

Besides problems resulting from noisy, biased, and incomplete data, an additional difficulty encountered by observational studies is that all parameters vary simultaneously so that it is not simple to determine how a particular cloud property is affected by one parameter independent of the rest. Furthermore, observations often only demonstrate the existence of a relationship, but not which parameter is forcing the other. In fact, it is possible for two parameters unrelated by a physical mechanism to show a statistical relationship solely because they are both forced by a common third parameter. For all of these reasons, it is essential to not only document, but also develop a physical understanding of observed co-variability in cloud properties and other climate parameters. This will provide confidence that the observed co-variability is real and not a statistical artifact arising from spurious variability. Furthermore, the greater understanding of processes influencing cloudiness and documentation of co-variability can be used to improve and evaluate GCM simulations in which cloud–climate feedbacks are implicated.

1.4 Previous studies of variability in stratiform cloud optical thickness

The fact that MSC and midlevel stratiform cloudiness produce strong negative net CRF suggests it is likely that interannual variability in net CRF over the summertime midlatitude ocean primarily results from interannual variability in stratiform cloud amount and stratiform cloud optical thickness. Synoptic surface cloud observations have a sufficiently long time record to be useful for studies of variability in cloud amount, but due to the lack of quantitative radiative information they are not useful for studies of cloud optical thickness, except perhaps for estimating variability in cloud optical thickness

resulting from changes in cloud type. Aside from macroscopic cloud structure and geometric cloud thickness, cloud optical thickness for warm clouds depends largely on liquid water content (LWC) and typical cloud droplet size (the relationship between optical thickness and ice crystals in cold clouds is a much more difficult problem). Although methods have been developed to estimate cloud droplet size and LWC from satellite observations (Han et al. 1994; Zuidema and Hartmann 1995), the data are not available for a sufficiently long time period to document long-term variability in cloud amount or optical thickness. For this reason, investigations of potential long-term variability in cloud optical thickness are often based on model simulations.

Several mechanisms have been proposed that could produce long-term changes in cloud optical thickness, but it is difficult to evaluate these hypotheses due to unrealistic models and lack of supporting observational data. Somerville and Remer (1984) suggested that global warming may increase cloud LWC and consequently optical thickness, thus producing a negative feedback. However, Tselioudis et al. (1992) examined geographical and seasonal variations of cloud optical thickness and cloud top temperature using ISCCP data and found that optical thickness generally decreases with increasing cloud temperature, implying a corresponding decrease in LWC and a positive feedback on the climate system (Tselioudis et al. 1993). Whether this controverts the hypothesis of Somerville and Remer is unclear, because subpixel clear-sky patches, which would cause cloud optical thickness to be underestimated, are more likely to occur with cumulus, which occurs more frequently in geographical regions and seasons with warmer temperatures.

Although cloud macrophysical properties appear to make the largest contribution to cloud optical thickness (Stephens and Greenwald 1991), cloud optical thickness can also be affected by changes in cloud microphysical properties. Twomey et al. (1984) suggested that increased cloud condensation nuclei (CCN) concentration due to pollution could increase cloud droplet concentration and consequently optical thickness (this effect is referred to as indirect forcing by aerosol, whereas direct forcing results from scattering by the aerosol). Thus, one potential source of long-term change in cloud optical thickness

is the production of sulfate aerosol from anthropogenic sources, which has greatly exceeded that from natural sources during the past century over and downwind from industrial regions (Langner et al. 1992). Charlson et al. (1987) propose that cloud albedo over the ocean may be particularly sensitive to sulfate aerosol concentration, the primary contributor to CCN over the ocean.

Observational studies have found increased CCN concentration, cloud droplet concentration, and reflectance in MBL stratocumulus near local (Radke et al. 1989) and regional (Twohy et al. 1995) sources of anthropogenic aerosols. However, the larger-scale impact of anthropogenic aerosols on cloud optical thickness and cloud albedo is much more uncertain (Charlson et al. 1992). Despite the dramatic increase in sulfate aerosol over much of the Northern Hemisphere, observational studies have found only a slight difference in droplet radius in marine clouds (Han et al. 1994) and no difference in cloud albedo between hemispheres (Schwartz 1988; Han et al. 1994), except perhaps adjacent to the coastline of industrial regions (Falkowski et al. 1992). Novakov et al. (1994) also find only a slight relationship between sulfate aerosol concentration and cloud droplet concentration in MBL stratocumulus at a site some distance away from sources of anthropogenic sulfate aerosol.

In addition to increasing cloud droplet concentration, increased CCN concentration also decreases typical cloud droplet radius if the LWC remains constant; this could have the effect of decreasing precipitation loss in MBL stratocumulus and hence increase cloud lifetime (Albrecht 1989). Parungo et al. (1994) attribute an observed increase in non-precipitating midlevel cloudiness over the Northern Hemisphere midlatitude oceans between 1952–1981 (Warren et al. 1988) to decreased precipitation loss and increased cloud lifetime resulting from the observed increase in sulfate aerosol concentration, but it is more likely that the correlation in trends is merely coincidental and that the increase in midlevel cloudiness primarily results from a change in atmospheric circulation (Norris and Leovy 1995).

Because it is difficult to observationally assess the impact of anthropogenic aerosols on cloud microphysical properties and cloud optical thickness at large scales, several

investigations have resorted to GCM simulations. Recent studies indicate that the climate system is sensitive to arbitrary changes in low cloud microphysical properties (Chen and Ramaswamy 1996a, 1996b), but it is more difficult to simulate realistic sulfate aerosol effects on clouds. Erickson et al. (1995) obtain the strange result of greater cooling during winter than summer, apparently the result of very inadequate production of MBL cloudiness over the ocean during summer in the model (Smith and Vonder Haar 1991). More realistic results of Jones et al. (1994) and Jones and Slingo (1996) suggest global annual mean TOA indirect forcing due to anthropogenic sulfate aerosol is –0.3 to –1.5 W m^{-2} with much higher values near industrial regions. The large range in estimated global forcing results from different parameterizations for aerosol formation and cloud microphysics (e.g. Lohmann and Feichter 1997). Although it is possible that the magnitude of indirect forcing by anthropogenic sulfate aerosol is a significant fraction of the magnitude of anthropogenic greenhouse forcing (e.g. Mitchell and Johns 1997), the actual value is highly uncertain, and likely to remain so until GCMs can successfully simulate cloud macrophysics and microphysics and the processes controlling CCN concentration. Further review can be found in Baker (1997).

1.5 Previous studies of variability in stratiform cloud amount

At the present time, cloud amount and cloud type are the only cloud properties for which it is possible to investigate interannual and interdecadal variability. The two primary datasets which have been developed to study interannual and interdecadal variability in cloud amount over the global ocean are the Comprehensive Ocean-Atmosphere Data Set (COADS) 2° x 2° monthly summaries of total cloud amount (Woodruff et al. 1987) and the Warren et al. (1988) (hereafter W88) dataset, which provides frequency-of-occurrence, amount-when-present, and average cloud amount for several cloud type categories. Both datasets are based on a similar collection of synoptic surface cloud observations. Although many previous studies have examined long-term variability in total cloud amount over land regions (e.g. Abakumova et al. 1996; Angell et al. 1984; Angell 1990; Baker et al. 1995; Dessens and Bücher 1995; Henderson-Sellers

1986a, 1986b, 1989; Jones and Henderson-Sellers 1992; McGuffie and Henderson-Sellers 1988; Plantico et al. 1990; Russak 1990; Seaver and Lee 1987; Wang et al. 1993), relatively few studies have examined interannual and interdecadal variability in cloudiness over the ocean (e.g. Bajuk and Leovy 1997a, 1997b).

Hanson (1991) examined forty years of interannual variability in COADS total cloud amount and SST in several eastern subtropical ocean regions. Although handicapped by a large amount of statistical noise resulting from the small number of observations contributing to each COADS monthly 2° x 2° value, he found negative local correlations between interannual anomalies in total cloud amount and SST over a large part of each region. Oreopoulos and Davies (1993) conducted a similar study for two eastern subtropical ocean regions using five years of monthly total cloud amount from ISCCP and monthly all-sky (cloudy plus clear) albedo from ERBE.* Although handicapped by the short five-year record, they found that anomalies in both total cloud amount and all-sky albedo were negatively correlated with anomalies in SST. Total cloud amount over eastern subtropical oceans is predominantly MSC, with a corresponding negative net CRF. Thus, a decrease in cloud amount will produce a relative increase in SST by allowing more insolation to reach the surface and be absorbed. The negative correlation between cloud amount and SST suggests the possibility of a positive cloud feedback over the eastern subtropical ocean, particularly if through some process, warmer surface water favors less cloud amount.

A substantial amount of research in recent years has been devoted towards understanding factors controlling cloud amount in inversion-capped MBLs using models (e.g. Lilly 1968; Schubert et al. 1979a, 1979b; Albrecht 1984; Moeng 1986; Bretherton and Wyant 1997; Wyant et al. 1997) and observations (e.g. Nicholls 1984; Nicholls and Leighton 1986; Albrecht et al. 1988; Klein and Hartmann 1993b; Norris and Leovy 1994; Paluch et al. 1994; Albrecht et al. 1995a; Albrecht et al. 1995b; Betts et al. 1995; Bretherton and Pincus 1995; Bretherton et al. 1995a; Bretherton et al. 1995b; Klein et al.

---

* It is likely that changes in all-sky albedo are dominated by variations in cloud amount instead of variations in cloud optical thickness.

1995; Norris 1997a; Norris 1997b) but only a small portion of it can be reviewed here.

Klein et al. (1995) examined interannual variability in low cloud amount over the eastern subtropical North Pacific during summer and found that increased cloud amount is associated with increased cold advection, decreased SST, and increased lower tropospheric static stability, defined as $S \equiv \theta(700\ \text{mb}) - \theta(\text{sfc})$, where both decreased SST and increased above-MBL temperature contribute to *S*. Anomalies in low cloud amount are best correlated with anomalies in SST and *S* that are 24–36 hours upwind, indicating that SST is not merely responding to CRF locally (as was also found by Ronca and Battisti 1997). The conceptual model of Bretherton (1992) and Wyant et al. (1997) proposes that increasing MBL depth and advection over increasingly warm water promotes decoupling of the cloud layer from the subcloud layer, thus causing the breakup of stratocumulus with large cloud amount to trade cumulus with small cloud amount. This is consistent with the results of Klein et al., since 24–36 hours is comparable to the timescale for temperature and moisture in the MBL to adjust to changes in environmental conditions (Schubert et al. 1979b; Albrecht 1984), and since increased *S* favors a shallower MBL. However, it is difficult to distinguish how variability in SST, *S*, and cold advection individually contribute to variability in low cloud amount since all are associated with variability in the strength of the subtropical anticyclone.

Klein and Hartmann (1993b) used the W88 "stratus" (identical to MSC) climatology to show that MSC is even more prevalent over the midlatitude ocean than over the eastern subtropical ocean. Moreover, they found that seasonal and geographical variations in MSC amount are well-related to seasonal and geographical variations in *S*. This suggested that the relationship between MSC amount, SST, and *S* previously observed in the eastern subtropical ocean may also exist in other regions of the ocean where MSC is common. Norris and Leovy (1994) (hereafter NL) examined thirty years of interannual variability in MSC amount and SST over the global ocean (interannual variability in *S* was not examined because 700-mb temperatures were not readily available prior to the decade of the 1980s). Their use of W88 seasonal values at 10° x 20° resolution considerably reduced the statistical noise encountered by the earlier Hanson

(1991) study. Similar to previous studies, NL found strong negative local correlations between interannual anomalies in MSC amount and SST over eastern subtropical oceans. Moreover, they found equally strong negative correlations at midlatitudes, as did Peterson (1991), particularly during summer. Significant upward trends in MSC amount and downward trends in SST were observed between 1952 and 1981 over the North Pacific and North Atlantic, particularly during summer.

As was also documented by Weare (1994), who examined five years of interannual variability in ISCCP total cloud amount and SST over the global ocean, the greatest negative correlations occurred along regions of strong SST and cloud gradient, suggesting that year-to-year meridional movements of these gradient regions are responsible for the observed correlations and long-term trends. A similar seasonal cycle of meridional movements of these gradient regions exists, as indicated by the strong negative intra-annual correlations between SST and cloudiness documented by Weare (1993, 1994). Since warm advection prevails in the western and central midlatitude ocean, it is likely that the MBL processes responsible for the observed negative correlation between MSC amount and SST at midlatitudes differ from those in the eastern subtropics. NL hypothesized that anomalously cold water along the SST gradient would shift the region of strongest SST gradient equatorward. This would produce an equatorward shift in the pattern of warm advection and likely a corresponding shift in stratus and fog, thus increasing MSC amount over the region of cold water.

The study of Weaver and Ramanathan (1996) indicates that the strongest CRF over the midlatitude North Pacific during summer results from midlevel clouds (presumably with underlying low clouds) associated with extratropical cyclones. Therefore, it is important to examine interannual variability in midlevel stratiform cloud amount as well as MSC amount. NL found that interannual anomalies in both precipitating and non-precipitating midlevel cloud amount were strongly negatively correlated with anomalies in SST along the midlatitude SST and cloud gradient region during summer. This suggested that, in addition to purely MBL processes, synoptic activity associated with shifts in the location of the storm track plays an important role in determining interannual

variability in cloudiness over midlatitude oceans during summer. However, NL did not quantitatively examine atmospheric circulation, synoptic activity, or variability in storm track location and SST.

1.6 Previous studies of atmosphere–ocean interaction

There have been many previous studies examining interaction between the atmosphere and ocean at midlatitudes (e.g. Davis 1976, 1978; Frankignoul 1985), but almost all of them have focused on the winter season and ignored the role of CRF. Observational studies have documented that coupled variability in monthly-mean and seasonal-mean atmospheric circulation and SST during winter (e.g. Wallace et al. 1990) is much stronger than coupled variability observed during summer (e.g. Zhang 1996, Norris et al. 1997), perhaps because anomalies in atmospheric circulation are much weaker during summer (Wallace et al. 1993). Coupled variability between atmospheric circulation and SST during summer may also be weaker because variability in CRF (ignored in almost all studies) has as much influence on SST as do the anomalous latent and sensible heat fluxes produced by variability in atmospheric circulation.

Coupled variability in atmospheric circulation and SST can arise from SST forcing of the atmosphere, atmospheric forcing of SST, or both; however, observational studies often have difficulty identifying the direction of causality in observed relationships. Kushnir (1994) indicates that patterns of atmosphere–ocean interaction over the wintertime North Atlantic are consistent with the atmosphere forcing the ocean on interannual timescales but suggests that the ocean may be forcing the atmosphere at interdecadal timescales. Peng and Fyfe (1996) observe two modes of atmosphere–ocean interaction and attribute one to atmospheric forcing of SST and the other to SST forcing of the atmosphere. However, most observational studies have concluded that SST is primarily forced by the atmosphere during winter.

Cayan (1992a, 1992b) and Deser and Timlin (1997) show that anomalous latent and sensible heat fluxes associated with changes in atmospheric circulation are largely responsible for interannual SST anomalies at northern midlatitudes during winter,

although Iwasaka and Wallace (1995) note that horizontal temperature advection and vertical mixing may be significant as well. Atmospheric forcing of the ocean is supported by the results of Luksch and von Storch (1992), Luksch (1996), and Battisti et al. (1995) who forced ocean models for the North Pacific and North Atlantic with observed wind anomalies and found that modeled SST was highly correlated with observed SST during winter. Lau (1988) shows that meridional displacements of the wintertime storm track occur with variations in certain large-scale circulation patterns, particularly the Pacific/ North America (PNA) pattern (described by Wallace and Gutzler 1981), the dominant pattern of Northern Hemisphere circulation during winter (Wallace et al. 1993). Namias et al. (1988) associate a decreasing trend in SST over the central North Pacific during winter with an increasing tendency for the selection or amplification of the positive phase of the PNA pattern. This provides evidence that the observed downward trend in SST over the central North Pacific during winter is forced by changes in large-scale atmospheric circulation. Zhang et al. (1997) demonstrate that wintertime SST anomalies persist into summer, suggesting that the observed downward trend in SST over the central North Pacific during summer documented in NL results in part from persistence.

The influence of midlatitude SST anomalies on atmospheric circulation has primarily been explored with atmospheric GCM experiments integrated over specified SST anomaly distributions (e.g. Palmer and Sun 1985; Pitcher et al. 1988; Lau and Nath 1990; Kushnir and Lau 1992; Ferranti et al. 1994; Kushnir and Held 1996; Peng et al. 1997), coupled to an oceanic mixed layer (e.g. Gallimore 1995), or an ocean GCM (Latif and Barnett 1996). Some, but far from all, indicate that the storm track shifts equatorward in response to negative SST anomalies and poleward in response to positive SST anomalies during winter, but the sensitivity of atmospheric circulation to midlatitude SST anomalies is weak. This lack of sensitivity may be due to the coarse spatial resolution of the GCMs, which produces insufficient eddy momentum fluxes (Kushnir and Held 1996), or due to differences in the background state of atmospheric circulation (Peng et al. 1997). The very few modeling studies which have examined forcing by SST anomalies during summer (e.g. Lau and Nath 1990) indicate that the atmospheric response is even weaker.

Thus, the effect of midlatitude SST anomalies on seasonal-mean atmospheric circulation and the location of storm tracks is not well-established, particularly during summer.

1.7 Overview of the present study

Although Fig. 1.1 indicates that MSC and midlevel stratiform cloudiness over the midlatitude ocean during summer have a very large impact on the TOA energy budget and likely also the surface energy budget, little research has been directed towards understanding the role of summertime midlatitude cloudiness in the climate system. Instead, most previous studies investigating coupling between eastern subtropical cloudiness and SST have largely focused on radiative and MBL processes and ignored the role of atmospheric circulation and latent and sensible heat fluxes (one exception is Ronca and Battisti 1997), and previous studies of coupling between midlatitude atmospheric circulation and SST have largely focused on latent and sensible heat fluxes during winter and ignored the role of midlatitude cloudiness and CRF during summer. However, the results of NL indicate that interannual variability in stratiform cloudiness is closely coupled to both interannual variability in SST and synoptic activity during summer. For these reasons, a study is needed which considers CRF, MBL processes, atmospheric circulation, latent and sensible heat fluxes together in producing interannual and interdecadal variability in MSC, midlevel stratiform cloudiness, and SST over the midlatitude ocean during summer. The potential for cloud feedbacks on local SST and the climate system as a whole should also be examined, particularly since variability in TOA net CRF represents a transfer of energy into and out of the Earth's climate system, while variability in sensible and latent heat fluxes represents an transfer of energy only between the ocean and the atmosphere.

Although the study of NL provided valuable information on interannual and interdecadal co-variability in MSC, midlevel cloud amount, and SST over the summer midlatitude ocean, many important questions remain:

- How are interannual and interdecadal variability in seasonal-mean MSC, midlevel

stratiform cloudiness, and SST related on the large scale?

- How is variability in seasonal-mean atmospheric circulation and synoptic activity quantitatively related to variability in MSC and midlevel stratiform cloudiness?
- What processes link SST and atmospheric circulation to low stratiform cloud types that contribute to MSC?
- What is the impact of variability in CRF on SST, and how does variability in CRF compare with other processes in producing variability in SST?
- What cloud feedbacks contribute to interdecadal variability in SST and the climate system?

These questions will be answered to the largest extent possible in the present study, which examines variability over the summertime North Pacific.

Chapter 2 examines the relationship between MSC, midlevel stratiform cloudiness, and SST on the large scale and interannual and interdecadal timescales using more advanced statistical techniques than the local correlation method employed by NL. The time period under analysis starts in 1952 and is extended from the 1981 endpoint of NL to 1992 using an improved, higher-resolution cloud dataset to examine whether the trends in MSC, midlevel stratiform cloudiness, and SST previously documented by NL continue through the 1980s. Furthermore, the role of seasonal-mean atmospheric circulation and synoptic activity is quantitatively investigated. The results are applied to testing the earlier hypothesis of NL that variability in MSC, midlevel stratiform cloudiness, and SST over the summertime midlatitude ocean is associated with meridional shifts in the storm track and the locations of the strongest gradients in SST and cloudiness. The degree to which variability in CRF is responsible for variability in SST is assessed by comparing an estimate of the change in SST produced by observed typical MSC anomalies to the actual SST anomalies.

Two substantial problems hinder the determination of processes responsible for interannual variability in MSC: (1) the low stratiform cloud types contributing to the MSC

category are produced by different advective and synoptic conditions, and (2) the different advective and synoptic conditions are largely averaged out in seasonal-mean data. Therefore, Chapter 3 uses data from several Ocean Weather Stations to composite soundings and surface meteorological observations for specific low cloud types. This provides information on representative MBL structures, advective, and synoptic conditions associated with low stratiform cloud types over the midlatitude ocean from which processes influencing MSC can be inferred. The climatological distribution of cloud amount and relative contribution to MSC amount for each low stratiform cloud type is documented in Chapter 4 for the summertime midlatitude North Pacific. Using these products, the roles of interannual variability in SST and synoptic activity in producing interannual variability in MSC can be understood as the cumulative effect of SST and advection on individual low stratiform cloud types. Chapter 4 furthermore confirms the OWS results in Chapter 3 by compositing low cloud type in the meridional direction over the central North Pacific for conditions of inferred warm and cold advection. Several satellite images are also presented which support the results obtained from surface observations.

Chapter 5 begins by repeating in greater detail many of the analyses undertaken in Chapter 2, this time focusing on interannual variability in the meridional direction over the central North Pacific during summer. The results from Chapters 3 and 4 are used to interpret regressions between low cloud types and time series of SST and an index of synoptic activity. This enables identification of the processes through which interannual variability in SST and storm track location produce interannual variability in MSC amount. The degree to which interannual variability in MSC amount radiatively forces interannual variability in SST during summer is also examined and compared to forcing by interannual variability in latent and sensible heat fluxes and zonal stress. The end result of this study is an improved understanding of the processes through which large-scale variability in MSC, midlevel stratiform cloudiness, SST, and atmospheric circulation interact over the midlatitude North Pacific during summer. Furthermore, the potential for a cloud feedback on SST is assessed, along with the role of radiative forcing

by MSC in producing interdecadal variability in SST. Chapter 6 reviews the present study and discusses possible relationships between variability in MSC amount over the summer midlatitude North Pacific and the global climate system. Possible directions of future research are described at the end.

Unfortunately, only variability in CRF due to changes in MSC amount and not optical thickness can be examined. The cloud dataset used in this study is based on synoptic surface cloud observations since only they provide a sufficiently long time record to undertake a study of interannual and interdecadal variability in cloudiness. Because quantitative radiative information is not available, it will not be possible to test the hypothesis that cloud optical thickness and cloud albedo has increased due to increased sulfate aerosols in particular, or to examine variability in cloud optical thickness and cloud albedo in general.* For this reason, only a partial cloud feedback based on variability in cloud amount can be obtained. Furthermore, it is beyond the scope of this study to investigate how SST anomalies potentially force variability in seasonal-mean atmospheric circulation and storm track location during summer. Nonetheless, the results of this study substantially increase our understanding of the processes producing large-scale co-variability in cloudiness, SST, and atmospheric circulation over the midlatitude ocean during summer, and provide a foundation for future modeling studies.

---

* Section 2.6 provides an estimate of the change in MSC optical thickness required to produce an anomaly in CRF equivalent to that produced by a typical anomaly in MSC amount.

Table 1.1: Seasonal variation of hemispheric and global mean net CRF (W m^{-2}) at the TOA (from Harrison et al. 1990) and the surface (from Gupta et al. 1993).

	TOA Net CRF			Surface Net CRF		
	NH	SH	Global	NH	SH	Global
April 1985	–18.6	–8.9	–13.8	–20.7	–4.9	–12.8
July 1985	–32.5	–0.8	–16.6	–34.9	10.9	–12.0
October 1985	–6.0	–30.0	–17.9	–11.0	–32.0	–21.5
January 1986	–0.1	–42.1	–21.1	3.4	–53.6	–25.1
Annual	–14.3	–20.4	–17.3	–15.8	–19.9	–17.9

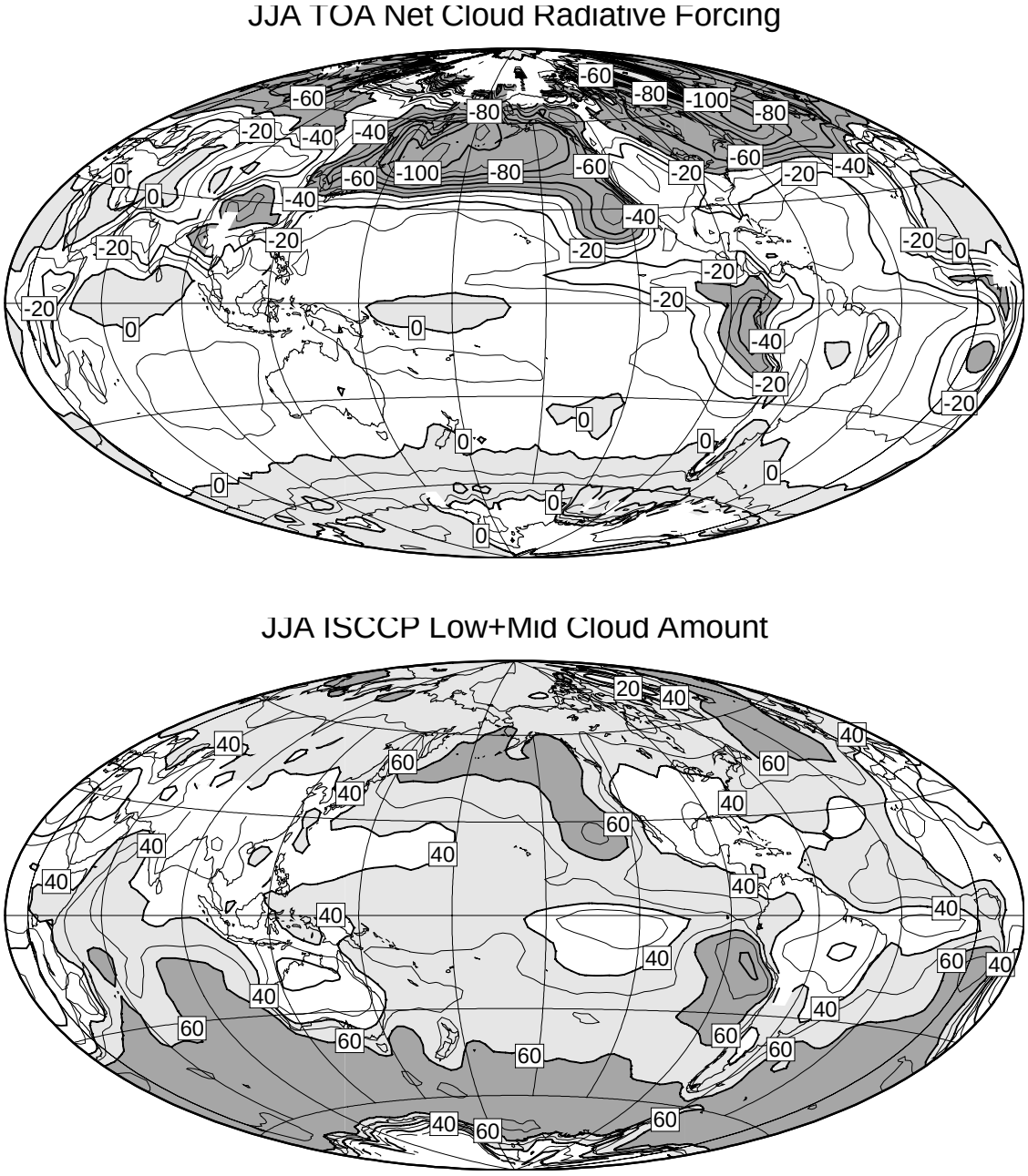

Figure 1.1: (Top) TOA net CRF during JJA. Contour interval is 10 W m^{-2}. Shading indicates values above 0 W m^{-2} (light) and below –40 W m^{-2} (dark). (Bottom) Amount of low and midlevel cloudiness seen by satellite during JJA. Contour interval is 10%; thresholds for lighter (darker) shading are 40% (60%).

CHAPTER 2

Large-Scale Interaction between Cloudiness, Sea Surface Temperature, and Atmospheric Circulation over the Summertime Midlatitude North Pacific

2.1 Introduction

The study of NL (1994) found strong negative local correlations between interannual anomalies in MSC amount and SST at midlatitudes, particularly during summer. In addition, between 1952 and 1981 over both the North Pacific and North Atlantic, a significant upward trend in MSC amount and downward trend in SST were observed. Similar trend patterns occurred in all seasons, but the MSC trend was greatest during summer. The fact that the greatest anomalies occurred along regions of strong SST and cloud gradient suggested that year-to-year meridional movements of these gradient regions were responsible for the observed correlations. Furthermore, strong negative local correlations between interannual anomalies in both precipitating and non-precipitating midlevel cloud amount and SST were found at these locations. This suggested that, in addition to purely MBL processes, synoptic activity associated with shifts in the location of the storm track played an important role in determining interannual variability in cloudiness over midlatitude oceans during summer. However, NL did not quantitatively examine seasonal-mean atmospheric circulation or synoptic activity.

This chapter extends NL in several important ways. Large-scale interaction between MSC, midlevel stratiform cloudiness, SST, and atmospheric circulation is examined using empirical orthogonal function (EOF) analysis and singular value decomposition (SVD) analysis instead of local correlations. The role of atmospheric circulation is evaluated by examining interannual variability in seasonal-mean sea level pressure (SLP) and the seasonal variance of daily meridional wind (VV). The cloud data are recalculated from the individual reports to avoid coarse resolution, biases due to

variability in spatial sampling, and biases due to inadequate nighttime sky illumination, all of which the original Warren et al. (1988) (W88) dataset suffered from. Furthermore, an additional eleven years of data are available to examine whether the previously observed trends in MSC amount and SST continue through the decade of the 1980s. The analysis focuses on the North Pacific because that is where the strongest relationships between cloudiness and SST are observed.

2.2 Data

The three basic parameters used to describe variability in cloud types are frequency of occurrence (FQ), amount-when-present (AWP), and average cloud amount (hereafter shortened to "cloud amount"), where cloud amount is defined as FQ x AWP. Interannual variability in MSC and midlevel stratiform cloudiness during summer is examined using MSC amount and nimbostratus (Ns) FQ. Since observers sometimes have difficulty identifying cloudiness under conditions of poor illumination (Hahn et al. 1995; Rozendaal et al. 1995; Norris 1997a), the present study uses only daytime (including twilight) observations. The W88 MSC and Ns data previously used by NL was obtained from all times of day without screening for poor illumination.

The present definition of MSC slightly differs from that of W88 in that all cases of sky-obscuring precipitation are now classified as MSC. Sky-obscuring precipitation during summer typically occurs as drizzle, consistent with the MSC classification, but the practical difference is negligible since sky-obscuring precipitation is rare. The present definition of Ns also differs from that of W88 in that all cases of drizzle precipitation are not classified as Ns. This was done to exclude the possibility of shallow precipitating stratus layers being identified as Ns. Furthermore, Ns FQ instead of Ns cloud amount is used to avoid assumptions about upper-level cloud cover when low-level cloud cover is overcast. Because Ns is identified by the occurrence of precipitation, Ns FQ can always be obtained despite the presence of obscuring low clouds. Nonetheless, Ns cloud amount is very close to Ns FQ since Ns AWP is typically nearly 100%. Although NL examined non-precipitating midlevel cloud amount, that is not repeated here due to frequent obscuration

of low clouds. The similarity between variations in non-precipitating midlevel cloud amount and Ns cloud amount (NL) suggest that Ns alone is a sufficient measure of variability in midtropospheric cloudiness.

The cloud data used in this study were calculated from the Extended Edited Cloud Report Archive (EECRA), an updated version of the Edited Cloud Report Archive (Hahn et al. 1996). The EECRA is a collection of individual reports which include coincident meteorological observations as well as synoptic surface cloud observations from December 1951 to December 1992. These were obtained from the COADS CMR and LMRF archives and are the same observations from which the W88 dataset was constructed for the time period 1952–1981. Observations before 1954 were not used in the present study because they inconsistently identify cloud type (W88). A major change in observing procedure was introduced in 1949 (Wright 1986), which substantially changed the cloud type categories reported by the synoptic code from previous categories (Berry et al. 1945); some nations (NCDC 1962) and apparently many ships did not adopt the new procedure until several years later. However, the additional eleven years of data after 1981 provide for a 39-year period of record (1954–1992) compared to a 30-year period of record. Due to a change in observing procedure in 1982 it was necessary to calculate FQ by a somewhat unconventional method to avoid introducing biases. Nonetheless, the formulas used are still exact and are described in Norris (1997b).

Two disadvantages of the W88 dataset are the coarse 10° x 20° resolution and the occurrence of spurious variability produced by changes in spatial sampling within a 10° x 20° grid box in the presence of a climatological cloudiness gradient.* These problems were avoided in the present study by a two-step process: (1) the individual reports of MSC amount and Ns FQ were averaged to monthly values at 2.5° x 5° resolution, and (2) the monthly 2.5° x 5° values were averaged to seasonal (JJA) values at 5° x 10° resolution with weighting by area but not the number of observations. Unfortunately, the smaller number of observations contributing to the 5° x 10° grid boxes compared to the

---

* Weare and Strub (1981) note that non-uniform sampling can produce significant biases even for 5° x 5° grid boxes

10° x 20° grid boxes resulted in greater statistical noise; this was reduced by 1–2–1 smoothing in latitude and longitude. The grid boxes were chosen to be longer in longitude than latitude because most features of the midlatitude North Pacific exhibit much shorter scales in the meridional direction than the zonal direction.

As in NL, the SST data used in this study are from the *Global Ocean Surface Temperature Atlas* (GOSTA) (Bottomley et al. 1990). Because the GOSTA data extend only to 1991, one year short of the cloud data, SST values obtained from the EECRA for 1992 were averaged to the GOSTA monthly 5° x 5° resolution and appended to the GOSTA dataset. The combined dataset (1954–1992) was then averaged to seasonal (JJA) 5° x 10° resolution to correspond with the cloud data, but no smoothing was needed.

Monthly SLP values at 5° x 5° resolution were obtained from the Data Support Section, Scientific Computing Division, NCAR. These data were corrected for errors and discontinuities due to changes in analysis procedure by K. Trenberth (NCAR). Similar to the SST data, the SLP data were averaged to seasonal (JJA) 5° x 10° resolution without smoothing for the time period 1954–1992; however, the SLP grid box centers are offset from the SST and cloud grid box centers by 2.5° in latitude and longitude (i.e. the northwesternmost 5° x 10° grid box is centered on 90°N, 2.5°E for the SLP dataset but 87.5°N, 5°E for SST and cloud datasets).

NL counted surface low center tracks recorded in the *Mariners Weather Log* (Anonymous 1958–1981) for the region 30–40°N, 160–180°E during JJA and found that years with colder water and greater MSC amount tend to have a greater frequency of cyclones. However, it is desirable to have a more quantitative and accessible measure of synoptic activity. Since surface wind direction will likely exhibit greater day-to-day variability when cyclones are more frequent, the seasonal variance of the daily surface meridional wind component (VV) may be a good measure of the strength of summertime synoptic activity during a particular year. The observational study of Blackmon et al. (1977) indicates that maximum VV at 500 mb coincides with the axes of climatological storm tracks over the ocean during winter. Due to the shallow nature of many summertime storm systems, surface wind may be a better measure of synoptic activity than wind in the

midtroposphere. Unfortunately, daily wind data are not yet directly available over most of the time period under study. Instead, daily meridional wind at 2.5° x 2.5° resolution was calculated assuming geostrophy from NCEP (known as the National Meteorological Center (NMC) prior to 1995) operational SLP analyses for 12 UTC obtained from NCAR through E. Recker (Department of Atmospheric Science, University of Washington). The long-term daily mean was subtracted from the data, and VV was obtained by calculating the variance of the resulting daily deviations over JJA for each year for the time period 1954–1992. The 2.5° x 2.5° VV data were then averaged to 5°x 10° resolution with weighting by area but no smoothing, and with the same grid box centers as for the SST and cloud data.

2.3 Analysis techniques

The results of NL suggested that interannual variability in stratiform cloudiness and SST is produced by large-scale meridional movement of the regions of strong gradients in cloudiness and SST; however, the local correlation method used by NL was unable to determine how variability in one area is related to variability in another area. Therefore, it is necessary to adopt more sophisticated analysis techniques which measure how variability in two parameters is related in space as well as time. Two such techniques used in the present study are empirical orthogonal function (EOF) analysis (e.g. Kutzbach 1967) and singular value decomposition (SVD) analysis (Bretherton et al. 1992). The input to these analyses are the covariance matrices of one or more data fields, measuring the temporal co-variability between each possible pair of gridpoints in the spatial domain. If the time series at each grid point is normalized to unit variance beforehand, the covariance matrix becomes the correlation matrix, but that was not done in this study.

EOF analysis calculates the eigenvectors, called EOFs, of the covariance matrix. The associated eigenvalues represent the fraction of total variance explained by each EOF. For this reason the EOFs are ordered according to decreasing eigenvalue, with the first EOF representing the dominant spatial pattern of temporal variability, the second EOF representing the second-most dominant pattern of spatial variability, etc. Because

the EOFs are constrained to be mutually orthogonal, only the leading EOFs typically have physical significance. The projection of the original data field onto an EOF, sometimes called the principal component (PC), produces the time series associated with that EOF. The time series, or PCs, of the EOFs are mutually uncorrelated. Because the behavior of the data field outside the EOF spatial domain is often of interest, the regression of the data field onto the normalized EOF time series will be displayed instead of the actual EOF pattern, but the difference between the two is insignificant. When the data field is regressed on the normalized EOF time series, the corresponding map shows typical fluctuations associated with that mode.

SVD analysis is similar to EOF analysis, but finds the singular vectors that explain the maximum squared cross-covariance between two data fields (typically referred to as right and left) in possibly two different spatial domains. Hence, each SVD mode contains patterns from both the right and the left field, each of which has a corresponding expansion coefficient time series, analogous to the PC of an EOF mode. SVD modes are ordered by their associated singular values (analogous to the eigenvalues of EOF analysis), which represent the fraction of total squared covariance explained by each SVD mode. Although squared covariance fraction (SCF) is useful for comparing the relative importance of modes in the same SVD expansion, it is less useful for comparing the strength of relationship between right and left fields in modes from different SVD expansions because the squared covariance between right and left fields may be much different. This problem can be mitigated by using normalized root-mean-squared covariance (NC), defined in Zhang et al. (1997), as a statistic.

The most important statistic for measuring coupling between two data fields is the correlation coefficient (r) between the expansion coefficient time series of the right and left patterns of an SVD mode. If two data fields are completely uncoupled, SVD analysis will still construct apparent coupling out of statistical noise; hence a non-zero value for r does not guarantee the existence of real coupling. It is generally not worthwhile to examine patterns associated with an SVD mode if $r < 65\%$ (J. M. Wallace, personal communication). SVD modes will be displayed by regressing the right (left) data field on

the normalized expansion coefficient of the left (right) pattern (called heterogeneous regression by Bretherton et al. 1992). Hence, the maps show the fluctuations in one data field associated with a typical anomaly pattern of the other data field. Further comments on the use of SVD analysis can be found in Newman and Sardeshmukh (1995), Cherry (1996, 1997), and Hu (1997).

Figure 2.1 shows the spatial domain on which EOF and SVD analyses involving MSC amount, Ns FQ, SST, and VV were conducted. Because the SLP grid box centers were offset 2.5° in latitude and longitude from the grid box centers of the other datasets, the domain for EOF and SVD analyses involving SLP was shifted 2.5° to the north and to the west of the region displayed in Fig. 2.1. With this minor exception, all datasets used the same domain for purposes of consistency and simplicity. The southern boundary was set at 25°N to focus on variability at midlatitudes, and the western and eastern boundaries were set at 140°E, and 120°W to exclude regions where variability in cloudiness is more related to variability in offshore flow rather than processes occurring in the central basin. The Bering Sea and the Sea of Okhotsk were also excluded from the domain due to low sampling density which produced large and spurious variability in the cloud data. In all EOF and SVD analyses, variances and covariances are weighted by the cosine of latitude so that equal areas have equal weighting.

2.4 Large-scale interaction between cloudiness and sea surface temperature

Figure 2.2 shows the climatological distribution of MSC amount during summer, the leading EOF of interannual variability in MSC amount, and the normalized time series corresponding to the leading EOF. The time series can be converted into absolute units by noting that the value of the EOF pattern at a particular location is equal to one standard deviation of the time series at that location. Table 2.1 documents the percentage of total variance explained by the first and second EOFs. The climatology displayed here was calculated from the smoothed 5° x 10° data to match the EOF analysis, but a finer-resolution climatology in Norris et al. (1997) (hereafter NZW) shows an even sharper gradient in MSC amount across the North Pacific. The dominant pattern of interannual

variability represented by the leading EOF is an increase or decrease in MSC amount along the gradient region in the central North Pacific. MSC amount over the eastern subtropical North Pacific varies in the opposite direction from MSC amount in the central North Pacific (although not shown in its entirety, part of this is apparent in Fig. 2.2). This is consistent with the results of NZW for the leading EOF of MSC amount north of 10°N. The fact that the leading EOF resembles the spatial pattern of trends in MSC amount between 1952–1981 shown in NL indicates it is largely responsible for long-term variability in MSC amount over the North Pacific. The time series associated with the leading EOF exhibits considerable variability at timescales longer than a year, and the long-term trend does indeed appear to continue past 1981.

Given the strength of the long-term trend, one might question whether there are sufficient temporal degrees of freedom to ensure that the results of the EOF analysis would be reproducible in an independent dataset. A further concern is that the substantial interdecadal variability might be at least partially spurious, given the sensitivity of cloud data to subtle changes in observing practices that may have occurred over the years (Bajuk and Leovy 1997b). To address these issues, the EOF calculation was repeated on the one-year (summer-to-summer) difference field (i.e., replacing the 1954 values with those for 1955 minus 1954, etc.), which emphasizes variability at less than five years and virtually eliminates any long-term trend. The resulting leading EOF pattern (not shown) is similar to that calculated on the undifferenced data, as shown by NZW. Therefore, it is highly unlikely the EOF pattern displayed in Fig 2.2 is merely an artifact of the interdecadal variability in the time series and has no physical significance on year-to-year timescales.

Figure 2.3 shows the climatological distribution of SST during summer, the leading EOF of interannual variability in SST, and the normalized time series corresponding to the leading EOF. The percentage variance explained by EOFs 1 and 2 is documented in Table 2.1. Similar to the case for MSC amount, a climatology at 1° x 1° resolution (not shown) exhibits a sharper gradient in SST than is apparent in the 5° x 10° climatology displayed here. The dominant pattern of interannual variability represented by the leading EOF is an increase or decrease in SST along the gradient region in the central North Pacific, but the

center of action is farther to the north than was the case for MSC amount. SST variability in the eastern subtropical North Pacific is opposite in sign to SST variability in the central North Pacific. This pattern is generally consistent with the leading EOF of SST north of 18°N calculated by Zhang (1996) and Zhang et al. (1997) for the slightly longer time period 1950–1993 using COADS instead of GOSTA (COADS is semi-independent from GOSTA). The time series associated with the leading EOF of summertime SST also exhibits considerable variability at timescales longer than a year. The spatial pattern of long-term trends in SST between 1952–1981 shown in NL are similar to the leading EOF, and the time series in Fig. 2.3 suggests the trends in SST continued at least through the mid-1980s. The pattern of the leading EOF and magnitude of the long-term trend are similar to the pattern and magnitude of the 1947–1986 annual-mean local SST trends calculated by Jones et al. (1987). The two time series corresponding to the leading EOFs of MSC amount and SST have a correlation coefficient (r_{PC}) of 66.0% (Table 2.2).

The study of NL described only the correlation between MSC amount and SST locally, but SVD analysis describes the correlation between coupled large-scale patterns of MSC amount and SST, displayed in Fig. 2.4 for the summer season. As was the case for local correlations, increased (decreased) MSC amount along the gradient region corresponds to decreased (increased) SST. Moreover, increased MSC amount and decreased SST along the gradient region are associated with decreased MSC amount and increased SST in the eastern subtropical Pacific and along the coast of North America, and vice versa. This is consistent with the results of NZW for the leading SVD patterns of MSC amount and SST poleward of 10°N. The SCF and NC listed in Table 2.2 indicate that the patterns shown in Fig. 2.4 explain a significant fraction of coupled MSC–SST variability, and the high value of r indicates these MSC and SST patterns are closely coupled. These MSC–SST patterns resemble, and have amplitudes almost as strong as their respective EOFs in Figs. 2.2 and 2.3. This indicates that the dominant patterns of interannual variability and long-term trends in MSC amount and SST individually are closely related to large-scale coupling between MSC and SST.

Given the fact that significant long-term trends exist in both the MSC and SST

datasets, one might question whether the apparent coupling between MSC amount and SST might only result from the trends and not variability at higher frequencies. As was done for the EOF analyses, the SVD analysis was repeated on MSC and SST one-year difference fields. The resulting leading SVD patterns (not shown) are similar to those calculated on the undifferenced data and are even more closely coupled (r = 91.9%), as was shown by NZW.

NL attributed the negative correlations between Ns amount and SST across the midlatitude ocean during summer to coinciding meridional shifts in the storm track and region of strong SST gradient. The top panel of Fig. 2.5 shows the summertime climatological distribution of Ns FQ, which has a lesser-amplitude but generally similar pattern to the W88 Ns climatology. The difference is largely due to the exclusion of all drizzle precipitation from Ns in the present study. The Ns in the vicinity of the SST gradient region coincides with climatological bands of enhanced cloud liquid water path (Weng et al. 1997) and mean upward motion in the midtroposphere (Hoskins et al. 1989). The middle and lower panels of Fig. 2.5 show the leading EOF of interannual variability in Ns FQ during summer and the normalized time series corresponding to the leading EOF. Table 2.1 documents the percentage of total variance explained by the first and second EOFs. The dominant pattern of interannual variability represented by the leading EOF is an increase (decrease) in Ns FQ along the equatorward Ns gradient region and a decrease (increase) in Ns FQ to the northwest. The Sea of Okhotsk and the Bering Sea were excluded from the analysis domain due to the overwhelming noise resulting from low sampling density, but the EOF calculation nevertheless identifies a see-saw relationship between Ns FQ at 35°N and at 50°N in the western North Pacific. This see-saw relationship is consistent with meridional movement of the storm track, or a tendency for cyclones to track in either a more zonal or more northeastward direction (e.g. Blender et al. 1997). The time series associated with the leading EOF exhibits an upward trend, consistent with the increase in annual W88 Ns amount over the central North Pacific documented by Norris and Leovy (1995).

Figure 2.6 shows the patterns associated with the leading SVD mode of Ns FQ and

SST during summer. Colder water along the SST gradient region is associated with increased Ns FQ in a band stretching southwest to northeast across the North Pacific along the Ns gradient region, and decreased Ns FQ northwest of the band. These Ns–SST patterns resemble their respective EOFs in Figs. 2.5 and 2.3, and the time series of the EOFs have a correlation coefficient of 65.3% (Table 2.2). This corroborates the hypothesis that the summertime storm track moves poleward and equatorward as the region of strong SST gradient moves poleward and equatorward. However, the lesser amplitudes of the centers of action in the SVD analysis compared to the EOF analyses and the statistics listed in Table 2.2 indicate that coupling between Ns FQ and SST is not as strong as the coupling between MSC amount and SST. SVD analysis between MSC amount and Ns FQ (the patterns are not shown, but the statistics are listed in Table 2.2) confirms that increased MSC amount occurs with increased Ns FQ in the gradient region. The MSC–Ns patterns resemble their respective EOFs.

2.5 Large scale interaction with atmospheric circulation

One shortcoming of NL was the lack of an explicit examination of the role of atmospheric circulation in cloud–SST interaction. Klein et al. (1995) found that cold advection was more frequent during years with greater low cloud amount over the eastern subtropical North Pacific, while NL hypothesized that increased MSC amount in the midlatitude North Pacific was associated with stronger warm advection over the SST gradient region resulting from anomalously cold water. Moreover, the fact that Ns as well as MSC is correlated with SST indicates that synoptic activity may have a significant influence on MSC variability. Therefore, it is important to specifically investigate how interannual variability in MSC over the midlatitude ocean during summer is related to changes in large-scale seasonal-mean atmospheric circulation and synoptic activity.

The simplest measure for seasonal-mean atmospheric circulation is the distribution of seasonal-mean SLP. Figure 2.7 shows the climatological distribution of SLP during summer, the leading EOF of interannual variability in SLP, and the normalized time series corresponding to the leading EOF. Table 2.1 documents the percentage of total

variance explained by the first and second EOFs. The dominant pattern of interannual variability represented by the leading EOF is a strengthening or weakening of the poleward portion of the subtropical anticyclone with a weak secondary center of action in the western North Pacific. This is consistent with the results of NZW for the leading EOF of COADS SLP north of 18°N. COADS SLP is only semi-independent from the Trenberth SLP used in the present study because the original SLP reports that were averaged into COADS were presumably also assimilated into the daily operational analyses from which the Trenberth SLP data were obtained. However, the Trenberth SLP are less noisy than COADS SLP in regions with low sampling density. It should be noted that the interannual variability in seasonal-mean circulation represented by Fig. 2.7 is much weaker than that observed during winter.

Figure 2.8 shows the patterns associated with the leading SVD mode of MSC amount and SLP during summer, which generally resemble their respective EOFs shown in Figs. 2.2 and 2.7. Consistent with the results of Klein et al. (1995) and NZW, decreased MSC amount in the eastern subtropical North Pacific is associated with a weakening of the seasonal-mean subtropical anticyclone and a corresponding reduction of cold advection. MSC amount increases on the western flank of the subtropical anticyclone all the way across the North Pacific along the MSC and SST gradient region. This indicates increased seasonal-mean MSC amount along the MSC and SST gradient region is associated with decreased seasonal-mean southerly flow, which, in the absence of a change in SST, would produce weaker seasonal mean warm advection. However, NZW show that the SLP pattern in Figs. 2.7 and 2.8 tends to be associated with a pattern resembling that of the leading EOF of SST, with decreased SST along the gradient region (although not shown, similar results were obtained by this study). Hence, it is difficult to separate the effect of weaker seasonal-mean warm advection due to reduced southerly flow from the effect of stronger seasonal-mean warm advection due to colder SST. However, the weaker coupling between MSC amount and SLP, as evidenced by the relatively low amplitudes of the centers of action in the SVD analysis and the low value of r (Table 2.2), suggests that seasonal-mean atmospheric circulation plays a lesser role than

SST in forcing interannual variability in cloudiness. This is also the case for Ns FQ, which exhibits a very weak equatorward shift in storm track associated with very weak seasonal-mean northerly flow over the central North Pacific poleward of 40°N (not shown). The associated statistics listed in Table 2.2 indicate the coupling between Ns FQ and SLP during summer is weak.

It is likely that coupling between MSC amount, Ns FQ, and seasonal-mean circulation is weak because seasonal-mean circulation poorly represents day-to-day flow. For example, enhanced southerly flow ahead of and northerly flow behind an extratropical cyclone are likely to be important contributors to cloud variability even though they largely average out over the long term. Therefore, the variance in meridional wind over the summer season (VV) may be more relevant than the seasonal-mean meridional wind in determining MSC and Ns anomalies. Figure 2.9 shows the climatological distribution of VV during summer, the leading EOF of interannual variability in VV, and the normalized time series corresponding to the leading EOF. Table 2.1 documents the percentage of total variance explained by the first and second EOFs. The climatology displays a clear storm track across the North Pacific, but the EOF pattern is more difficult to interpret. In contrast to the other fields, the EOF of VV has practically the same sign over the entire basin and somewhat resembles the mean field, suggesting that a significant part of the observed interannual variability results from a uniform relative increase or decrease of the mean distribution. This feature is suspicious because a bias proportional to the magnitude of VV would exhibit similar behavior. In fact, data from 1987 were excluded from the EOF analysis because values of VV were unrealistically high over a large part of the domain. The time series associated with the leading EOF of VV also does not exhibit an upward trend as might be expected from the trend in the time series associated with the leading EOF of Ns FQ. Furthermore, the results of Lambert (1996) suggest that more intense synoptic activity might be expected to be associated with the trend of decreasing SST in the central North Pacific, and the decreases in 500-mb geopotential height over the summertime midlatitude North Pacific documented by Reiter and Westhoff (1982) between 1951–1978 and Shabbar et al.

(1990) between 1946–1985 suggest an equatorward shift in the storm track.

Because the VV dataset was calculated from daily operational SLP analyses, it is quite possible that spurious variability can be introduced by changes in the analysis procedure or assimilation of SLP reports (e.g. Trenberth and Paolino 1980); however, the specific cause of the apparent problem with 1987 data is not clear. In order to better assess the possibility of spurious variability in the VV dataset, VV during JJA was calculated from daily wind observations reported at 12 UTC for several Ocean Weather Stations (OWS) (locations displayed in Fig. 3.1) and correlated with SLP-derived VV from the closest grid box (or grid boxes if the OWS was located near the border between two). The results are listed in Table 2.3. For comparison note that Ronca (1995) found only a 66% correlation between daily wind speed anomalies measured at OWS N and calculated from SLP analyses. Since the OWS observations were presumably assimilated into the operational SLP analyses used to calculate the VV dataset, the fact that correlations of VV are not very high suggests that spurious interannual variability is present in the VV dataset. Furthermore, substantial noise will result from the lack of sampling at daily timescales over the ocean, particularly during the earlier part of the record. The EOF analysis was repeated on VV one-year difference fields, and the resulting pattern was almost identical to that for the un-differenced data (not shown). This indicates that real variability in VV, or possible biases in VV which obscure real variability, is dominated by frequencies with periods of a few years or less.

Although possible biases and noise may obscure a real signal in the EOF analysis, better results may be obtained with SVD analysis if the biases and noise in VV are uncorrelated with variability in the other field. Figure 2.10 shows the patterns associated with the leading SVD mode of Ns FQ and VV during summer (excluding data from 1987). Although the Ns FQ pattern resembles its EOF, that is definitely not the case for the VV pattern. Instead, bands of increased and decreased VV occur across the North Pacific, generally co-located with increased and decreased Ns FQ. However, the fraction of squared covariance explained by the leading mode of coupled Ns–VV variability is quite small (Table 2.2), probably the result of substantial noise and spurious variability. The

value of *r* (Table 2.2) may also be underestimated for this reason. Nevertheless, Ns FQ is better-coupled with the frequency of synoptic activity, as inferred from VV, than with the seasonal-mean circulation. The leading patterns resulting from SVD analysis on MSC amount and VV fields (not shown, but the associated statistics are listed in Table 2.2) are more noisy, but indicate that increased MSC amount along the gradient region tends to occur with bands of increased and decreased VV with some resemblance to those displayed in Fig. 2.10.

In order to more directly test the hypothesis of NL that the summertime storm track shifts poleward and equatorward as the region of strong SST gradient shifts poleward and equatorward, SVD analysis was conducted on VV and SST fields (excluding data from 1987); the results are displayed in Fig. 2.11. Colder water along the gradient region, representing an equatorward shift in the region of strongest SST gradient is associated with a poleward band of decreased VV and equatorward band of slightly increased VV. This suggests surface low centers tend to cross the North Pacific farther south during summers with anomalously low SST. The studies of Blender (1997), Rogers (1997), and Serreze et al. (1997) indicate that cyclones over the North Atlantic during winter travel in a more zonal rather than northeastward direction when the subtropical anticyclone is relatively weak. SVD analysis conducted on VV and SLP fields (not shown, but the associated statistics are listed in Table 2.2) over the North Pacific during summer produces patterns that appear to have little physical relationship except that the VV pattern generally has positive sign and SLP pattern negative sign over the basin. This and the low values for VV–SLP coupling listed in Table 2.2 suggest that the frequency and distribution of synoptic activity during the summer season is only very weakly reflected in the seasonal-mean circulation. It is possible that stronger results could be obtained for EOF and SVD analyses using VV from the NCEP/NCAR Reanalysis Project (Kalnay et al. 1996) when it becomes available, since it applies a recent analysis procedure uniformly over the period of record.

2.6 A preliminary look at radiative forcing of sea surface temperature

Although it is difficult to determine surface net CRF from data based on synoptic surface cloud observations, NL estimate that net downward surface radiation is reduced by 1 W m^{-2} for every 1% increase in MSC amount (a comparison of the top panels of Figs. 1.1 and 2.2 also suggests this number is of the right magnitude). Thus, the typical anomaly in MSC amount associated with a typical anomaly in SST changes surface net CRF by about 3 W m^{-2}. Assuming every other process affecting SST remained unchanged, the SST anomaly, ΔSST, produced by a radiative anomaly, ΔCRF, can be estimated using the following equation,

$$\Delta \mathrm{SST} \approx \frac{\Delta t \Delta \mathrm{CRF}}{\rho_w c d} \tag{2.1}$$

where ρ_w and c are the density and specific heat of liquid water, d is the depth of the oceanic mixed layer, and Δt is the time period over which the radiative anomaly acts. Equation 2.1 assumes that all incident radiation is absorbed by the oceanic mixed layer, but about 6% of the incident SW radiation will be reflected (Payne 1972) and another 5-10% may penetrate beneath the oceanic mixed layer (Ohlmann et al. 1996).

For a typical summertime oceanic mixed-layer depth of 25 m in the SST gradient region (Bathen 1972; Deser et al. 1996), a decrease in surface downward radiation equal to 3 W m^{-2} associated with a 3% increase in MSC amount would produce a –0.2°C change in SST over the summer season, which is less than half the magnitude of observed typical SST anomalies. Ronca and Battisti (1997) show that variability in latent heat flux plays a stronger role than variability in surface SW radiative flux in changing SST at Ocean Weather Station N in the eastern subtropical North Pacific; therefore, the role of latent heat flux should not be ignored at midlatitudes. Because latent heat flux tends to be negatively correlated with MSC amount over the midlatitude ocean (NL), the decrease in SST is probably less than that estimated above.

Surface net CRF may be stronger when Ns and associated non-precipitating midlevel clouds occur, although the 1 W m^{-2} for every 1% change in MSC amount estimation described in the previous paragraph assumes the observed SW CRF is due to

solely to MSC (NL) and thereby already implicitly includes contributions from overlapping midlevel cloudiness. Nonetheless, even assuming that additional midlevel cloudiness increases surface net CRF to the large value of 1.5 W m^{-2} for every 1% change in overlapping MSC–midlevel amount, the magnitude of the resulting radiatively-forced SST anomalies would only increase from 0.2°C to 0.3°C. Since typical SST anomalies associated with MSC anomalies have a magnitude of 0.5°C (Fig. 2.4), a large part of the observed SST variability must result from processes other than radiative forcing by changes in MSC amount. The impact of radiative forcing on SST due to variability in MSC amount will be examined in more detail in Section 5.5.

Radiative forcing of SST can also be produced by changes in MSC optical thickness, but this cannot be directly evaluated using surface observations. Instead, the change in MSC optical thickness required to produce a radiative forcing equivalent to that of a typical anomaly in MSC amount will be estimated. The transmittance, t, through a purely scattering medium can be related to the optical thickness, τ, by the following equation (S. Warren, class notes to ATMS 534),

$$t \approx \frac{1}{1 + (1 - g)\tau} \tag{2.2}$$

where g is the asymmetry factor. Assuming a daily average summertime insolation equal to 450 W m^{-2} (Hartmann 1994), a clear-sky transmittance equal to 0.75 (Wallace and Hobbs 1977), an asymmetry factor equal to 0.87 (Slingo and Schrecker 1982), and typical MSC optical thicknesses equal to 10–30 (Nakajima et al. 1991), a 3 W m^{-2} decrease in transmitted SW radiation would be produced by an optical thickness increase equal to 0.4 at $\tau = 10$ and 1.7 at $\tau = 30$. Typical satellite calibration errors in ISCCP cloud optical thickness averaged between 50°S–50°N are on the order of 1 (Klein and Hartmann 1993a). Thus, it appears that it is not possible at this time to determine whether significant interannual variability in MSC optical thickness has occurred. However, Klein and Hartmann (1993b) conclude that it is unlikely that CRF resulting from variability in MSC optical thickness is greater than CRF resulting from variability in MSC amount.

2.7 Summary and conclusions

This chapter extends the local-correlation study of NL by examining coupled large-scale patterns of MSC amount, Ns FQ, and SST over the midlatitude North Pacific during summer using EOF and SVD analysis. An improved cloud dataset is used, which provides a longer period of record and higher spatial resolution than was available with the previous W88 dataset. Moreover, the original individual synoptic surface cloud reports were averaged into the gridded data using a revised procedure which largely eliminates biases associated with variations in spatial sampling over time. An important extension to the previous study of NL is an explicit examination of the influence of seasonal-mean circulation and synoptic activity on cloud variability. SLP is used to infer the seasonal-mean circulation, and the seasonal variance of meridional wind is used to infer the frequency and distribution of synoptic activity.

The greatest interannual variability in MSC amount and SST individually over the North Pacific during summer occurs along the region of strong gradient in MSC amount between about 30–40°N (Fig. 2.2) and SST between about 35–45°N (Fig. 2.3), representing a nearly basin-wide meridional shift of the boundary between extensive MSC and cold water at midlatitudes and little MSC and warm water in the subtropics. SVD analysis (Fig. 2.4), indicates that interannual variations in MSC amount are closely related to variations in SST during summer. Increased (decreased) MSC amount occurs with decreased (increased) SST along the gradient region. The greatest interannual variability in Ns FQ in the central North Pacific during summer also occurs along the SST gradient region (Fig. 2.5), although both the climatology and variability of Ns FQ have a slight southwest-to-northeast rather than zonal orientation. Increased Ns FQ along the Ns gradient region is associated with a decreased Ns FQ to the northwest. The pattern associated with coupled Ns–SST variability (Fig. 2.6) is similar to the EOF patterns, indicating that interannual variations in Ns FQ tend to be related to variations in SST during summer. Increased Ns FQ in the vicinity of the SST gradient region and decreased Ns FQ to the northwest occurs with decreased SST along the SST gradient region. However, Ns–SST coupling is not nearly as strong as MSC–SST coupling (Table 2.2).

Since estimated radiative forcing by changes in MSC amount is too small to account for the observed SST anomalies, a large part of the observed coupling between MSC and SST must result from SST variability forcing MSC variability. In this case, what is the origin of the observed SST anomalies? Surface latent and sensible heat flux and oceanic dynamical processes also have a role in producing SST anomalies (e.g. Ronca and Battisti 1997), but the results of Zhang et al. (1997) indicate that persistence from the preceding winter is an important contributor to summertime SST anomalies over the midlatitude North Pacific. The role of persistence is examined in Fig. 2.12, which displays monthly-mean SST along the gradient region averaged from the ten coldest JJA seasons and ten warmest JJA seasons from the time series associated with the leading EOF of SST over the midlatitude North Pacific (Fig. 2.3), along with the 39-year climatology. The bottom panel of Fig. 2.12 shows that half the magnitude of an anomaly during JJA can be attributed to persistence of an anomaly from the previous winter. It is also interesting to note that the composite cold and warm anomalies are behind or ahead of the climatological seasonal cycle by only 1–2 weeks.

Although MSC amount, Ns FQ, and SST are weakly coupled with seasonal-mean SLP over the North Pacific during summer (Fig. 2.8), the associated seasonal-mean circulation anomalies are only 0.1–0.3 m s^{-1}. This suggests that day-to-day variations in atmospheric flow produced by synoptic activity have a greater influence on cloud variability. Examination of the variance in meridional wind over each summer season, used to infer the strength of synoptic activity, shows similar patterns are associated with coupled Ns–VV variability (Fig. 2.10). Increased Ns FQ and increased VV occur along the Ns gradient region and decreased Ns FQ and decreased VV occur to the northwest, and vice versa. Although the coupling between Ns–VV coupling is not as strong as Ns–SST coupling, this may simply be a result of excess noise and spurious variability in the VV dataset. Since Ns results from synoptic activity, it is possible that with a better dataset, Ns would be more closely coupled to VV than SST. Analysis of VV–SST coupling shows the same general patterns for VV and SST (Fig. 2.11) as were previously seen for Ns FQ and SST. Increased (decreased) VV in the vicinity of the SST gradient

region and decreased (increased) VV to the northwest is associated with decreased (increased) SST along the SST gradient region, indicating that the summertime storm track occurs equatorward of its climatological position when water is colder along the SST gradient region, and poleward when water is warmer.

The weak relationship between interannual variability in seasonal-mean SLP and MSC and the strong relationship between interannual variability in Ns and MSC indicates it is not sufficient to examine seasonal-mean variability to understand processes influencing MSC. Previous studies have approached coupled cloud–SST variability from the standpoint of surface radiative forcing (e.g. Oreopoulos and Davies 1993) or static stability and local MBL processes (Klein and Hartmann 1993b). However, the connection between synoptic activity and cloud variability suggests it is essential to consider advection as well. A similar situation exists between synoptic activity and latent and sensible heat fluxes, which can vary substantially with the sign and magnitude of advection.

Although the role of cold advection in producing interannual variability in low cloud amount over the eastern subtropical North Pacific was examined by Klein et al. (1995), the situation over the midlatitude North Pacific is more complicated since both warm and cold advection occur in that region, and changes in advection occur on smaller timescales. In this case, it will be necessary to use more specific categories of low stratiform cloudiness than MSC. Stratocumulus, stratus, and sky-obscuring fog all contribute to MSC, but often occur with different advective and synoptic situations. Because the relative contribution of each cloud type to variability in MSC amount is not clear, the specific processes by which SST and synoptic activity produce variability in MSC are not clear. Therefore, interannual variability in each cloud type must be examined while taking into account day-to-day changes in advection; from this, the processes responsible for variability in MSC amount can be inferred. However, it will be necessary to first establish relationships between low cloud type, MBL structure, and advection, since these have not been previously documented.

Table 2.1: Percentage of total variance explained by the first and second EOFs.*

Parameter	EOF 1	EOF 2
MSC amount	22.9	16.2
SST	26.7	18.7
Ns FQ	17.6	13.3
SLP	35.9	18.4
VV	23.1	14.7

* Every leading EOF is well-separated from the second EOF according to the criterion of North et al. (1982).

Table 2.2: Summary statistics for the SVD analyses (in percent).

Left field	Right field	SCF	NC	r	Variance explained	r_{PC}
MSC amount	SST	53.4	16.0	84.3	15.9/17.5	66.0
Ns FQ	SST	52.6	15.7	77.1	9.8/15.1	65.3
MSC amount	Ns FQ	58.1	17.0	84.7	15.8/11.5	71.7
MSC amount	SLP	55.1	16.1	67.0	8.3/14.0	38.4
SST	SLP	55.4	16.5	65.4	9.5/12.2	32.4
Ns FQ	SLP	44.2	12.8	69.0	5.2/15.2	25.9
Ns FQ	VV	27.9	9.5	73.0	7.4/6.9	7.5
MSC amount	VV	31.2	9.4	63.3	7.3/5.1	12.7
VV	SST	39.9	10.7	68.6	5.3/10.8	–1.6
VV	SLP	39.7	12.9	62.7	5.0/13.7	21.3

SCF = squared covariance fraction

NC = normalized root-mean-squared covariance (defined in Zhang et al. 1997)

r = correlation coefficient between left and right SVD expansion coefficient time series

Variance explained = variance explained by the first SVD mode of the left/ right field as a percentage of total variance of the left/right field

r_{PC} = correlation coefficient between the EOF time series (PCs) of the left and right fields

Table 2.3: Local correlations between VV from Ocean Weather Stations (OWS) and VV from SLP analyses (in percent).

OWS B	OWS C	OWS N	OWS P	OWS V
25.8	34.4	–4.2	68.0	40.1

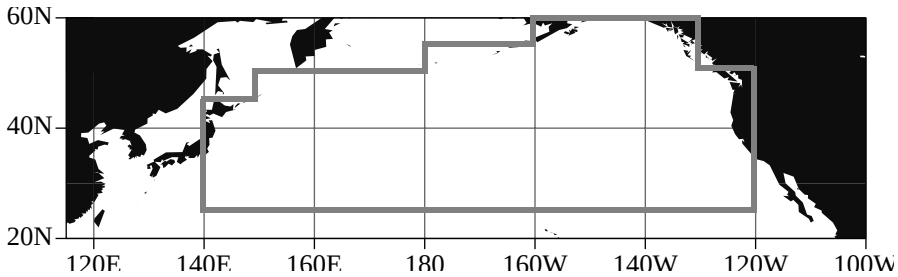

Figure 2.1: Domain used for EOF and SVD analyses.

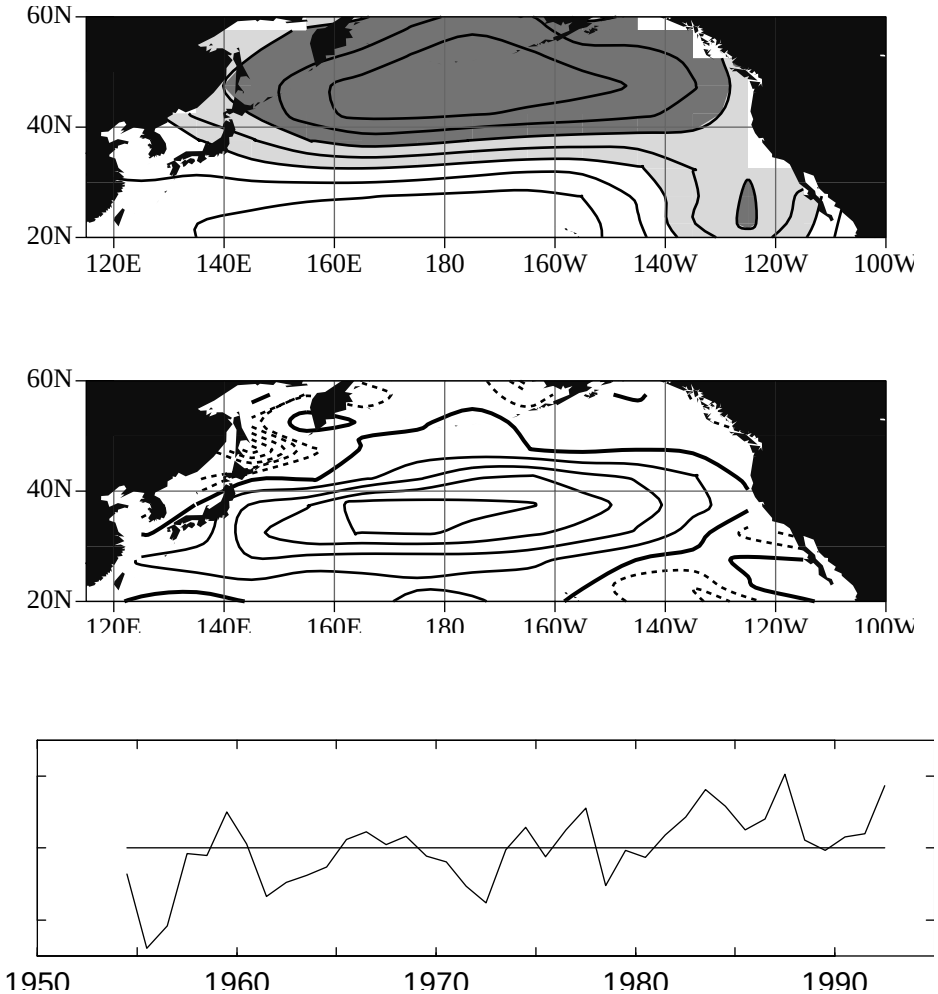

Figure 2.2: (Top) Climatological daytime MSC amount during JJA. Contour interval is 10%; thresholds for lighter (darker) shading are 40% (60%). (Middle) Leading EOF of seasonal-mean daytime MSC amount during JJA. Contour interval 1%; the zero contour is thickened and negative contours are dashed. (Bottom) Normalized time series corresponding to the leading EOF. One tick mark represents two standard deviations. Summary statistics are presented in Table 2.1.

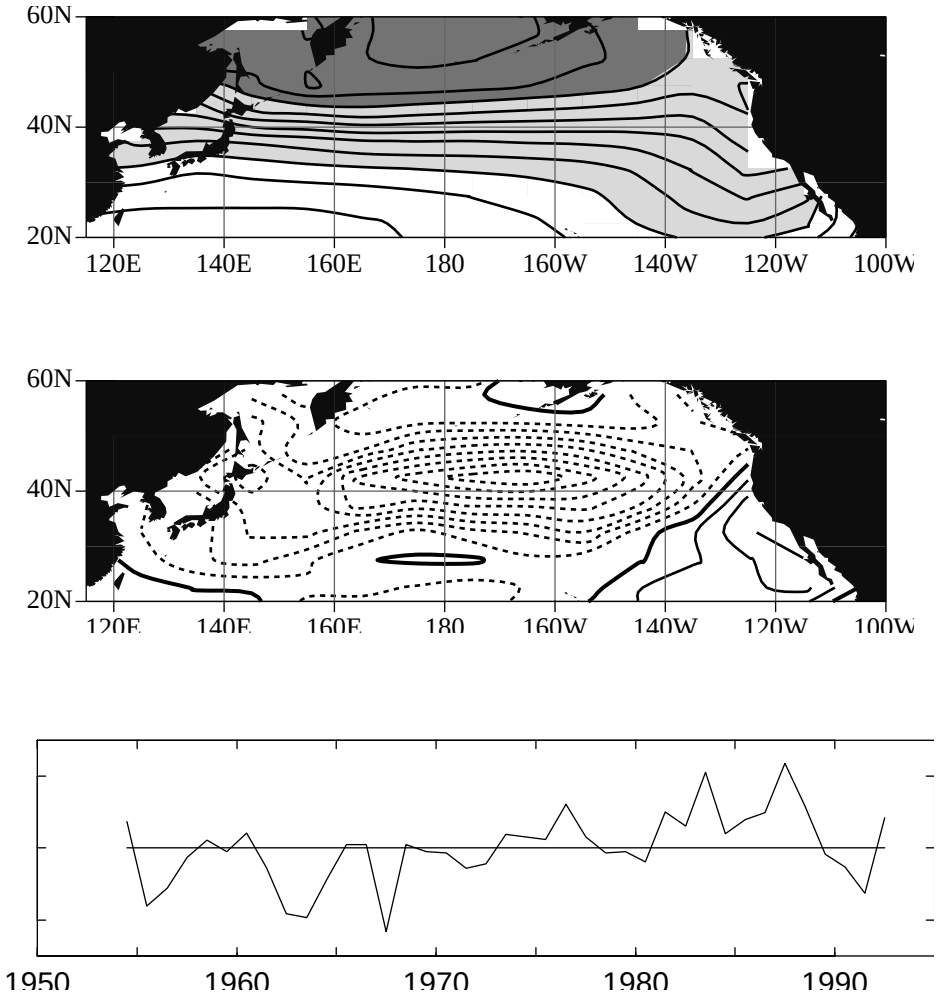

Figure 2.3: (Top) Climatological SST during JJA. Contour interval is 2°C; thresholds for lighter (darker) shading are 24°C (12°C). (Middle) Leading EOF of seasonal-mean SST during JJA. Contour interval 0.1°C; the zero contour is thickened and negative contours are dashed. (Bottom) Normalized time series corresponding to the leading EOF. One tick mark represents two standard deviations. Summary statistics are presented in Table 2.1.

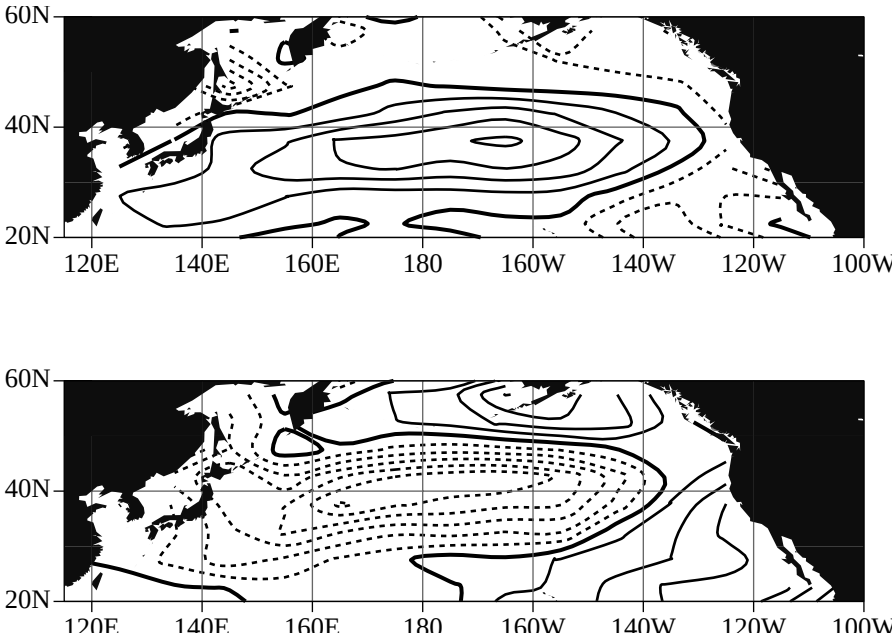

Figure 2.4: Leading SVD mode for seasonal-mean (top) daytime MSC amount paired with (bottom) SST during JJA. Contour intervals are 1% and 0.1°C; the zero contour is thickened and negative contours are dashed. Summary statistics are presented in Table 2.2.

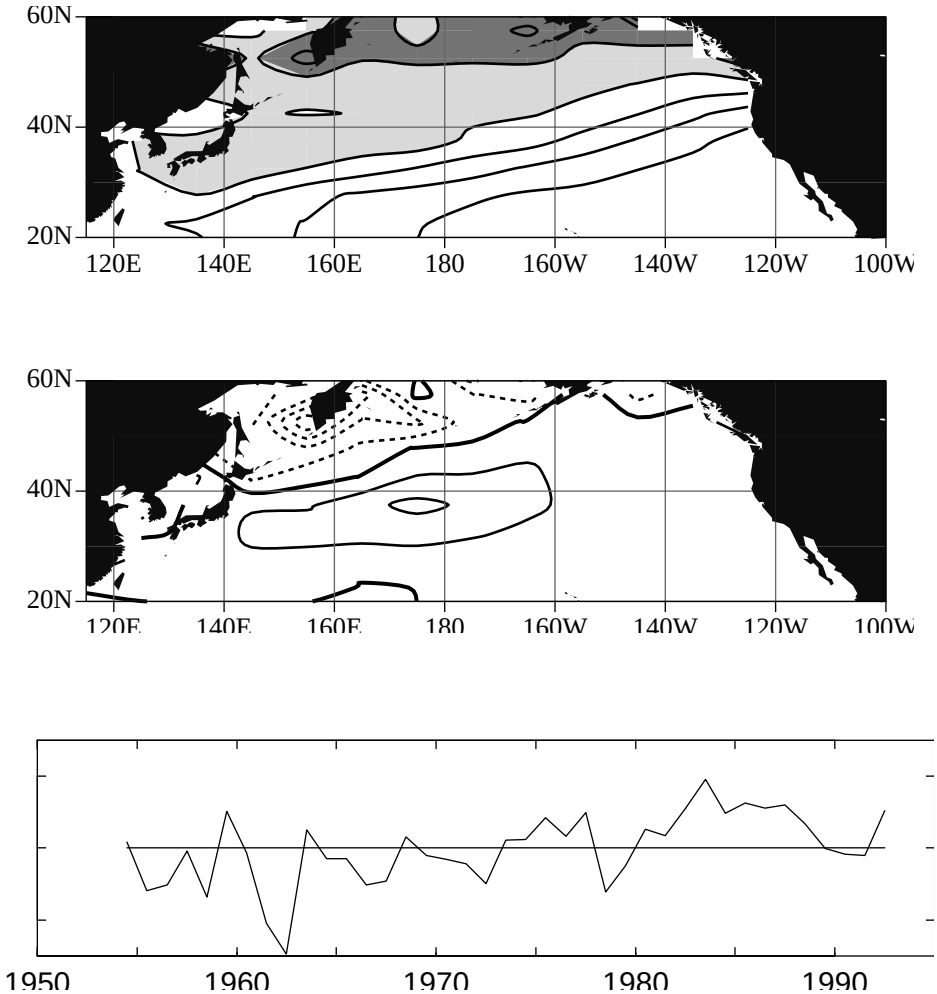

Figure 2.5: (Top) Climatological daytime Ns FQ during JJA. Contour interval is 1%; thresholds for lighter (darker) shading are 4% (5%). (Middle) Leading EOF of seasonal-mean daytime Ns FQ during JJA. Contour interval 0.5%; the zero contour is thickened and negative contours are dashed. (Bottom) Normalized time series corresponding to the leading EOF. One tick mark represents two standard deviations. Summary statistics are presented in Table 2.1.

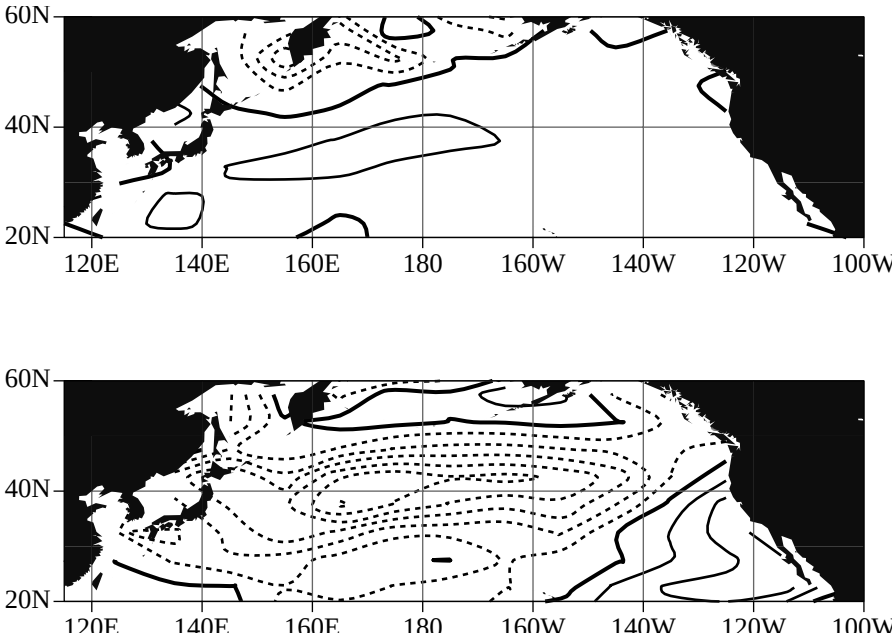

Figure 2.6: Leading SVD mode for seasonal-mean (top) daytime Ns FQ paired with (bottom) SST during JJA. Contour intervals are 0.5% and 0.1°C; the zero contour is thickened and negative contours are dashed. Summary statistics are presented in Table 2.2.

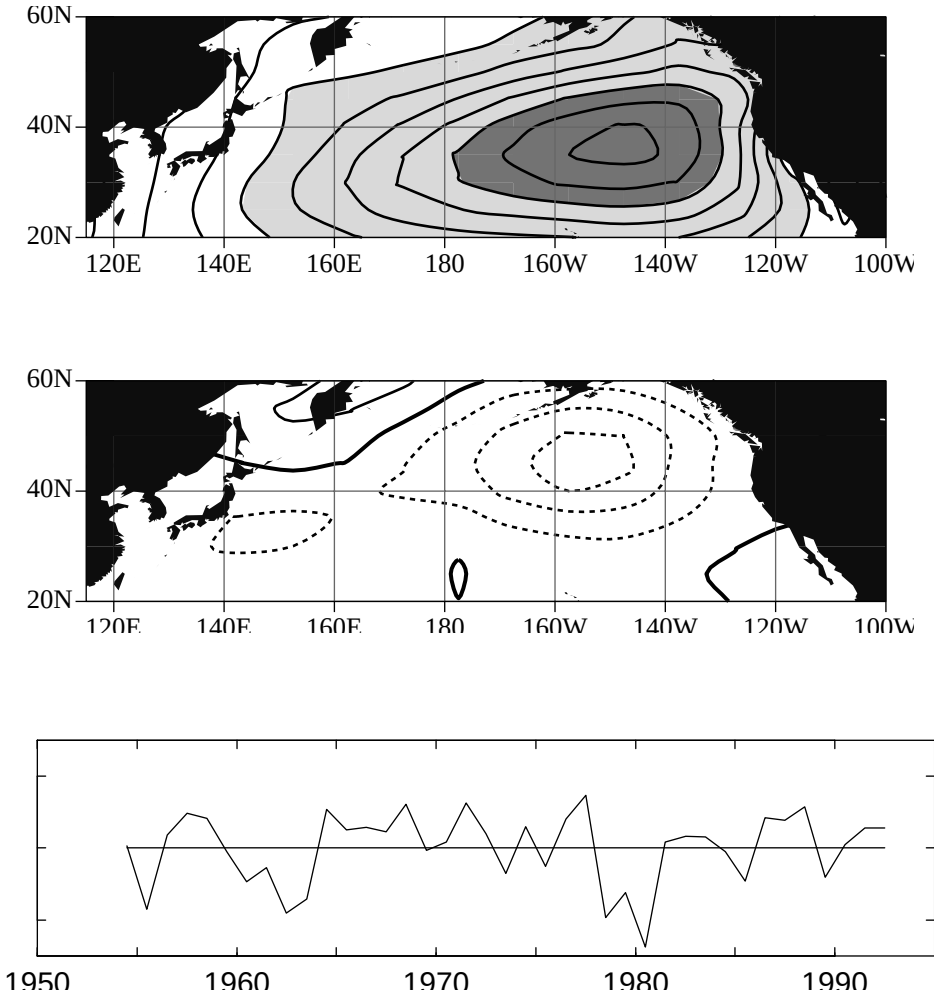

Figure 2.7: (Top) Climatological SLP during JJA. Contour interval is 2 mb; thresholds for lighter (darker) shading are 1012 mb (1020 mb). (Middle) Leading EOF of seasonal-mean SLP during JJA. Contour interval 0.5 mb; the zero contour is thickened and negative contours are dashed. (Bottom) Normalized time series corresponding to the leading EOF. One tick mark represents two standard deviations. Summary statistics are presented in Table 2.1.

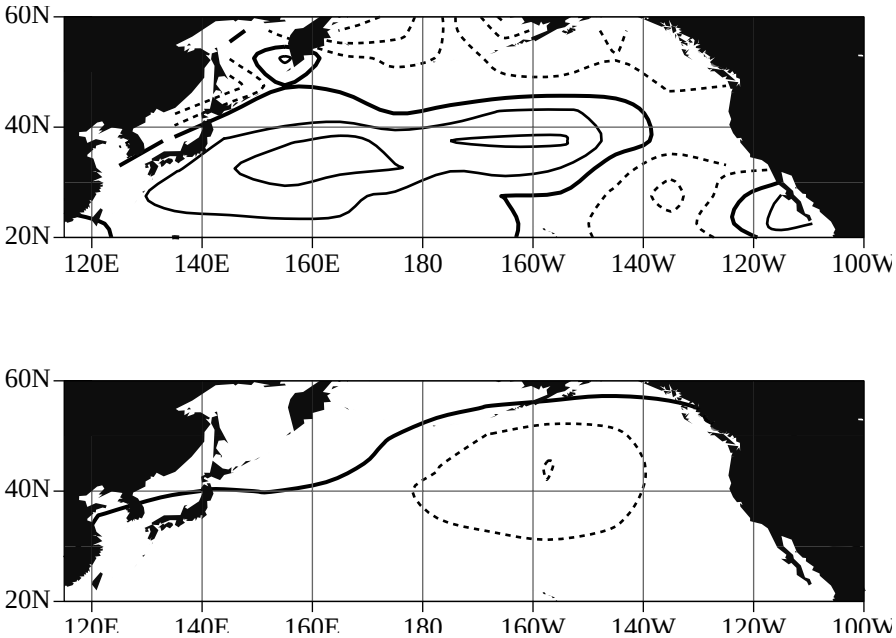

Figure 2.8: Leading SVD mode for seasonal-mean (top) daytime MSC amount paired with (bottom) SLP during JJA. Contour intervals are 1% and 0.5 mb; the zero contour is thickened and negative contours are dashed. Summary statistics are presented in Table 2.2.

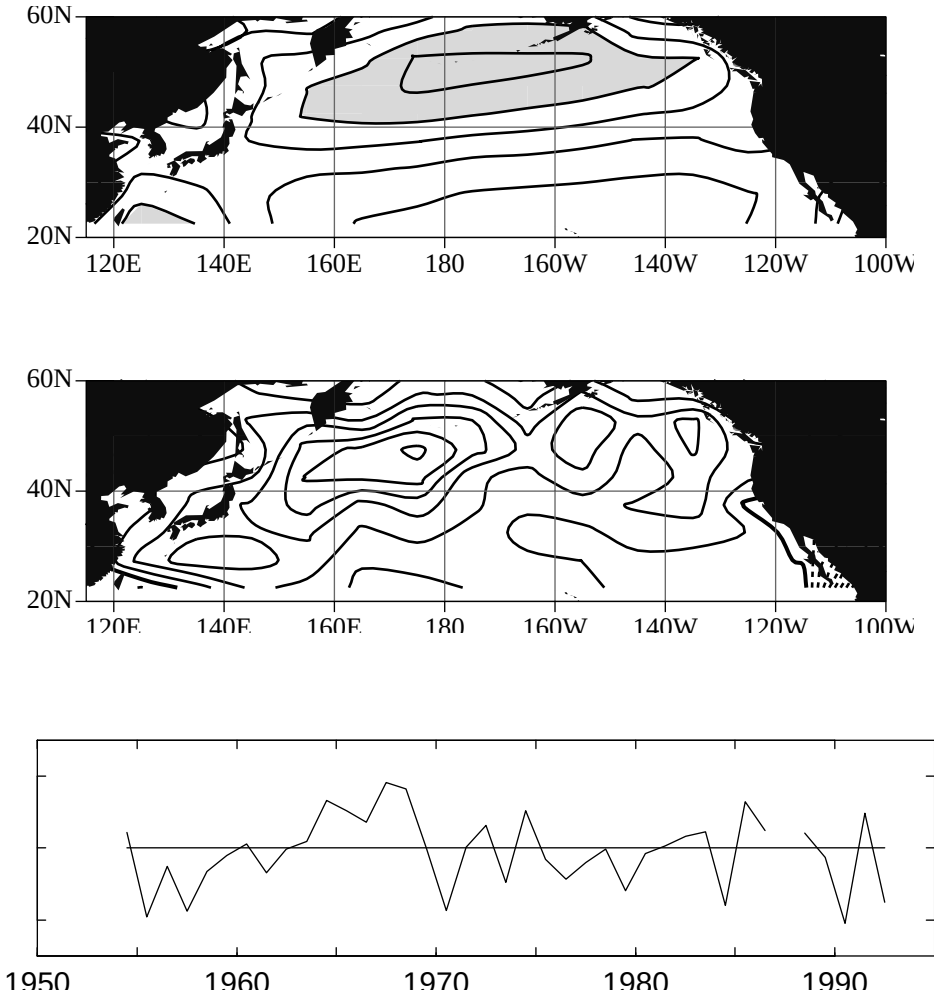

Figure 2.9: (Top) Climatological VV during JJA. Contour interval is 10 $m^2\ s^{-2}$; threshold for shading is 40 $m^2\ s^{-2}$. (Middle) Leading EOF of seasonal-mean VV during JJA. Contour interval 1 $m^2\ s^{-2}$; the zero contour is thickened and negative contours are dashed. (Bottom) Normalized time series corresponding to the leading EOF. One tick mark represents two standard deviations. Summary statistics are presented in Table 2.1.

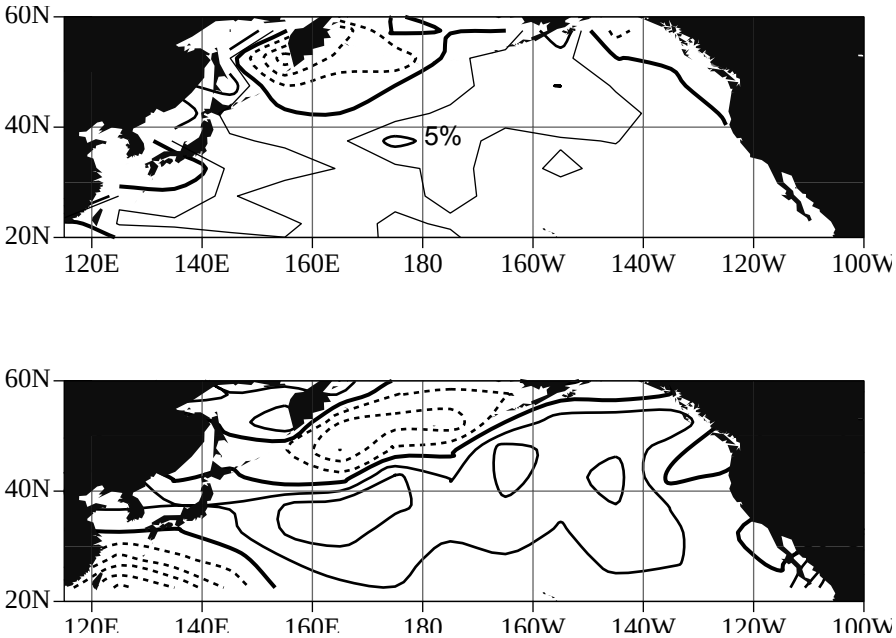

Figure 2.10: Leading SVD mode for seasonal-mean (top) daytime Ns FQ paired with (bottom) VV during JJA. Contour intervals are 0.5% and 1 m^2 s^{-2}; the zero contour is thickened and negative contours are dashed. A thin contour has been added for 0.25% Ns FQ. Summary statistics are presented in Table 2.2.

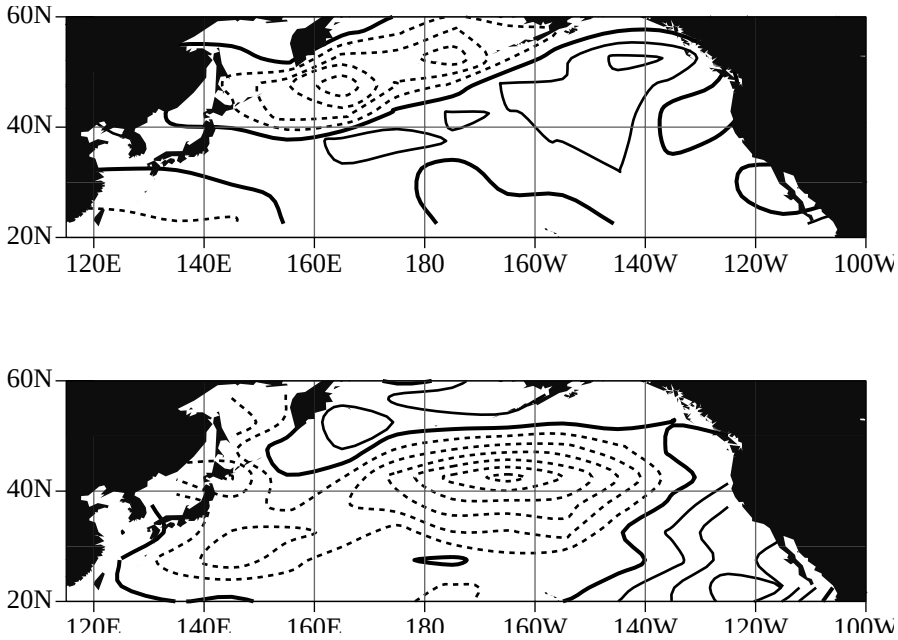

Figure 2.11: Leading SVD mode for seasonal-mean (top) VV paired with (bottom) SST during JJA. Contour intervals are 1 m^2 s^{-2} and 0.1°C; the zero contour is thickened and negative contours are dashed. Summary statistics are presented in Table 2.2.

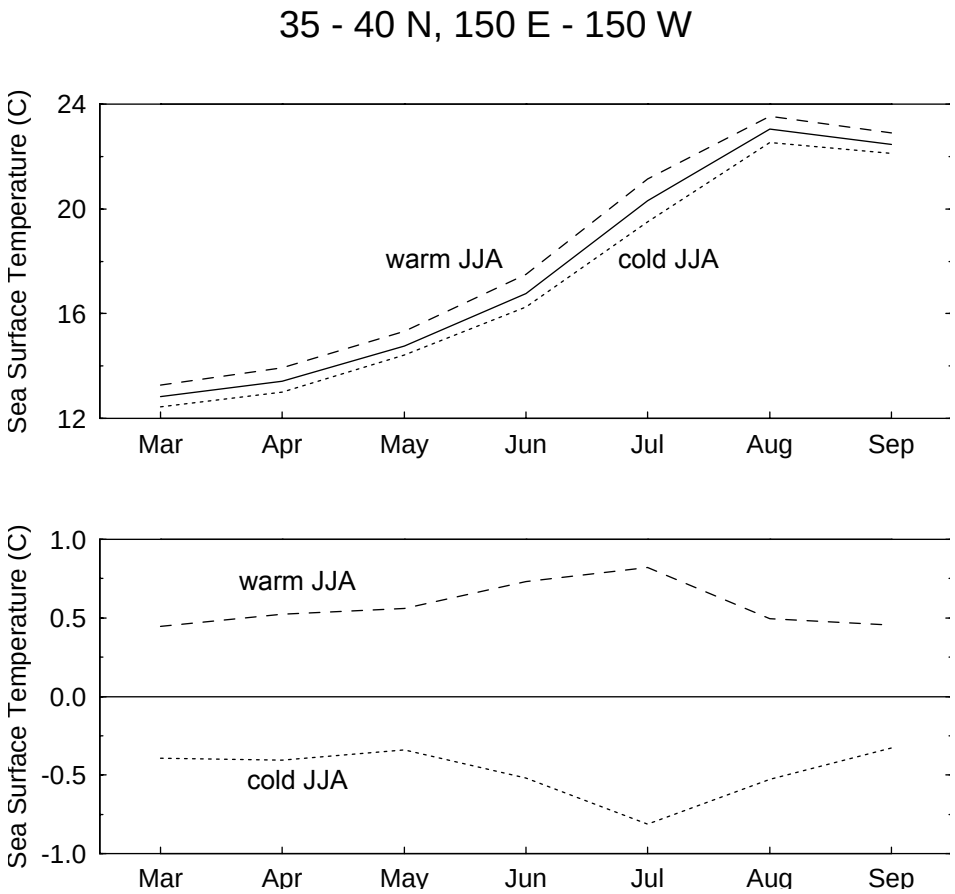

Figure 2.12: (a) Monthly mean SST averaged between 35–40°N, 150°E–150°W for the 39-year climatology (solid), the ten coldest JJA seasons (dotted) and the ten warmest JJA seasons (dashed) from the time series in Fig. 2.3. (b) Monthly difference between the cold-JJA composite and the climatology (dotted) and the warm-JJA composite and the climatology (dashed).

CHAPTER 3

Relationships between Low Cloud Type, Inferred Advection, and the Vertical Distribution of Temperature and Moisture

3.1 Introduction

The previous chapter examined large-scale interannual co-variability between MSC amount, Ns FQ, SST, and atmospheric circulation over the midlatitude North Pacific during summer. In the region of strong cloud and SST gradient across the North Pacific, increased (decreased) MSC amount and Ns FQ were found to occur with decreased (increased) SST and an equatorward (poleward) shift in the storm track. The magnitude of SST anomalies estimated to result from radiative forcing by the observed MSC anomalies was found to be substantially less than that of the observed SST anomalies. This suggested the observed relationship between MSC amount and SST during summer primarily results from SST forcing MSC. However, the processes by which variability in SST produces variability in MSC are unclear. Although, until recently, previous studies have considered cloud–SST variability from a static point of view, the presence of frequent synoptic activity at midlatitudes, even during summer, indicates that it is essential to sort out how advection influences cloudiness. The MSC category comprises stratocumulus, stratus, and sky-obscuring fog, but each of these typically occurs under different advective and synoptic conditions. Therefore, in order to understand variability in MSC, it is necessary to examine the specific processes which are responsible for producing variability in each low stratiform cloud type.

Factors controlling the amount and optical thickness of low cloudiness, particularly that over the midlatitude ocean, are not completely understood. Field experiments such as the First ISCCP Regional Experiment (FIRE) (Albrecht et al. 1988) and the Atlantic Stratocumulus Transition Experiment (ASTEX) (Albrecht et al. 1995a) have been conducted to investigate how MBL processes and the large-scale environment influence

cloud properties and the transition between stratocumulus and trade cumulus cloud regimes in the eastern subtropical ocean. Although these and similar projects have produced a wealth of detailed information on the radiative and microphysical properties of clouds and the dynamical and thermodynamical properties of the MBL, the data exist only for short periods of time at a few locations and focus on the subtropical ocean. Since the basic meteorological conditions associated with the occurrence of specific low stratiform cloud types over the midlatitude ocean are not well-documented, this chapter establishes representative MBL structure and surface meteorological conditions associated with various low cloud types using coincident soundings and surface observations from several Ocean Weather Stations (OWS).

3.2 Ocean Weather Station surface observations and soundings

The OWS data were obtained from the National Climatic Data Center (NCDC) in Asheville, North Carolina through S. Klein (now at the European Center for Medium-Range Weather Forecasts (ECMWF), Reading, UK). Most of the OWS operated for several decades until the early 1970's, and synoptic surface meteorological and cloud observations are available every three hours during the time periods listed in Table 3.1. Twice-daily soundings are also available for most of the time that surface observations are available, but prior to July 1970 the soundings were archived at 50 mb resolution, which is insufficient to accurately specify the depth of the MBL or the strength of a capping inversion. For the few remaining years (see Table 3.1) soundings were archived at significant levels (described in WMO 1974) and include data measured at or interpolated to every 50 mb as well.

Figure 3.1 displays the locations of the OWS along with the climatological distribution of summertime SST to provide meteorological context. OWS N was located in the transition region between stratocumulus and trade wind cumulus in the eastern subtropical North Pacific. OWS P was located in the eastern midlatitude North Pacific, but unfortunately only 50 mb resolution soundings are available. OWS V was located on the equatorward side of the SST gradient near the region of large MSC–SST co-variability.

Because no OWS poleward of the SST gradient in the North Pacific had significant-level sounding data, data from OWS B and C in the western and central midlatitude North Atlantic were included in the study. These OWS are poleward of the region of strong SST gradient in the North Atlantic and experience generally similar meteorological conditions to those of the northwestern midlatitude North Pacific.

Surface observers identify cloud type according to the synoptic code (WMO 1975), and Table 3.2 gives non-technical descriptions of each low cloud type (C_L), including no-low-cloud. If more than one cloud type is present, certain cloud types have priority over others in designating the low type code even if they cover only a small fraction of the sky. Descending preferential order of low cloud type identification is C_L = 9, 3, 4, 8, 2. If only C_L = 1, 5, 6, or 7 are present then the low type code is designated by whatever type has the greatest sky cover. If no low cloud is present then C_L = 0. Occasionally it is not possible to observe low cloudiness due to sky-obscuring fog or precipitation; the latter is declared when total cloud cover (N) identifies sky-obscured (N = 9) and when the present weather code (ww) (WMO 1974) identifies fog (ww = 10–12, 40–49) or precipitation (ww = 50–75, 77, 79, 80–99) at the time and location of the observation. The fact that clouds are identified by morphological type means that the low cloud type code provides a qualitative description of the dynamical and thermodynamical environment in which the clouds occur from which specific processes influencing cloud type and cloud amount can be inferred.

Solar heating of the radiosonde hygristor caused daytime relative humidity to be substantially underestimated in the OWS soundings (Teweles 1970; Elliott and Gaffen 1991; Klein 1994). The amount of underestimation varies with cloud cover and solar angle and consequently is impossible to correct in individual soundings. To avoid introducing an unknown humidity bias into the results, daytime soundings and coincident surface observations were excluded from the analysis*. One drawback of this policy is

* June soundings at OWS B were still included in the analysis even though the sun is slightly above the horizon at 0 UTC, but any solar heating should be negligible.

that diurnal cycles in MBL decoupling (Betts 1990; Hignett 1991; Betts et al. 1995) that help drive diurnal cycles in cloud type (Klein et al. 1995; Rozendaal et al. 1995) will not be uniformly sampled. Furthermore, usually more than half of the nighttime cloud observations lack sufficient illumination (Table 3.1). Figure 3.2 shows the climatological FQ of each low cloud type during JJA* at 0 UTC for OWS B and C and at 12 UTC for OWS N, P, and V. These hours are the times of the nighttime sounding and correspond to 2036, 2138, 0240, 0220, and 2256 local time at OWS B, C, N, P, and V, respectively. Frequencies are calculated separately for nights with and without sufficient moonlight or twilight (using the criterion of Hahn et al. 1995), since surface observers sometimes have difficulty identifying clouds on dark nights (Hahn et al. 1995). This is mainly a problem for the detection of middle and high clouds but also affects the identification of low cloud type (Rozendaal et al. 1995), as Fig. 3.2 illustrates.

3.3 Low cloud type compositing procedure

Relationships between low cloud type, surface meteorology, and the vertical distribution of temperature and moisture were examined by compositing significant-level soundings and averaging surface meteorological observations for which the same low cloud type was observed at the time of the sounding. In order to increase the sample size, cloud observations made without sufficient illumination were included if the climatological FQ of the reported cloud type under poor illumination did not exceed the frequency under good illumination at the 80% significance level for that location and season. For example, at OWS N during JJA it is likely that cumulus-under-stratocumulus (C_L 8) is sometimes misidentified as ordinary stratocumulus (C_L 5) under conditions of poor illumination (Fig. 3.2). Therefore, all C_L 8 observations are accepted but poor-illumination C_L 5 observations are rejected. Table 3.1 shows the total number of soundings with coincident surface cloud observations at each location during JJA and also the number with good illumination. A few hundred soundings are available for each OWS

* Norris (1997a) shows December–January–February (DJF) values.

but usually only a fraction have good illumination.

Some cloud types have many soundings contributing; in these cases only the subset for which the cloud type had been persistent three hours before and/or after the time of the sounding was used. This should improve the quality of the results by eliminating cases on the borderline between two cloud types. Additional improvement was obtained by removing a small fraction of soundings (typically 15%) that did not share the MBL structure commonly associated with the given cloud type. Although excluding such ambiguous soundings could bias the results, the practical result of including them is simply added noise, not a change in the basic properties of the composite soundings. Nonetheless, it should be kept in mind that observers occasionally identify a particular cloud type under conditions not represented in the corresponding composite sounding. The number of soundings contributing to the composites at each OWS during each season are recorded in Tables 3.3 and 3.5. These numbers are not large enough for climatological significance, but the composites do show representative vertical distributions of temperature and moisture associated with particular cloud types. Moreover, the OWS soundings used in the composites are sampled from an entire season over a period of several years and thus have a much greater level of independence than those from short-term field projects (e.g. FIRE, ASTEX).

As noted by Albrecht et al. (1995b) and Klein et al. (1995), directly averaging temperature and moisture parameters on a pressure axis will smear out the sharpness of the capping inversion due to fluctuations in MBL height. In order to preserve the temperature and moisture structure at the top of the MBL all soundings were normalized by the height of the MBL prior to averaging. After averaging, the vertical axis of the composite sounding was rescaled to the mean MBL height. In all cases, MBL height was determined by visual inspection of the soundings.

For clouds occurring under capping inversions (stratocumulus and cumulus cloud types at OWS B, C, and N), MBL height was identified as the height of temperature minimum at the base of the inversion. This almost always corresponded closely to the base of the layer in which potential temperature began to increase substantially and both

relative and specific humidity began to decrease substantially. In a few soundings the slope of potential temperature experienced a short decrease immediately above the apparent cloud top, suggesting the occurrence of spurious cooling due to the evaporation of cloud droplets off the radiosonde*; in these cases MBL height was identified as the base of the layer where relative humidity began to decrease substantially. Sky-obscuring fog and no-low-cloud at OWS B and C occur with surface-based inversions; their soundings were normalized by the height of the temperature maximum at the top of this inversion. Fair-weather stratus at OWS B and C typically has a clearly-defined cloud top but often occurs without a clearly-defined capping inversion or stable layer. For this reason fair-weather stratus soundings at OWS B and C were normalized by the height at which relative humidity began to significantly decrease with height. Bad-weather stratus at all locations and cumulus and stratus at OWS V during summer typically did not have MBLs that could be clearly defined by either potential temperature or relative humidity; their soundings were not normalized. Additional information about the vertical distribution and overlap of multiple cloud layers obtained from OWS soundings and surface observations can be found in Wang and Rossow (1995).

Surface observations of low cloud fraction, SST, air-sea temperature difference ($\Delta T \equiv T_{air} - \mathrm{SST}$), wind speed, zonal and meridional wind components, and frequencies of fog and various precipitation types, were averaged for each cloud type over the entire multidecadal time period. The lower tropospheric static stability, $S \equiv \theta(700\ \mathrm{mb}) - \theta(\mathrm{SST,SLP})$, was averaged for each cloud type using the entire sounding data set. However, a slightly different definition of S from that of Klein and Hartmann (1993b) was used where SST is substituted for surface air temperature. Only observations at the time of day of the nighttime sounding made under conditions of sufficient sky illumination were averaged. In order to obtain averages which more strongly distinguish between cloud types, observations were averaged only when the

---

* Superadiabatic decreases in potential temperature were corrected by interpolating temperature between the base of the superadiabatic layer and the nearest level above the superadiabatic layer.

cloud type had been persistent three hours before and after the observation. When less than 40 observations were available, the persistence criterion was relaxed to allow more observations to contribute.

3.4 Low cloud type composites with capping inversions

A temperature inversion almost always caps the MBL over eastern subtropical oceans and frequently caps the MBL over midlatitude oceans, particularly during summer (e.g. Klein and Hartmann 1993b). Both subsidence associated with the subtropical anticyclone and subsidence behind a cold front probably contribute to inversions during summer. Figures 3.3 and 3.4 show composite vertical distributions of water vapor mixing ratio (q), saturation water vapor mixing ratio (q_s),* virtual potential temperature (θ_v), and equivalent potential temperature (θ_e)* for stratocumulus (C_L 5) and cumulus-under-stratocumulus (C_L 8) at OWS B, C, N, and V during JJA. A composite for moderate and large cumulus (C_L 2) is also shown at OWS N, but not at the other OWS. This is because cumulus rarely occurs at OWS B and C during summer and cumulus at OWS V during summer typically occurs without a capping inversion. Stratocumulus cloud types at OWS B, C, and N and cumulus cloud types at OWS N occur without an inversion less than 10% of the time. Although the large-scale environments at the locations displayed in Figs. 3.3 and 3.4 are different, each set of soundings shares common features. The depth of the MBL and the increase in θ_v and decrease in q within the MBL above the surface layer typically increases from stratocumulus to cumulus-under-stratocumulus to cumulus. Similar features are seen at these locations during the winter season (Norris 1997a). The fact that MBL height is slightly larger for stratocumulus than for cumulus-under-stratocumulus at OWS V may simply be due to the small number of soundings contributing to the composite (Table 3.3).

The conceptual model of Bretherton (1992) and Wyant et al. (1997) proposes that a generally well-mixed MBL with stratocumulus becomes increasingly decoupled as it is

---

* Calculated following Bolton (1980).

advected by the trade winds over increasingly warm water. In a decoupled MBL (described by Nicholls 1984) intermittent cumuli carry moisture from the subcloud layer to the cloud layer to maintain the stratocumulus deck (Martin et al. 1995). In a more strongly decoupled MBL, entrainment may evaporate the stratocumulus deck leaving only cumulus in the cloud layer. Inspection of soundings coincident with observations of cumulus-under-stratocumulus and cumulus cloudiness from the ASTEX R/V *Valdivia* (not shown) indicates most of the change in stratification and humidity within the MBL above the surface layer frequently occurs in a single jump near the middle of the MBL, similar to the structure of the trade-wind MBL reported by Augstein et al. (1974). Unfortunately, the OWS significant level soundings lack sufficient resolution to discern a jump in θ_v and q between a decoupled cloud layer and subcloud layer, but the ASTEX soundings suggest that the change in stratification and humidity within the MBL seen at the OWS may often result from decoupling.

Since the best measure of decoupling is probably the decrease in q from subcloud layer to cloud layer (C. Bretherton, personal communication), the parameter $\delta q \equiv q(z/z_i = 0.2) - q(z/z_i = 0.9)$, where z_i is the height of the MBL, is introduced. These are the same locations in the MBL that Albrecht et al. (1995b) chose to sample in the subcloud layer and near the top of the cloud layer. Because the present study focuses on the relative differences in δq between cloud types and not the specific values of δq, the conversion of water vapor to liquid water will not bias the results unless cloud liquid water in the sounding profiles increases with decoupling. This is unlikely to be the case since the stratocumulus deck is expected to be thinner for cumulus-under-stratocumulus than for stratocumulus alone, and only about 10% of the soundings pass through cumulus clouds. Although not shown, similar results are obtained using decoupling parameters based on θ_v and θ_e instead of q.

Figure 3.5 shows average MBL height, δq / q_{SST}, ΔT, and S for stratocumulus, cumulus-under-stratocumulus, and moderate and large cumulus occurring under an inversion for various locations during summer. The lines connect values for each cloud type at a single location. Because a smaller δq could occur in the colder midlatitude MBLs

simply due to the non-linear Clausius-Clapeyron relationship, δq is normalized by the SST saturation water vapor mixing ratio, q_{SST}. Table 3.3 records the means and standard deviations of the data displayed in Fig. 3.5. Although not shown, the distributions of δq often exhibited considerable skewness, with the tail towards greater magnitude. Although the large standard deviations indicate that the cloud types are not well-separated in parameter space, the differences in mean MBL height and δq / q_{SST} between the cloud types at each location are generally significant by a one-tailed *t*-test (Table 3.4). Even if it is assumed that the occasional occurrence of soundings nearby in time reduces the actual number of degrees of freedom to only 75% of the number of soundings, the values in Table 3.4 would be reduced by only 2-3%.

The results from the four OWS collectively suggest that MBL height and normalized δq are significantly less for stratocumulus than for cumulus-under-stratocumulus and significantly less for cumulus-under-stratocumulus than for moderate and large cumulus (Fig. 3.5a and b). Similar results with unknown significance were obtained by Norris (1997a) for composite soundings based on the same cloud types at these locations during the winter season, and by Klein (1997), Betts et al. (1995), and Albrecht et al. (1995b) for composite soundings based on cloud amount at several locations in the subtropical and tropical oceans. The fact that similar associations between cloud type, increased decoupling inferred from δq, and increased MBL height are observed at midlatitudes as well as in the subtropics suggests this general relationship tends to occur whenever the MBL is capped by an inversion.

Figure 3.5c shows that the average ΔT associated with stratocumulus and cumulus cloud types at these locations is always negative, suggesting the presence of cold advection. This is certainly the case for the trade-wind regime at OWS N; examination of coincident surface winds at the other OWS (not shown) indicates a tendency for stratocumulus and cumulus cloud types to occur with flow from the direction of cooler water. The study of Lau and Crane (1995), who composited ISCCP cloud data with ECMWF analyses, found that clouds of varying optical thickness with low tops are associated with cold advection and subsidence. Assuming no overlying higher clouds, a

satellite would identify stratocumulus, cumulus-under-stratocumulus, and cumulus as clouds of varying optical thickness with low tops. A subsequent study by Lau and Crane (1997) using surface cloud observations confirms that stratocumulus and cumulus are most common in the cold-advection region west of the low pressure center. The summertime midlatitude ΔT is distinctly lower than the trade wind ΔT, which, along with the colder water, contributes to a weaker latent heat flux.

Klein and Hartmann (1993b) documented that increased cloud amount of combined stratus, stratocumulus, and fog is associated with a greater lower tropospheric static stability (S) for both the seasonal cycle and interannual anomalies. Figure 3.5d shows that S is greatest for stratocumulus, less for cumulus-under-stratocumulus, and least for cumulus at every location (Norris 1997a shows this is also the case during winter), suggesting that a large part of the relationship documented by Klein and Hartmann is due to the fact that stratiform cloud types occur more frequently when S is greater. A further contribution results from the fact that stratocumulus typically has greater cloud amount than cumulus-under-stratocumulus, which typically has greater cloud amount than cumulus. The observed relationship between low cloud type and S is consistent with increased subsidence promoting a shallower MBL (Schubert et al. 1979a) and warmer temperatures at 700 mb. The fact that the midlatitude MBL at OWS B and C is much shallower than the trade wind MBL at OWS N during summer suggests that greater subsidence, weaker entrainment-generating turbulence, or both occurs at midlatitudes. The shallower MBL depth at midlatitudes may also account for the more well-mixed stratocumulus MBL indicated by $\delta q / q_{SST}$.

3.5 Low cloud type composites without capping inversions

A variety of structures occur when the MBL is not capped by a temperature inversion, such as surface-based inversions, strongly stratified layers, or weakly stratified layers, as illustrated in Figures 3.6–8. Average ΔT and S for low cloud types displayed in these figures and those from the previous section are shown in Fig. 3.9, with Table 3.5 recording the means and standard deviations of the data from this section.

Figure 3.6 shows composite vertical distributions of q, q_s, θ_v, and θ_e for no-low-cloud (C_L 0) and sky-obscuring fog at OWS B and C during JJA. The extremely strong surface stratification, positive ΔT, large S (Fig. 3.9), and strong southerly wind component (not shown) associated with observations of no-low-cloud and sky-obscuring fog at midlatitudes are consistent with subsidence and strong advection of warmer air over colder water, as has been documented by previous studies of fog over the ocean (Taylor 1917; Tsukuda 1932). The no-low-cloud composite has much less low-level moisture than the sky-obscuring fog composite. Figure 14 of Norris (1997b) shows that no-low-cloud generally occurs only very close to the coast, or sometimes poleward and eastward of continents at midlatitudes during summer. This suggests the occurrence of no-low-cloud at OWS B and C during summer corresponds to air masses of recent continental origin, as is the case for stratocumulus cloud clearing episodes off the coast of California (Kloesel 1992).

Fair-weather stratus at OWS B and C during summer occurs in a saturated layer that is often shallow but sometimes quite deep, but bad-weather stratus usually has no clear MBL or cloud top and is nearly saturated through much of the troposphere (Fig. 3.7). Fair-weather stratus is frequently accompanied by fog and drizzle, and bad-weather stratus is associated with particularly strong winds and substantial precipitation (not shown). The relatively large values of S, positive or slightly negative values of ΔT (Fig. 3.9), and deep cloud layers suggest that fair-weather stratus as well as bad-weather stratus tends to be associated with warm advection and synoptic ascent. The fact that fair-weather stratus typically has a well-defined cloud top and largely occurs with drizzle whereas bad-weather stratus generally has no well-defined cloud top and largely occurs with rain suggests these two types differ by the degree of synoptic ascent. The study of Lau and Crane (1995) found that optically thick clouds with high tops, likely corresponding to nimbostratus, are associated with warm advection and ascent. Lau and Crane (1997) confirms that surface-observed nimbostratus is most frequent in the warm-advection region east of the low pressure center.

The greatest difference between OWS V and the other OWS is the frequent lack of

a discernible MBL or cloud top during the summer season, resulting from weaker or negligible subsidence at OWS V compared to the other locations. Furthermore, in contrast to the other locations, OWS V reported stratocumulus without a capping inversion about two thirds of the time. The cases without an inversion bore some resemblance to those for fair-weather stratus (not shown), and were not added to the stratocumulus composite sounding displayed in Fig. 3.4. No abrupt decrease in humidity occurs in the moderate and large cumulus composite sounding at OWS V (Fig. 3.8), suggesting that the cumuli have a broad distribution of cloud top heights.

Both the moderate and large cumulus composite sounding and fair-weather stratus composite sounding at OWS V (Fig. 3.8) show a similar gradual decrease of temperature and humidity with height with the only difference being that the stratus composite is more saturated and stratified near the surface. This suggests that stratus at OWS V may often be associated with a very shallow, shear-driven stratus layer. Such a cloud type was documented by Nicholls and Leighton (1986), who observed a shear-driven cloud layer with a very low base and a flat, uniform, and featureless top over the wintertime midlatitude North Atlantic. Rogers (1989) and Koracin and Rogers (1990) use observations and a modeling study to show that advection of a well-mixed, inversion-capped MBL from the warm side to the cold side of a sharp SST gradient causes a stable, shear-driven internal boundary layer to form at the surface. Although no inversion is present with stratus at OWS V, it is likely that the stable layer at the surface forms by similar processes. Nicholls et al. (1983) suggest that the depth of a weakly-turbulent layer scales by u_*/f with observationally-determined proportionality constant 0.2, where u_* is the friction velocity and f is the Coriolis parameter. Using this formulation and typical surface meteorological values associated with stratus at OWS V yields a depth of 600 m, somewhat less than but comparable to a depth of 800 m obtained by assuming the top of the stable layer occurs where the stratus θ_v composite departs from the cumulus θ_v composite (Fig. 3.8).

The difference between cumulus and stratus at OWS V largely seems to depend on the SST associated with each (25.6 °C for cumulus and 20.8 °C for stratus). This

substantial difference in SST between cloud types does not occur at the other OWS and largely stems from cumulus replacing stratus as the strong SST gradient between subtropics and midlatitudes moves poleward during summer (stratus is observed during June and July and cumulus is observed during July and August). Hence, the cumulus composite at OWS V may be viewed as corresponding to a location equatorward of OWS V during June, and the stratus composite at OWS V may be viewed as corresponding to a location poleward of OWS V during August. In this sense, the stratus composite shows how the lower part of the cumulus composite is modified as it is advected poleward from the subtropics over increasingly cold water, along with a corresponding increase in S and change from negative to positive ΔT (Fig. 3.9). This is consistent with the results of NL, who found a strong negative correlation between interannual anomalies in seasonal-mean MSC and SST in this region during JJA and attributed it to meridional shifts in the strong MSC and SST gradients which usually exist slightly north of OWS V. An equatorward shift in the region of strong SST gradient could produce significantly stronger warm advection at OWS V and result in more stratus compared to cumulus. Fig. 2.12 suggests that SST anomalies can be interpreted as a delay or advance of seasonal warming of surface water in the central North Pacific.

3.6 Summary and conclusions

The preceding results for OWS composite soundings and surface observations suggest that advection and vertical motion have a large influence on MBL structure and consequently low cloud type over the midlatitude ocean. Figure 3.9a shows that ΔT is typically less than –0.25 °C for stratocumulus (C_L 5), cumulus-under-stratocumulus (C_L 8), and moderate and large cumulus (C_L 2), implying that cold advection is typical in each of these situations, and that ΔT is typically greater than 0 °C for bad-weather stratus (C_L 7), fair-weather stratus (C_L 6), and sky-obscuring fog, and no-low-cloud (C_L 0), implying that warm advection is typical in each of these situations. The cold-advection cloud types typically occur within a generally well-mixed MBL capped by a temperature inversion (Figs. 3.3 and 3.4), implying the presence of subsidence. MBL height and

inferred decoupling of the cloud layer from the subcloud layer generally increase from stratocumulus to cumulus-under-stratocumulus to cumulus (Fig. 3.5ab). Sky-obscuring fog typically occurs with a strong surface-based inversion (Fig. 3.6), implying the presence of subsidence. Figure 3.7 shows that fair-weather stratus generally occurs in a deep stratified layer with frequent drizzle, implying the presence of weak and shallow ascent, and that bad-weather stratus occurs in very deep stratified layer with rain, implying the presence of strong and vertically extensive ascent. Cumulus near the western subtropical ocean has no discernible MBL, implying near-zero vertical motion (e.g., Bajuk and Leovy 1997a). Fair-weather stratus in the same region has a similar vertical profile, except for a very shallow stratified layer near the surface. Table 3.6 summarizes the conditions associated with these cloud types.

The fact that low stratiform cloud types form under a large variety of conditions over the midlatitude ocean has not been sufficiently appreciated by previous studies. Figure 3.9b shows that, with the exception of infrequently-occurring no-low-cloud (C_L 0), large S is associated with low stratiform cloud types, thus producing the strong relationship between S and MSC amount documented by Klein and Hartmann (1993b). However, different processes are responsible for producing the large S associated with different cloud types. Subsidence warming produces the large S associated with stratocumulus, warm advection and ascent produce the large S associated with stratus, and subsidence warming and warm advection produce the very large S associated with sky-obscuring fog. Therefore, although S may be a useful diagnostic for MSC amount, it is necessary to explicitly examine the underlying processes of advection and vertical motion to understand variability in MSC.

Table 3.6 indicates that particular advective conditions promote certain cloud types, suggesting that variability in advection produces variability in the relative frequencies of cloud types. Vertical motion and other processes are important as well, particularly those that affect internal properties like MBL decoupling, but these are not examined in the present study due to lack of observations. It is likely that more frequent cold advection favors increased stratocumulus, cumulus-under-stratocumulus, or cumulus, depending on

the strength of MBL decoupling. More frequent warm advection likely favors increased sky-obscuring fog, fair-weather stratus, or bad-weather stratus, and no-low-cloud, depending on the direction and magnitude of vertical motion. However, variability in advection may not necessarily produce variability in MSC amount if some low stratiform cloud types are simply replaced by other low stratiform cloud types, although such replacement might produce variability in MSC optical thickness. Cloud amount associated with each low stratiform cloud type, its relative contribution to MSC amount, and the role of advection is documented for the summertime midlatitude North Pacific in the next chapter.

Table 3.1: Availability of good OWS data.

	OWS B	OWS C	OWS N	OWS P	OWS V
surface observations	Jan 54 – Apr 74	Jan 54 – Dec 87	Jan 54 – Apr 74	Jan 54 – Jun 81	Jan 54 – Jan 72
significant-level soundings	Jul 70 – Jun 74	Jul 70 – Dec 73	Jul 70 – Jun 74	not available	Jul 70 – Jan 72
number of JJA soundings*	254 (226)	299 (141)	249 (69)	0	149 (37)

* The parentheses indicate the number of soundings with conditions of good illumination.

Table 3.2: WMO low cloud classification.

C_L Code	Non-technical cloud type description
0	No stratocumulus, stratus, cumulus or cumulonimbus
1	Cumulus with little vertical extent and seemingly flattened, or ragged cumulus other than of bad weather*, or both
2	Cumulus of moderate or strong vertical extent, generally with protuberances in the form of domes or towers, either accompanied or not by other cumulus or by stratocumulus, all having their bases at the same level
3	Cumulonimbus the summits of which, at least partially, lack sharp outlines, but are neither clearly fibrous (cirriform) nor in the form of an anvil; cumulus, stratocumulus or stratus may also be present
4	Stratocumulus from the spreading out of cumulus; cumulus may also be present
5	Stratocumulus not resulting from the spreading out of cumulus
6	Stratus in a more or less continuous sheet or layer, or in ragged shreds, or both, but no stratus fractus of bad weather*
7	Stratus fractus of bad weather* or cumulus fractus of bad weather, or both (pannus), usually below altostratus or nimbostratus
8	Cumulus and stratocumulus other than that formed from the spreading out of cumulus; the base of the cumulus is at a different level than that of the stratocumulus
9	Cumulonimbus, the upper part of which is clearly fibrous (cirriform), often in the form of an anvil, either accompanied or not by cumulonimbus without anvil or fibrous upper part, by cumulus, stratocumulus, stratus or pannus

* "Bad weather" denotes the conditions which generally exist during precipitation and a short time before and after.

Table 3.3: Number of significant-level soundings used in the composites, and means and standard deviations from Fig. 3.5.

	number of soundings	MBL Height (km)	$\delta q/q_{SST}$ (x 100)	ΔT (K)	S (K)
OWS B C_L 5	33	0.67 ± 0.24	2.6 ± 12.2	–0.5 ± 1.0	19.0 ± 4.1
OWS B C_L 8	7	0.92 ± 0.34	2.8 ± 10.8	–0.8 ± 0.8	14.8 ± 3.8
OWS C C_L 5	46	0.86 ± 0.32	5.2 ± 8.5	–0.4 ± 1.2	18.7 ± 4.0
OWS C C_L 8	12	1.13 ± 0.49	13.1 ± 11.1	–0.6 ± 0.9	15.6 ± 3.9
OWS N C_L 5	7	1.26 ± 0.39	10.4 ± 5.9	–1.6 ± 0.8	18.3 ± 2.7
OWS N C_L 8	68	1.67 ± 0.42	14.0 ± 6.5	–1.5 ± 0.8	17.3 ± 2.0
OWS N C_L 2	15	1.88 ± 0.56	18.5 ± 7.6	–1.6 ± 0.9	16.6 ± 3.1
OWS P C_L 5				–0.4 ± 0.8	17.3 ± 3.1
OWS P C_L 8				–0.5 ± 0.7	15.5 ± 3.2
OWS V C_L 5	4	1.38 ± 0.65	4.8 ± 5.6	–0.2 ± 1.8	17.5 ± 2.8
OWS V C_L 8	8	1.35 ± 0.55	12.6 ± 4.5	–0.7 ± 0.9	16.1 ± 2.2

Table 3.4: Statistical significance of differences in MBL height and $\delta q/q_{SST}$ between low cloud types using a one-tailed *t*-test and values from Table 3.3 (in percent).

	difference in MBL Height	difference in $\delta q/q_{SST}$
C_L 5 and C_L 8 at OWS B	94.8	not significant
C_L 5 and C_L 8 at OWS C	95.4	98.2
C_L 5 and C_L 8 at OWS N	98.4	91.6
C_L 5 and C_L 2 at OWS N	99.6	99.2
C_L 8 and C_L 2 at OWS N	94.0	97.7
C_L 5 and C_L 8 at OWS V	not significant	97.0

Table 3.5: Number of significant-level soundings used in the composites, and means and standard deviations from Fig. 3.9.

	number of soundings	ΔT (K)	S (K)
OWS B C_L 7	15	0.1 ± 1.0	18.3 ± 3.6
OWS B C_L 0	12	0.7 ± 1.2	20.9 ± 3.7
OWS B C_L 6	17	–0.1 ± 0.9	19.9 ± 3.9
OWS B FOG	21	0.0 ± 1.2	23.6 ± 3.8
OWS C C_L 7	29	0.2 ± 1.0	18.0 ± 4.1
OWS C C_L 0	13	0.6 ± 1.0	19.9 ± 2.9
OWS C C_L 6	28	0.2 ± 1.2	21.5 ± 3.5
OWS C FOG	25	1.0 ± 1.0	23.7 ± 2.6
OWS P C_L 7		0.0 ± 0.8	20.7 ± 3.5
OWS P C_L 6		–0.1 ± 0.6	20.1 ± 3.4
OWS P FOG		0.1 ± 0.9	21.3 ± 4.3
OWS V C_L 2	22	–0.5 ± 1.0	14.2 ± 2.0
OWS V C_L 0		0.3 ± 1.9	17.4 ± 2.6
OWS V C_L 6	10	0.3 ± 1.1	18.6 ± 18

Table 3.6: Typical conditions associated with various low cloud types over the midlatitude ocean inferred from Figs. 3.3–9.

low cloud type	advection	vertical motion	MBL structure
stratocumulus	cold	subsidence	weakly decoupled mixed layer*
cumulus-with-stratocumulus	cold	subsidence	decoupled mixed layer*
deep midlatitude cumulus	cold	subsidence	strongly decoupled mixed layer*
deep midlatitude stratus	warm	weak ascent	deep stratified layer
bad-weather stratus	warm	strong ascent	very deep stratified layer
sky-obscuring fog	warm	subsidence	strongly stratified surface layer
near-western subtropical stratus	warm	near-zero	weakly stratified near-surface layer
near-western subtropical cumulus	near-zero	near-zero	no discernible MBL

* The term “mixed layer” refers to a generally well-mixed MBL under a capping inversion.

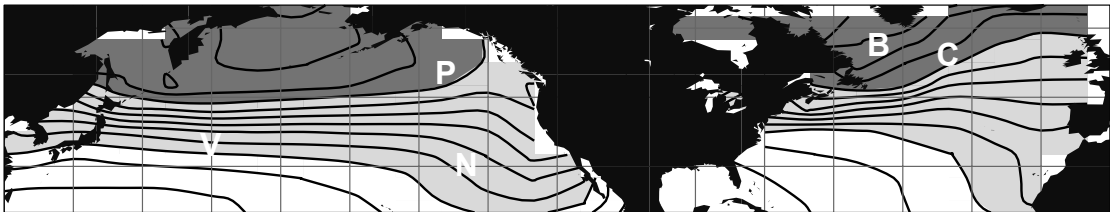

Figure 3.1: Locations of OWS B (56.5°N, 51°W), C (52.75°N, 35.5°W), N (30°N, 140°W), P (50°N, 145°W), and V (34°N, 164°E) which contributed soundings and surface observations for this investigation. Climatological SST during JJA is provided for meteorological context. Contour interval is 2°C; thresholds for lighter (darker) shading are 24°C (12°C)

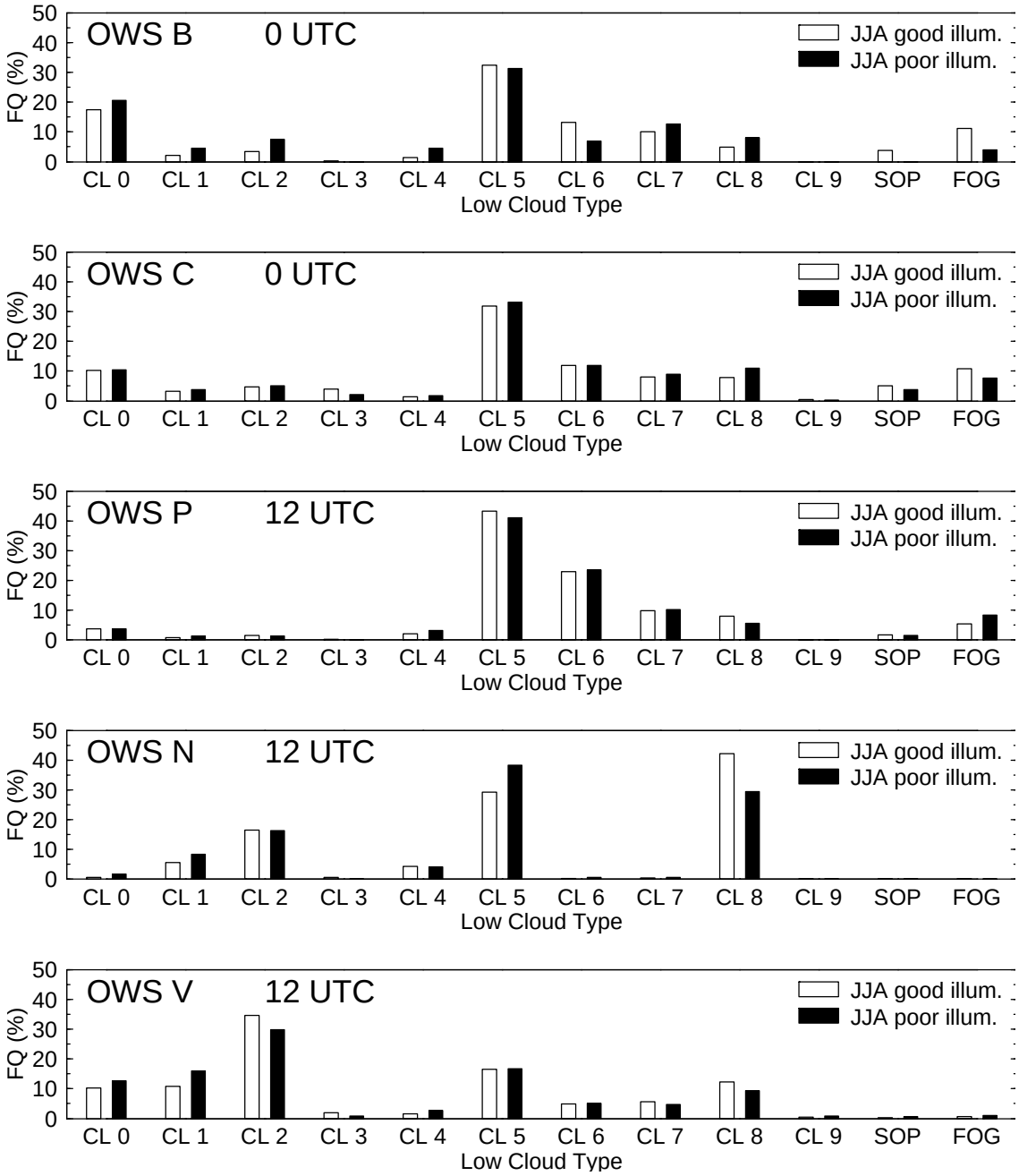

Figure 3.2: FQ of the low cloud types described in Table 3.2 along with sky-obscuring precipitation (SOP) and sky-obscuring fog (FOG) at OWS B, C, N, P, and V during JJA. Observations are from 0 UTC or 12 UTC (nighttime) under conditions of good illumination and poor illumination according to the criterion of Hahn et al. (1995). Color coding of bars: white – good; black – poor.

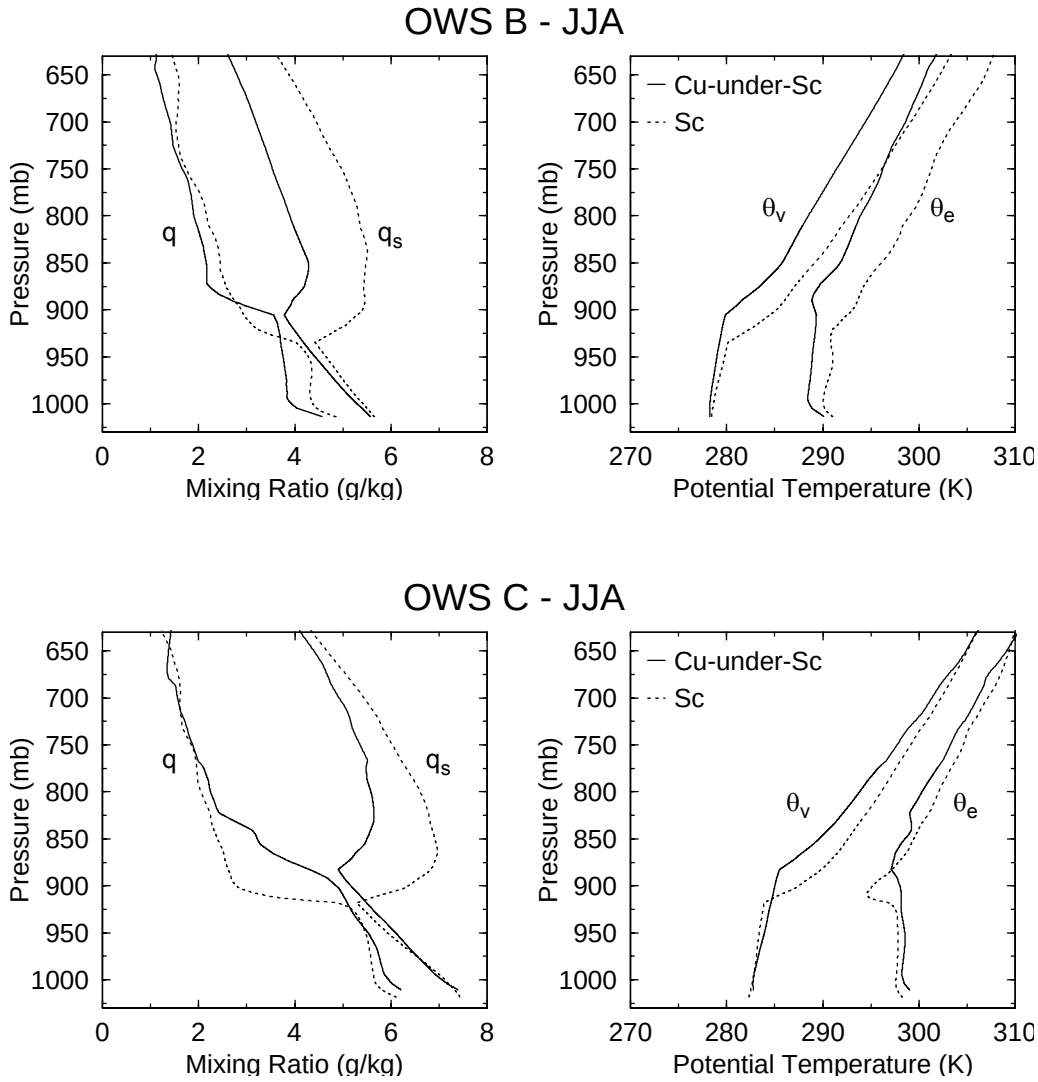

Figure 3.3: Composite water vapor mixing ratio (q) and saturation water vapor mixing ratio (q_s) (left) and virtual potential temperature (θ_v) and equivalent potential temperature (θ_e) (right) for cumulus-under-stratocumulus (C_L 8) (solid) and stratocumulus (C_L 5) (dotted) at OWS B (top) and C (bottom) during JJA.

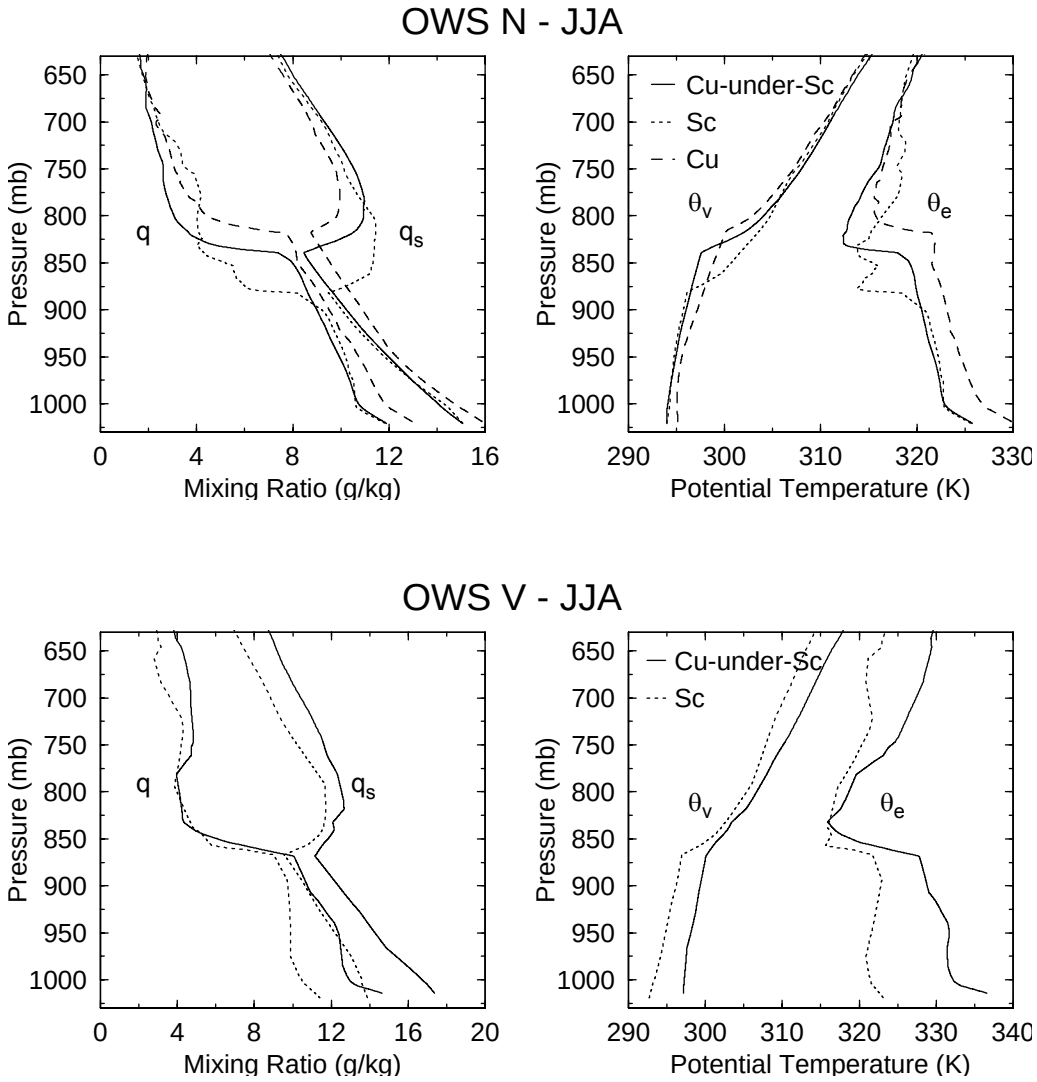

Figure 3.4: As in Fig. 3.3, except for cumulus-under-stratocumulus (C_L 8) (solid), stratocumulus (C_L 5) (dotted), and moderate and large cumulus (C_L 2) at OWS N (top) and V (bottom). Moderate and large cumulus at OWS V does not occur under a capping inversion and is therefore not displayed here.

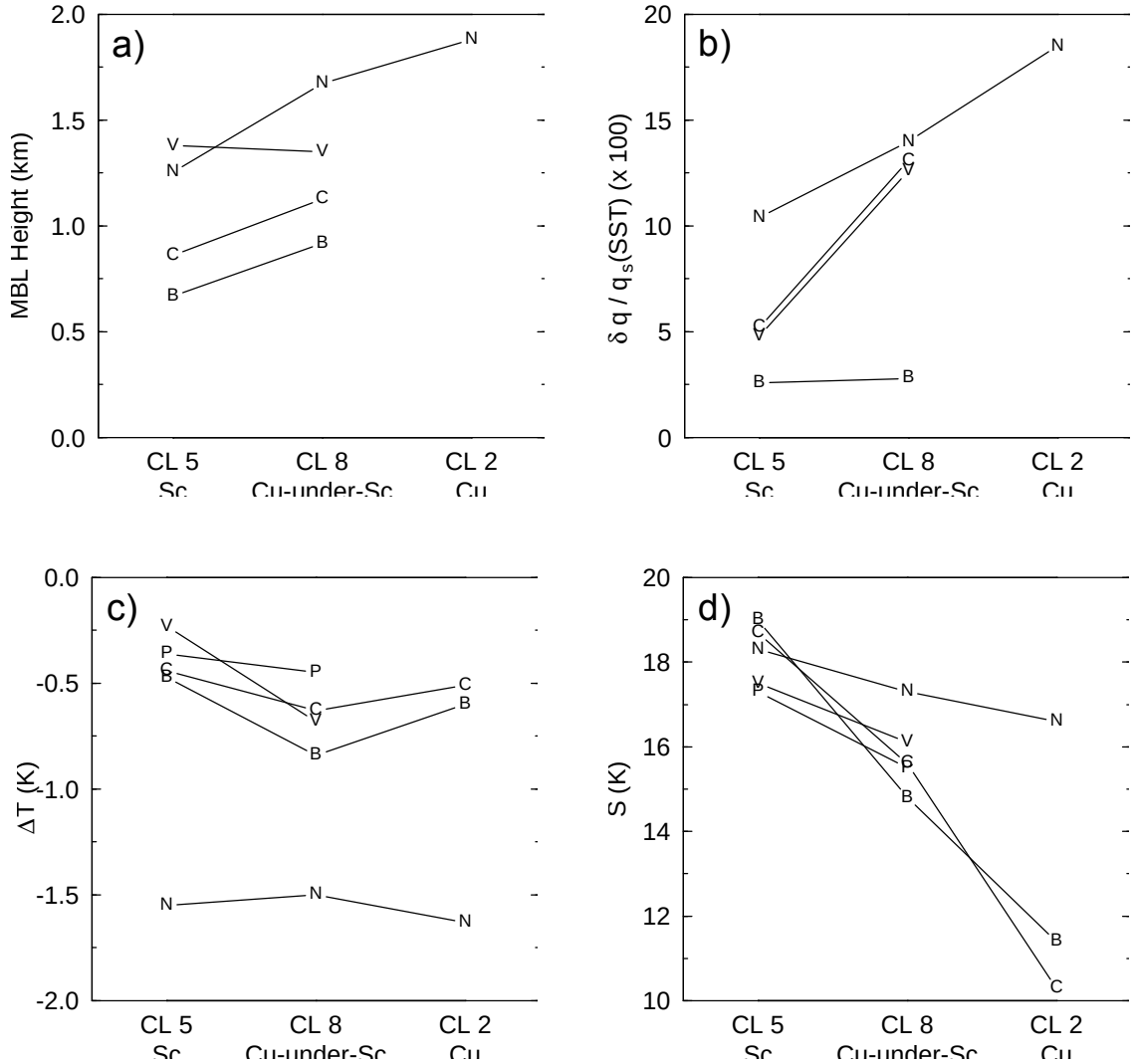

Figure 3.5: (a) MBL height from significant-level sounding composites, (b) δq / q_{SST} from significant-level sounding composites, (c) ΔT from surface observations, and (d) S from 50 mb-resolution soundings, for stratocumulus (C_L 5), cumulus-under-stratocumulus (C_L 8), and moderate and large cumulus (C_L 2) during JJA. OWS locations are identified by letter and connected by lines.

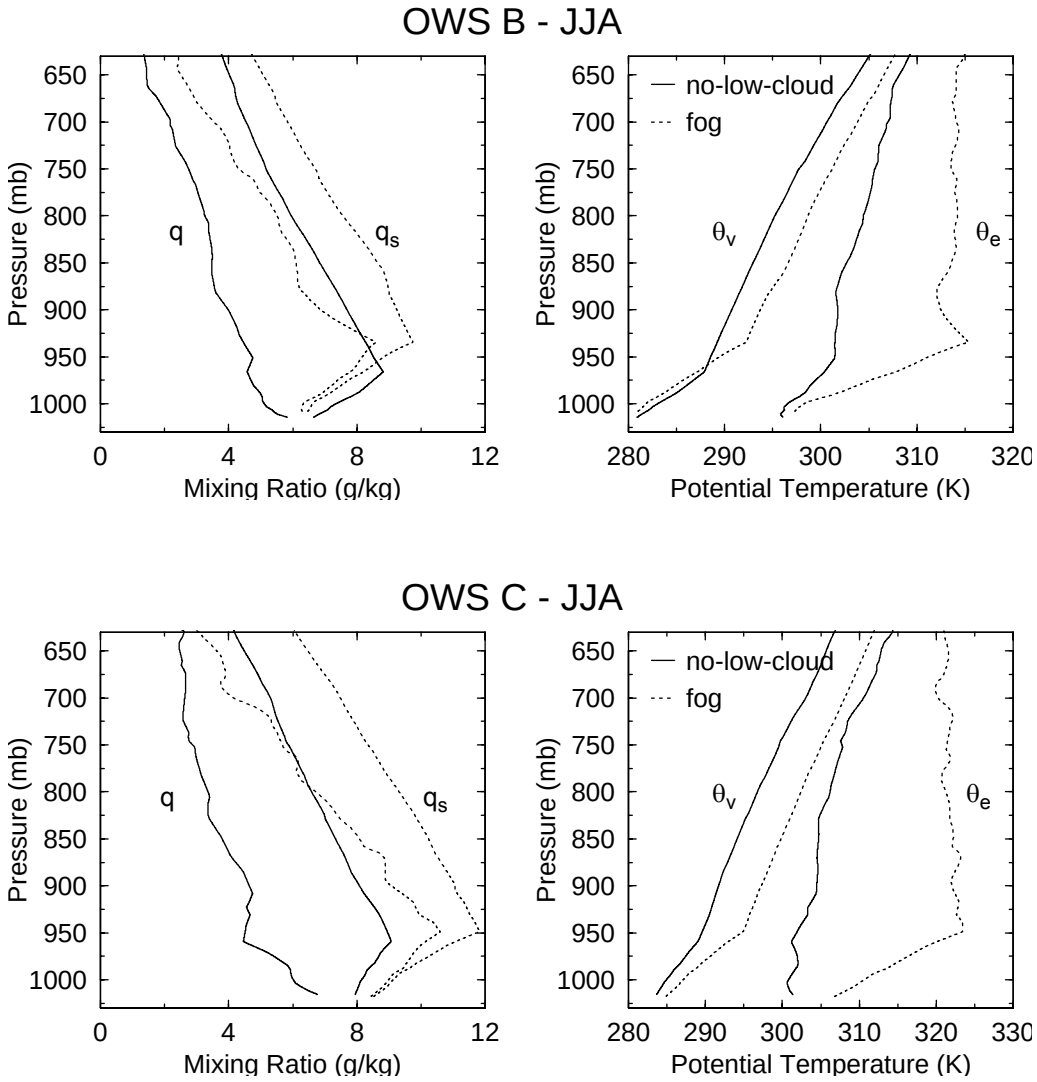

Figure 3.6: As in Fig. 3.3, except for no-low-cloud (C_L 0) (solid) and sky-obscuring fog (dotted) at OWS B (top) and C (bottom).

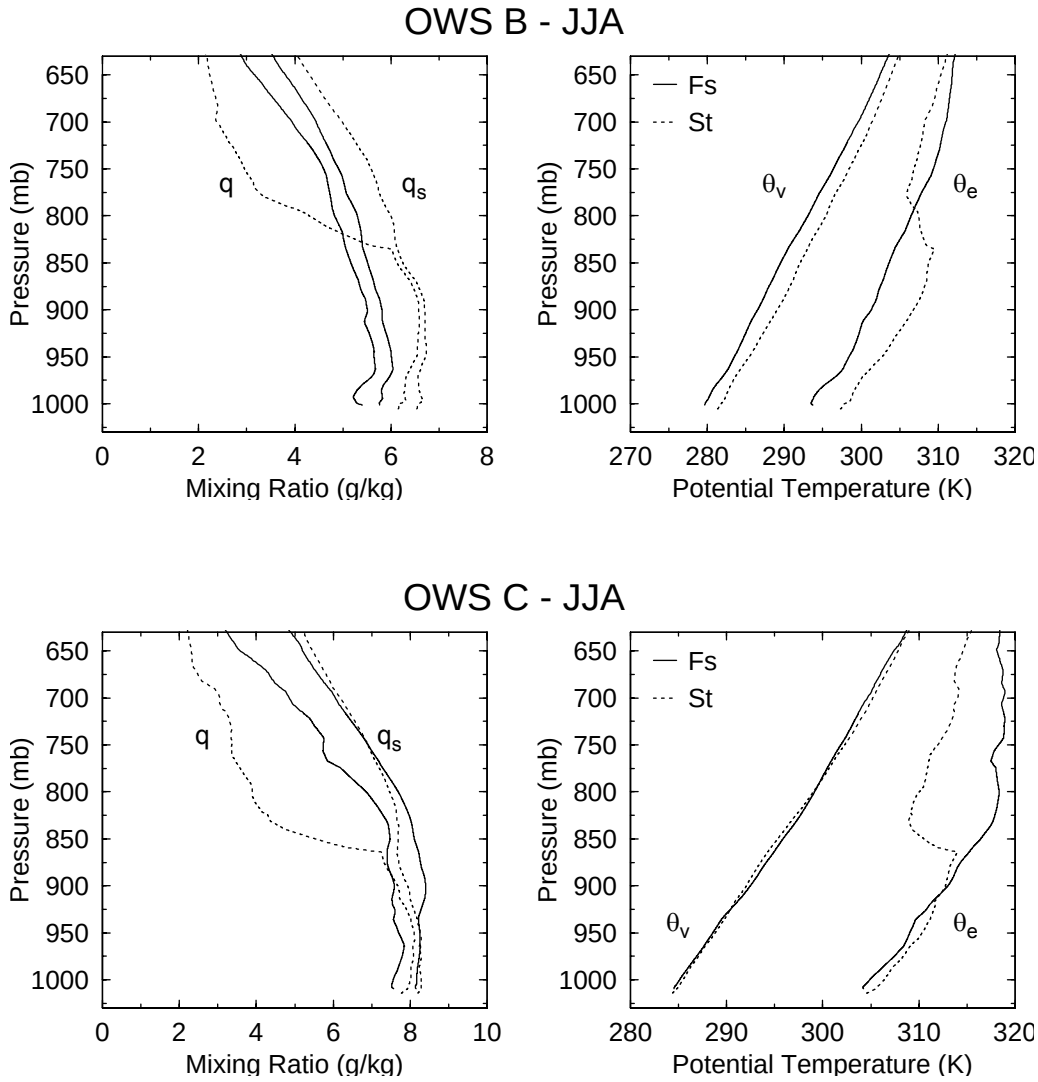

Figure 3.7: As in Fig. 3.3, except for bad-weather stratus (Fs) (C_L 7) (solid) and fair-weather stratus (C_L 6) (dotted) at OWS B (top) and C (bottom).

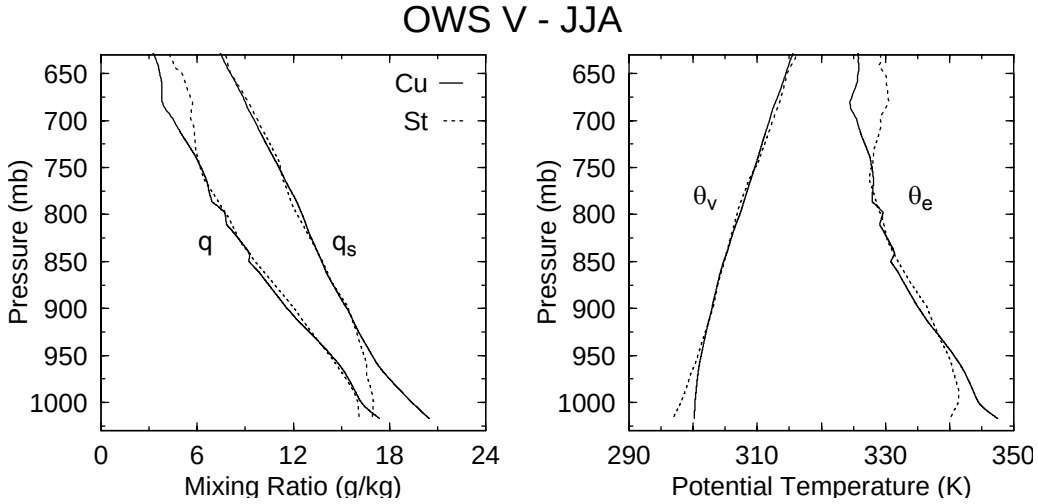

Figure 3.8: As in Fig. 3.3, except for moderate and large cumulus (C_L 2) (solid) and fair-weather stratus (C_L 6) (dotted) at OWS V.

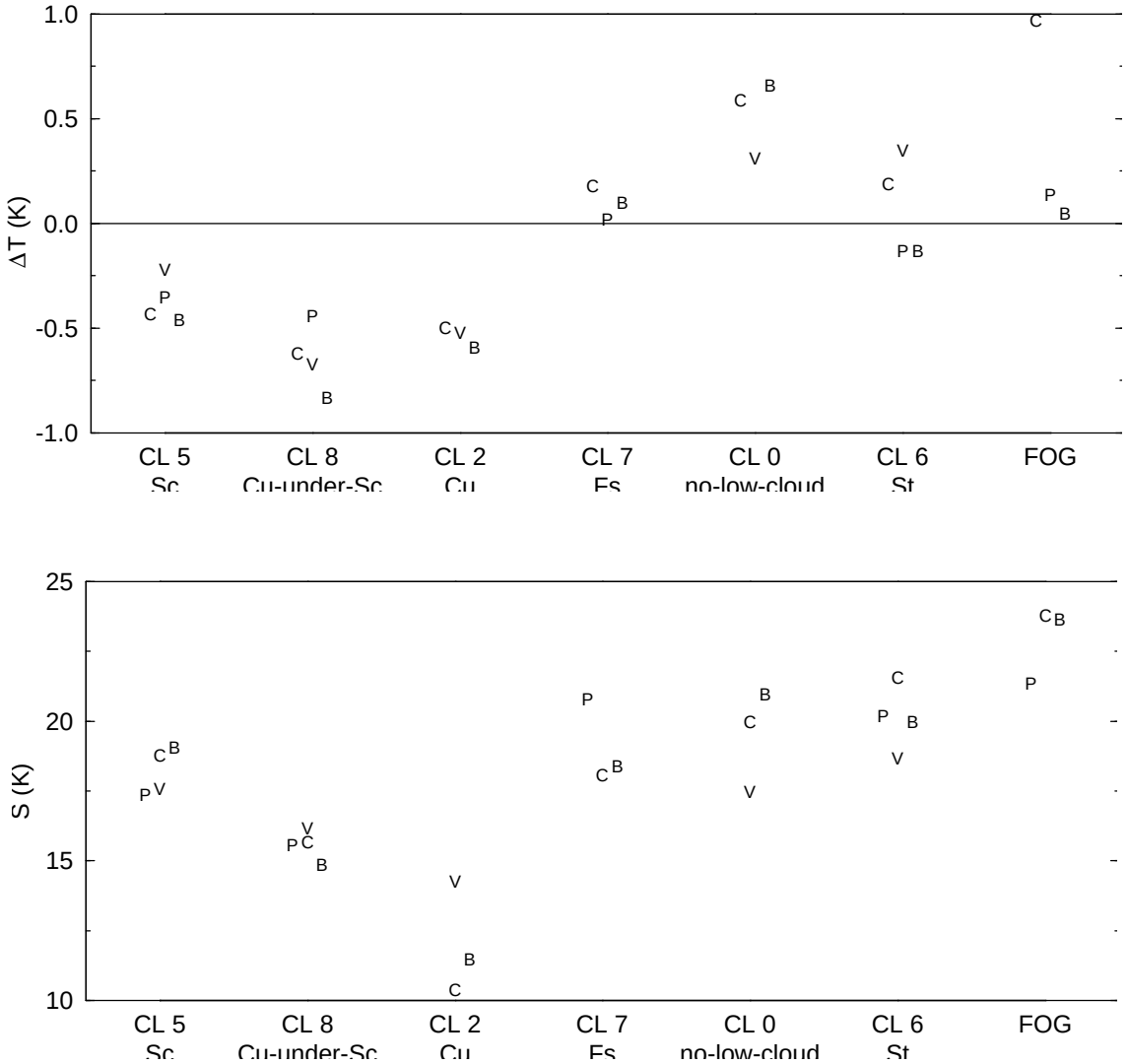

Figure 3.9: (Top) ΔT from surface observations and (bottom) S from 50 mb resolution soundings, for stratocumulus (C_L 5), cumulus-under-stratocumulus (C_L 8), moderate and large cumulus (C_L 2), bad-weather stratus (Fs) (C_L 7), no-low-cloud (C_L 0), fair-weather stratus (C_L 6), and sky-obscuring during JJA. OWS locations are identified by letter. Some values have been slightly offset along the x-axis to improve readability.

CHAPTER 4

Low Stratiform Cloud Types over the Summertime Midlatitude North Pacific and Variability Associated with Different Inferred Advective Conditions

4.1 Introduction

The previous chapter documented representative MBL structures and surface meteorology associated with various low cloud types over the midlatitude ocean during summer. The observed conditions suggested that stratocumulus types typically occur with cold advection and subsidence, sky-obscuring fog typically occurs with warm advection and subsidence, and stratus types typically occur with warm advection and ascent (Table 3.6). In order to understand the role of advection in producing variability in MSC, it is necessary not only to determine how advection produces variability in each low stratiform cloud type, but also how each low stratiform cloud type contributes to MSC. Since this has not been previously documented, the present chapter shows the amount of each low stratiform cloud type and its relative contribution to MSC amount over the summertime midlatitude North Pacific. Cloud amounts of cumulus types, cumulonimbus, and the FQ of no-low-cloud are also presented to include all possible low cloud conditions. The role of advection in producing variability in low stratiform cloud types over the midlatitude North Pacific is examined by comparing MSC amount, amounts of low cloud types, and meteorological parameters composited on conditions of local cold and warm advection, as inferred from wind direction or air-sea temperature difference. These results receive support from several satellite images presented at the end of the chapter which suggest similar relationships between inferred low cloud type, advection, and the SST gradient.

4.2 Construction of low cloud type climatologies

Summertime (JJA) climatological amounts of all low cloud types were calculated for the 1954–1992 time period using individual daytime (including twilight) observations from the EECRA (Hahn et al. 1996). In addition to the ten low cloud types identified by the synoptic code (Table 3.2), sky-obscuring fog and sky-obscuring precipitation were identified as "low cloud types" for the purposes of the present study. These twelve types include every possible sky condition for low cloud identification. Clouds types contributing to MSC are sky-obscuring fog, sky-obscuring precipitation, cumulus-with-stratocumulus types (C_L 4 and 8), stratocumulus (C_L 5), fair-weather stratus (C_L 6), and bad-weather stratus (C_L 7). Cumulus cloud types are moderate and large cumulus (C_L 2) and small cumulus (C_L 1). Cumulonimbus cloud types are C_L 3 and 9.

It is important to keep in mind that the frequency and amount of lesser-priority cloud types may be underestimated. This should not be so great a problem for low stratiform cloud types since several of them (C_L = 5, 6, or 7) have the same priority. However, conditions which are identified as sky-obscured generally prevent identification of low cloud type, and mixed cumuliform and stratiform cloud types (C_L = 4 or 8) always have priority over purely stratiform cloud types. Cumulonimbus types (C_L = 3 or 9) always have priority over other cloud types, and moderate and large cumulus (C_L 2) has priority over purely stratiform types, but these should be of small effect over the summertime midlatitude North Pacific due to the rarity of purely cumuliform cloud types.

Most of the synoptic surface cloud observations compiled in the EECRA were reported by observers on Volunteer Observing Ships (VOS), who sometimes identified cloud type differently from OWS observers, probably because they did not receive as much training. Figure 4.1 compares the daytime FQ of each cloud type calculated from OWS observations to the FQ calculated from nearby VOS observations during JJA (Norris 1997b shows DJF values). Only VOS observations made within a 2° x 2° box centered on the OWS were used, and both OWS and VOS observations are from the time period 1954–1972. Although OWS and VOS observers generally agree on which cloud types are most frequent and which are least frequent, the VOS observers tend to identify

the more frequently occurring cloud types less often and the less frequently occurring cloud types more often than do OWS observers. This tendency is consistent with increased random errors in cloud identification by less skillful VOS observers. Paired OWS and VOS observations (near in space and coincident in time) were examined to see if there were consistent patterns relating a specific cloud type identified by OWS to that identified by VOS. The results were inconclusive, probably because most paired OWS and VOS observations were insufficiently close to exclude natural mesoscale variability in cloud type. All observations from the EECRA near OWS locations were excluded from the calculation of climatological and yearly cloud data used in this study since OWS observers identify certain cloud types differently from VOS observers.

Results from Norris (1997b) suggest that, in the context of the midlatitude North Pacific during summer, it is appropriate to combine sky-obscuring precipitation and sky-obscuring fog in one category, and C_L 4 and C_L 8 in one category. Sky-obscuring precipitation occasionally occurs at midlatitudes, usually as drizzle during summer. The similarity between geographical distributions of sky-obscuring precipitation and sky-obscuring fog during summer (Norris 1997b) suggests that reports of sky-obscuring precipitation due to drizzle actually result from sky-obscuring fog with coincident drizzle. The present-weather code requires the largest applicable number to be reported, so drizzle (ww = 50-59) has priority over fog (ww = 10–12, 40-49). For this reason, the very small amount of sky-obscuring precipitation which occurs over the ocean during summer will be classified as sky-obscuring fog in this and succeeding chapters. C_L 8 and C_L 4 both consist of cumulus with stratocumulus, and are distinguished from each other by whether the cumulus clouds widen as they reach the stratocumulus layer, the case for C_L 4. Otherwise cumulus with stratocumulus is identified as C_L 8. This appears to be a subtle difference in practice, however, and the great similarity between the geographical and seasonal distributions of C_L 8 and C_L 4 over the summertime midlatitude North Pacific (Norris 1997b) suggests observers have difficulty distinguishing between the two. For this reason, C_L 4 and C_L 8 will be classified as a single cumulus-with-stratocumulus cloud type in this and subsequent chapters.

As was done in Chapter 2, average cloud amount was obtained by separately averaging FQ and AWP and then multiplying them. Because the distribution of ships over the global ocean is highly non-uniform, the irregular averaging grid for JJA displayed in Fig. 2 of Norris (1997b) was used to preserve resolution in regions with many observations and to increase statistical significance in regions with few observations. The base grid box size in the North Pacific was 2.5° x 2.5°, and no grid box was more than four times the grid area of the base box. Grid boxes in well-sampled regions typically had several thousand observations contributing to the average, and grid boxes with less than 100 observations contributing to the FQ average were discarded. The 1982 change in observing procedure affecting the calculation of FQ was taken into account using formulas given in Norris (1997b). After calculating average cloud amount, the value of each large grid box was assigned to all of the 2.5° x 2.5° base boxes within it. MSC amount is the sum of the amounts of each contributing cloud type, and the percentage contribution of each cloud type to MSC was obtained by dividing the amounts of each cloud type by MSC amount. 1–2–1 smoothing in latitude and longitude was applied to the 2.5° x 2.5° climatologies of low stratiform cloud type amount and percentage contribution to MSC amount. These climatologies are complementary to those of low cloud type FQ presented in Norris (1997b).

4.3 Midlatitude North Pacific low cloud type climatologies

Figures 4.2 and 4.3 show the climatological cloud amounts and the percentage contributions to MSC amount for ordinary stratocumulus and cumulus-with-stratocumulus, respectively, over the midlatitude North Pacific during summer. There is a general geographical correspondence between regions with large cloud amount of stratocumulus types and regions where the climatological conditions favor frequent cold advection. Both stratocumulus types are very prevalent on the eastern flank of the subtropical anticyclone (Fig. 2.7), where they are the dominant contributors to MSC. Maximum cumulus-with-stratocumulus cloud amount occurs downwind from the maximum in stratocumulus cloud amount, consistent with a transition from stratocumulus

to cumulus-with-stratocumulus to cumulus as the MBL is advected equatorward over warmer water by the steady, cold-advection trade winds (Bretherton 1992; Wyant et al. 1997). Although MSC is rare over the central and western subtropical North Pacific, it usually occurs as cumulus-with-stratocumulus. Stratocumulus is also common at midlatitudes, particularly near the Bering Sea, but cumulus-with-stratocumulus tends to occur only over the SST gradient region (Fig. 2.3). Although both warm and cold advection occur over the central and western midlatitude North Pacific, warm advection prevails and the amount of stratocumulus is correspondingly less south of 55°N.

Figure 4.4 shows the climatological distribution of the amount of sky-obscuring fog and precipitation and the percentage contribution to MSC amount over the midlatitude North Pacific during summer. Because sky-obscured does not specify actual cloud cover, AWP of sky-obscuring fog and precipitation is assumed to be 100%. Therefore, the top map is basically a higher-resolution version of W88 Map 102. Sky-obscuring fog is very prevalent in the western midlatitude North Pacific and Sea of Okhotsk during summer where substantial warm advection occurs (Klein and Hartmann 1993b), and maximum sky-obscuring fog occurs where mean warm advection at 1000 mb (calculated from daily ECMWF analyses) is greatest (not shown). Sky-obscuring fog is the dominant contributor to MSC amount in the western North Pacific poleward of 40°N. Negligible sky-obscuring fog occurs in the subtropics and east of the subtropical cyclone, except over the coastal upwelling region along Oregon and northern California where the seasonal cycle of SST strongly decreases from spring into summer (e.g. Strub et al. 1987). Fog is often initiated when warm air is advected over the cold upwelled water along the immediate coast (e.g. Palmer 1917; Leipper 1994).

Figure 4.5 shows the climatological distribution of fair-weather stratus cloud amount and the percentage contribution to MSC amount over the midlatitude North Pacific during summer. As was the case for sky-obscuring fog, there is a general geographical correspondence between regions with large stratus cloud amount and regions where warm advection is frequent. Fair-weather stratus is very prevalent in the central midlatitude North Pacific during summer and it is the greatest contributor to MSC

amount there. Because fair-weather stratus and fog frequently co-occur, the lesser amount of fair-weather stratus over the western midlatitude North Pacific may simply result from the fact that relatively deep stratus layers which have a cloud base at the surface will be identified only as sky-obscuring fog. Fair-weather stratus is negligible in the subtropics, but sometimes occurs near the coast of California. Soundings from coastal stations indicate that this eastern subtropical stratus occurs in a very shallow mixed layer under a strong inversion (Lilly 1968), a MBL structure more typical for cold instead of warm advection. Cloudiness occurring in well-mixed MBLs probably has less horizontal inhomogeneity than cloudiness occurring in less well-mixed MBLs, prompting observers to identify it as stratus instead of stratocumulus. The area of fair-weather stratus next to the California coast roughly corresponds to the area where Bretherton and Wyant (1997) predict coupled cloud-topped MBLs. Fair-weather stratus may also result from advection of stratocumulus over colder coastal waters.

Figure 4.6 shows the climatological distribution of bad-weather stratus cloud amount and the percentage contribution to MSC amount over the midlatitude North Pacific during summer. Bad-weather stratus has the least cloud amount of all low stratiform cloud types and only makes a significant contribution to MSC amount in the western subtropical North Pacific. Other low stratiform types are relatively rare in this region, and bad-weather stratus is probably associated with stratiform precipitation regions of mesoscale convective systems (Houze 1993). Bad-weather stratus over the midlatitude North Pacific occurs in a relatively weak but well-defined storm track immediately poleward of the gradient in Ns FQ (Fig. 2.5), generally equatorward of maximum VV (Fig. 2.9), and coinciding with bands of enhanced cloud liquid water path (Weng et al. 1997) and mean upward motion in the midtroposphere (Hoskins et al. 1989). However, bad-weather stratus cloud amount decreases instead of increases poleward of 50°N, in contrast to Ns FQ.

For purposes of comparison, the climatological distributions of moderate and large cumulus cloud amount and small cumulus cloud amount over the North Pacific during summer are presented in Fig. 4.7. Cumulus cloud amount is largest over the western and

central subtropics, but negligible at midlatitudes where warm advection prevails (Klein and Hartmann 1993b). More cold advection occurs in the eastern midlatitude North Pacific than farther west, and cumulus is relatively more frequent there. Moderate and large cumulus cloud amount is greater than small cumulus cloud amount everywhere because it is has larger AWP and usually occurs more frequently (some part of the difference may also be due to the fact that C_L 2 has priority over C_L 1 in designating the low cloud type code). Figure 4.8 shows the climatological distribution of cumulonimbus cloud amount over the North Pacific during summer, and this map is basically a higher-resolution version of W88 Map 50. Although cumulonimbus has larger AWP than that for moderate and large cumulus, it occurs less frequently and consequently has lesser cloud amount. Otherwise the distribution of cumulonimbus cloud amount is similar to that for the cumulus types. No-low-cloud is very frequent near the coast due to offshore flow, but note in particular the band of no-low-cloud FQ across the North Pacific over the SST gradient region (Fig. 4.9).

4.4 Construction of zonal averages of cloud and meteorological parameters

The results of Chapter 2 indicate that interannual variability in MSC amount, Ns FQ, VV, and SST over the midlatitude North Pacific during summer is largely associated with meridional shifts in the location of the storm track and the regions of strong cloud gradient and SST gradient. The fact that both interannual anomalies and the climatological distributions of cloud and meteorological parameters exhibit much more variability in the meridional direction than the zonal direction suggests the analysis can be simplified by the use of zonal averages. Accordingly, cloud and meteorological parameters were averaged between 150°E–150°W over the central North Pacific at 2.5° resolution in latitude during the summer season (JJA) for the time period 1954–1992. All meteorological observations except for VV were obtained from the EECRA instead of the Trenberth SLP and GOSTA datasets used in Chapter 2. All observations contributing to a 2.5° x 60° grid box were averaged together without prior aggregation, but potential biases resulting from changes in spatial sampling (described in Section 2.2) should be

minimal since the zonal variation of most parameters is very small between 150°E–150°W. Values of VV at 2.5° x 2.5° resolution were averaged to 2.5° x 60° resolution. This focus on the meridional direction will facilitate the interpretation of the results and additionally decrease statistical noise by increasing the number of observations contributing to the averages.

Several new meteorological parameters are also introduced. The results of Chapter 3 suggest that advection has a large influence on cloud type, but unfortunately advection cannot be directly measured using only local observations. One proxy for advection is the strength of surface flow parallel to the climatological SST gradient (Klein et al. 1995) which can be approximated by the meridional wind component for the central North Pacific since SST is nearly zonally uniform over the SST gradient region (Fig. 2.3). The percentage contribution of various terms to the interannual variance of seasonal-mean advection calculated from SLP-derived daily wind and the monthly SST gradient are listed in Table 4.1. The majority of the interannual variance in seasonal-mean advection is explained by variability in meridional wind, but variability in the meridional SST gradient also makes a significant contribution. This chapter neglects the role of variability in the meridional SST gradient in order to focus on how the meridional wind influences low cloud type and surface meteorology. Observations of meridional wind component coincident with cloud observations are obtained from EECRA meteorological observations.

ΔT will also be used as a proxy for advection for purposes of comparison with the results of Chapter 3. Positive ΔT implies warm advection, but negative ΔT does not necessarily imply cold advection, particularly in the subtropics. ΔT can suffer substantial biases during daytime as a result of deck heating (Goerss and Duchon 1980). Although average daytime ΔT was approximately 0.8 °C greater than average nighttime ΔT over the central North Pacific (not shown), the amount of overestimation of ΔT varies with cloud cover and solar angle (Kent et al. 1993a; Kent et al. 1993b) and consequently is impossible to correct in individual observations; therefore, only nighttime (including twilight) observations from the EECRA were used to calculate ΔT in the present analysis

(ΔT in Chapter 3 did not suffer from biases since it was averaged only at the time of day of the nighttime sounding).

In order to ascertain the importance of surface latent and sensible heat fluxes relative to surface radiative fluxes over the midlatitude North Pacific during summer, seasonal-mean values were calculated from EECRA observations of ΔT and wind speed using bulk formulas* and exchange coefficients from Smith (1988). Since individual values were calculated with exchange coefficients as a function of wind speed and surface stratification prior to averaging, values of surface latent and sensible heat fluxes used in the present study are superior to those available from the COADS 2° x 2° summaries, which require an exchange coefficient be applied to the 2° x 2° monthly mean. Due to the absence of any reference-height documentation, observations of surface air temperature, dew point depression, and wind speed for the exchange coefficients and flux calculations were assumed to be measured at or previously adjusted to a height of 10 m. Since average anemometer height is 20 m (Cardone et al. 1990), it is likely that anemometer-measured wind speeds used in the 10 m calculations are biased upward by about 5% (Smith 1988). On the other hand, estimations of wind speed from sea-state identified by the Beaufort code are defined for a height of 10 m, but are likely systematically underestimated due to incorrect transformation from Beaufort values to wind speed (Isemer and Hasse 1991). Although errors in wind speed (perhaps on the order of 1 m s^{-1} during JJA) will causes errors in fluxes (perhaps on the order of 20% during JJA) (Isemer and Hasse 1991), no corrections were attempted due to lack of specific information on anemometer height, ignorance of the original Beaufort values, and sometimes lack of knowledge whether wind speed had been measured by anemometer or estimated using the Beaufort scale.

Because of the previous possible bias and others, Weare (1989) estimates that bulk calculations of long-term mean latent heat flux over the tropical and subtropical ocean

---

* Latent heat flux was obtained using the saturation mixing ratio for surface air temperature instead of SST. This would produce about a 6% difference in latent heat flux when ΔT has a magnitude of 1 °C.

have uncertainties on the order of ± 30 W m^{-2}, although this may be less over the colder midlatitude ocean. Blanc (1986) estimates that typical uncertainties for individual calculations of latent and sensible heat fluxes at OWS C are ±40 W m^{-2} and ±25 W m^{-2}, respectively, but these can be considerably reduced when a large number are averaged. Uncertainties for VOS observations are probably greater due to lesser-quality observers and instrumentation; however, Husby (1980) found that the difference between climatological latent heat flux estimated from observations at OWS V and that estimated from nearby VOS observations was only 7 W m^{-2} for the April–September season. Because biases in ΔT can greatly affect estimates of latent and sensible heat fluxes (Kent et al. 1993b), values were calculated only for nighttime, another advantage over the COADS 2° x 2° summaries.

4.5 Meridional variation of cloud and meteorological parameters

Figure 4.10 shows the climatological meridional variation of seasonal-mean MSC amount, Ns FQ, SST, ΔT, VV, meridional wind (V), latent heat flux, and sensible heat flux over the central North Pacific during summer. As was seen previously in Chapter 2, strong gradients in MSC amount, Ns FQ, SST, and VV occur between 30–45°N. Climatological V is southerly poleward of 25°N, and flow over northward decreasing SST produces mean warm advection. Climatological ΔT goes from negative to positive between the subtropics and midlatitudes and has meridional variation very similar to that of seasonal mean temperature advection at 1000 mb calculated from daily ECMWF analyses (not shown). Climatological sensible heat flux is weak at all latitudes and becomes negative (the ocean gains energy) where ΔT is negative. Climatological latent heat flux (defined as positive out of the ocean) greatly decreases from subtropics to midlatitudes as a result of increasing stratification and decreasing SST saturation mixing ratio. Assuming that overcast MSC reduces net downward surface radiation flux by about 100 W m^{-2} during JJA (NL), the reduction in net downward surface radiation flux due to the climatological MSC amount is comparable to the latent heat flux in the gradient region between 30–40°N.

Processes responsible for the transition between the subtropical cumuliform regime

and the midlatitude stratiform regime may be elucidated by examining the climatological meridional variation of the amount of specific low cloud types, presented in Fig. 4.11. This is complementary to the climatological meridional variation of the FQ of specific low cloud types displayed in Fig. 18 of Norris (1997b). Figure 4.11a shows a poleward decrease in cumulus cloud amount with a poleward increase in the relative contribution of small cumulus to total cumulus cloud amount, and Norris (1997b) shows that at midlatitudes the FQ of small cumulus is actually greater than the FQ of moderate and large cumulus. This is consistent with decreasing convective available potential energy (CAPE) resulting from decreasing SST, which will decrease the maximum height attained by cumulus and increase the probability that cumulus clouds will be identified as "small" instead of "moderate or large".

Flow over rapidly decreasing SST may increase the stratification of the near-surface layer to the point where no cumulus clouds can form, consistent with the observed increase in no-low-cloud FQ over the SST gradient (Fig. 4.11c). Because the region under examination is far from the coast, no-low-cloud in Fig. 4.11c is probably not associated with air masses of recent continental origin. Subsequent advection of a no-low-cloud stratified near-surface layer over decreasing SST will likely bring the temperature down to the dew point and produce a very shallow stratus layer similar to that displayed in Fig. 3.8. The poleward increase in fair-weather stratus cloud amount (Fig. 4.11c) is consistent with the transformation from cumulus to stratus near OWS V suggested by Fig. 3.8. It is likely that further advection of this shallow stratus layer over decreasing SST will produce sky-obscuring fog under conditions of subsidence (e.g. Fig. 3.6) or a deeper stratus layer (e.g. Fig. 3.7) under conditions of weak ascent. The amount of sky-obscuring fog is greatest (Fig. 4.11c) where ΔT is most positive (Fig. 4.10b). Figure 4.12 conceptually illustrates the "cumulus to stratus" transition.

Persistent warm advection rarely occurs at midlatitudes due to frequent synoptic activity, which can cause equatorward flow as well as poleward flow over the SST gradient. Norris (1997b) shows that flow over increasingly warm water in the eastern subtropical North Pacific and eastern equatorial North Pacific is associated with a

transition from stratocumulus to cumulus-with-stratocumulus to cumulus, consistent with increasing decoupling of the cloud layer from the subcloud layer. Figure 4.11b suggests a similar transition occurs at midlatitudes when flow over increasing SST produces cold advection. Maximum stratocumulus cloud amount is located over relatively cold water, maximum cumulus-with-stratocumulus cloud amount over relatively warmer water, and maximum cumulus cloud amount occur over the warmest water. Figure 4.13 conceptually illustrates the "stratocumulus to cumulus" transition.

Figure 4.11d shows that cumulonimbus cloud amount is greatest in the subtropics and bad-weather stratus cloud amount is greatest at midlatitudes. Maximum bad-weather stratus cloud amount is co-located with maximum Ns FQ. This is slightly south of the region of strongest SST gradient and coincides with bands of enhanced cloud liquid water path (Weng et al. 1997) and mean upward motion in the midtroposphere (Hoskins et al. 1989).

4.6 Diagnosing advection from wind and air-sea temperature difference

Figure 3.9a suggests low cloud types over the midlatitude ocean may be classified into cold and warm advection categories. Stratocumulus and cumulus-with-stratocumulus occur with cold advection, and fair-weather stratus, bad-weather stratus, sky-obscuring fog, and no-low-cloud occur with warm advection. Cumulus occurs with cold advection at midlatitudes but with near-zero advection in the subtropics. However, these results were obtained only at the locations of the five OWS. Therefore, it is desirable to verify whether the association between low cloud type and inferred advection observed at the OWS occurs in general over the midlatitude ocean. This can be accomplished by extending the analysis of the previous section to separately examine the meridional variation of cloud and meteorological parameters for conditions of inferred cold advection and conditions of inferred warm advection.

Because advection cannot be measured using only local observations, it is necessary to adopt proxy measures such as ΔT or the strength of surface flow parallel to the climatological SST gradient, both of which have advantages and disadvantages. For the

case of the central North Pacific, the meridional wind is parallel to the SST gradient; therefore, the strength of southerly or northerly winds over the SST gradient identifies how quickly the MBL experiences a change in temperature at its bottom boundary. However, due to the circular motion of air masses around low pressure centers it is possible for air colder than the SST to be advected from the south or for air warmer than the SST be advected from the north. Given this possibility, it might be considered preferable to instead use ΔT as a proxy for advection. However, ΔT also may not always exhibit a consistent relationship with low cloud type. Since the adjustment time for ΔT is faster than the adjustment time for the entire MBL, it is possible that ΔT may identify a new advective situation while the remnants of the old MBL structure and corresponding cloud type still persist. Therefore, since neither wind direction nor ΔT definitively identify the advective conditions experienced by the MBL, cold-advection and warm-advection composites based on these proxies may not be as distinct from each other as would be the case for better measures of cold and warm advection.

As was done in the previous section, cloud and meteorological parameters were zonally-averaged over the central North Pacific, but this time only for observations when conditions of cold advection or warm advection were diagnosed. Composites were constructed for both advection inferred from ΔT and advection inferred from wind direction. For the ΔT composites, cold advection was diagnosed when $\Delta T \leq -0.25$ °C and warm advection was diagnosed when $\Delta T \geq 0$ °C, following Fig. 3.9a. To avoid biases due to deck heating, the ΔT composites were necessarily constructed only for nighttime observations, and the cloud composites were accordingly constructed only for nighttime observations with good illumination.

For the wind direction composites, cold and warm advection were diagnosed when the wind direction was within 30° of north or south and when the wind speed was at least 2 m s^{-1} (to exclude near-calm conditions). Although the strength of advection is better related to the magnitude of the meridional wind component rather than wind direction, diagnosis by near-southerly or near-northerly winds was chosen for ease of interpretation. The seasonal-mean frequency of northerly wind and the seasonal-mean frequency of

southerly wind have correlations of 43% (48%) and –31% (–53%) with seasonal-mean advection, all averaged over 35–40°N, 150°E–150°W (the parentheses indicate advection calculated with the climatological SST gradient). Although the frequencies of northerly and southerly winds are not well-correlated with the strength of advection, the goal of the present study is to demonstrate that low cloud type differs between conditions of cold and warm advection rather than to establish a quantitative relationship between low cloud type and the strength of seasonal-mean advection.

Figure 4.14 shows the percentage of cases where cold and warm advection is inferred. In terms of wind direction, warm advection is twice as frequent as cold advection over the central North Pacific, but near-southerly or near-northerly winds do not often occur, especially equatorward of 25°N where synoptic activity seldom reaches. In terms of ΔT, warm advection occurs twice as often as cold advection around 45°N but much less often around 25°N. This is because ΔT is typically –1 °C over the subtropical ocean under conditions of near-zero advection (and consequently is not a good proxy for cold advection in this region). Since almost all cases are included in either cold or warm advection categories according to ΔT (only $-0.25\ ^\circ\mathrm{C} < \Delta T < 0\ ^\circ\mathrm{C}$ are excluded), this represents a less exclusive standard than that for wind direction.

4.7 Meridional variation associated with cold and warm advection

Figure 4.15 shows typical meteorological conditions over the central North Pacific during summer associated with cold and warm advection inferred from wind direction and ΔT. For the case of advection inferred from wind direction, typical southerly winds at midlatitudes are 6–7 m s^{-1} and typical northerly winds are 5–6 m s^{-1} (Fig. 4.15c). Since northerly winds over the western and central midlatitude North Pacific most likely occur behind a front, subsidence is probably also present. Ascent is likely to be present with southerly winds occurring ahead of a front. ΔT associated with southerly winds exhibits a nearly linear poleward increase (Fig. 4.15a). Although this analysis does not track individual MBL parcel trajectories, this behavior is consistent with increasing near-surface stratification as the MBL is advected northward over decreasing SST. On the other

hand, ΔT associated with northerly winds substantially decreases and then remains relatively constant as the MBL is advected southward over the increasing SST. For the case of advection inferred from ΔT, typical warm-advection ΔT is 1–1.5 °C and typical cold-advection ΔT is –1.5–2 °C (Fig. 4.15b). V associated with warm-advection ΔT is southerly, but V associated with cold-advection ΔT is near-zero (Fig. 4.15d).

The difference between SST associated with cold and warm advection is not the same for advection inferred from wind direction as for ΔT. Figure 4.15a shows that SST is about 0.8 °C greater for southerly winds than for northerly winds, but Fig. 4.15b shows that SST is about 1.5 °C less for warm-advection ΔT than for cold-advection ΔT. Both of these features probably arise from the seasonal variation of wind and SST during JJA. SST over the central North Pacific is less (Fig. 2.12) and northerly winds are more frequent at the beginning of JJA; hence, the meridional profiles of SST displayed in Fig. 4.15a are to some extent sampled from different parts of the summer season. Similarly, ΔT is more frequently positive at the beginning of JJA and more frequently negative at the end of JJA, apparently due to the northward movement of the SST gradient, which has greater effect than the decrease in the frequency of northerly winds over the summer season. The fact that differences between composites in Fig. 4.15 and following figures reflect the seasonal cycle in addition to synoptic variability should not negate the applicability of the results to understanding interannual variability because interannual variations in the SST gradient and synoptic activity resemble seasonal variations.

Figure 4. shows typical MSC amount, Ns FQ, and latent and sensible heat fluxes over the central North Pacific during summer associated with cold and warm advection inferred from wind direction and ΔT. Ns occurs much more frequently with southerly winds than northerly winds (Fig. 4.a), consistent with the results of Lau and Crane (1995, 1997). MSC amount is about 5–10% greater for northerly winds than southerly winds between 30–40°N (Fig. 4.a). However, little difference is seen for compositing on ΔT (Fig. 4.b), probably because low stratiform cloud types contributing to MSC occur with both positive and negative ΔT (Fig. 3.9a). As expected, increased latent and sensible fluxes occur with inferred cold advection and decreased fluxes with inferred warm

advection at midlatitudes.* The difference is about 15–20 W m^{-2} for latent heat flux and about 10–25 W m^{-2} for sensible heat flux between 30–40°N; these fluxes act in the same direction and are larger than the estimated 5–10 W m^{-2} difference in surface downward radiation resulting from the difference in MSC amount. Net surface downward radiation may also differ if low stratiform cloud types associated with cold and warm advection have different optical thicknesses, but it is not possible to investigate this at the present time since no information is available on typical cloud optical thickness or CRF associated with low cloud types identified by the synoptic code.

The meridional variation in cloud amount associated with conditions of inferred cold and warm advection was calculated for warm-advection (Figs. 4.17 and 4.18cd) and cold-advection (Fig. 4.18ab) low cloud types to verify that the association between low cloud type and advection suggested by the OWS observations occurs in general over the central North Pacific during summer. The differences in cloud amount and FQ between conditions of cold and warm advection inferred from ΔT are less than those between conditions of cold and warm advection inferred from wind direction for almost every low cloud type in Figs. 4.17 and 4.18, probably due to the less-strict ΔT criteria. The one exception is fair-weather stratus, perhaps because substantial surface buoyancy flux may quickly transform stratus into stratocumulus. Because wind direction and ΔT imperfectly diagnose advection, cold-advection low cloud types occur a significant amount of the time with inferred "warm advection" and warm-advection low cloud types occur a significant amount of the time with inferred "cold advection".

Figure 4.17a shows that no-low-cloud occurs much more frequently with southerly winds than northerly winds, consistent with increased near-surface stratification resulting from advection over increasingly cold water. The amount of sky-obscuring fog is similarly much greater for southerly winds than for northerly winds (Fig. 4.17c). Fair-weather stratus cloud amount is also slightly greater for southerly winds than for northerly winds between 32.5–40°N, consistent with the transformation from cumulus to stratus near OWS

* Equatorward of 27.5°N, latent heat flux is greater when $\Delta T \geq 0$ °C than when $\Delta T \leq -0.25$ °C because weaker winds occur with the latter.

V suggested by Fig. 3.8, but is less poleward of 40°N (Fig. 4.17c). This latter feature likely represents the lowering of cloud base by southerly flow over cold water which prompts observers to identify sky-obscuring fog instead of stratus; hence, in some situations it may be more appropriate to consider fair-weather stratus and sky-obscuring fog as a single cloud type.

Figure 4.18a shows that both stratocumulus cloud amount and cumulus-with-stratocumulus cloud amount are greater for northerly winds than for southerly winds, consistent with advection over increasingly warm water. Cumulus cloud amount is also greater for northerly flow than for southerly flow (Fig. 4.17a). This suggests subtropical cumulus quickly dissipates as it is advected poleward over colder water, but equatorward advection of midlatitude stratocumulus over warmer water results in decoupling and subsequent breakup into cumulus. Unlike the case for Ns FQ, little difference in bad-weather stratus cloud amount occurs between southerly and northerly flow. Little difference in cumulonimbus cloud amount occurs between southerly and northerly flow at midlatitudes, and perhaps subsidence associated with northerly flow inhibits cumulonimbus in the subtropics.

Relationships between cloud type and advection as inferred from satellite images supporting the preceding results are presented in Figs. 4.19–22.

4.8 Summary and conclusions

The preceding results suggest that the occurrence and geographical distribution of low cloud types over the midlatitude North Pacific during summer are substantially related to advection and the SST gradient, confirming the previous OWS results presented in Chapter 3. Stratocumulus typically occurs with cold advection and subsidence and is prevalent at midlatitudes, but stratocumulus cloud amount is greatest over the eastern subtropics where steady cold advection occurs on the eastern flank of the subtropical anticyclone (Fig. 4.2). Cumulus-with-stratocumulus also typically occurs with cold advection and subsidence, but is less prevalent than stratocumulus at midlatitudes. Maxima in cumulus-with-stratocumulus cloud amount occur over SST

gradient regions equatorward of maxima in stratocumulus cloud amount, both at midlatitudes and in the eastern subtropics (Fig. 4.3). This is consistent with increasing decoupling of the cloud layer from the subcloud layer associated with advection of a deepening MBL over increasing SST (Bretherton 1992; Wyant et al. 1997), as illustrated by Fig. 16 of Norris (1997b) for the climatological transition from stratocumulus to trade cumulus over the eastern subtropical North Pacific. A similar climatological transition from stratocumulus to cumulus-with-stratocumulus to cumulus occurs when a midlatitude MBL is advected equatorward over the stronger and sharper SST gradient in the central North Pacific (Fig. 4.18a) (conceptually illustrated in Fig. 4.13).

Sky-obscuring fog occurs with warm advection and is prevalent at midlatitudes, especially the western North Pacific, but is negligible in the eastern North Pacific except over coastal upwelling regions (Fig. 4.4). Fair-weather stratus also occurs with warm advection and is prevalent at midlatitudes, particularly the central North Pacific (Fig. 4.5). Some fair-weather stratus occurs over the eastern subtropical ocean near the coast, but has MBL structure more related to stratocumulus (Lilly 1968) than stratus at midlatitudes (Fig. 3.7). A climatological transition from cumulus to no-low-cloud to shallow fair-weather stratus occurs when a subtropical MBL is advected poleward over the strong SST gradient in the central North Pacific (Fig. 4.17ac), consistent with increasing near-surface stratification produced by decreasing SST (Fig. 3.8). Subsequent poleward advection transforms the shallow stratus layer to sky-obscuring fog (Fig. 3.6) or a deep stratus layer (Fig. 3.7) (conceptually illustrated in Fig. 4.12). Bad-weather stratus occurs with warm advection and strong ascent along the storm track across the midlatitude North Pacific (Figs. 4.6), but makes a lesser contribution to MSC amount than do the other low stratiform cloud types.

Ns FQ is much greater for southerly winds, which are likely to occur ahead of a front, than for northerly winds, which are likely to occur with subsidence behind a front. Because low stratiform cloud types occur with both cold and warm advection, MSC amount does not greatly vary with advection. However, greater MSC amount occurs over the SST gradient region with northerly winds than with southerly winds due to the greater

frequency of occurrence of stratocumulus types and lesser frequency of occurrence of no-low-cloud. Less MSC amount occurs poleward of 42.5°N with northerly winds than with southerly winds because stratocumulus types with AWP < 100% are replaced with sky-obscuring fog with AWP = 100%. In addition to changing MSC amount, replacement of one low stratiform cloud type by another may change cloud optical thickness, but this cannot be assessed at the present time. Surface downward radiation is estimated to be 5–10 W m^{-2} less for northerly winds than for southerly winds, compared to an estimated 25–45 W m^{-2} more in combined latent and sensible heat fluxes for northerly winds than for southerly winds.

The fact that the direction of advection, particularly over the SST gradient, is an important factor determining low cloud type provides a foundation for understanding coupled interannual variability in MSC, SST, and atmospheric circulation. Variability in SST causes meridional shifts in the location of the SST gradient, and variability in the location and strength of synoptic activity causes changes in vertical motion and the frequency of poleward and equatorward advection. Hence, SST anomalies likely produce meridional shifts in the location of cloud type transitions, and anomalies in synoptic activity likely produce changes in the relative frequency of cloud types associated with cold advection and subsidence and warm advection and ascent. These hypotheses will be examined in the next chapter, along with the potential for feedbacks on SST.

Table 4.1: Percentage of the interannual variance of seasonal-mean $\boldsymbol{V} \cdot \nabla \mathrm{SST}$ averaged over 35–40°N, 150°E–150°W explained by various terms. v and y are in the meridional direction, u and x in the zonal direction, and the overbar signifies the climatological mean.

$v\frac{\partial \overline{\mathrm{SST}}}{\partial y}$	$\bar{v}\frac{\partial \mathrm{SST}}{\partial y}$	$u\frac{\partial \mathrm{SST}}{\partial x}$
61	22	4

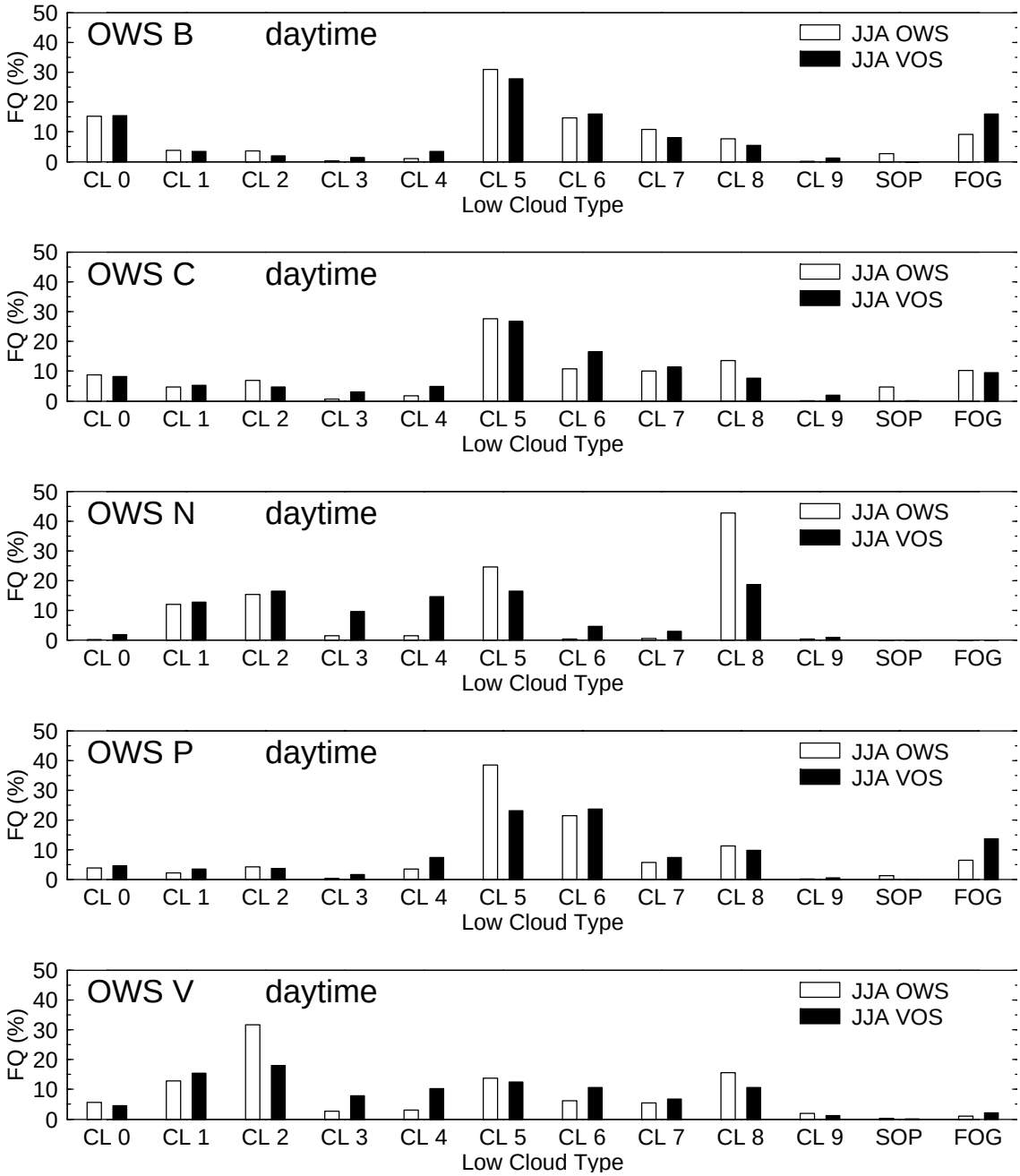

Figure 4.1: Daytime FQ of the low cloud types described in Table 3.2 along with sky-obscuring precipitation (SOP) and sky-obscuring fog (FOG) for OWS B, C, N, P, and V and nearby VOS during JJA. VOS observations are from a 2° x 2° box centered on the OWS. Both OWS and VOS data are from the time period 1954–1972. Color coding of bars: white - OWS; black - VOS.

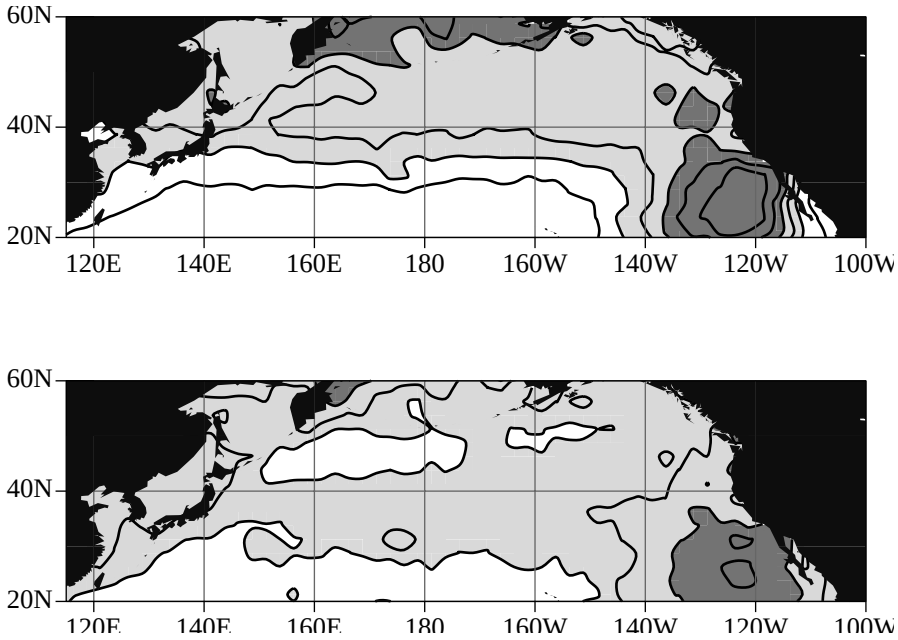

Figure 4.2: (Top) Climatological daytime stratocumulus (C_L 5) cloud amount during JJA. Contour interval is 5%. Shading indicates amounts above 10% (light) and 20% (dark). (Bottom) Percentage contribution by stratocumulus to daytime MSC amount during JJA. Contour interval is 10%. Shading indicates contributions above 20% (light) and 40% (dark).

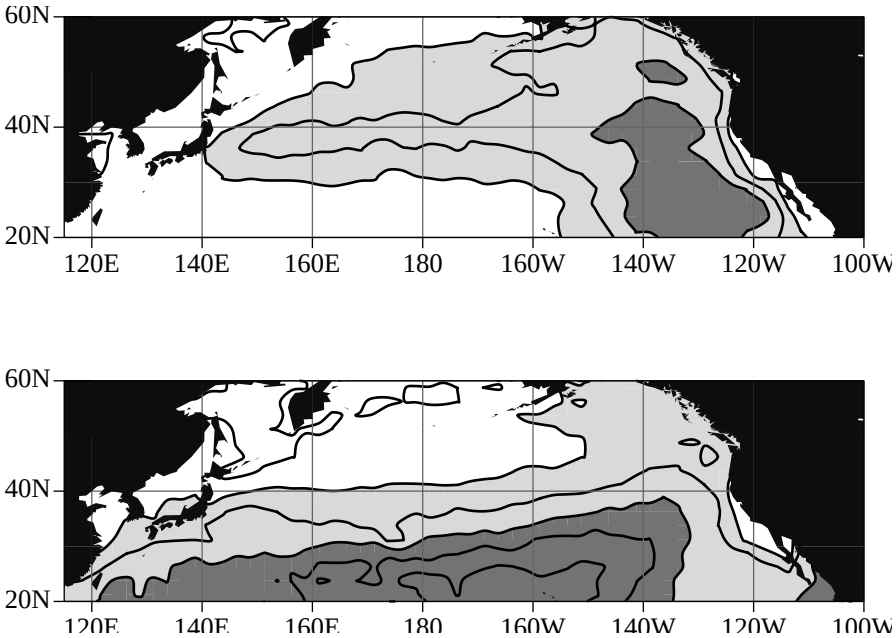

Figure 4.3: As in Fig. 4.2, except for cumulus-with-stratocumulus (C_L 4 + 8).

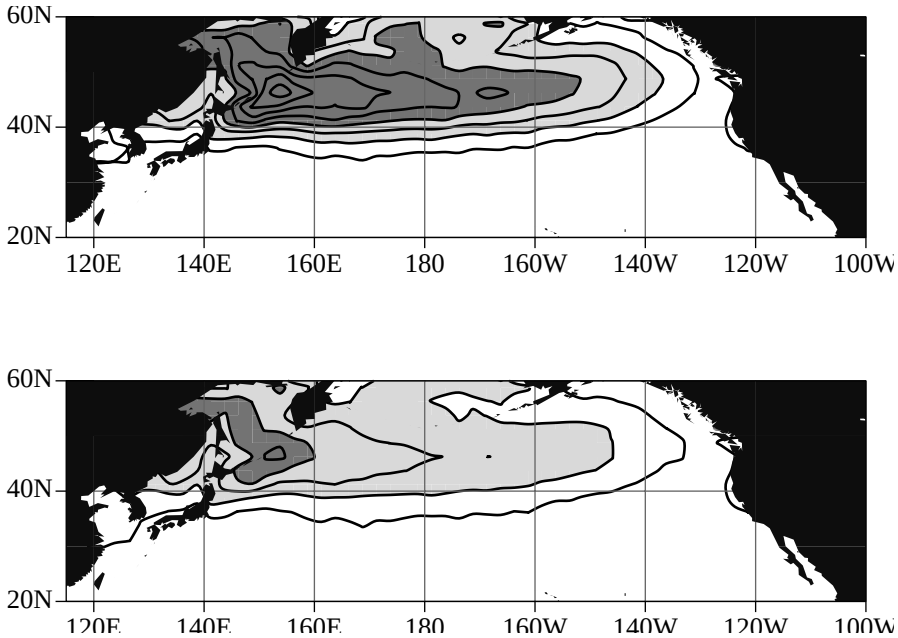

Figure 4.4: As in Fig. 4.2, except for sky-obscuring fog and precipitation.

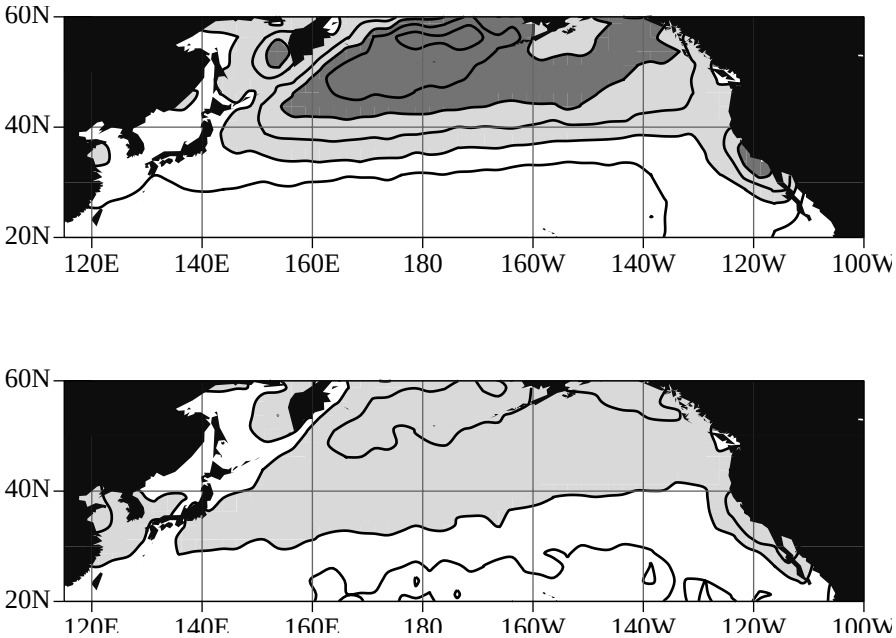

Figure 4.5: As in Fig. 4.2, except for fair-weather stratus (C_L 6).

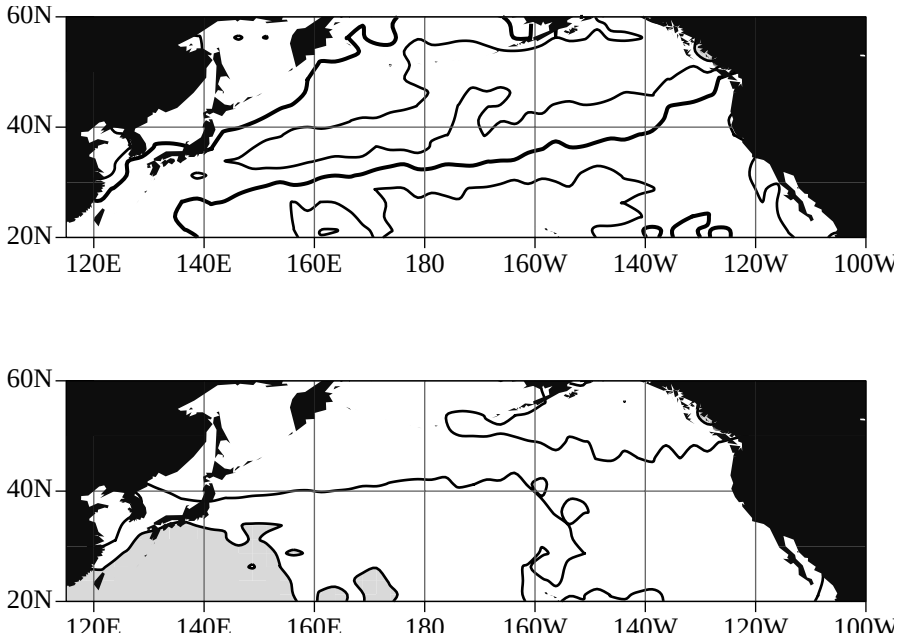

Figure 4.6: As in Fig. 4.2, except for bad-weather stratus (C_L 7) with contours for cloud amount at every 2.5% and the 5% contour thickened.

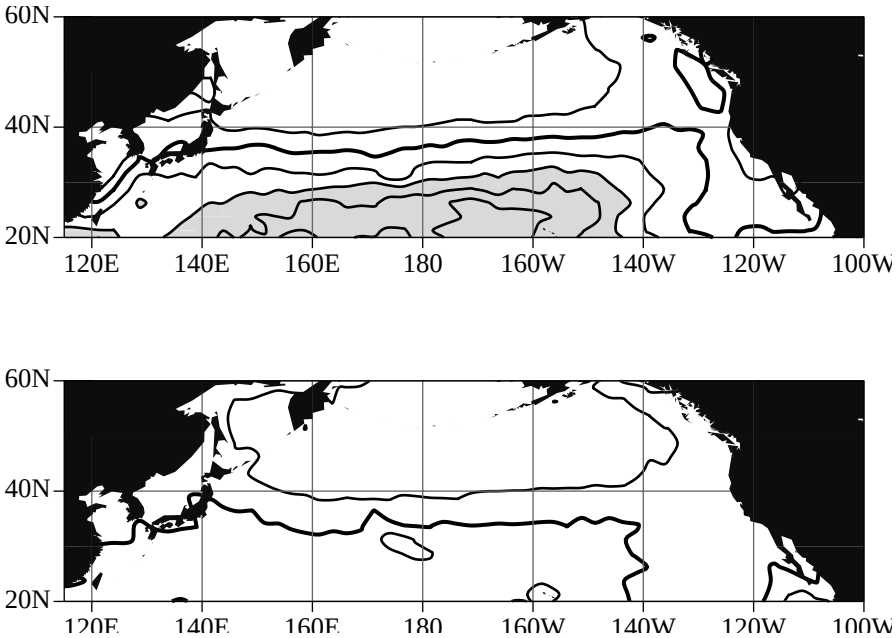

Figure 4.7: Climatological daytime moderate and large cumulus (C_L 2) cloud amount (top) and small cumulus (C_L 1) cloud amount (bottom) during JJA. Contour interval is 2.5%. Shading indicates amounts above 10% (light) and the 5% contour is thickened.

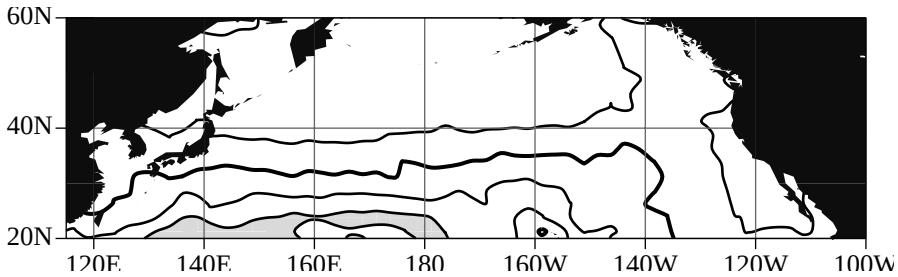

Figure 4.8: As in Fig. 4.7, except for cumulonimbus (C_L 3+9).

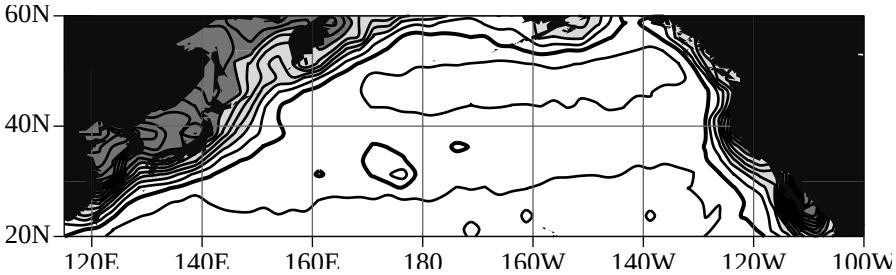

Figure 4.9: Climatological daytime FQ of no-low-cloud (C_L 0) during JJA. Contour interval is 2.5%. Shading indicates amounts above 10% (light) and the 5% contour is thickened.

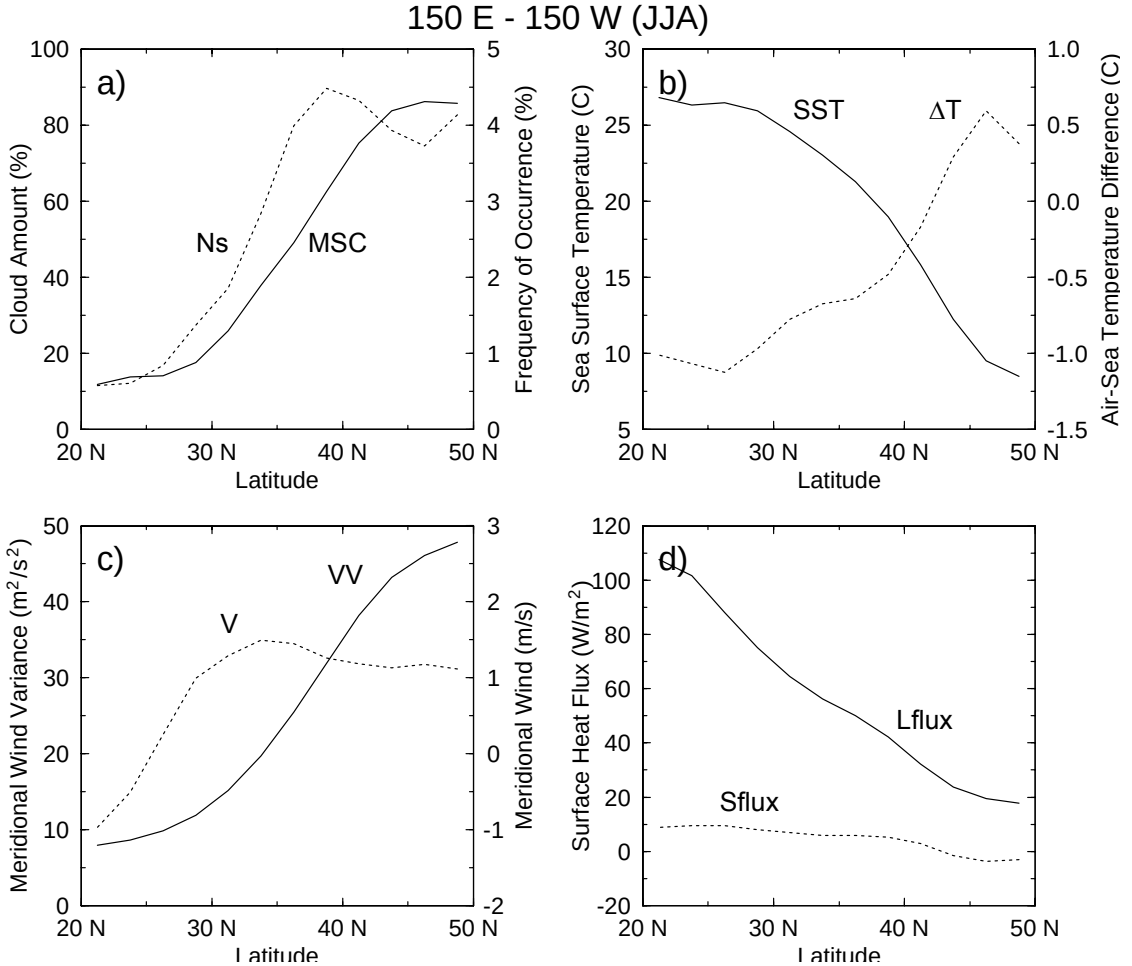

Figure 4.10: (a) Meridional profile of climatological daytime MSC amount (solid) and Ns FQ (dotted) zonally averaged over 150°E–150°W in the North Pacific during JJA. (b) As in (a), except for SST (solid) and nighttime ΔT (dotted). (c) As in (a), except for VV (solid) and V (dotted). (d) As in (a), except for nighttime latent heat flux (solid) and nighttime sensible heat flux (dotted).

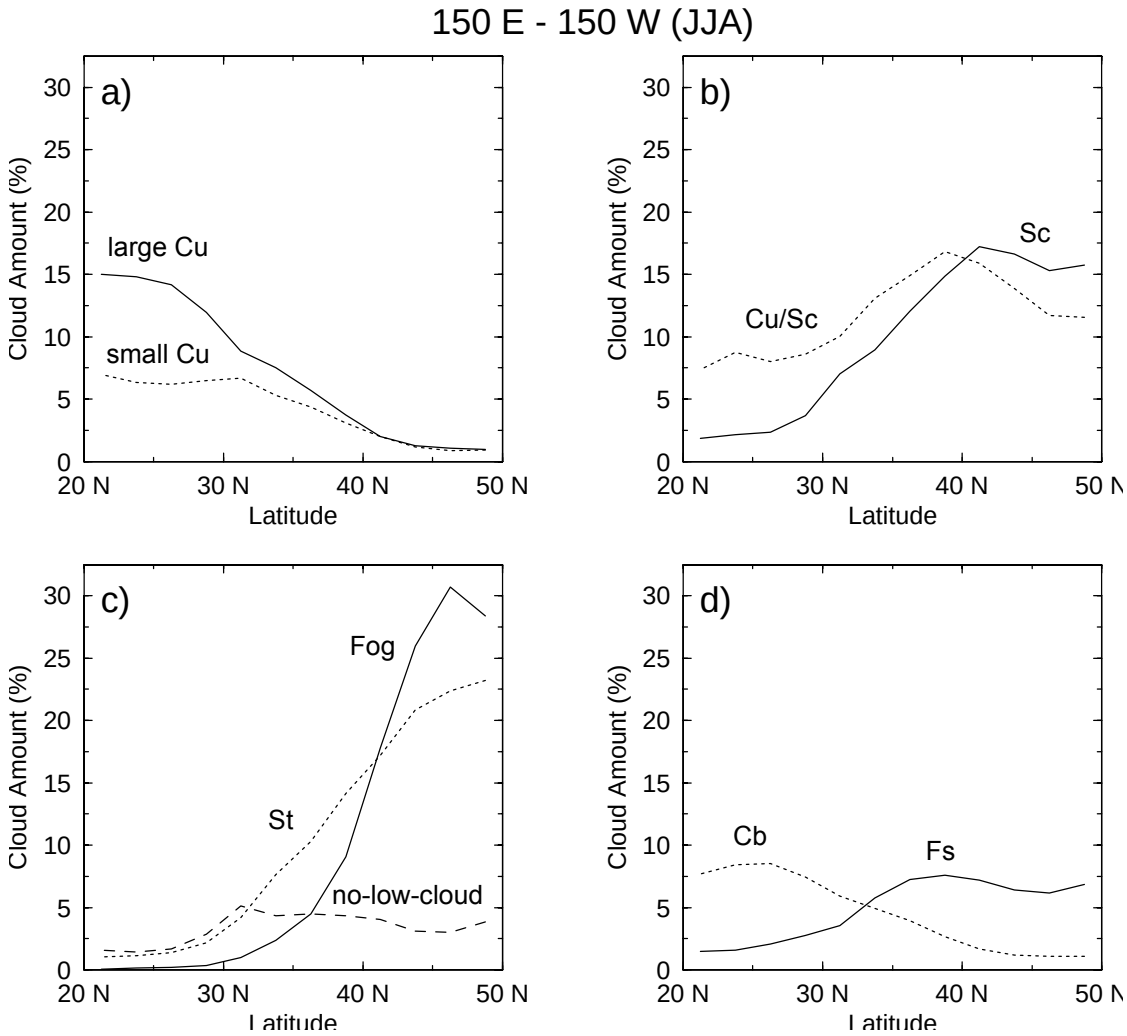

Figure 4.11: (a) As in Fig. 4.10a, except for moderate and large cumulus (C_L 2) cloud amount (solid) and small cumulus (C_L 1) cloud amount (dotted). (b) As in (a), except for stratocumulus (C_L 5) (solid) and cumulus-with-stratocumulus (C_L 4+8) (dotted). (c) As in (a), except for sky-obscuring fog (solid), fair-weather stratus (C_L 6) (dotted), and no-low-cloud (C_L 0) FQ (in same units as cloud amount) (dashed). (d) As in (a), except for bad-weather stratus (C_L 7) (solid) and cumulonimbus (C_L 3+9) (dotted). All values are for daytime only.

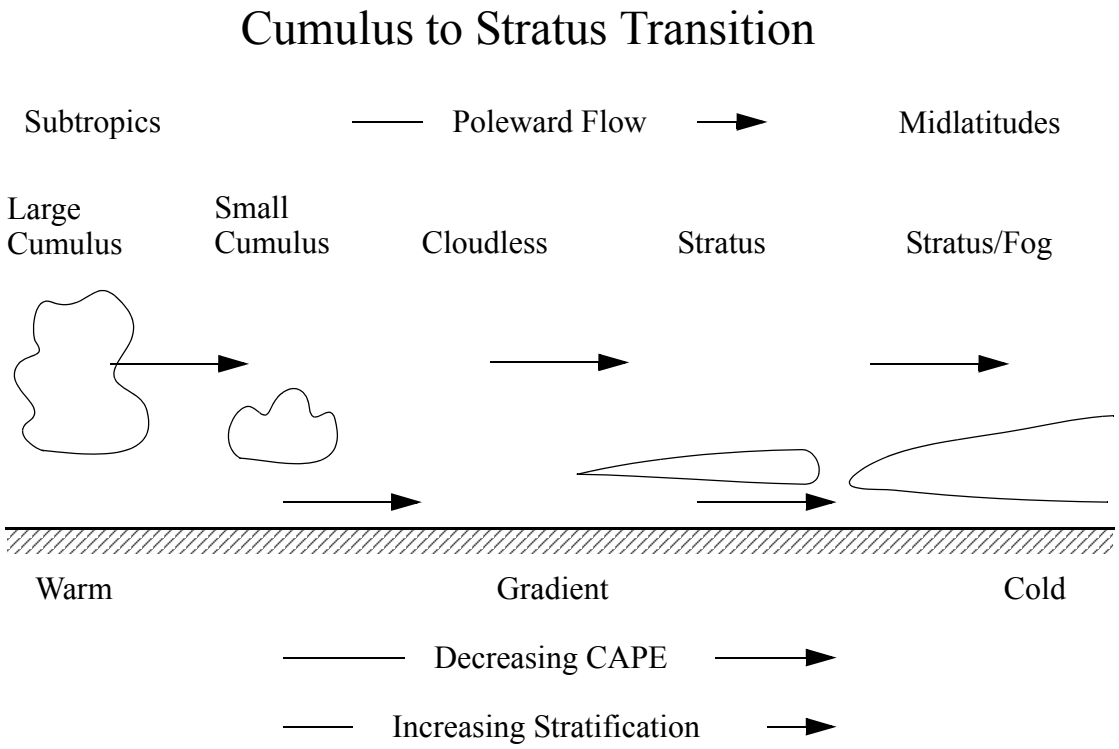

Figure 4.12: Conceptual model illustrating the cumulus-to-stratus transition.

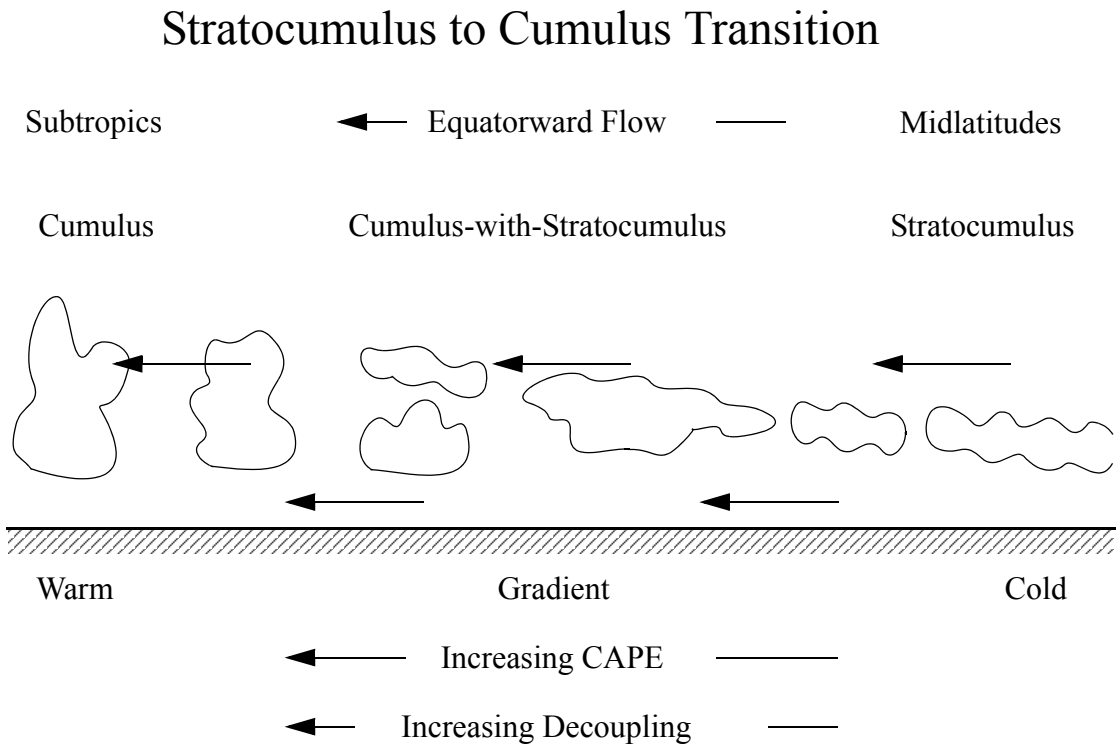

Figure 4.13: Conceptual model illustrating the stratocumulus-to-cumulus transition [adopted from the conceptual model of Bretherton (1992) and Wyant et al. (1997) for the transition from stratocumulus to trade cumulus in the eastern subtropical ocean].

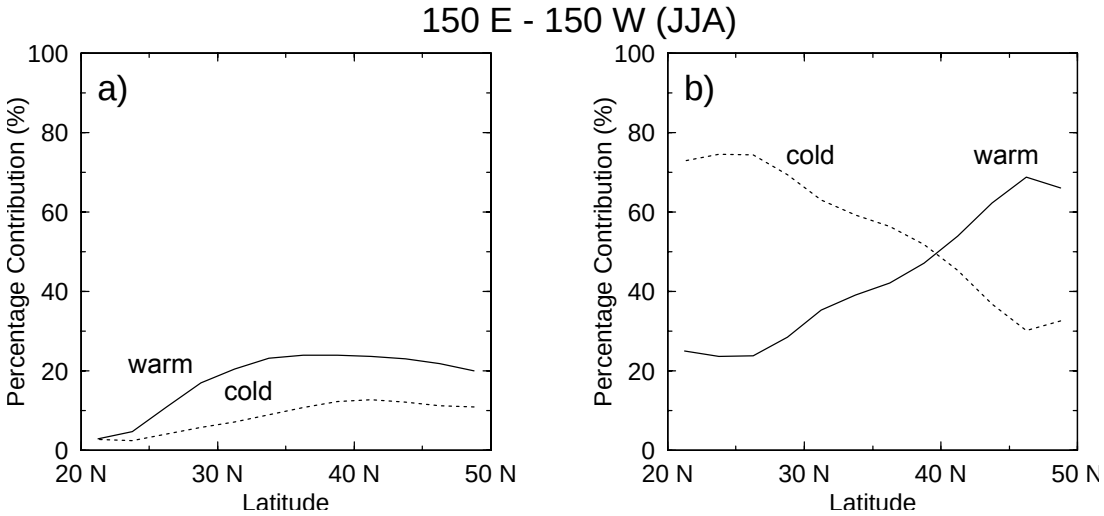

Figure 4.14: Percentage contribution of warm advection cases (solid) and cold advection cases (dotted) to all cases for advection inferred from wind direction (a) and nighttime ΔT (b).

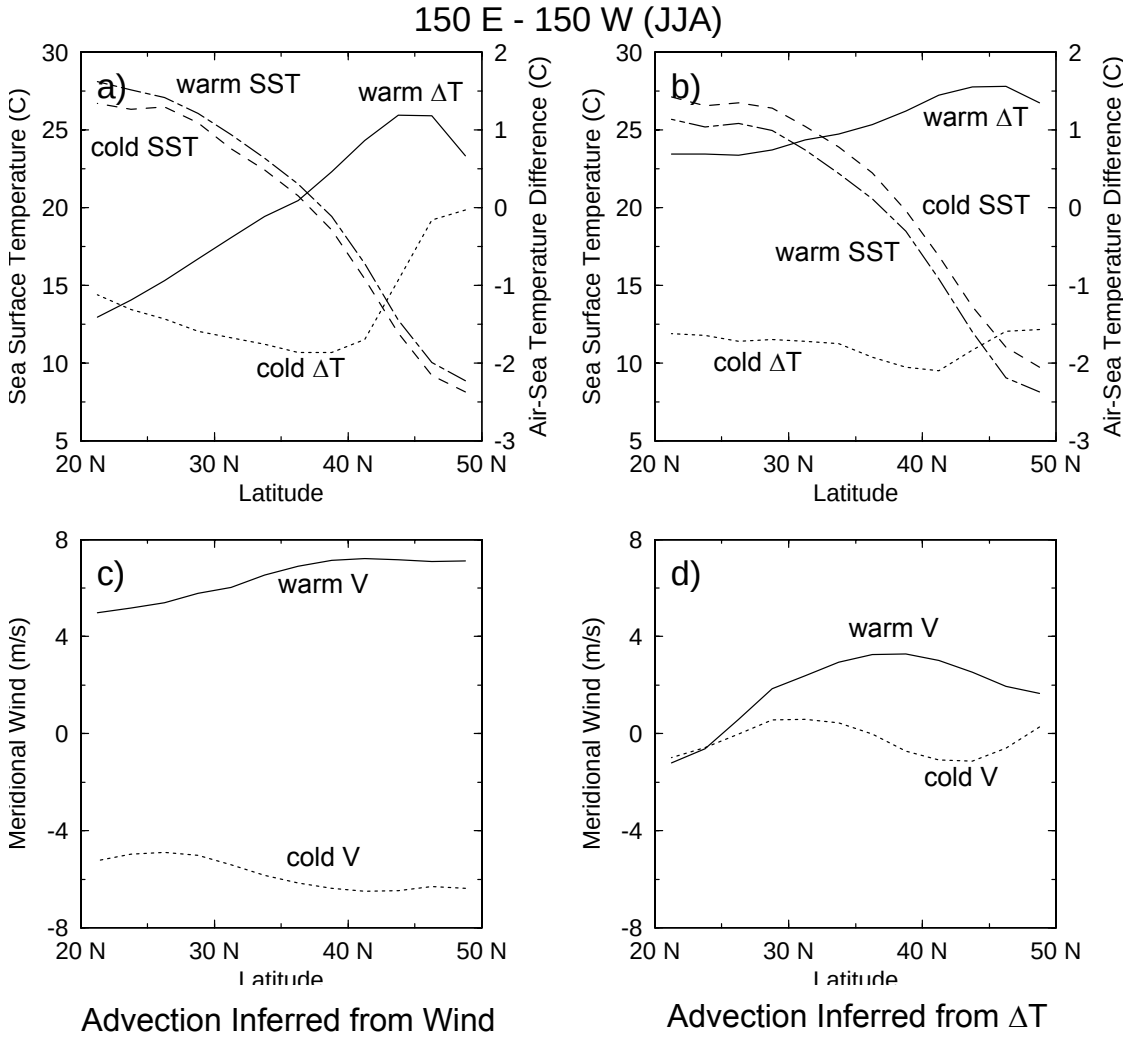

Figure 4.15: (a) Meridional profiles of climatological ΔT associated with warm (solid) and cold (dotted) advection and SST associated with warm (dot-dash) and cold (dashed) advection inferred from wind direction zonally averaged over 150°E–150°W in the North Pacific during JJA. (b) As in (a), except for advection inferred from ΔT. (c) As in (a), except for V associated with warm (solid) and cold (dotted) advection. (d) As in (c) except for advection inferred from ΔT. Values for ΔT and advection inferred from ΔT are for nighttime only.

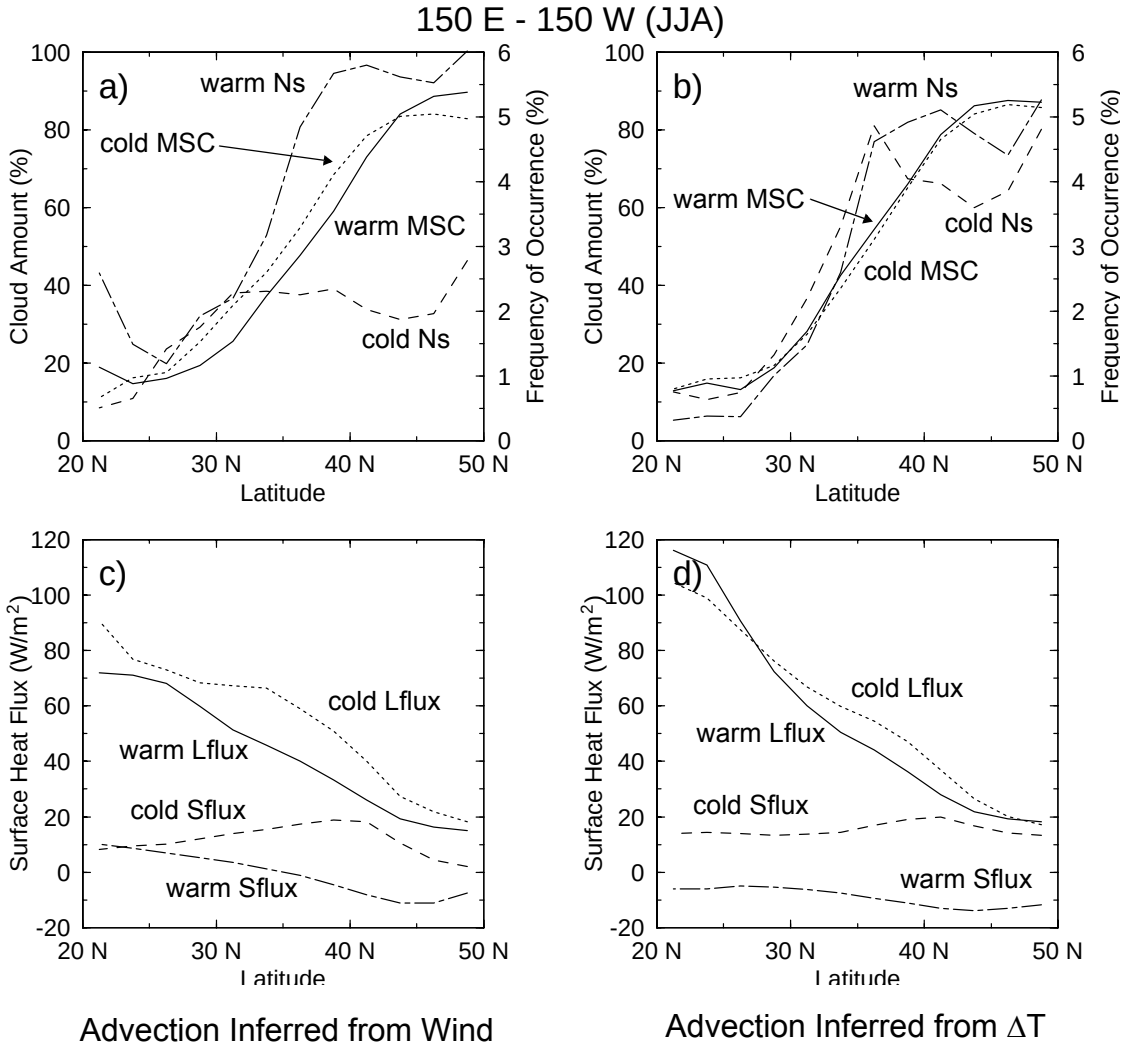

Figure 4.16: (a) As in Fig. 4.15a, except for MSC amount associated with warm (solid) and cold (dotted) advection and Ns FQ associated with warm (dot-dash) and cold (dashed) advection. (b) As in (a), except for advection inferred from ΔT. (c) As in (a), except for nighttime latent heat flux associated with warm (solid) and cold (dotted) advection and nighttime sensible heat flux associated with warm (dot-dash) and cold (dashed) advection. (d) As in (c) except for advection inferred from ΔT. Cloud values for advection inferred from ΔT are for nighttime good illumination conditions only; otherwise daytime only.

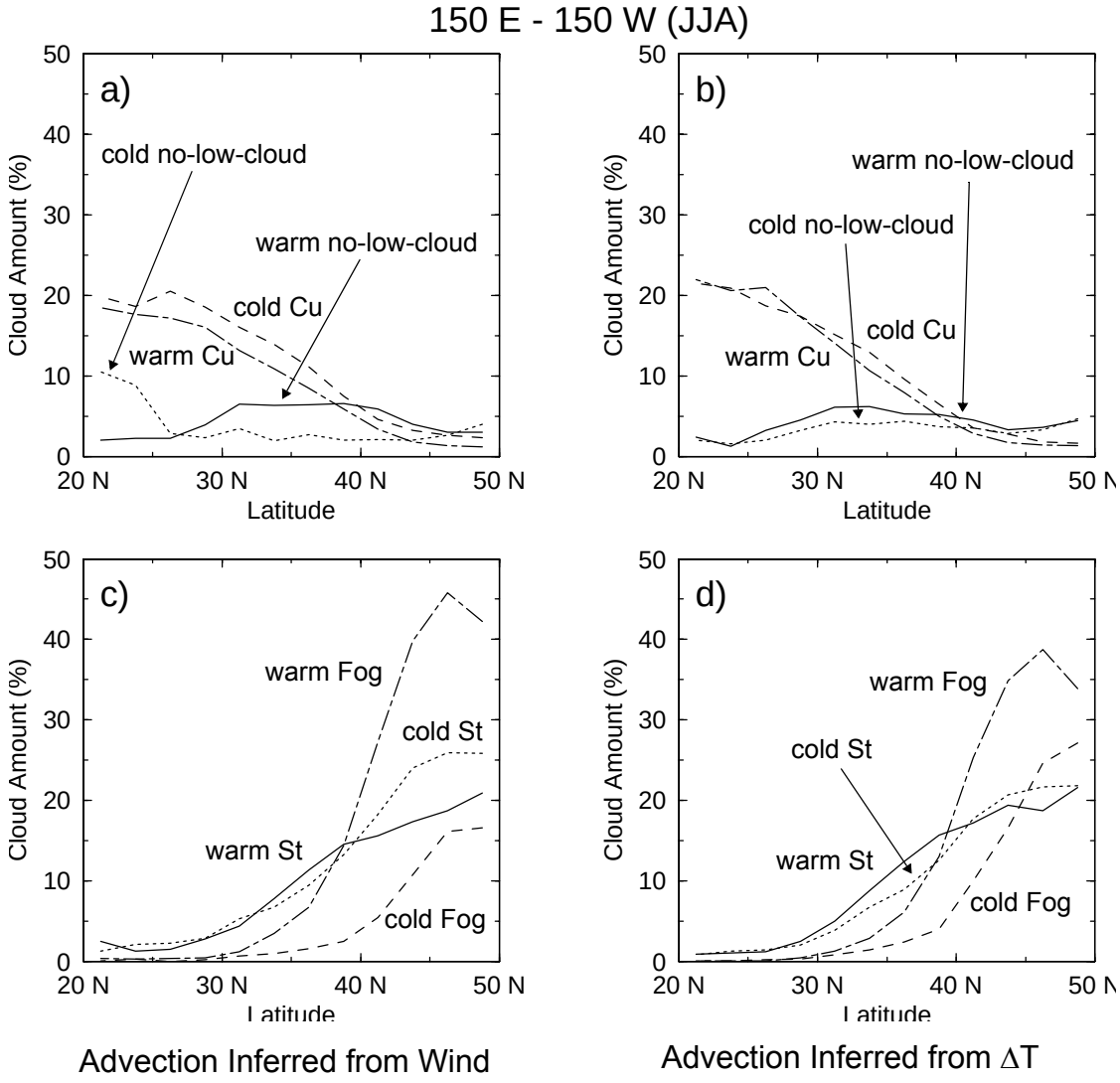

Figure 4.17: (a) As in Fig. 4.15a, except for no-low-cloud (C_L 0) FQ (in same units as cloud amount) associated with warm (solid) and cold (dotted) advection and cumulus (C_L 1+2) cloud amount associated with warm (dot-dash) and cold (dashed) advection. (b) As in (a), except for advection inferred from ΔT. (c) As in (a), except for fair-weather stratus (C_L 6) cloud amount associated with warm (solid) and cold (dotted) advection and amount of sky-obscuring fog associated with warm (dot-dash) and cold (dashed) advection. (d) As in (c) except for advection inferred from ΔT. Cloud values for advection inferred from ΔT are for nighttime good illumination conditions only; otherwise daytime only.

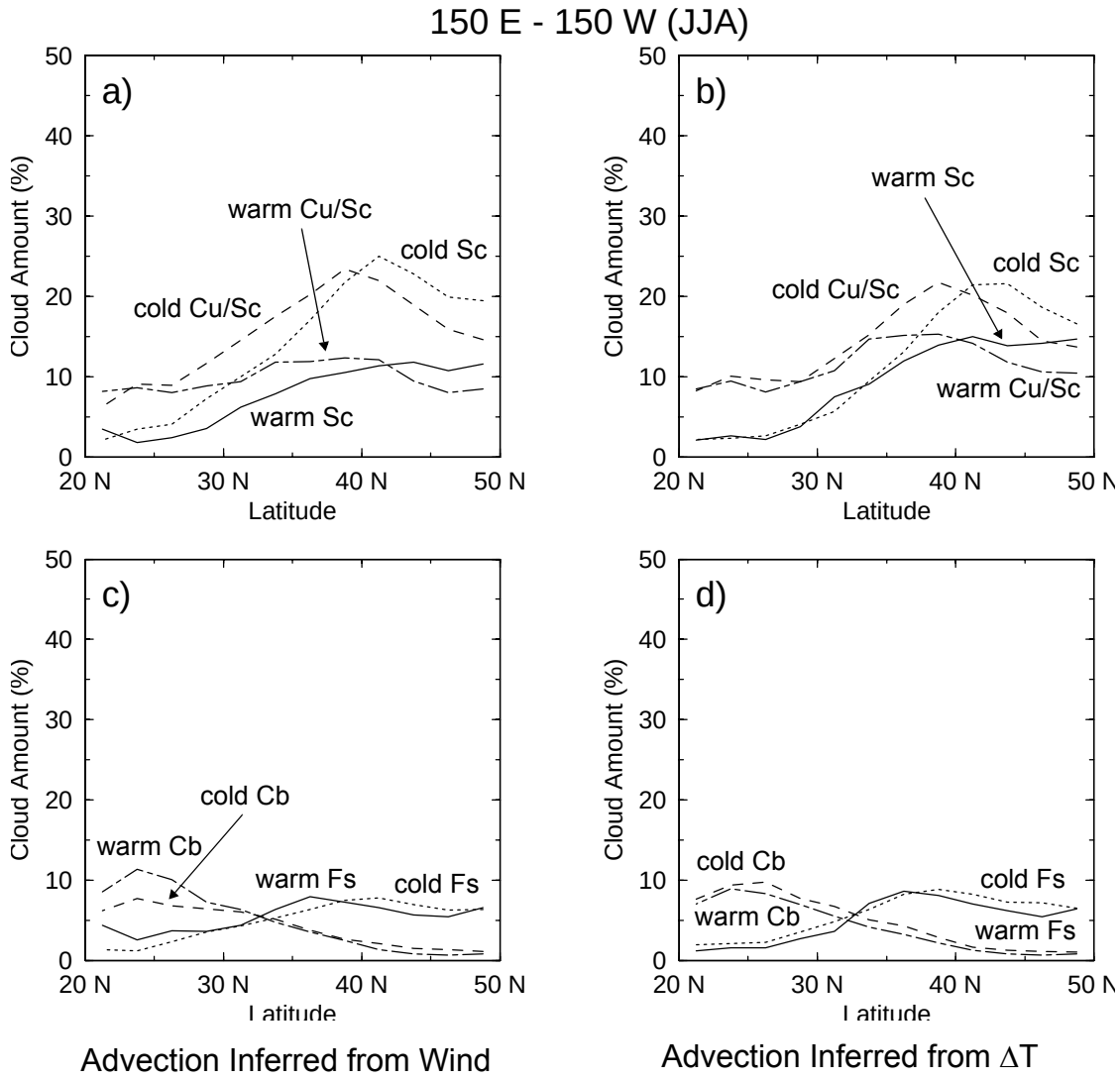

Figure 4.18: (a) As in Fig. 4.15a, except for stratocumulus (C_L 5) cloud amount associated with warm (solid) and cold (dotted) advection and cumulus-under stratocumulus (C_L 4+8) cloud amount associated with warm (dot-dash) and cold (dashed) advection. (b) As in (a), except for advection inferred from ΔT. (c) As in (a), except for bad-weather stratus (C_L 7) cloud amount associated with warm (solid) and cold (dotted) advection and cumulonimbus (C_L 3+9) cloud amount associated with warm (dot-dash) and cold (dashed) advection. (d) As in (c) except for advection inferred from ΔT. Cloud values for advection inferred from ΔT are for nighttime good illumination conditions only; otherwise daytime only.

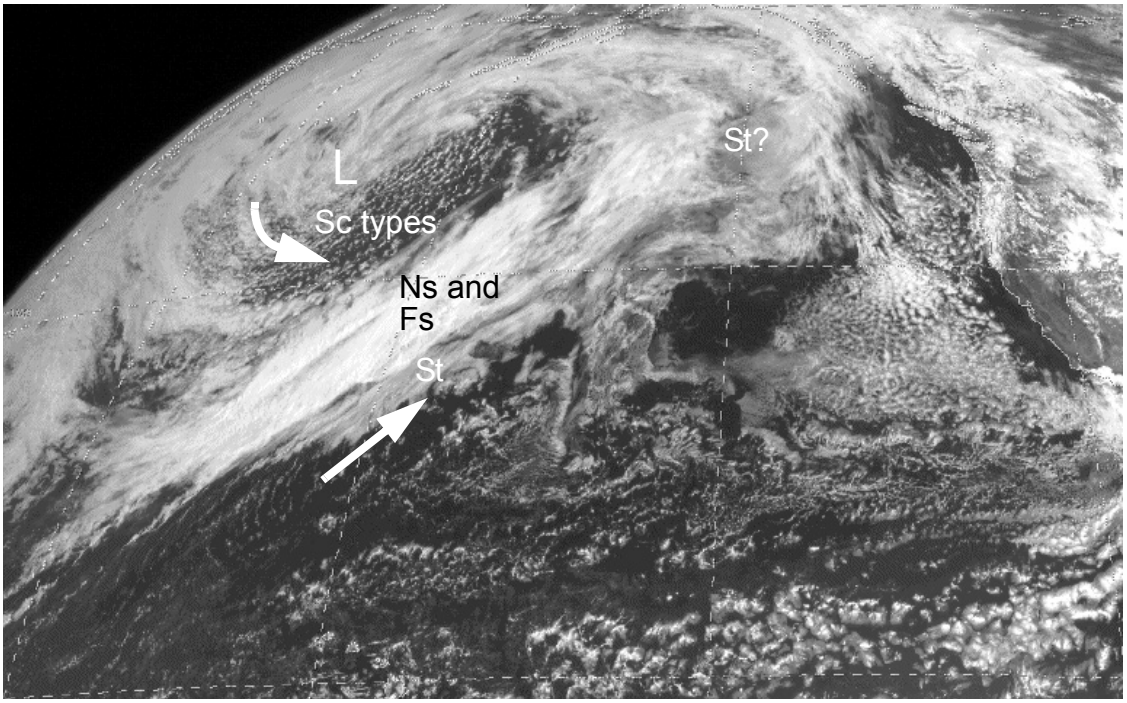

Figure 4.19: GOES-W satellite image for 20 UTC on June 12, 1997 (4 km resolution). Arrows indicate low cloud motion obtained from the satellite loop; inferred cloud type and the location of the low center are marked. Note how stratocumulus types occur in the cold advection region behind the front whereas fair-weather stratus occurs in the warm advection region ahead of the front.

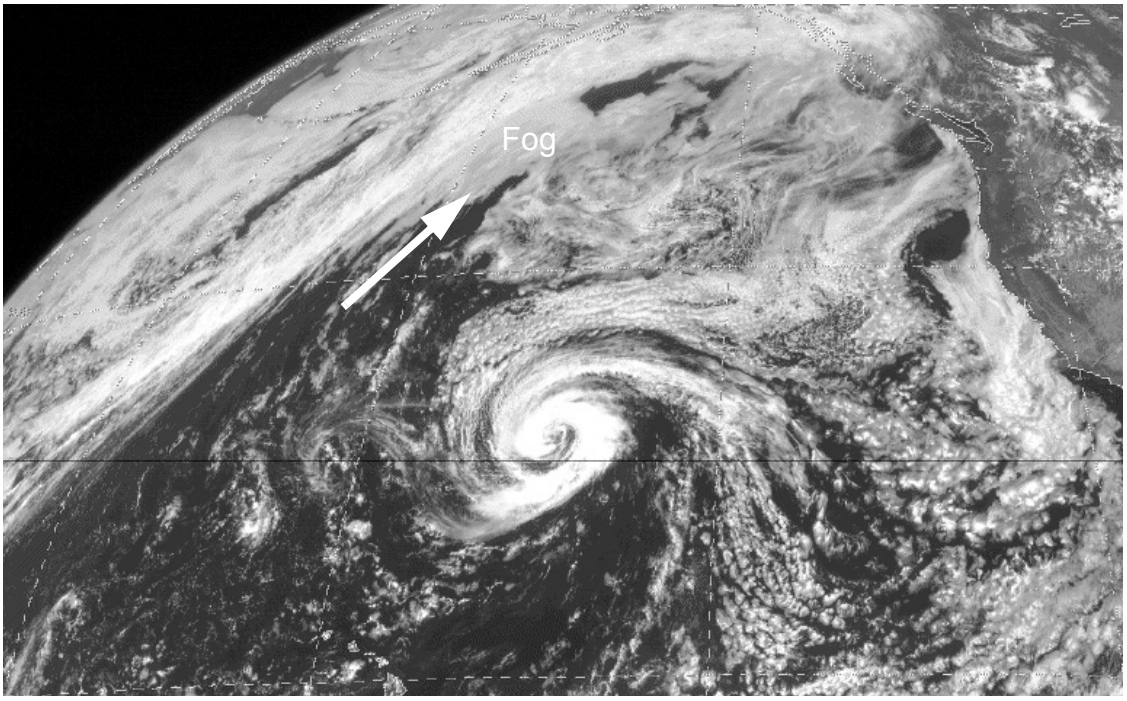

Figure 4.20: GOES-W satellite image for 22 UTC on August 12, 1997 (4 km resolution). Arrows indicate low cloud motion obtained from the satellite loop; inferred cloud type is marked. Note the large area of fog (perhaps fair-weather stratus?) ahead of the front and the generally cloudless region equatorward of it.

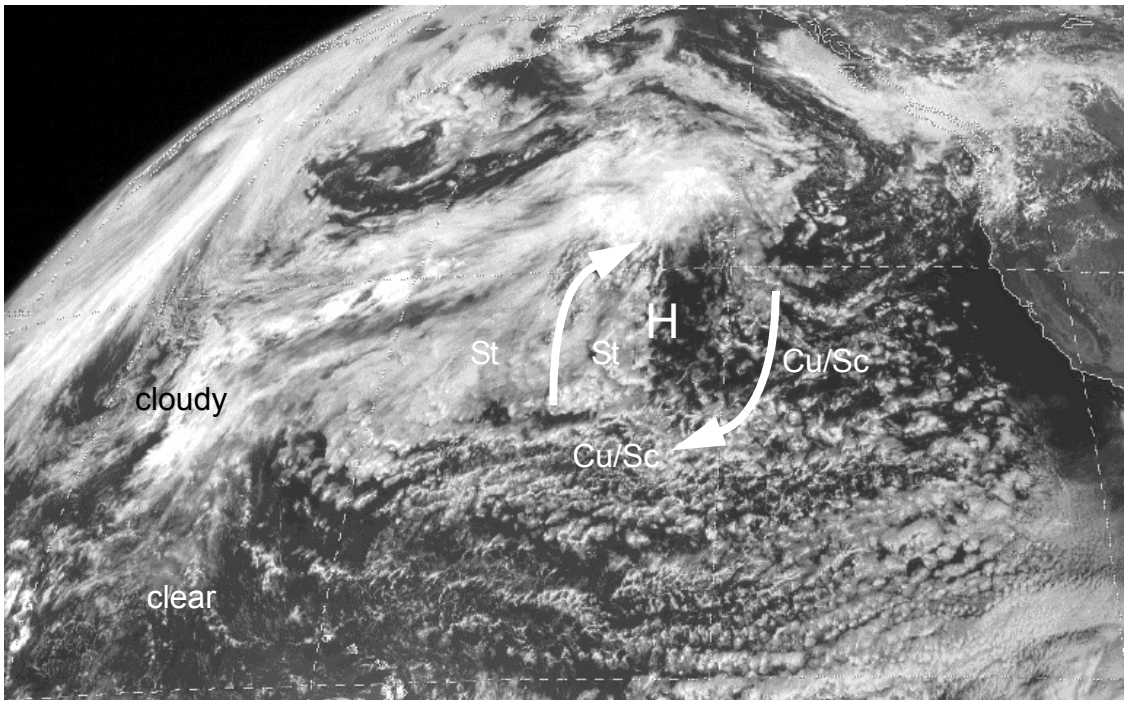

Figure 4.21: GOES-W satellite image for 00 UTC on June 23, 1997 (4 km resolution). Arrows indicate low cloud motion obtained from the satellite loop; inferred cloud type and the location of the subtropical anticyclone are marked. Note the apparent mixture of fair-weather stratus with mesoscale stratocumulus elements southwest of the anticyclone, suggesting that stratocumulus on the eastern flank of the cyclone has been advected around to the western flank of the anticyclone and is now undergoing transformation into stratus as a result of poleward advection over decreasing SST. Also note that much of the stratocumulus cover of the cumulus-with-stratocumulus has dissipated during the afternoon whereas the fair-weather stratus has not (although some thinning may have occurred). Finally, note the distinction between the cloudy midlatitudes and less cloudy subtropics apparent in the central North Pacific; the division occurs around the latitude of the SST gradient.

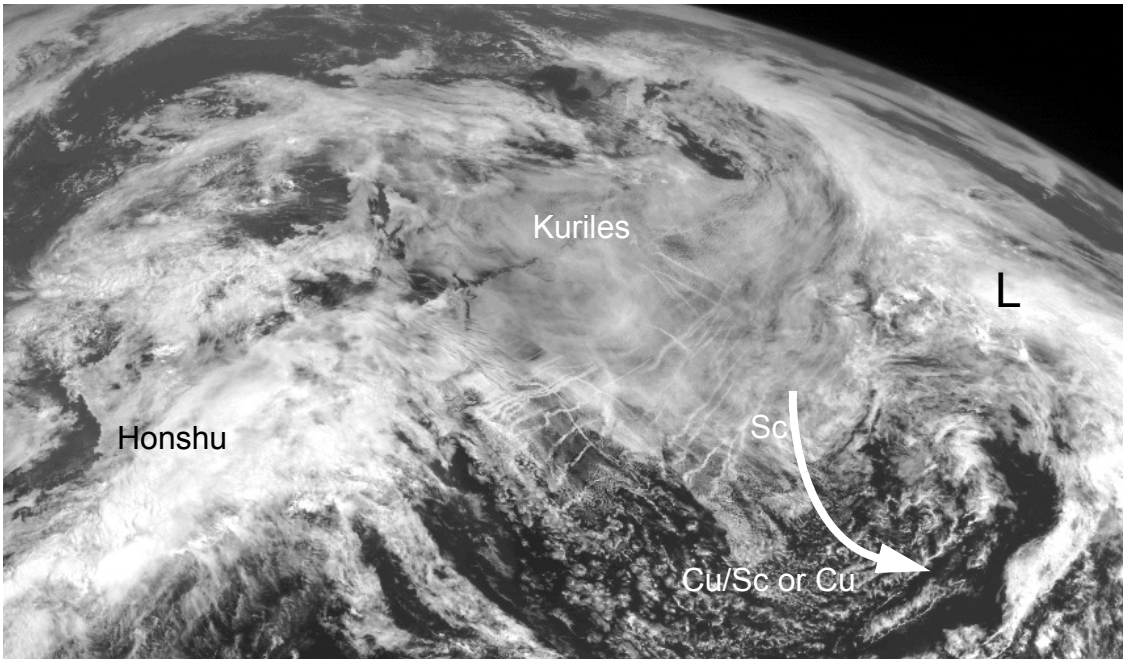

Figure 4.22: GMS satellite image for 01 UTC on June 19, 1993 (8 km resolution) (provided by S. Klein). Arrows indicate low cloud motion obtained from the satellite loop; inferred cloud type and the location of the low center are marked. Note how stratocumulus in the cold advection region behind the front breaks up as it passes over the approximate latitude of the SST gradient.

CHAPTER 5

Processes Responsible for Interannual Variability in Cloudiness and Sea Surface Temperature over the Summertime Midlatitude North Pacific

5.1 Introduction

The previous chapter documented the climatological distributions of the amounts of low cloud types over the midlatitude North Pacific during summer, along with the relative contribution of low stratiform clouds types to MSC amount. Climatological transitions in low cloud type occurring over the SST gradient in the central North Pacific were investigated by examining meridional variations of zonally-averaged cloud and meteorological parameters. The associations between inferred advection and cloud type observed in Chapter 3 were confirmed by zonally averaging cloud and meteorological parameters separately for conditions of northerly or southerly wind and $\Delta T \leq -0.25$ °C or $\Delta T \geq 0$ °C over the central North Pacific. Stratocumulus, cumulus-with-stratocumulus, and cumulus cloud amounts were found to be greater for northerly winds, and combined sky-obscuring fog and fair-weather stratus cloud amount and no-low-cloud FQ were found to be greater for southerly winds. Because low stratiform cloud types occur with both cold and warm advection, MSC amount over the SST gradient region is only slightly greater for northerly winds than for southerly winds. Although the climatological meridional variation of latent heat flux between 30–40°N is comparable to the estimated reduction in downward surface radiative flux due to the meridional variation of MSC amount, the difference in latent heat flux between conditions of northerly winds and southerly winds is much greater than the difference in estimated downward surface radiative flux due to differing MSC amount.

The locations of maximum climatological stratocumulus, cumulus-with-stratocumulus, and cumulus cloud amounts were found to occur progressively equatorward, particularly for conditions of inferred cold advection. This is consistent

with increasing decoupling of the cloud layer from the subcloud layer in an inversion-capped MBL as it is advected over increasing SST (conceptually illustrated in Fig. 4.13). The locations of maximum moderate and large cumulus cloud amount, small cumulus cloud amount, no-low-cloud FQ, and combined sky-obscuring fog and fair-weather stratus cloud amount were found to occur progressively poleward, particularly for conditions of inferred warm advection. This is consistent with decreasing CAPE and increasing near-surface stratification associated with advection over decreasing SST (conceptually illustrated in Fig. 4.12).

These results suggest that meridional shifts in the SST gradient will produce meridional shifts in the location of low cloud type transitions, and that changes in the frequency of northerly and southerly winds will produce changes in the frequency of cold-advection and warm-advection low cloud types. Variations in the strength of synoptic activity will also produce variations in the frequency of low cloud types associated with subsidence and the strength of ascent. The present chapter examines year-to-year meridional co-variability of MSC, midlevel stratiform cloudiness, SST, seasonal-mean atmospheric circulation, and synoptic activity over the central North Pacific. The specific processes by which interannual variability in SST and synoptic activity produce meridional changes in MSC are examined by regressing meteorological parameters and cloud amount of low cloud types on variability in SST and VV over the region of strong SST gradient. The potential for cloud feedbacks on SST is examined, along with a comparison with other processes which modify SST.

5.2 Interannual meridional co-variability over the central North Pacific

Chapter 2 showed that coupled interannual variability in SST, MSC, Ns FQ, and VV over the central North Pacific was primarily composed of meridional shifts in the region of strong SST gradient, cloud gradient, and storm track location. In order to more closely examine this co-variability, SVD analysis was performed on interannual anomalies of summertime (JJA) MSC amount, Ns FQ, SST, SLP, and VV zonally averaged between 150°E–150°W at 2.5° resolution between 20–50°N, as described in Section 4.4. These are

the same parameters which were analyzed in Chapter 2, except SST and SLP were obtained from the EECRA instead of the GOSTA and Trenberth SLP datasets. As was done in Chapter 2, data from 1987 were excluded from analyses involving VV because of the unrealistically high values of VV that year. Because zonal averages of SLP cannot describe circulation in the meridional direction, interannual anomalies of summertime V obtained from the EECRA were also analyzed.

Simple averaging of all observations into 2.5° x 60° grid boxes was justified in Chapter 4 by the fact that zonal variations of the parameters are small between 150°E–150°W; however, this is not the case for SLP and related parameters. Because it is possible that changes in spatial sampling in the presence of a climatological gradient could produce spurious variability, SVD analysis was performed on Trenberth SLP aggregated from 5° x 10° grid boxes to 5° x 60° grid boxes. The results were almost identical to those obtained from EECRA SLP averaged to 2.5° x 60° grid boxes, indicating that spatial sampling biases are minimal, probably because most long-term variation in spatial sampling over the central North Pacific occurs in the meridional instead of zonal direction.

Table 5.1 documents the summary statistics associated with the SVD analyses and includes the same parameter pairs listed in Table 2.2 with the addition of V. The much-higher values of SCF and NC in Table 5.1 compared to those in Table 2.2 are the result of 12 instead of 57 gridpoints contributing to the analysis. For this reason, *r* is likely to be the best measure of the strength of coupling between two fields, and for simplicity of presentation, statistics for SVD pairs in Table 5.1 are listed in order of decreasing *r*. As was the case for the basin-wide SVD analyses presented in Chapter 2, the strongest relationships are between MSC amount, Ns FQ, and SST, where increased (decreased) MSC amount and Ns FQ are associated with decreased (increased) SST between 30–45°N (not shown). Other SVD pairs had weaker coupling, although the associated patterns were generally consistent with expected physical processes (not shown).

As discussed in Chapter 2, the presence of significant long-term trends in several of the parameters brings into question whether apparent coupling between SVD pairs might

only result from the trends and not variability at higher frequencies. Furthermore, Bajuk and Leovy (1997b) show that substantial variations in the frequency of identification of various low cloud types over the ocean have occurred between 1952–1992. Substantial spurious variations also occur in the frequency of identification of sky-obscured (N = 9) and clear sky (N = 0), along with increasing trends in total cloud cover (N) and cloud cover of the lowest layer (N_h) (Norris 1997c). These probably do not greatly affect calculations involving MSC because variations in MSC amount are dominated by variations in MSC FQ, which has minimal spurious variability since changes in the frequency of identification of one contributing low stratiform cloud type are likely compensated by changes in the frequency of identification of other contributing low stratiform cloud types. Calculations involving Ns FQ are probably also not greatly affected because Ns is identified by the presence of rain or snow, and the small amount of apparent spurious variability in the frequency of precipitation over the ocean (Petty 1995) does not resemble the time series associated with the leading EOF of interannual variability in Ns FQ over the North Pacific during summer (Fig. 2.5).

The wind speed data also suffer from spurious interdecadal variability. An upward trend in wind speed over the ocean has been observed since 1950, which is attributed to increasing use of anemometers to measure wind speed instead of estimations from sea-state diagnosed by Beaufort code (Ramage 1987; Cardone et al. 1990). Because the scale used to transform Beaufort values to wind speed systematically underestimates wind speed compared to measurements (discussed in Section 4.4), an upward trend in the fraction of wind speed observations contributed by anemometer measurements will produce a spurious upward trend in average wind speed. This does not affect calculations involving VV, which was estimated from SLP gradients, and probably does not greatly affect calculations involving V, which at midlatitudes is influenced more by variability in wind direction than wind speed. However, the spurious trend in wind speed can produce a spurious trend in calculated latent and sensible heat fluxes (Ramage 1987) and wind stress. In order to avoid problems due to the spurious trend in wind speed and spurious interdecadal variability in low cloud type identification, the SVD analyses were repeated

on the one-year (summer-to-summer) difference fields (i.e., replacing the 1954 values with those for 1955 minus 1954, etc.). This emphasizes variability at less than five years and virtually eliminates any long-term trend. Ward and Hoskins (1996) compared COADS wind with wind derived from COADS SLP and concluded COADS wind data (of which EECRA wind observations are a subset) is reliable for use in studies of interannual variability.

Table 5.2 documents the summary statistics associated with the SVD analyses of the one-year difference fields, presented in the same order as in Table 5.1. Values of *r* for SVD pairs indicate that MSC amount is more closely coupled to SST and Ns FQ for one-year difference fields than for undifferenced fields. The corresponding meridional patterns shown in Fig. 5.1a (MSC–SST) and Fig. 5.1b (MSC-Ns) are consistent with the basin-wide analyses from Chapter 2. However, the difference in *r* between Tables 5.1 and 5.2 indicates that Ns FQ and SST are less coupled for one-year difference fields, suggesting that long-term trends in SST and Ns FQ (Figs. 2.3 and 2.5) account for much of the apparent coupling between the undifferenced fields and that another parameter, such as synoptic activity, is more influential in producing variability in Ns FQ at yearly timescales. Such coupling with synoptic activity is not apparent for the Ns–VV SVD pair (Table 5.2), but perhaps the low *r* value is due to the inadequacies of the VV dataset used in the present study. Instead, one-year difference fields of Ns FQ are much better-coupled with V (Table 5.2). The corresponding meridional patterns (Fig. 5.1c) indicate latitudes of increased (decreased) Ns FQ tend to be co-located with convergence (divergence) of V.

It is interesting to observe that one-year difference fields of SST are as closely coupled to SLP as they are to MSC (Table 5.2), particularly since previous basin-wide SVD analyses of SST and SLP over the North Pacific during summer have exhibited only weak coupling (Zhang 1996; NZW). Figure 5.1d shows that poleward decreasing (increasing) SLP from 30°N to 50°N is associated with decreased (increased) SST between 40–50°N. Poleward decreasing (increasing) SLP produces positive (negative) zonal wind anomalies which will force anomalous Ekman transport in the equatorward

(poleward) direction. Because anomalous equatorward (poleward) Ekman transport in the presence of poleward decreasing SST can produce local negative (positive) SST anomalies, the possibility arises that the atmosphere forces SST through wind stress as well as surface fluxes. However, the SST pattern in Fig. 5.1d is not consistent with forcing by Ekman transport because the SST anomaly is minimal between 27.5–37.5°N despite the presence of SLP and SST gradients. Nonetheless, the potential for zonal wind anomalies to produce SST anomalies will be assessed since Qiu and Kelly (1993) demonstrate Ekman transport is a significant term in the upper-ocean heat balance in the Kuroshio Extension region (30–40°N, 141–175°E, which overlaps the domain of this chapter, 20–50°N, 150°E–150°W).

5.3 Cloud response to anomalous sea surface temperature

The results of Chapter 4 suggested that meridional shifts in the SST gradient will produce meridional shifts in the location of low cloud type transitions. The present section examines this hypothesis by regressing one-year difference fields of various cloud and meteorological parameters on the normalized time series of SST between 35–40°N using summertime (JJA) data zonally averaged between 150°E–150°W at 2.5° resolution between 20–50°N, as described in Section 4.4. Regression analysis is undertaken instead of SVD analysis in order to better establish how SST produces variability in cloudiness, and the regressions are based on SST averaged between 35–40°N since that latitude band exhibits the greatest amplitude of coupled variability with MSC (Fig. 5.1a), is at the center of the climatological SST gradient region (Fig. 4.10b), and has the greatest correlation (86.3%) with the time series associated with the leading basin-wide EOF of the one-year difference field of SST (not shown). Since the parameters are regressed on the normalized time series, the associated amplitudes represent the magnitude of response to typical SST anomalies. For purposes of consistency with previous figures, all regressions will be illustrated as corresponding to a negative SST anomaly, but the opposite results occur for a positive SST anomaly.

Figure 5.2a displays the meridional variations of SST and ΔT regressed on SST

between 35–40°N during summer. A typical negative SST anomaly spans the entire climatological gradient region (Fig. 4.10b) and strengthens the gradient equatorward and weakens the gradient poleward of approximately 40°N. This is generally consistent with the meridional variation of ΔT, since flow over decreasing SST is likely to produce relatively more positive ΔT where the SST gradient is stronger and relatively more negative ΔT where the SST gradient is weaker. Figure 5.2b shows the meridional variation in MSC amount and Ns FQ associated with a typical negative SST anomaly during summer. As previously seen in Figs. 2.4, 2.6, and 5.1, increased (decreased) MSC amount and Ns FQ occur with decreased (increased) SST. This corresponds to mutual poleward or equatorward shifts in the gradient regions of MSC amount, Ns FQ, and SST (Fig. 4.10).

Because seasonal-mean atmospheric circulation and synoptic activity are weakly coupled to SST during summer (Table 2.2), it is possible that some variability in the regressed cloud parameters attributed to processes affected by anomalies in SST actually results from processes better related to anomalies in atmospheric circulation. Unfortunately, it is not possible to hold all other parameters constant in the SST regressions, aside from perhaps developing a multi-category and likely inadequate compositing procedure. For this reason, the results of the SST regressions will generally be interpreted as arising from anomalies in SST, with the possibility left open for other factors to play a role. Nonetheless, the meridional variation of VV and V associated with a typical negative SST anomaly during summer is documented in Fig. 5.2c. Decreased (increased) SST occurs with a slight equatorward (poleward) shift in the location of the storm track, as observed in Fig. 2.11, and anomalous seasonal-mean northerly (southerly) wind at midlatitudes, as observed by Zhang (1996) and Norris et al. (1997). Figure 5.2d shows that northerly winds are slightly more frequent and southerly winds less frequent at midlatitudes when the water is colder than usual.

Figure 5.3 displays the meridional variations of low cloud types regressed on SST between 35–40°N during summer. Poleward of about 27.5°N, less moderate and large cumulus cloud amount occurs with negative SST anomalies (Fig. 5.3a), consistent with

decreased CAPE resulting from decreased SST. Negative SST anomalies act to shift the region of strongest SST gradient equatorward, which under conditions of poleward advection will produce stronger near-surface stratification closer to the subtropics. This is consistent with increased frequency of no-low-cloud on the equatorward side and decreased frequency of no-low-cloud on the poleward side (Fig. 5.3a) of climatological maximum no-low-cloud (Fig. 4.11c). Poleward advection over anomalously cold water produces increased cloud amount of fair-weather stratus and sky-obscuring fog equatorward of about 40°N. The substantial decrease in the amount of sky-obscuring fog poleward of 40°N probably results from the relatively weaker SST gradient at those latitudes, and it appears much of the fog is lifted into stratus (Fig. 5.3c).

It is likely that the equatorward shift of the region of strongest SST gradient associated with a negative SST anomaly decreases the rate of decoupling of stratocumulus MBLs as they are advected equatorward. This is consistent with increased stratocumulus cloud amount between 30–40°N (Fig. 5.3b). It is unclear why there is not a corresponding increase in cumulus-with-stratocumulus cloud amount equatorward of increased stratocumulus cloud amount (Fig. 5.3c), given that cumulus-with-stratocumulus is a transitional cloud type between stratocumulus and cumulus (Bretherton 1992; Wyant et al. 1997) and that the climatological maximum of cumulus-with-stratocumulus is located on the equatorward side of the climatological maximum of stratocumulus (Fig. 4.11b). Increased cloud amount of stratocumulus types at midlatitudes may also result from increased frequency of cold advection, as inferred by wind direction (Fig. 5.2d). Slight decreases in small cumulus cloud amount and cumulonimbus cloud amount occur with negative SST anomalies (Fig. 5.3d). The increase in bad-weather stratus cloud amount between 30–40°N may be more related to increased synoptic activity (e.g. Fig. 5.2bc) than decreased SST.

5.4 Cloud response to anomalous synoptic activity

Variability in the frequency and strength of synoptic activity produces variability in vertical motion and the relative frequency of cold and warm advection. The results of

Chapter 4 suggest that cold advection favors the occurrence of stratocumulus, cumulus-with-stratocumulus, and cumulus, and warm advection favors the occurrence of no-low-cloud, fair-weather stratus, and sky-obscuring fog. The results of Chapter 3 suggest that strong ascent with warm advection favors the occurrence of bad-weather stratus instead of fair-weather stratus and sky-obscuring fog. Therefore, it is likely that increased synoptic activity will produce more cold-advection cloud types and bad-weather stratus. The present section examines this hypothesis by regressing one-year difference fields of various cloud and meteorological parameters on the normalized time series of summertime VV between 35–40°N in a manner similar to that of the previous section. As was done in Chapter 2, data from 1987 were excluded from analyses involving VV because of the unrealistically high values of VV that year. The VV regressions are based on the 35–40°N latitude band for consistency with the SST regressions and because a center of action in the basin-wide SVD analyses is located approximately between 35–40°N (Figs. 2.10 and 2.11). For purposes of consistency with previous figures, all regressions will be illustrated as corresponding to a positive VV anomaly, but the opposite results occur for a negative VV anomaly.

Figure 5.4 displays summertime VV regressions with identical scaling to Fig. 5.2 for ease of comparison. The meridional variation of VV associated with a typical anomaly between 35–40°N resembles the leading basin-wide EOF of VV (Fig. 2.9) more than the basin-wide SVD patterns of VV paired with Ns FQ and SST (Figs. 2.10 and 2.11). This implies a significant amount of spurious variability may be present in the VV time series, but previous results suggest this adds noise to but does not bias the data. The regression calculations were repeated on the normalized time series of the difference between VV at 35–40°N and 45–50°N, but the results were less satisfactory, probably because more noise was added by taking a difference than spurious variability removed. Increased synoptic activity favors northerly winds but has little effect on the frequency of southerly winds (Fig. 5.4b). The negative ΔT anomalies associated with positive anomalies in VV (Fig. 5.4c) are consistent with the greater frequency of northerly winds and greater inferred cold advection. As previously seen in Fig. 2.10, increased

(decreased) Ns FQ between 35–40°N tends to occur with increased (decreased) VV between 35–40°N. Slightly increased MSC amount occurs equatorward and slightly decreased MSC amount occurs poleward of 40°N with positive VV anomalies, reminiscent of the meridional pattern of the difference in MSC amount between conditions of northerly and southerly winds (Fig. 4.16a).

Figure 5.5 displays the meridional variations of low cloud types regressed on VV between 35–40°N during summer with scaling equal to half of that used in Fig. 5.3. The amplitudes of the VV regressions may be smaller either because synoptic activity has less influence on low cloud types or because the VV dataset used in the present study is inadequate. Increased moderate and large cumulus cloud amount and cumulus-with-stratocumulus cloud amount occur with positive VV anomalies (Fig. 5.5ab), consistent with the greater frequency of inferred cold advection (Fig. 4.17ab). The location of maximum moderate and large cumulus is generally equatorward of the location of maximum cumulus-with-stratocumulus, consistent with cumulus resulting from the breakup of stratocumulus in an increasingly decoupled MBL advected over increasing SST (e.g. Bretherton 1992; Wyant et al. 1997). When synoptic activity is stronger or more frequent, the ratio of poleward flow to equatorward flow decreases (e.g. Fig. 5.4b), and it is likely that poleward flow is more often accompanied by relatively stronger ascent. Such a scenario is consistent with the lesser occurrence of no-low-cloud, fair-weather stratus, and sky-obscuring fog and increased occurrence of bad-weather stratus at midlatitudes. Slightly less cumulonimbus occurs with positive VV anomalies, but the meridional patterns of stratocumulus cloud amount and small cumulus cloud amount are more difficult to interpret.

5.5 Processes and feedbacks influencing sea surface temperature

Given the observed coupling between SST and MSC, it is important to investigate not only the processes by which variability in SST produces variability in MSC amount, but also the degree to which radiative forcing resulting from variability in MSC amount produces variability in SST. This will enable the potential for a cloud feedback on SST to

be estimated. In order to assess the relative importance of radiative forcing due to anomalous MSC amount, it is necessary to examine the degree to which other processes such as anomalous latent and sensible heat fluxes and Ekman transport due to anomalous zonal wind stress produce variability in SST. This is particularly the case since NL (1994) suggest interannual variability in latent heat flux opposes interannual variability in MSC radiative forcing over the midlatitude North Pacific during summer. The magnitude of anomalies in surface flux and SST tendency associated with anomalies in SST during summer is estimated by regressing one-year difference fields of flux parameters and SST tendency on the time series of SST between 35–40°N, as was done previously in Section 5.3. Because MSC and other processes influencing SST vary with synoptic activity, regressions on the time series of VV between 35–40°N (as was done in Section 5.4) are also displayed. For the purpose of convenient comparisons, the results are displayed for negative SST anomalies and positive VV anomalies, along with the meridional patterns of SST (previously shown in Fig. 5.2a) or VV (previously shown in Fig. 5.4a).

The SST tendency over a summer season is defined as the difference between August monthly-mean SST and June monthly-mean SST.* Following NL, radiative forcing by MSC is estimated to be a loss to the ocean of 1 W m^{-2} for every 1% increase in MSC amount (Section 2.6 provides more detailed discussion). In this case, the amount of lost downward surface radiation (hereafter referred to as "radiation loss") may be easily obtained by substituting units of W m^{-2} for units of percentage cloud amount. Seasonal-mean values of zonal wind stress during summer were calculated from nighttime EECRA observations of wind speed and ΔT using bulk formulas and exchange coefficients from Smith (1988) assuming a reference height of 10 m (more detailed discussion of potential biases is provided in Section 4.4). The calculated meridional variation of climatological zonal wind stress between 150°E–150°W was generally comparable to the climatologies of Hellerman and Rosenstein (1983) and Trenberth et al. (1990). In order to facilitate comparison with the radiation loss and latent and sensible heat fluxes, anomalies in zonal

* Note that the SST tendency is on the order of two months whereas the seasonal-mean flux values occur over three months.

wind stress, ΔX_0, were converted to anomalies in "equivalent energy flux" (hereafter referred to as "zonal stress flux") by assuming that the resulting anomalous Ekman mass transport, $\Delta X_0 / f$, acted on a meridional temperature gradient identical to the climatological SST gradient displayed in Fig. 4.10b, adopting the formulation of Ronca and Battisti (1997),

$$-\left(\frac{\Delta X_0}{f}\right) \times \left(c\frac{\partial \overline{\mathrm{SST}}}{\partial y}\right) \tag{5.1}$$

where f is the Coriolis parameter and c is the specific heat of liquid water.

Figure 5.6a shows that for year-to-year differences, SST tendency anomalies are in the opposite direction and as large as the SST anomalies equatorward of 40°N (SST tendency anomalies are only a third as large as the SST anomalies for regressions on the undifferenced time series). This suggests a strong negative feedback on SST may be operating equatorward of 40°N. One candidate is the combined latent and sensible heat flux out of the ocean (hereafter referred to as "turbulent heat flux"), which is less (greater) for decreased (increased) SST. Note that the center of action for the turbulent heat flux is not collocated with the center of action for SST, but instead occurs where the SST anomaly changes the strength of the SST gradient and likely the strength of near-surface stratification in the presence of poleward advection. As noted by NL, MSC anomalies associated with SST anomalies (Fig. 5.2b) work in an opposite way from the turbulent heat flux and increase (decrease) the loss of radiative energy to the ocean when water is cold (warm) (Fig. 5.6c). Anomalous zonal wind stress acts to decrease negative SST anomalies and increase positive SST anomalies, but this is of second order compared to the radiative flux and heat flux (Fig. 5.6d), as is also the case for the eastern subtropical North Pacific during summer (Ronca and Battisti 1997).

Anomalies in radiation loss and SST tendency are considerably weaker when regressed on VV instead of SST (identical scaling is used in Figs. 5.6 and 5.7), and the turbulent heat flux is half as strong. Increased VV is associated with increased turbulent heat flux out of the ocean (Fig. 5.7b), consistent with greater frequency of inferred cold advection (Fig. 5.4b) and greater wind speed (not shown). Anomalies in zonal stress flux

are slightly positive equatorward of and slightly negative poleward of 40°N (Fig. 5.7d), consistent with an equatorward shift in the storm track. Although little change in MSC amount is associated with anomalous VV (Fig. 5.4d), it is possible that the associated radiation loss is different than that estimated in Fig. 5.7c if anomalous VV causes typical MSC optical thickness to change. The slightly negative anomaly in SST tendency between 35–45°N when VV is greater than usual (Fig. 5.7a) is consistent with enhanced turbulent heat flux.

Coupling between SST, SST tendency, and processes potentially influencing SST is directly examined over the central North Pacific during summer using SVD analysis on the one-year difference fields as described in Section 5.2. Table 5.3 documents the summary statistics associated with the SVD analyses, listed in order of decreasing *r*. Fig. 5.8ab shows that the SVD patterns of radiation loss and turbulent heat flux paired with SST largely resemble their respective regressions on SST (Fig. 5.6bc). Anomalies in radiation loss work to enhance SST anomalies and anomalies in turbulent heat flux work to reduce SST anomalies and hence oppose each other (Fig. 5.8c), albeit weakly (*r* is only 68.3%). Although the change in radiation lost to the ocean is of the same magnitude as the change in turbulent heat flux out of the ocean, the maxima are not co-located, suggesting that poleward of approximately 35°N the radiation loss is stronger and provides a positive feedback on SST and that equatorward of 35°N the turbulent heat flux is stronger and provides a negative feedback on SST. However, this hypothesis greatly depends on the magnitude of the radiative forcing associated with MSC amount, which is uncertain in the present analysis by perhaps as much as 50%.

Coupling between most flux parameters and the SST tendency is negligible (Table 5.3). Turbulent heat flux poleward of 27.5°N is weakly coupled to SST tendency (r = 64.4), with decreased (increased) turbulent heat flux out of the ocean associated with warming (cooling) water (Fig. 5.8d). However, the magnitude of typical SST tendency anomalies is much larger than what would be generated by the associated turbulent heat flux anomalies (following the formulation of Eq. 2.1). Negligible relationship is apparent between SST tendency anomalies and radiation loss due to MSC anomalies (Table 5.3). It

is possible that the tendency for cancelation between radiation loss and turbulent heat flux anomalies causes the overall flux anomaly to be small and consequently produce little change in SST.

Ronca and Battisti (1997) found that anomalies in latent heat flux at OWS N in the eastern subtropical North Pacific were primarily due to anomalies in wind speed, and it would be interesting see if this is also the case for the central North Pacific. The conventional bulk formulation for latent heat flux (Smith 1988)* can be rewritten as

$$C_E L \rho |\boldsymbol{V}| q_{\mathrm{SST}} \left(\frac{q_{\mathrm{SST}} - q}{q_{\mathrm{SST}}} \right) \tag{5.2}$$

where C_E is the evaporation exchange coefficient, L is the latent heat of vaporization, ρ is the density of air, $|\boldsymbol{V}|$ is the wind speed, q_{SST} is the SST saturation water vapor mixing ratio, and q is the surface water vapor mixing ratio. Thus, to first order, latent heat flux varies linearly with wind speed, SST saturation mixing ratio, and the relative humidity deficit.** A comparison of the magnitude of seasonal-mean anomalies in wind speed, q_{SST}, relative humidity, and latent heat flux regressed on SST to the magnitude of their climatological values for the 30–32.5°N latitude band suggests that variability in relative humidity can account for 95% of the observed variability in latent heat flux whereas variability in wind speed and q_{SST} can account for only 5% and 20% of the observed variability in latent heat flux.

5.6 Summary and conclusions

The preceding results indicate that interannual meridional shifts in the location of the SST gradient in the central North Pacific during summer produce corresponding

---

* Latent heat flux in this study was actually obtained using the saturation mixing ratio for surface air temperature instead of SST. This would produce about a 6% difference in latent heat flux when ΔT has a magnitude of 1 °C.

** Strictly speaking, relative humidity is measured as $q / q_s(T_{air})$ instead of q / q_{SST}, but there is little practical difference between the two.

meridional shifts in the location of low cloud type transitions. For MBLs undergoing equatorward advection, anomalously cold (warm) water delays (advances) the onset of strong MBL decoupling along the trajectory and hence delays (advances) the breakup of stratocumulus into cumulus (Fig. 5.3b). For MBLs undergoing poleward advection, anomalously cold (warm) water advances (delays) the onset of strong near-surface stratification and decreased CAPE along the trajectory and hence advances (delays) the replacement of subtropical cumulus by fair-weather stratus and sky-obscuring fog (Fig. 5.3ac). Thus, increased (decreased) cloud amount of low stratiform cloud types is strongly coupled to decreased (increased) SST for both poleward and equatorward advection (e.g., Figs. 5.1a and 5.2b and Table 5.2).

Interannual variability in VV is observed to have much less influence on the overall cloud amount of low stratiform cloud types (Fig. 5.4d and Table 5.2), largely because decreases in one low stratiform cloud type are compensated by increases in another. Aside from the obvious increase in bad-weather stratus (Fig. 5.5d), regressions of low cloud type on VV suggest increased synoptic activity favors stratocumulus types at the expense of fair-weather stratus and sky-obscuring fog (Fig. 5.5bc), probably because synoptic activity produces more cold advection, as suggested by the increased frequency of northerly winds in Fig. 5.4b. The compensation in cloud amount between cold-advection cloud types (stratocumulus and cumulus-with-stratocumulus) and warm-advection cloud types (fair-weather stratus and sky-obscuring fog) poleward of 40°N is illustrated by SVD analysis of the one-year difference fields of combined stratocumulus and cumulus-with-stratocumulus cloud amount and combined sky-obscuring fog and fair-weather stratus cloud amount (Fig. 5.9). Note the strong coupling of cold-advection and warm-advection cloud types with each other but relatively weak coupling with MSC amount (Table 5.4), suggesting that variability in advective conditions produces much more change in the relative amounts of various low stratiform cloud types than change in the overall amount of all low stratiform cloud types. However, Fig. 5.7b suggests that increased synoptic activity favors increased turbulent heat flux out of the ocean.

The fact that decreased SST favors increased MSC amount over the SST gradient

region during summer provides the basis for a positive cloud feedback on SST if increased MSC amount reduces surface insolation and thus decreases SST. Although the large CRF associated with MSC over the midlatitude ocean during summer strongly suggests increased MSC amount reduces surface insolation (Fig. 1.1), seasonal-mean anomalies in MSC amount are observed to have negligible coupling with seasonal SST tendency (Table 5.3). Three possible reasons for this lack of a relationship are: (1) variability in MSC amount produces insignificant variability in radiative forcing, (2) radiation loss due to variability in MSC amount largely occurs below the oceanic surface layer, or (3) other processes work against or obscure the role of radiation loss due to variability in MSC amount. Possibility (1) cannot be evaluated until surface net CRF associated with surface-observed cloudiness is better established. Possibility (2) could occur if a large fraction of the surface insolation penetrates beneath an oceanic surface layer which poorly mixes with the layer beneath (e.g. Ohlmann et al. 1996). In this case, the effects of the radiation loss would not be felt by the SST until some later time when mixing occurs.

Possibility (3) has the best support. Fig. 5.8c indicates that variability in turbulent heat flux is weakly coupled to the SST tendency and tends to oppose estimated variability in radiation loss due to MSC. Assuming surface net CRF due to MSC amount has been correctly estimated, turbulent heat flux dominates equatorward and radiation loss due to MSC dominates poleward of 35°N, although the remaining signals may be too weak to clearly discern. The regression of the SST tendency on SST (Fig. 5.6a) lends support to the possible existence of a negative feedback on the equatorward side of the SST anomaly and a positive feedback on the poleward side. An investigation of the influence of Ekman transport due to anomalous zonal wind stress on SST indicates it is of second order compared to anomalous turbulent heat flux and anomalous radiation loss due to MSC considered individually. Other processes affecting SST not examined are geostrophic advection, horizontal mixing, vertical entrainment, and variability in oceanic mixed layer depth.

Although the results of this chapter provide substantial support for the existence of a positive cloud feedback on SST over the midlatitude ocean during summer, before this can

be definitively established it will be necessary to more accurately determine how surface net CRF varies with cloud amount and cloud type and better understand the processes influencing SST and the surface layer of the ocean.

Table 5.1: Summary statistics for the SVD analyses (in percent).

Parameters	SCF	NC	*r*
MSC amount and SST	92.3	42.5	75.9
MSC amount and Ns FQ	89.9	30.9	73.9
Ns FQ and SST	90.5	30.2	71.8
Ns FQ and V	49.6	12.3	63.1
MSC amount and SLP	89.9	28.0	55.0
SST and SLP	86.5	29.5	54.2
SST and V	57.1	17.5	54.1
VV and SLP	93.1	23.9	52.9
Ns FQ and VV	64.2	14.9	51.0
MSC amount and V	55.6	12.7	49.1
Ns FQ and SLP	68.2	16.0	42.8
MSC amount and VV	90.1	21.9	41.2
SST and VV	82.0	18.5	35.8
VV and V	70.4	11.2	33.8

Table 5.2: Summary statistics for the SVD analyses of the one-year difference fields (in percent).

Parameters	SCF	NC	*r*
MSC amount and SST	69.4	31.5	83.5
MSC amount and Ns FQ	77.1	24.5	79.4
Ns FQ and SST	55.8	18.4	60.2
Ns FQ and V	47.4	16.5	79.5
MSC amount and SLP	66.0	19.6	51.9
SST and SLP	87.1	30.4	82.2
SST and V	51.0	20.2	65.0
VV and SLP	81.7	23.2	48.7
Ns FQ and VV	63.5	15.9	56.5
MSC amount and V	75.8	22.1	59.4
Ns FQ and SLP	62.8	14.9	67.9
MSC amount and VV	51.4	10.8	47.4
SST and VV	54.5	13.5	34.4
VV and V	68.9	17.0	43.0

Table 5.3: Summary statistics for the SVD analyses of the one-year difference fields of flux parameters, SST, and SST tendency (in percent).

Parameters	SCF	NC	*r*
radiation loss and SST	69.4	31.5	83.5
radiation loss and turbulent heat flux	78.6	26.5	68.3
turbulent heat flux and SST	67.2	23.9	67.2
turbulent heat flux and SST tendency*	73.0	23.7	64.4
SST tendency and SST	81.2	24.6	63.8
zonal stress flux and SST	90.2	27.9	63.2
turbulent heat flux and zonal stress flux	70.5	18.5	59.3
zonal stress flux and SST tendency	69.3	16.4	52.0
radiation loss and zonal stress flux	66.6	16.0	44.1
radiation loss and SST tendency	54.1	12.0	41.8

* Turbulent heat flux anomalies equatorward of 27.5°N were set to zero to prevent the analysis from constructing a strongly coupled (r = 80.7%) SVD mode that had minimal local relationship but was instead based on a "teleconnection" between turbulent heat flux equatorward of 27.5°N and SST tendency between 35–40°N.

Table 5.4: Summary statistics for the SVD analyses of the one-year difference fields of combined stratocumulus and cumulus-with-stratocumulus cloud amount, combined sky-obscuring fog and fair-weather stratus cloud amount, and MSC amount (in percent).

Parameters	SCF	NC	*r*
Sc + Cu/Sc amount and St + Fog amount	89.6	38.9	85.8
Sc + Cu/Sc amount and MSC amount	73.4	27.7	74.9
St + Fog amount and MSC amount	77.4	29.2	70.5

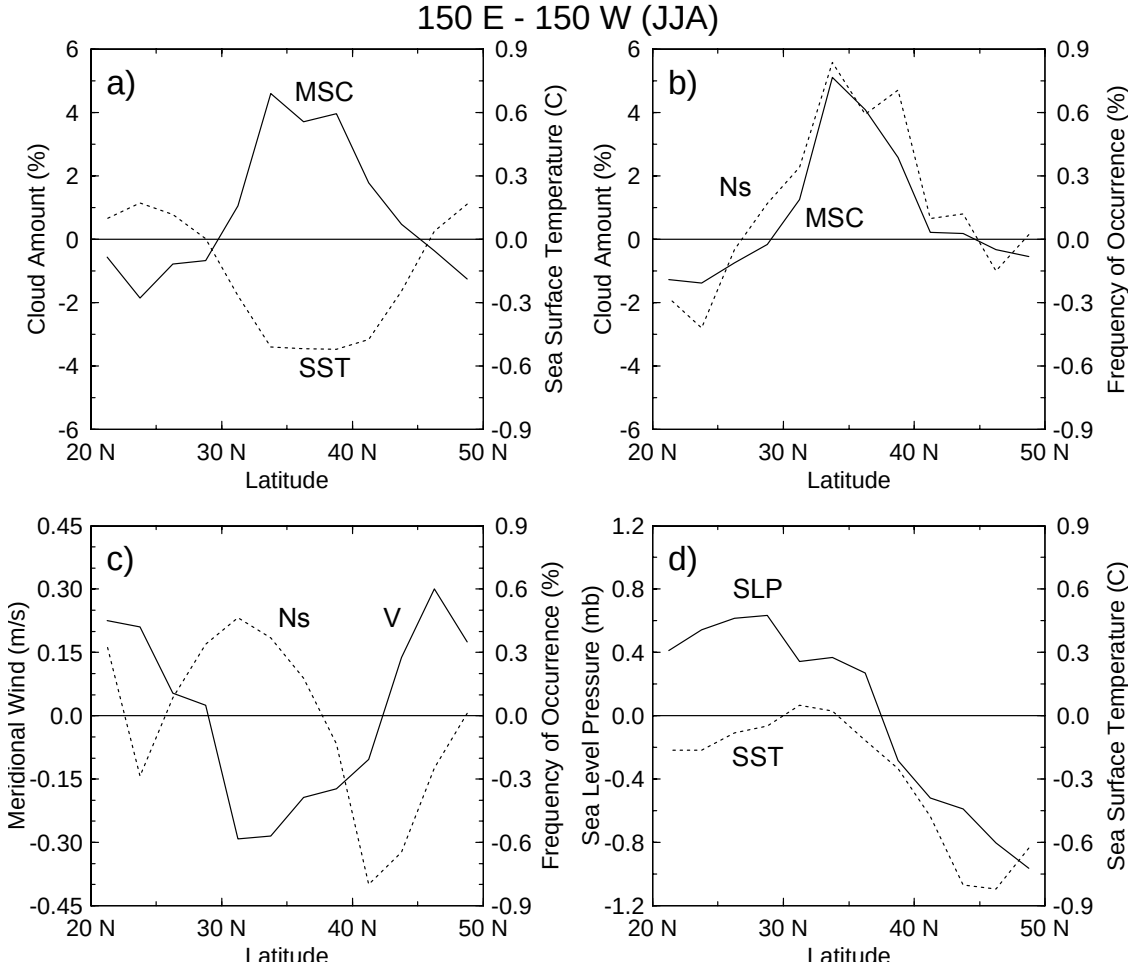

Figure 5.1: (a) Leading SVD modes for one-year difference fields of zonally-averaged seasonal-mean daytime MSC amount (solid) paired with SST (dotted) during JJA. (b) As in (a), except for daytime MSC amount (solid) paired with daytime Ns FQ (dotted). (c) As in (a), except for V (solid) paired with daytime Ns FQ (dotted). (d) As in (a), except for SLP (solid) paired with SST (dotted). Summary statistics are presented in Table 5.2.

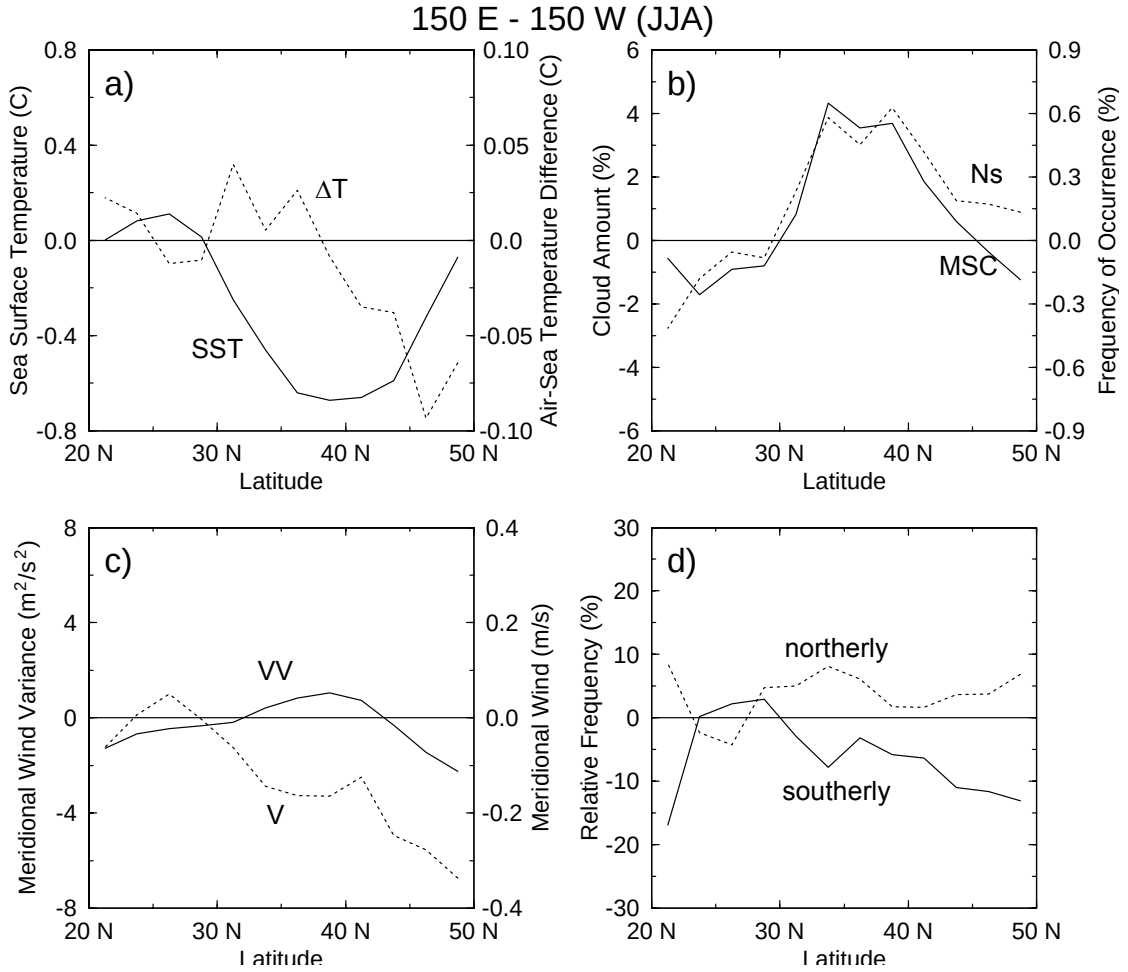

Figure 5.2: (a) One-year difference fields of zonally-averaged seasonal-mean SST (solid) and nighttime ΔT (dotted) regressed on the normalized time series of SST averaged between 35–40°N during JJA. (b) As in (a), except for daytime MSC amount (solid) and daytime Ns FQ (dotted). (c) As in (a), except for VV (solid) and V (dotted). (d) As in (a), except for the relative change in the frequency of southerly (solid) and northerly (dotted) winds, as defined in Section 4.6.

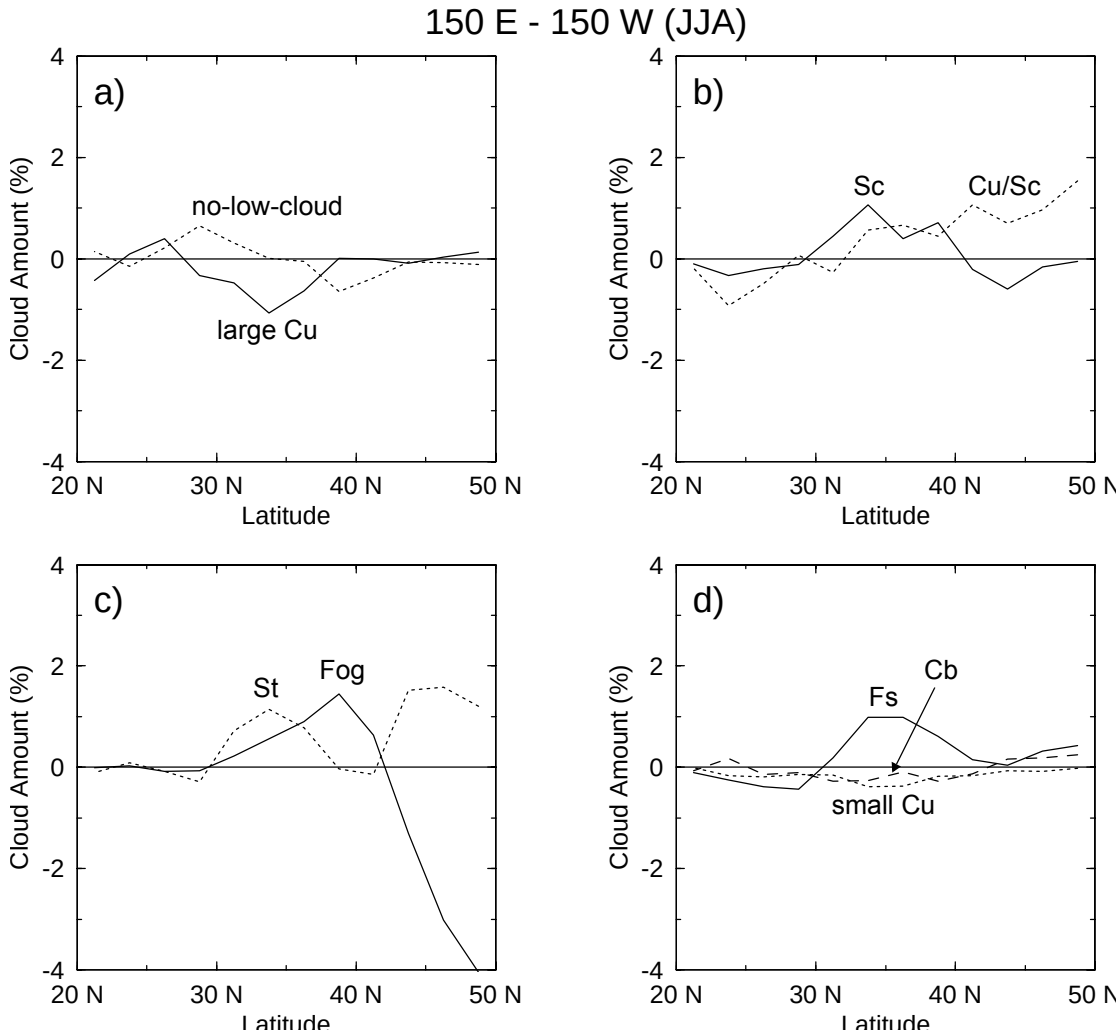

Figure 5.3: (a) As in Fig. 5.2a, except for moderate and large cumulus (C_L 2) cloud amount (solid) and no-low-cloud (C_L 0) FQ (in same units as cloud amount) (dotted). (b) As in (a), except for stratocumulus (C_L 5) (solid) and cumulus-with-stratocumulus (C_L 4+8) (dotted). (c) As in (a), except for sky-obscuring fog (solid) and fair-weather stratus (C_L 6) (dotted). (d) As in (a) except for bad-weather stratus (C_L 7) (solid), small cumulus (C_L 1) (dotted), and cumulonimbus (C_L 3+9) (dashed). All values are for daytime only.

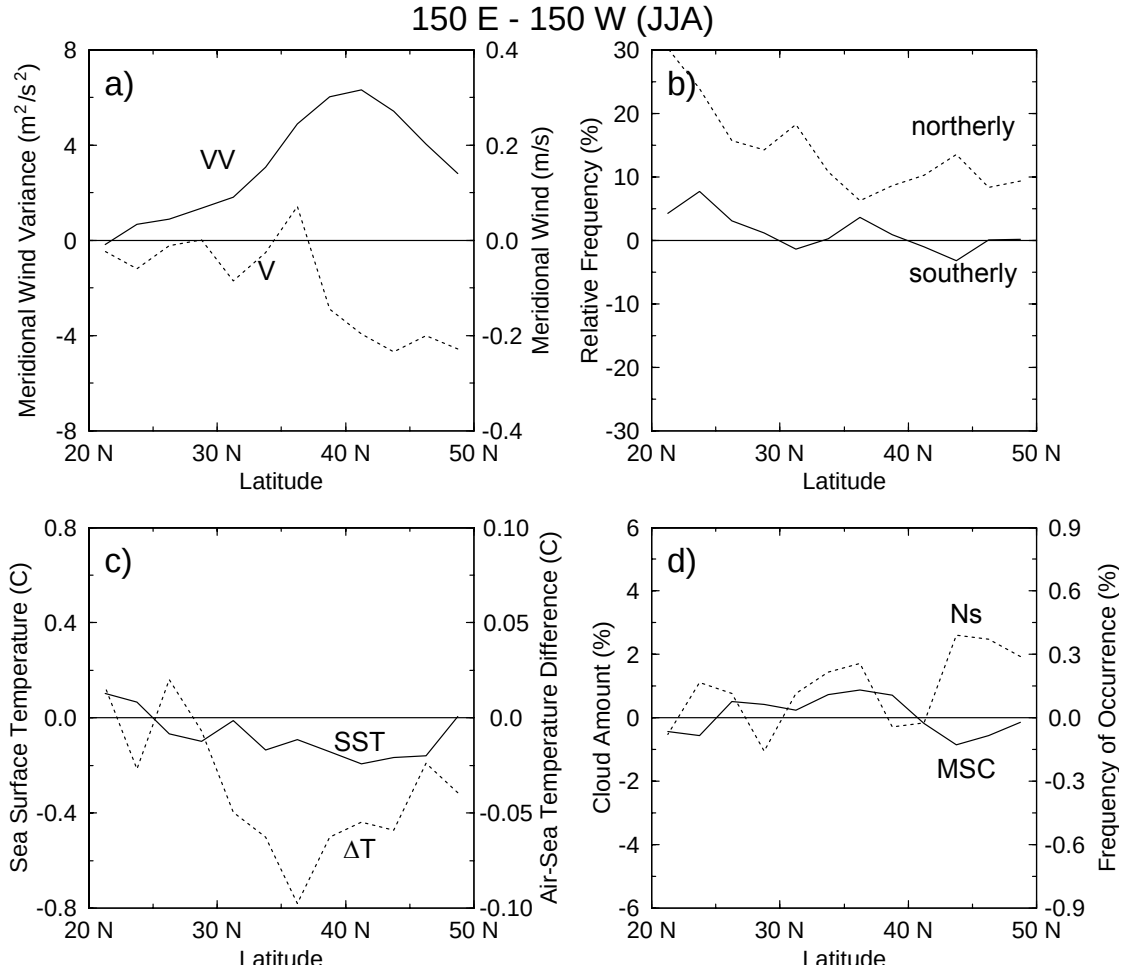

Figure 5.4: (a) One-year difference fields of zonally-averaged seasonal-mean VV (solid) and V (dotted) regressed on the normalized time series of VV averaged between 35–40°N during JJA. (b) As in (a), except for the relative change in the frequency of southerly (solid) and northerly (dotted) winds, as defined in Section 4.6. (c) As in (a), except for SST (solid) and nighttime ΔT (dotted). (d) As in (a), except for daytime MSC amount (solid) and daytime Ns FQ (dotted).

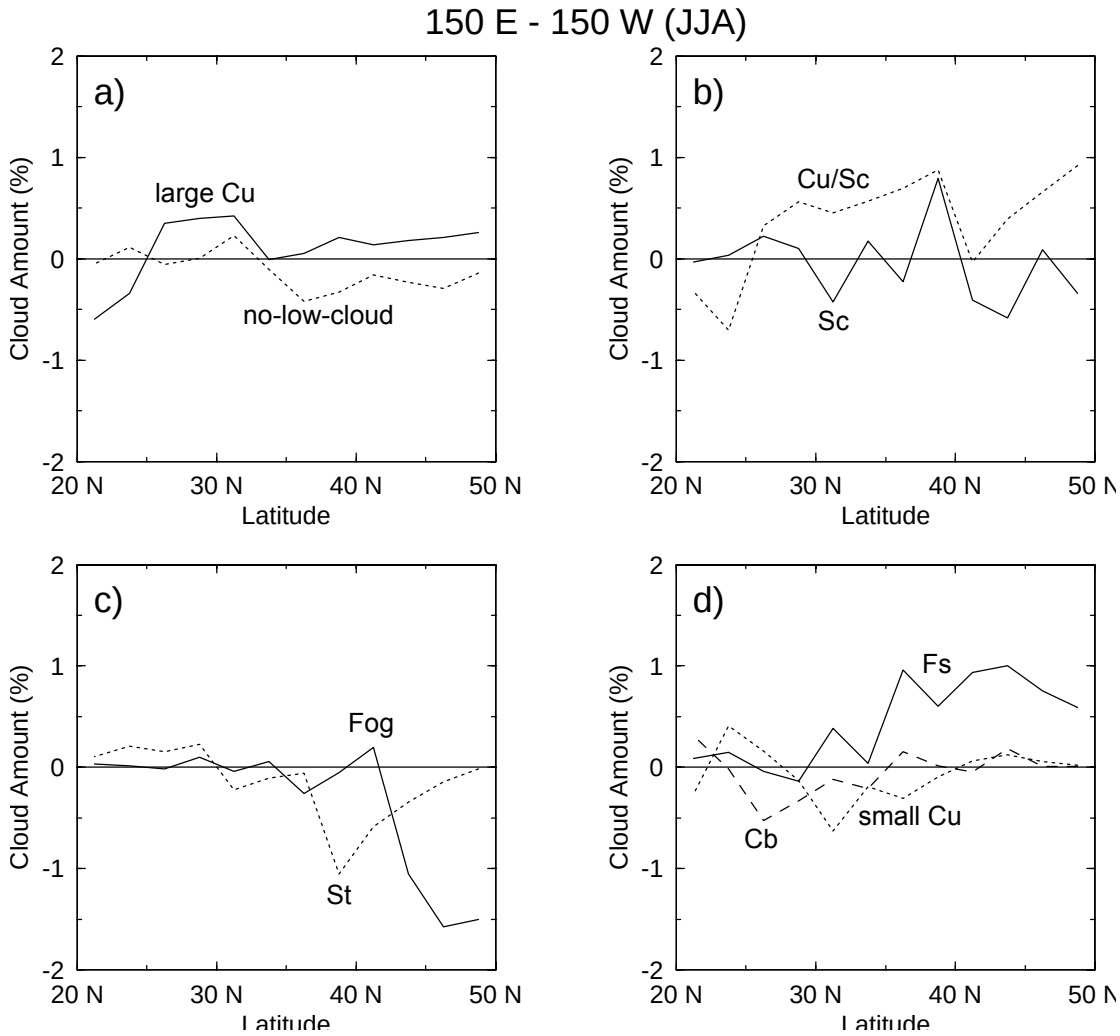

Figure 5.5: (a) As in Fig. 5.4a, except for moderate and large cumulus (C_L 2) cloud amount (solid) and no-low-cloud (C_L 0) FQ (in same units as cloud amount) (dotted). (b) As in (a), except for stratocumulus (C_L 5) (solid) and cumulus-with-stratocumulus (C_L 4+8) (dotted). (c) As in (a), except for sky-obscuring fog (solid) and fair-weather stratus (C_L 6) (dotted). (d) As in (a) except for bad-weather stratus (C_L 7) (solid), small cumulus (C_L 1) (dotted), and cumulonimbus (C_L 3+9) (dashed). All values are for daytime only.

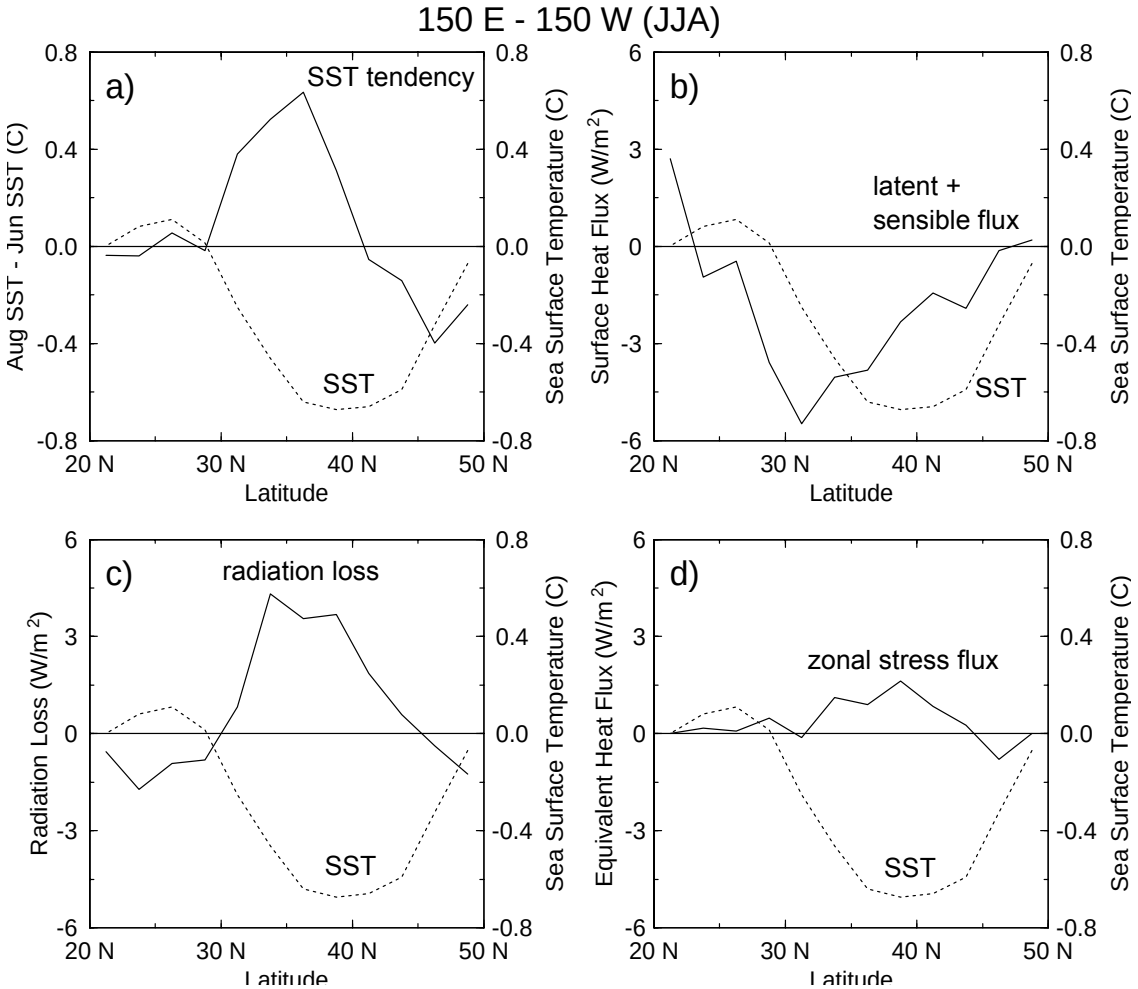

Figure 5.6: (a) As in Fig. 5.2a, except for SST tendency (solid) and SST (dotted). (b) As in (a), except for nighttime turbulent heat flux (solid) and SST (dotted). (c) As in (a) except for radiation loss due to MSC amount (solid) and SST (dotted). (d) As in (a), except nighttime zonal wind stress equivalent flux (solid) and SST (dotted). Positive flux is out of the ocean.

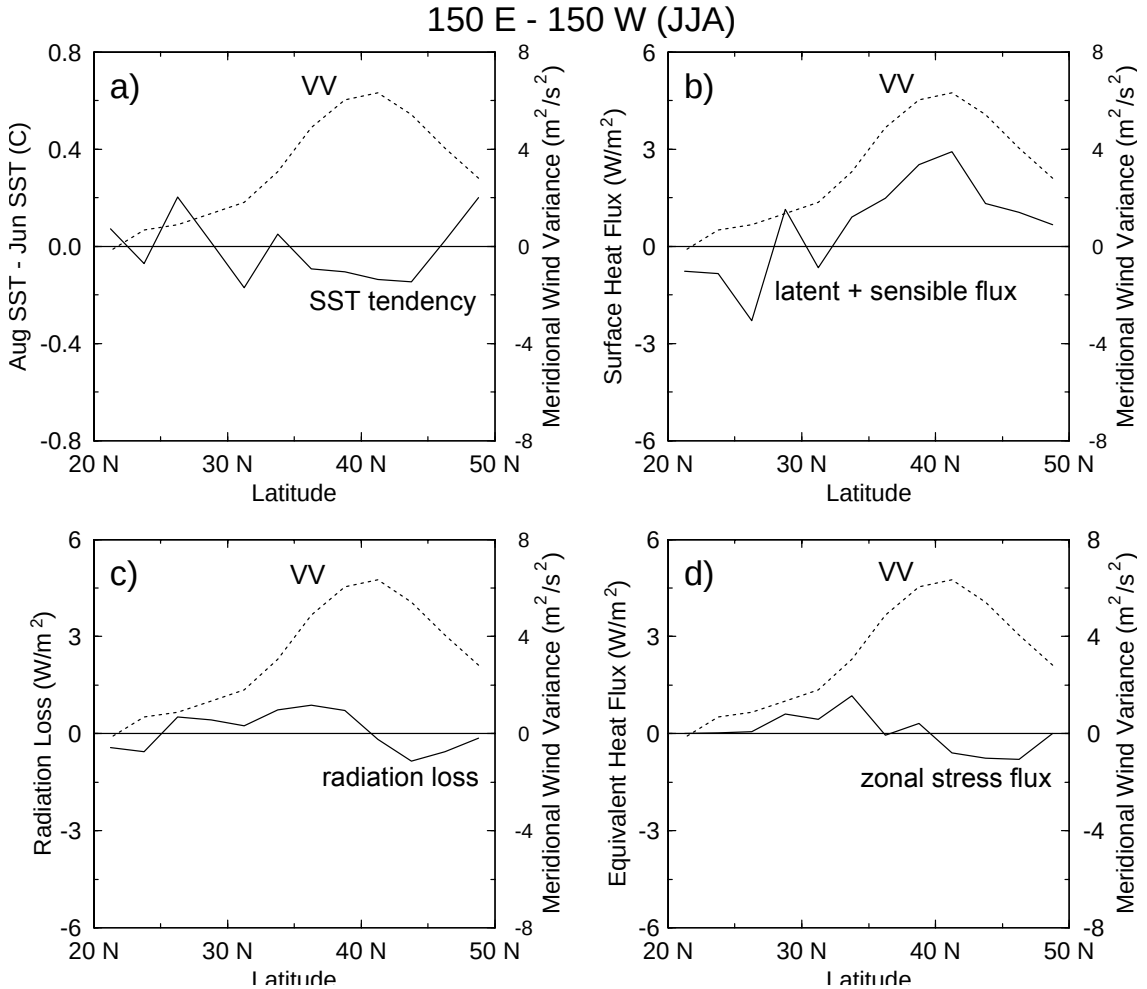

Figure 5.7: (a) As in Fig. 5.4a, except for SST tendency (solid) and VV (dotted). (b) As in (a), except for nighttime turbulent heat flux (solid) and VV (dotted). (c) As in (a) except for radiation loss due to MSC amount (solid) and VV (dotted). (d) As in (a), except nighttime zonal wind stress equivalent flux (solid) and VV (dotted). Positive flux is out of the ocean.

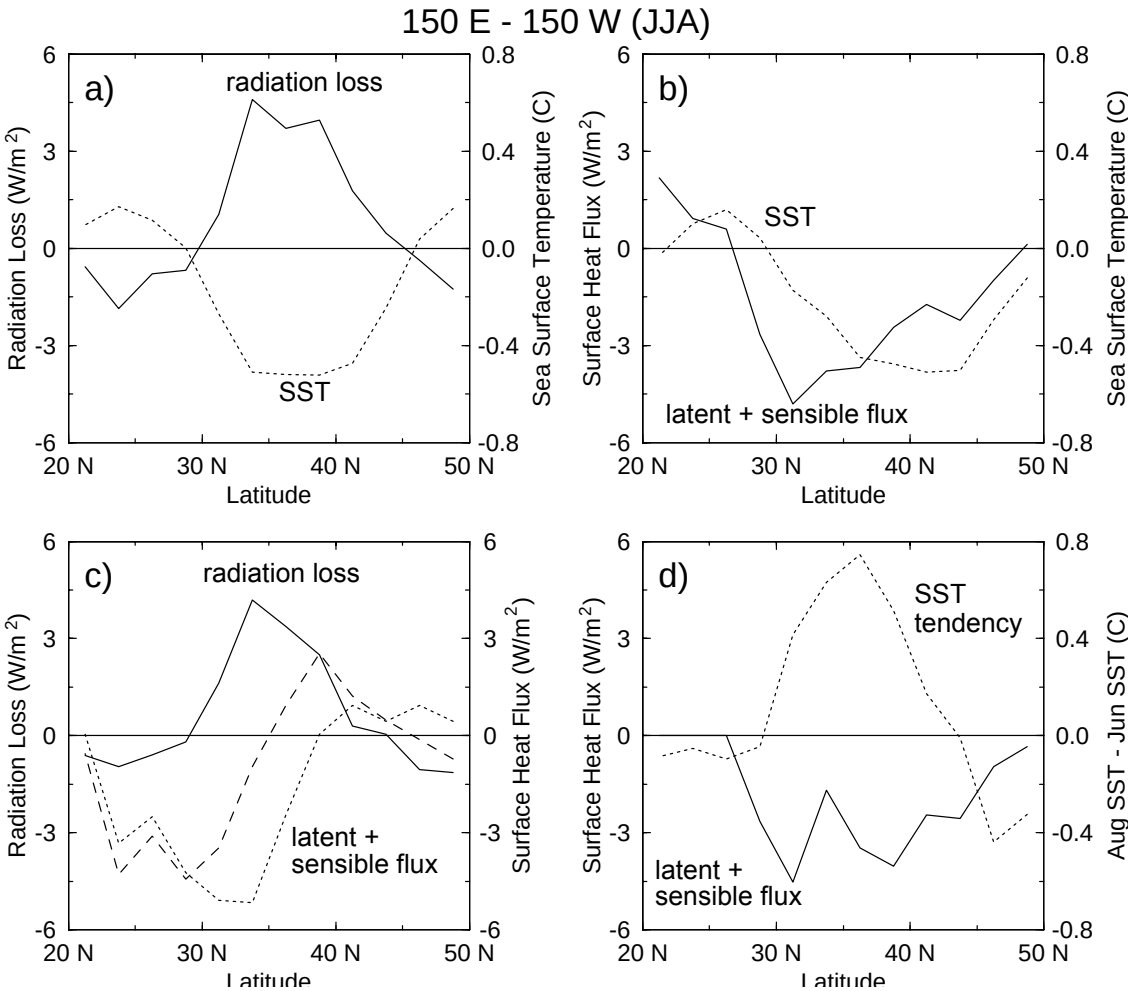

Figure 5.8: (a) As in Fig. 5.1a, except for radiation loss due to MSC amount (solid) paired with SST (dotted). (b) As in (a), except for nighttime turbulent heat flux (solid) paired with SST (dotted). (c) As in (a), except for radiation loss due to MSC amount (solid) paired with nighttime turbulent heat flux (dotted). The dashed line is the sum of solid and dotted lines. (d) As in (a), except for nighttime turbulent heat flux (solid) paired with SST tendency (dotted). Positive flux is out of the ocean. Summary statistics are presented in Table 5.3.

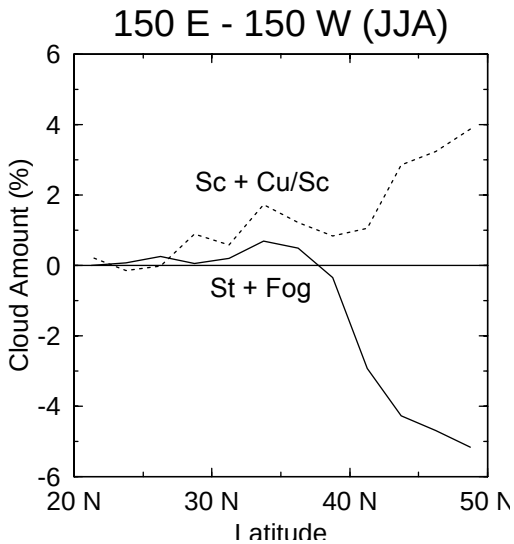

Figure 5.9: As in Fig. 5.1a, except for combined sky-obscuring fog and fair-weather stratus cloud amount (solid) paired with combined stratocumulus and cumulus-with-stratocumulus cloud amount (dotted). Summary statistics are presented in Table 5.4.

CHAPTER 6

Summary, Discussion, and Conclusions

6.1 Review of the present study

The present study is a first attempt to comprehensively investigate the processes which relate large-scale, seasonal-mean variations in MSC, midlevel stratiform cloudiness, SST, and synoptic activity over the midlatitude ocean during summer. Chapter 2 provided confirmation that interannual variability and long-term trends in MSC amount and Ns FQ are closely coupled to interannual variability and long-term trends in SST along the region of strong SST and cloud gradient between the subtropics and midlatitudes over the central North Pacific. Increased (decreased) MSC amount and Ns FQ were found to occur with decreased (increased) SST. A quantitative examination of the frequency and strength of synoptic activity demonstrated that year-to-year meridional shifts in storm track location were consistent with the observed variability in Ns FQ. Although a slightly weaker (stronger) subtropical anticyclone was observed during summers with increased (decreased) MSC amount and Ns FQ, relationships between seasonal-mean cloudiness and circulation were found to be generally weak.

In order to understand the processes by which variability in SST and synoptic activity produce variability in MSC, it was necessary to document the typical MBL structure and meteorological conditions associated with various low stratiform cloud types contributing to MSC. Chapter 3 presented soundings and surface meteorological observations composited on low cloud type for several locations in the midlatitude and subtropical oceans. Stratocumulus types were observed to occur in relatively well-mixed, inversion-capped MBLs with inferred cold advection, and fair-weather stratus, sky-obscuring fog, and no-low-cloud were observed to occur in stratified MBLs with inferred warm advection. Chapter 4 examined the association between the SST gradient, inferred advection, and climatological meridional distributions of the amount of low cloud types

over the central North Pacific. The results suggested that equatorward advection over increasing SST produces a transition from stratocumulus to cumulus-under-stratocumulus to cumulus as the MBL becomes increasingly decoupled (conceptually illustrated in Fig. 4.13), and that poleward advection over decreasing SST produces a transition from cumulus to no-low-cloud to fair-weather stratus and sky-obscuring fog as CAPE decreases and the near-surface layer becomes increasingly stratified (conceptually illustrated in Fig. 4.12). Several satellite images were presented which supported the results obtained from surface observations.

The documented low cloud type composites and climatological transitions in low cloud type provided a foundation for understanding processes through which variability in SST and synoptic activity produces variability in MSC amount during summer. For MBLs undergoing equatorward advection, anomalously cold (warm) water delays (advances) the onset of strong MBL decoupling along the trajectory and hence delays (advances) the breakup of stratocumulus into cumulus. For MBLs undergoing poleward advection, anomalously cold (warm) water advances (delays) the onset of strong near-surface stratification and decreased CAPE along the trajectory and hence advances (delays) the replacement of subtropical cumulus by fair-weather stratus and sky-obscuring fog. Thus, whether or not advection is poleward or equatorward, MSC amount increases (decreases) with decreased (increased) SST.

Variability in synoptic activity was observed to have less impact on MSC amount than SST, although increased synoptic activity tends to favor stratocumulus types, and, of course, bad-weather stratus over fair-weather stratus and sky-obscuring fog. No attempt was made to determine whether such a change in the relative contribution of each low stratiform cloud type to MSC amount would change the typical MSC optical thickness. Information about time and space variations in cloud optical thickness associated with extratropical cyclones can be obtained only using satellite observations, not the surface observations of cloud amount and type used in the present study.

An attempt was made to assess the radiative impact of variability in MSC amount on SST during summer, but negligible correlation was found between seasonal-mean

anomalies in MSC amount and anomalies in SST tendency over the season. Although it is possible that variability in MSC amount has a much smaller effect on the surface energy budget than estimated in the present study, it seems more likely that other processes such as anomalies in turbulent heat flux tend to compensate for MSC-induced radiative anomalies in the net surface energy budget. However, the existence of compensating processes to anomalous radiative forcing by MSC does not negate the possible importance of a cloud feedback on SST because there is no guarantee that the amount of compensation will remain the same in a changing climate. Moreover, any GCM which correctly simulates one but not the other will produce a biased surface energy budget. Therefore, it will be necessary to develop a more quantitative understanding of processes influencing SST at midlatitudes during summer in general and the variability in surface net CRF associated with variability in cloud amount and cloud type in particular before the magnitude of a positive feedback of cloudiness on SST can be determined.

6.2 Variability in the surface energy budget and sea surface temperature

In order to better understand the role of CRF in producing variability in the surface energy budget and SST of the midlatitude SST gradient region during summer, it is useful to compare the different roles of CRF and latent heat flux in producing variability in the surface energy budget and SST of the eastern subtropical ocean during summer and the midlatitude SST gradient region during winter.

Ronca (1995) and Ronca and Battisti (1997) examined monthly variations in surface fluxes, SST, and SST tendency at OWS N during summer and winter seasons. They found that variability in SST tendency was best correlated with variability in latent heat flux, even during summer. Since most of the variability in latent heat flux resulted from variability in wind speed, they concluded that the atmosphere was driving the ocean, with negligible direct SST feedback on wind speed. On the other hand, variability in SW radiation (estimated from surface-observed cloud amount using a bulk formula) was best correlated with variability in SST, but had little correlation with variability in SST tendency.* The lack of correlation between variability in SW and variability in SST

tendency was attributed to compensation by latent heat flux and LW radiation; i.e., negative feedbacks in latent heat flux and LW radiation balanced the positive SW cloud feedback. The negative latent heat flux feedback was attributed to the Clausius-Clapeyron relationship (less evaporation occurs with cold anomalies and more evaporation occurs with warm anomalies), but was not directly assessed. Figure 6.1 conceptually illustrates how latent heat flux and SW radiation are related to SST anomalies in the summertime eastern subtropical ocean.

In contrast to variability in latent heat flux over the eastern subtropical ocean, variability in latent heat flux over the midlatitude SST gradient region during summer primarily results from variability in relative humidity (not shown). Although this can be produced by changes in advection over the SST gradient, it appears that most of the variability in seasonal-mean relative humidity is due to variability in SST; i.e., seasonal-mean poleward advection over anomalously cold (warm) water produces increased (decreased) ΔT and relative humidity, particularly on the equatorward side of the SST gradient region.* Thus, latent heat flux has a significant response to variability in SST in addition to producing variability in SST, which provides a significant negative feedback on SST. This negative feedback is not important in the eastern subtropical ocean because relative humidity variations do not have as much influence on latent heat flux (probably because near-surface air can more easily adjust to SST when it is negatively instead of positively stratified). Thus, MSC provides a positive feedback on SST in both the

* The relative weakness of variability in SW CRF compared to variability in latent heat flux at OWS N is probably not representative of a large part of the eastern subtropical ocean. The interannual variance of summertime MSC amount is low at the location of OWS N compared to elsewhere in the eastern subtropical ocean (NZW); also note that OWS N (30°N, 140°W) is located along a zero line of the leading MSC EOF (Fig. 2.2) and MSC–SST SVD (Fig. 2.4).

* Negative SST anomalies are associated with anomalous northerly flow (Fig. 5.2c), which would produce decreased ΔT (Fig. 4.15a) and relative humidity. The fact that decreased relative humidity is not observed with decreased SST suggests that variability in seasonal-mean advection is not as important as variability in SST for producing variability in latent heat flux.

midlatitude and eastern subtropical oceans, but latent heat flux has a strong negative feedback on SST only at midlatitudes. Figure 6.2 conceptually illustrates how latent heat flux and SW radiation are related to SST anomalies in the summertime midlatitude ocean.

Seasonally reduced insolation considerably reduces SW CRF and the greater land-ocean temperature contrast substantially increases latent and sensible heat fluxes over the midlatitude ocean during winter. Although the interannual variance of seasonal-mean SST is slightly lower during winter than summer (Zhang et al. 1997), the variability in the heat content of the oceanic mixed layer is much larger during winter due to the much deeper mixed layer. In fact, Namias and Born (1970, 1974) hypothesized, and Alexander and Deser (1995) observationally confirmed, that temperature anomalies created in a deep wintertime mixed layer can disappear below a shallow unrelated summertime mixed layer and reappear at the surface the following winter. Accordingly, if the memory of the ocean is solely from winter to winter, it may not matter how much radiative forcing associated with variability in MSC amount impacts SST during summer since that perturbation will be overwhelmed when the anomaly from the previous winter is mixed up from subsurface water.

On the other hand, recent results of Zhang et al. (1997) indicate that, although the persistence of local SST anomalies from winter into summer may be minimal, the persistence of large-scale anomaly patterns from winter into summer and from summer into winter is significant. If large-scale autumn and winter SLP anomalies over the North Pacific are influenced by SST patterns from the previous summer, as suggested by Davis (1978) (but without confirmation in more recent studies), then persistent summertime SST anomalies may influence patterns of atmospheric circulation the following winter. If these atmospheric circulation patterns act to reinforce the existing SST anomalies, then positive feedback on SST due to summertime MSC may act as a bridge from winter to winter along with subsurface heat content anomalies and thus contribute an additional mechanism for interdecadal variability in SST.

6.3 Long-term trends in cloudiness and sea surface temperature

The time series of the leading EOFs of MSC amount and SST presented in Figs. 2.2 and 2.3 exhibit substantial trends of increasing MSC amount and decreasing SST over the central North Pacific during summer. Deser et al. (1996) also observe a decreasing trend in subsurface temperature in the central North Pacific. Although the origins of interdecadal variability in the climate system are not well-understood, processes possibly responsible for the observed trends will now be considered. Of particular interest are climate forcings of anthropogenic origin such as increased greenhouse gases. Given the large uncertainties and many gaps in our understanding of interdecadal variability in the climate system, the following discussion should be viewed as speculative.

The results of the present study suggest that, although variability in surface net CRF associated with variability in MSC amount may have a non-negligible impact on SST, it is primarily variability in SST that drives variability in MSC amount over the midlatitude North Pacific during summer. Thus, a positive MSC feedback on SST may reinforce SST anomalies, but the initial SST variability is probably generated by a different process. Given the relative weakness and tendency for cancelation of fluxes during summer, it is likely that SST anomalies have their origin in the winter season and then persist into the summer season.

A substantial amount of research has been directed towards examining the source of wintertime SST anomalies (Lau 1997) and whether they primarily result from purely midlatitude atmosphere–ocean interaction or from a midlatitude atmospheric response to tropical forcing associated with El Niño / Southern Oscillation (ENSO) (Horel and Wallace 1981; Rassmusson and Wallace 1983). SST in the central North Pacific is observed to generally be anomalously low during winters when SST in the eastern and central equatorial Pacific is anomalously high (Weare et al. 1976). Several GCM studies indicate that wintertime Northern Hemisphere atmospheric circulation is more sensitive to tropical Pacific SST anomalies than midlatitude North Pacific SST anomalies (e.g. Alexander 1992a; Graham et al. 1994; Lau and Nath 1994), and the anomalous atmospheric circulation which develops in turn forces SST anomalies over the midlatitude

North Pacific (Alexander 1992b). Trenberth (1990) and Trenberth and Hurrell (1994) attribute interdecadal variability in SST and atmospheric circulation over the midlatitude North Pacific to recent changes in the frequency and intensity of El Niño versus La Niña events. This scenario suggests the observed upward trend in MSC amount over the central midlatitude North Pacific during summer results from the following processes:

1) increasing tendency toward the warm phase of ENSO, which generates
2) anomalous wintertime Northern Hemisphere atmospheric circulation, which produces
3) a downward trend in SST in the central North Pacific during winter, which
4) through persistence becomes a downward trend in SST during summer, and
5) produces an upward trend in MSC amount.

On the other hand, observational studies have found significant variability in SST and atmospheric circulation over the midlatitude North Pacific that occurs independently of ENSO (Deser and Blackmon 1995; Zhang et al. 1996). The observational and modeling studies of Latif and Barnett (1994, 1996) with supporting observations of Zhang and Levitus (1997) suggest that the internal dynamics of the midlatitude North Pacific atmosphere–ocean system can produce decadal variability in atmospheric circulation and SST. This scenario suggests the observed upward trend in MSC amount over the central midlatitude North Pacific during summer results from the following processes:

1) interdecadal cycle due to extratropical atmosphere–ocean interaction and gyre circulation results in
2) a downward trend in SST in the central North Pacific during winter, which
3) through persistence becomes a downward trend in SST during summer, and
4) produces an upward trend in MSC amount.

Of course, both scenarios may contribute to the observed upward trend in MSC amount. Moreover, Gu and Philander (1997) hypothesize that subsurface exchange between the eastern subtropical and tropical Pacific can produce interdecadal variability and is

responsible for the persistence of the warm phase of ENSO in recent years.

Possible impacts of increasing greenhouse gases on the observed trends are even more difficult to determine. Trenberth and Hoar (1996) speculate that the recent prolonged warm event during 1990–1995 may be partly caused by increased greenhouse gases, but GCM studies of ENSO behavior show little change under conditions of increased warming and CO_2 concentration (Knutson et al. 1997; Smith et al. 1997). In the long term, the global ocean will eventually warm and come to an equilibrium with a greenhouse-gas enriched atmosphere. For the case of this future scenario, the results of the present study suggest global midlatitude MSC amount may decrease and thus provide a positive feedback. Decreased MSC amount would probably result even if the strength of the midlatitude SST gradient remained unchanged because a uniform increase in SST would contribute to greater CAPE and therefore encourage the breakup of stratocumulus into cumulus and resist the transition from cumulus to stratus.

Of course, this assumes there would be no compensating changes in above-surface atmospheric temperature structure and dynamics. For example, Miller (1997) simulated the response of tropical and subtropical MSC to doubled CO_2 using a model based on that of Pierrehumbert (1995) and a parameterization for MSC amount based on the relationship with S found by Klein and Hartmann (1993). He found that, although SST increased with doubled CO_2, 700-mb temperature increased even more, causing MSC amount to increase and producing a negative feedback on SST. A stronger hydrological cycle resulting from global warming could produce increased monsoon circulations which lead to increased heating over continents and increased subsidence over oceans (suggested by C. Leovy). In this scenario, Fig. 2.8 suggests a strengthened subtropical anticyclone would favor increased MSC amount over the eastern subtropical North Pacific and decreased MSC amount over central midlatitude North Pacific. Thus, both increased SST and a possible change in atmospheric circulation resulting from global warming contribute to decreased MSC amount over the midlatitude ocean. These scenarios preclude the attribution of global warming as the cause of the observed increase in MSC amount over the summertime central midlatitude North Pacific during the past several decades.

Although summertime midlatitude MSC acts as a positive feedback on SST in the short term, it can only be tentatively concluded that summertime midlatitude MSC acts as a positive feedback on the climate system in the long term due to the great uncertainties involved with understanding climate variability and climate change.

6.4 Directions of future research

The greatest weakness of the present study is the lack of quantitative radiative information because it prevents a precise assessment of the impact of variability in MSC amount and low stratiform cloud types on SST. Although bulk models have been developed to provide downward SW and LW radiation as a function of surface-observed cloud amount and cloud type, it is unlikely that these will ever provide an accurate and universal estimate of surface net CRF over the ocean due to large and unmeasured variations in cloud optical thickness, even for individual cloud types. Thus, obtaining a reasonably precise quantitative record of interdecadal variability in surface net CRF over the ocean will remain an intractable problem. Instead, efforts would be better directed towards examining interannual variability in satellite-estimated surface net CRF to obtain a more reliable estimate of typical anomalies in MSC radiative forcing than the 1 W m^{-2} per 1% cloud amount used in the present study. Furthermore, it is essential to determine whether geographic variations in MSC optical thickness occur and whether systematic differences in MSC optical thickness exist between warm-advection stratus and fog and cold-advection stratocumulus types, both of which were neglected in the present study. Weaver and Ramanathan (1996) noted that optically thick midlevel cloudiness produced by extratropical cyclones during summer was associated with the largest observed negative TOA net CRF; therefore, a study should be undertaken to determine the relative contributions of midlevel cloudiness and MBL cloudiness to seasonal-mean CRF.

Another problem of the present study was the use of a VV dataset which appeared to suffer from significant spurious interannual variability; therefore, the analyses should be repeated with VV data obtained from the NCEP/NCAR Reanalysis Project (Kalnay et al. 1996). This may eliminate much of the spurious variability which could be obscuring

relationships with MSC amount and other parameters and thus better illuminate the role of variability in synoptic activity in producing variability in MSC amount and low stratiform cloud types. It may also be possible to use vertical motion as an index of synoptic activity. Reanalysis data would also provide above-surface and non-local information back to 1957 so that relationships between low cloud type, advection, and vertical motion could be directly composited instead of merely inferred.

Although extensive modeling of the eastern subtropical stratocumulus-to-cumulus transition has been done, Fig. 3.5 suggests that the MBL is typically shallower and ΔT is typically weaker for stratocumulus at midlatitudes. For this reason, it would be useful to model midlatitude stratocumulus and the midlatitude stratocumulus-to-cumulus transition to better understand the conditions which promote stratocumulus breakup. It is even more important to model the cumulus-to-stratus transition since that has received little previous attention. In particular, it would be useful to know whether there is some "critical" SST at which stratus forms or stratocumulus breaks up. This could help the development and validation of improved MBL cloud parameterizations in GCMs, especially since most GCMs poorly simulate MBL cloudiness at midlatitudes at the present time. However, in order to better carry out modeling simulations of MBL cloudiness at midlatitudes, more detailed observations of MBL structure and microphysical properties associated with various low cloud types are needed, particularly those which occur with warm advection and near-surface stratification. For this reason it would be useful to undertake field programs to investigate processes associated with MBL cloudiness at midlatitudes similar to those undertaken over the eastern subtropical ocean (e.g., FIRE, ASTEX).

The results of Table 5.3 indicate that neither anomalies in turbulent heat flux nor anomalies in radiation loss due to MSC amount are strongly coupled to anomalies in SST tendency in the summertime central midlatitude North Pacific. This suggests processes besides surface fluxes are important for generating SST variability during summer. Although "equivalent flux" due to anomalous zonal stress was found to be much weaker than the surface fluxes, the sum of the contributions due to anomalous Ekman transport, geostrophic advection, horizontal mixing, turbulent entrainment, and variations in mixed

layer depth may be as important for producing anomalies in SST tendency as anomalies in surface flux. A good ocean model and a better understanding of ocean dynamics will be required to sort this out.

Although farther beyond the scope of a study such as this, the issue of interdecadal variability in SST cannot be settled until coupled ocean-atmosphere interaction and dynamics are better understood, specifically the role of SST anomalies in generating anomalous atmospheric circulation, especially during summer. It would be desirable to use a GCM to investigate the potential for a positive MSC feedback on SST since other processes can be held constant to focus on the relationship between MSC and SST. However, this cannot be done until, among other things, GCMs more accurately simulate MBL cloudiness at midlatitudes during summer. In fact, GCM MBL cloud parameterizations can be tested by examining whether the model is able to correctly simulate the observed interannual and interdecadal co-variability between MSC and SST.

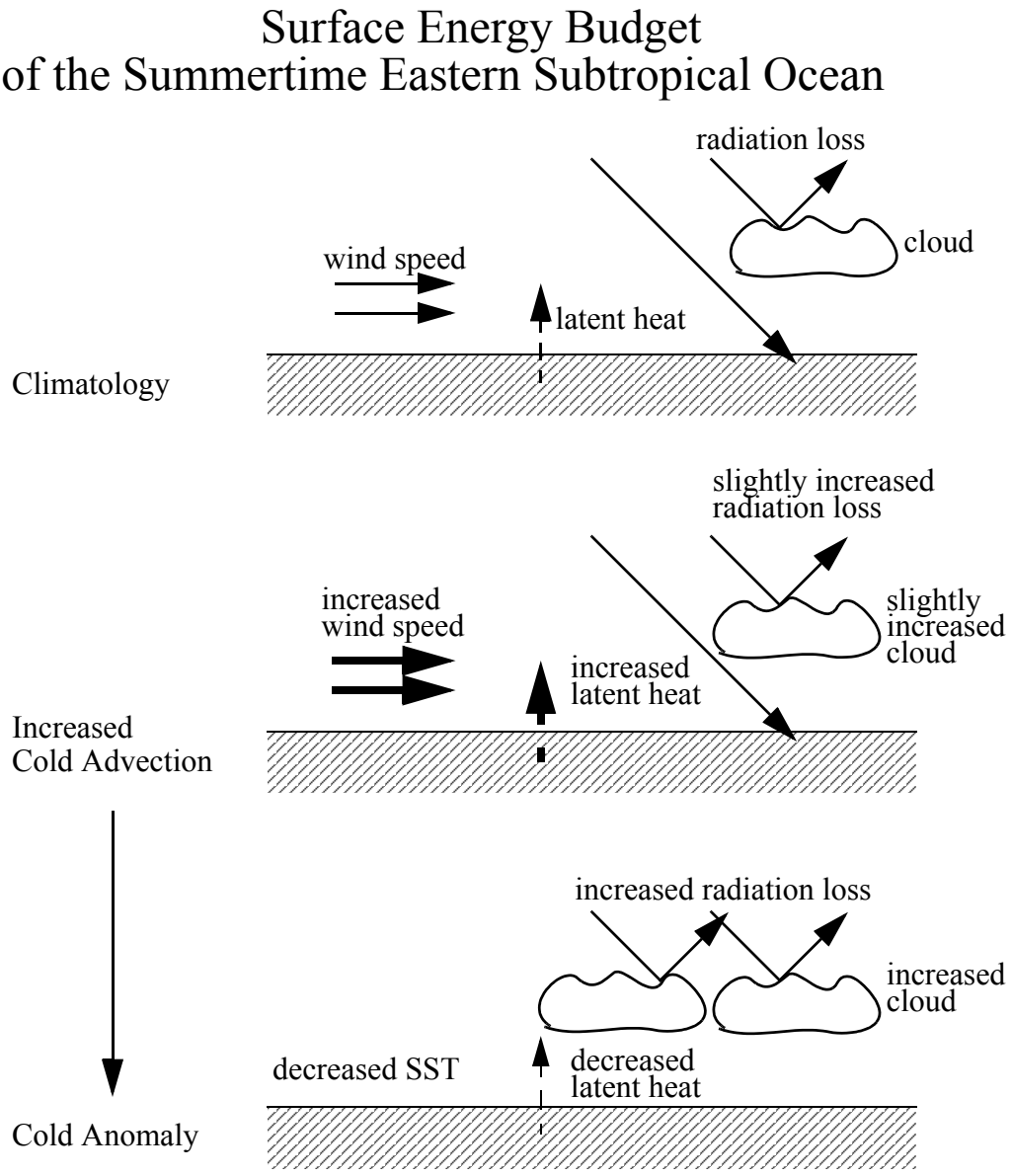

Figure 6.1: Conceptual model illustrating the surface energy budget of the summertime eastern subtropical ocean (adopted from Ronca and Battisti 1997).

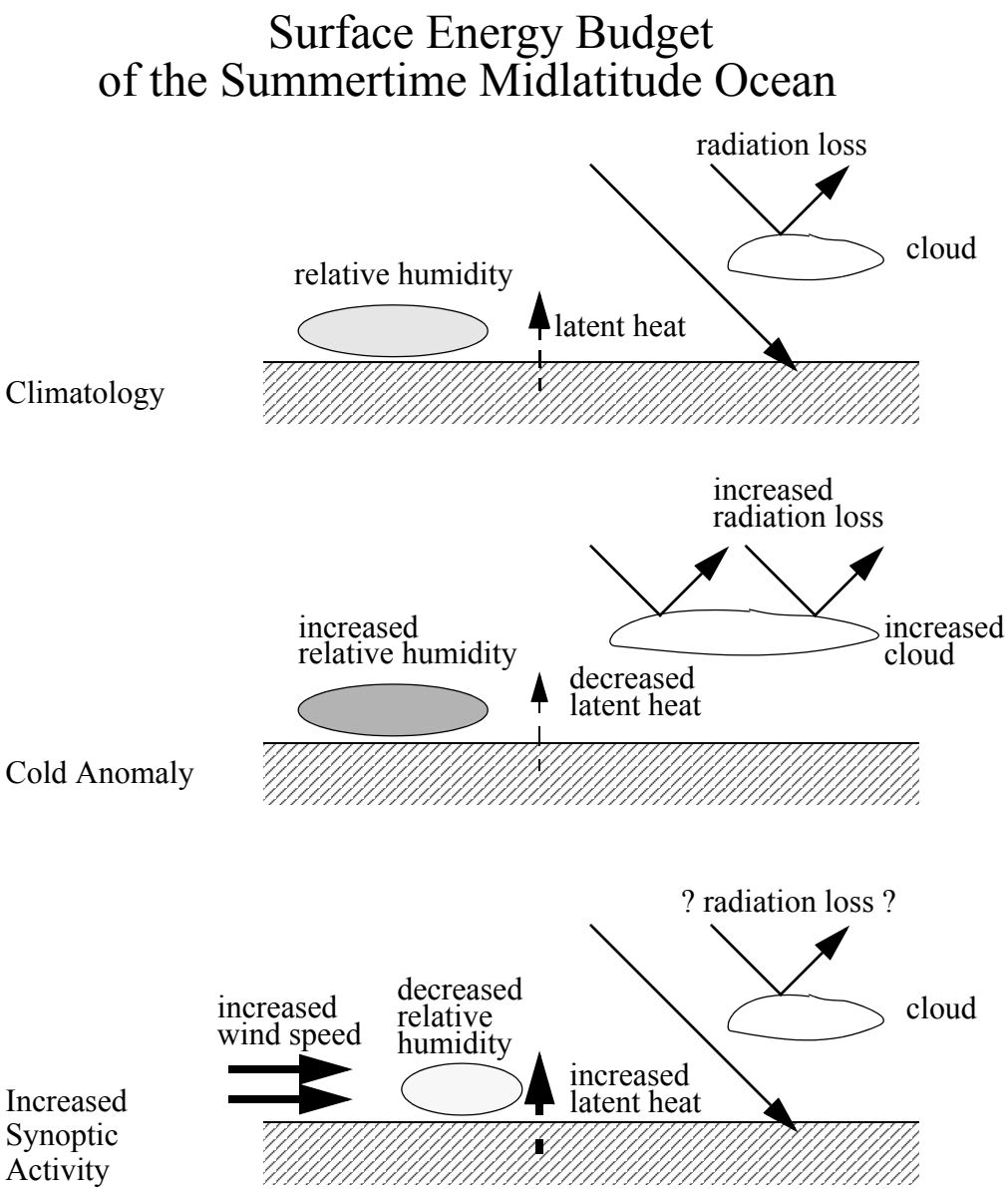

Figure 6.2: Conceptual model illustrating the surface energy budget of the summertime midlatitude ocean.

BIBLIOGRAPHY

Abakumova, G. M., E. M. Feigelson, V. Russak, and V. V. Stadnik, 1996: Evaluation of long-term changes in radiation, cloudiness, and surface temperature on the territory of the Former Soviet Union. *J. Climate*, **9**, 1319-1327.

Albrecht, B. A., 1984: A model study of downstream variations of the thermodynamic structure of the trade winds. *Tellus*, **36A**, 187-202.

———, 1989: Aerosols, cloud microphysics, and fractional cloudiness. *Science*, **245**, 1227-1230.

———, D. A. Randall, and S. Nicholls, 1988: Observations of marine stratocumulus clouds during FIRE. *Bull. Amer. Meteor. Soc.*, **69**, 618-626.

———, C. S. Bretherton, D. Johnson, W. H. Schubert, and A. S. Frisch, 1995a: The Atlantic Stratocumulus Transition Experiment – ASTEX. *Bull. Amer. Meteor. Soc.*, **76**, 889-904.

———, M. P. Jensen, and W. J. Syrett, 1995b: Marine boundary layer structure and fractional cloudiness. *J. Geophys. Res.*, **100**, 14209-14222.

Alexander, M. A., 1992a: Midlatitude atmosphere–ocean interaction during El Niño. Part I: the North Pacific ocean. *J. Climate*, **5**, 944-958.

———, 1992b: Midlatitude atmosphere–ocean interaction during El Niño. Part II: the Northern Hemisphere atmosphere. *J. Climate*, **5**, 959-972.

———, and C. Deser, 1995: A mechanism for the recurrence of wintertime midlatitude SST anomalies. *J. Phys. Oceangr.*, **25**, 123-137.

Angell, J. K., 1990: Variation in United States cloudiness and sunshine duration between 1950 and the drought year of 1988. *J. Climate*, **3**, 296-308.

———, J. Korshover, and G. F. Cotton, 1984: Variation in United States cloudiness and sunshine, 1950-82. *J. Climate Appl. Meteor.,* **23**, 752-761.

Anonymous, 1958-1981: Principal tracks of centers of cyclones at sea level, North Pacific. *Mar. Wea. Log*, **2-26**.

Arking, A., 1991: The radiative effects of clouds and their impact on climate. *Bull. Amer. Meteor. Soc.*, **72**, 795-813.

———, 1996: Absorption of solar energy in the atmosphere: discrepancy between model and observations. *Science*, **273**, 779-782.

Atwater, M. A., and J. T. Ball, 1981: Surface solar radiation model for cloudy atmospheres. *Mon. Wea. Rev.*, **109**, 878-888.

Augstein, E., H. Schmidt, and F. Ostapoff, 1974: The vertical structure of the atmospheric

planetary boundary layer in undisturbed trade winds over the Atlantic Ocean. *Bound.-Layer Meteor.*, **6**, 129-150.

Bajuk, L. J., and C. B. Leovy, 1997a: Marine clouds from surface observations. Part I: seasonal and interannual variations in tropical low cloud types. *J. Climate*, submitted.

———, and C. B. Leovy, 1997b: Marine clouds from surface observations. Part II: interdecadal variations. *J. Climate*, submitted.

Baker, C. B., R. G. Quayle, and W. Wanlin, 1995: The influence of night time cloud cover on the observed minimum temperature in China. *Atmos. Res.*, **37**, 27-35.

Baker, M. B., 1997: Cloud microphysics and climate. *Science*, **276**, 1072-1078.

Barkstrom, B., E. Harrison, G. Smith, R. Green, J. Kibler, R. Cess, and the ERBE Science Team, 1989: Earth Radiation Budget Experiment (ERBE) archival and April 1985 results. *Bull. Amer. Meteor. Soc.*, **70**, 1254-1262.

Bathen, K. H., 1972: On the seasonal changes in the depth of the mixed layer in the North Pacific ocean. *J. Geophys. Res.*, **77**, 7138-7150.

Battisti, D. S., U. S. Bhatt, and M. A. Alexander, 1995: A modeling study of the interannual variability in the wintertime North Atlantic ocean. *J. Climate*, **8**, 3067-3083.

Berry, F. A., E. Bollay, and N. R. Beers, 1945: *Handbook of Meteorology.* McGraw-Hill Book Company, 1068 pp.

Betts, A. K., 1990: Diurnal variation of the California coastal stratocumulus from two days of boundary layer soundings. *Tellus*, **42A**, 302-304.

———, C. S. Bretherton, and E. Klinker, 1995: Relation between mean boundary-layer structure and cloudiness at the R/V *Valdivia* during ASTEX. *J. Atmos. Sci.*, **52**, 2752-2762.

Bishop, J. K. B., and W. B. Rossow, 1991: Spatial and temporal variability of global surface solar irradiance. *J. Geophys. Res.*, **96**, 16839-16858.

———, W. B. Rossow, and E. G. Dutton, 1997: Surface solar irradiance from the International Satellite Cloud Climatology Project 1983-1991. *J. Geophys. Res.*, **102**, 6883-6910.

Blackmon, M. L., J. M. Wallace, N.-C. Lau, and S. L. Mullen, 1977: An observational study of the Northern Hemisphere wintertime circulation. *J. Atmos. Sci.*, **34**, 1040-1053.

Blanc, T. V., 1986: The effect of inaccuracies in weather-ship data on bulk-derived estimates of flux, stability and sea-surface roughness. *J. Atmos. Ocean Technol.*, **3**, 12-26.

Blender, R., K. Fraedrich, and F. Lunkeit, 1997: Identification of cyclone-track regimes in

the North Atlantic. *Quart. J. Roy. Meteor. Soc.*, **123**, 727-741.

Bolton, D., 1980: The computation of equivalent potential temperature. *Mon. Wea. Rev.*, **108**, 1046-1053.

Bottomley, M., C. K. Folland, J. Hsiung, R. E. Newell, and D. E. Parker, 1990: *Global Ocean Surface Temperature Atlas.* U.K. Meteorological Office, Massachusetts Institute of Technology, Department of Earth, Atmospheric, and Planetary Sciences, 20 pp. + 313 maps.

Bretherton, C. S., 1992: A conceptual model of the stratocumulus-trade-cumulus transition in the subtropical oceans. *Proc. 11th Int. Conf. on Clouds and Precipitation*, Montreal, Canada, 374-377.

———, and R. Pincus, 1995: Cloudiness and marine boundary layer dynamics in the ASTEX Lagrangian experiments. Part I: synoptic setting and vertical structure. *J. Atmos. Sci.*, **52**, 2707-2723.

———, and W. C. Wyant, 1997: Moisture transport, lower-tropospheric stability, and decoupling of cloud-topped boundary layers. *J. Atmos. Sci.*, **54**, 148-167.

———, C. Smith, and J. M. Wallace, 1992: An intercomparison of methods for finding coupled patterns in climate data. *J. Climate*, **5**, 541-560.

———, P. Austin, and S. T. Siems, 1995a: Cloudiness and marine boundary layer dynamics in the ASTEX Lagrangian experiments. Part II: cloudiness, drizzle, surface fluxes, and entrainment. *J. Atmos. Sci.*, **52**, 2724-2735.

———, E. Klinker, A. K. Betts, and J. A. Coakley, 1995b: Comparison of ceilometer, satellite, and synoptic measurements of boundary-layer cloudiness and the ECMWF diagnostic cloud parameterization scheme during ASTEX. *J. Atmos. Sci.*, **52**, 2736-2751.

Cardone, V. J., J. G. Greenwood, and M. A. Cane, 1990: On trends in historical marine wind data. *J. Climate*, **3**, 113-127.

Cayan, D. R., 1992a: Latent and sensible heat flux anomalies over the northern oceans: driving the sea surface temperature. *J. Phys. Oceanogr.*, **22**, 859-881.

———, 1992b: Latent and sensible heat flux anomalies over the northern oceans: the connection to monthly atmospheric circulation. *J. Climate*, **5**, 354-369.

Cess, R. D., G. L. Potter, J. P. Blanchet, G. J. Boer, S. J. Ghan, J. T. Kiehl, H. Le Treut, Z.-X. Li, X. Z. Liang, J. F. B. Mitchell, J.-J. Morcrette, D. A. Randall, M. R. Riches, E. Roeckner, U. Schlese, A. Slingo, K. E. Taylor, W. M. Washington, R. T. Wetherald, and I. Yagai, 1989: Interpretation of cloud-climate feedback as produced by 14 atmospheric general circulation models. *Science*, **245**, 513-516.

———, G. L. Potter, J. P. Blanchet, G. J. Boer, A. D. Del Genio, M. Déqué, V. Dymnikov, V. Galin, W. L. Gates, S. J. Ghan, J. T. Kiehl, A. A. Lacis, H. Le Treut, Z.-X. Li, X. Z.

Liang, B. J. McAvaney, V. P. Meleshko, J. F. B. Mitchell, J.-J. Morcrette, D. A. Randall, L. Rikus, E. Roeckner, J. F. Royer, U. Schlese, D. A. Sheinin, A. Slingo, A. P. Sokolov, K. E. Taylor, W. M. Washington, R. T. Wetherald, I. Yagai, and M.-H. Zhang, 1990: Intercomparison and interpretation of climate feedback processes in 19 atmospheric general circulation models. *J. Geophys. Res.*, **95**, 16601-16615.

———, E. F. Harrison, P. Minnis, B. R. Barkstrom, V. Ramanathan, and T. Y. Kwon, 1992: Interpretation of seasonal cloud-climate interactions using Earth Radiation Budget Experiment data. *J. Geophys. Res.*, **97**, 7613-7617.

———, M. H. Zhang, P. Minnis, L. Corsetti, E. G. Dutton, B. W. Forgan, D. P. Garber, W. L. Gates, J. J. Hack, E. F. Harrison, X. Jing, J. T. Kiehl, C. N. Long, J.-J. Morcrette, G. L. Potter, V. Ramanathan, B. Subasilar, C. H. Whitlock, D. F. Young, and Y. Zhou, 1995: Absorption of solar radiation by clouds: observations versus models. *Science*, **267**, 496-499.

———, M. H. Zhang, W. J. Ingram, G. L. Potter, V. Alekseev, H. W. Barker, E. Cohen-Solal, R. A. Colman, D. A. Dazlich, A. D. Del Genio, M. R. Dix, V. Dymnikov, M. Esch, L. D. Fowler, J. R. Fraser, V. Galin, W. L. Gates, J. J. Hack, J. T. Kiehl. H. Le Treut, K. K.-W. Lo, B. J. McAvaney, V. P. Meleshko, J.-J. Morcrette, D. A. Randall, E. Roeckner, J. F. Royer, M. E. Schlesinger, P. V. Sporyshev, B. Timbal, E. M. Volodin, K. E. Taylor, W. Wang, and R. T. Wetherald, 1996: Cloud feedback in atmospheric general circulation models: an update. *J. Geophys. Res.,* **101**, 12791-12794.

Charlson, R. J., J. E. Lovelock, M. O. Andreae, and S. G. Warren, 1987: Oceanic phytoplankton, atmospheric sulphur, cloud albedo and climate. *Nature*, **326**, 655-661.

———, S. E. Schwartz, J. M. Hales, R. D. Cess, J. A. Coakley, J. E. Hansen, and D. J. Hofmann, 1992: Climate forcing by anthropogenic aerosols. *Science*, **255**, 423-430.

Chen, C.-T., and V. Ramaswamy, 1996a: Sensitivity of simulated global climate to perturbations in low-cloud microphysical properties. Part I: globally uniform perturbations. *J. Climate*, **9**, 1385-1402.

———, ———, 1996b: Sensitivity of simulated global climate to perturbations in low-cloud microphysical properties. Part II: spatially localized perturbations. *J. Climate*, **9**, 2788-2801.

Cherry, S., 1996: Singular value decomposition analysis and canonical correlation analysis. *J. Climate*, **9**, 2003-2009.

———, 1997: Some comments on singular value decomposition analysis. *J. Climate*, **10**, 1759-1761.

Chertock, B., R. Frouin, and R. C. J. Somerville, 1991: Global monitoring of net solar irradiance at the ocean surface: climatological variability and the 1982-1983 El Niño. *J. Climate*, **4**, 639-650.

Davis, R. E., 1976: Predictability of sea surface temperature and sea level pressure

anomalies over the North Pacific ocean. *J. Phys. Oceanogr.*, **6**, 249-266.

———, 1978: Predictability of sea level pressure anomalies over the North Pacific ocean. *J. Phys. Oceanogr.*, **8**, 233-246.

Del Genio, A. D., M.-S. Yao, W. Kovari, and K. K.-W. Lo, 1996: A prognostic cloud water parameterization for global climate models. *J. Climate*, **9**, 270-304.

Deser, C., and M. Blackmon, 1995: On the relationship between Tropical and North Pacific sea surface temperature variations. *J. Climate*, **8**, 1677-1680.

———, and M. S. Timlin, 1997: Atmosphere–ocean interaction on weekly timescales in the North Atlantic and Pacific. *J. Climate*, **10**, 393-408.

———, M. A. Alexander, and M. S. Timlin, 1996: Upper-ocean thermal variations in the North Pacific during 1970-1991. *J. Climate*, **9**, 1840-1855.

Dessens, J., and A. Bücher, 1995: Changes in minimum and maximum temperatures at the Pic du Midi in relation with humidity and cloudiness, 1882-1984. *Atmos. Res.*, **37**, 147-162.

Dobson, F. W., and S. D. Smith, 1988: Bulk models of solar radiation at sea. *Quart. J. Meteor. Soc.*, **114**, 165-182.

Elliott, W. P., and D. J. Gaffen, 1991: On the utility of radiosonde humidity archives for climate studies. *Bull. Amer. Meteor. Soc.*, **72**, 1507-1520.

Erickson, D. J., R. J. Oglesby, and S. Marshall, 1995: Climate response to indirect anthropogenic sulfate forcing. *Geophys. Res. Lett.*, **22**, 2017-2020.

Falkowski, P. G., Y. Kim, Z. Kolber, C. Wilson, C. Wirick, and R. Cess, 1992: Natural versus anthropogenic factors affecting low-level cloud albedo over the North Atlantic. *Science*, **256**, 1311-1313.

Ferranti, L., F. Molteni, and T. N. Palmer, 1994: Impact of localized tropical and extratropical SST anomalies in ensembles of seasonal GCM integrations. *Quart. J. Roy. Meteor. Soc.*, **120**, 1613-1645.

Frankignoul, C., 1985: Sea surface temperature anomalies, planetary waves, and air-sea feedback in the middle latitudes. *Rev. Geophys.*, **23**, 357-390.

Gallimore, R. G., 1995: Simulated ocean-atmosphere interaction in the North Pacific from a GCM coupled to a constant-depth mixed layer ocean. *J. Climate*, **8**, 1721-1737.

Goerss, J. S., and C. E. Duchon, 1980: Effect of ship heating on dry-bulb temperature measurements in GATE. *J. Phys. Oceanogr.*, **10**, 478-479.

Graham, N. E., T. P. Barnett, R. Wilde, M. Ponater, and S. Schubert, 1994: On the roles of tropical and midlatitude SSTs in forcing interannual to interdecadal variability in the winter Northern Hemisphere circulation. *J. Climate*, **7**, 1416-1441.

Gu, D., and S. G. H. Philander, 1997: Interdecadal climate fluctuations that depend on exchanges between the Tropics and extratropics. *Science*, **275**, 805-807.

Gupta, S. K., W. F. Staylor, W. L. Darnell, A.C. Wilber, and N. A. Ritchey, 1993: Seasonal variation of surface and atmospheric cloud radiative forcing over the globe derived from satellite data. *J. Geophys. Res.*, **98**, 20761-20778.

Hahn, C. J., S. G. Warren, and J. London, 1995: The effect of moonlight on observation of cloud cover at night, and application to cloud climatology. *J. Climate*, **8**, 1429-1446.

———, ———, ———, 1996: *Edited synoptic cloud reports from ships and land stations over the globe, 1982-1991*. Rep #NDP026B, 45 pp. [Available from Carbon Dioxide Information Analysis Center, Oak Ridge National Laboratory, P. O. Box 2008, Oak Ridge, TN 37831-6050]

Han, Q., W. B. Rossow, A. A. Lacis, 1994: Near-global survey of effective droplet radii in liquid water clouds using ISCCP Data. *J. Climate*, **7**, 465-497.

Hanson, H. P., 1991: Marine stratocumulus climatologies. *International Journal of Climatology*, **11**, 147-164.

Harrison, E. F., P. Minnis, B. R. Barkstrom, V. Ramanathan, R. D. Cess, and G. G. Gibson, 1990: Seasonal variation of cloud radiative forcing derived from the Earth radiation Budget Experiment. *J. Geophys. Res.*, **95**, 18687-18703.

Hartmann, D. L., 1994: *Global Physical Climatology.* Academic Press, 408pp.

———, and D. Doelling, 1991: On the net radiative effectiveness of clouds. *J. Geophys. Res.*, **96**, 869-891.

———, M. E. Ockert-Bell, and M. L. Michelsen, 1992: The effect of cloud type on Earth's energy balance: global analysis. *J. Climate*, **5**, 1281-1304.

Haskins, R. D., T. P. Barnett, M. M. Tyree, and E. Roeckner, 1995: Comparison of cloud fields from atmospheric general circulation model, in situ and satellite measurements. *J. Geophys. Res.*, **100**, 1367-1378.

Hellerman, S., and M. Rosenstein, 1983: Normal monthly wind stress over the world ocean with error estimates. *J. Phys. Oceangr.*, **13**, 1093-1104.

Henderson-Sellers, A., 1986a: Cloud changes in a warmer Europe. *Clim. Change*, **8**, 25-52.

———, 1986b: Increasing cloud in a warming world. *Clim. Change*, **9**, 267-309.

———, 1989: North American total cloud amount variations this century. *Global Planet. Change*, **1**, 175-194.

Hignett, P., 1991: Observations of diurnal variation in a cloud-capped marine boundary layer. *J. Atmos. Sci.*, **48**, 1474-1482.

Horel, J. D., and J. M. Wallace, 1981: Planetary-scale atmospheric phenomena associated with the Southern Oscillation. *Mon. Wea. Rev.*, **109**, 813-829.

Hoskins, B. J., H. H. Hsu, I. N. James, M. Masutani, P. D. Sardeshmukh, and G. H. White, 1989: Diagnostics of the global atmospheric circulation based on ECMWF analyses 1979-1989. WCRP-27, WMO/TD - No. 326., WMO, 219 pp

Houze, R. A., 1993: *Cloud Dynamics*. Academic Press, 573 pp.

Hu, Q., 1997: On the uniqueness of the singular value decomposition in meteorological applications. *J. Climate*, **10**, 1762-1766.

Husby, D. M., 1980: A comparison of surface heat flux estimates from Ocean Weather Station V and merchant vessels in its vicinity in the western North Pacific region, 1956-1970. *J. Phys. Oceanogr.*, **10**, 971-975.

Imre, D. G., E. H. Abramson, and P. H. Daum, 1996: Quantifying cloud-induced shortwave absorption: an examination of uncertainties and of recent arguments for large excess absorption. *J. Appl. Meteor.*, **35**, 1991-2010.

Intergovernmental Panel on Climate Change (IPCC), 1996: *Climate Change 1995: The Science of Climate Change*. J. T. Houghton, L. G. Meira Filho, B. A. Callander, N. Harris, A. Kattenberg, and K. Maskell (eds.), Cambridge University Press, Cambridge, UK

Isemer, H.-J., and L. Hasse, 1991: The scientific equivalent scale: effects on wind statistics and climatological air-sea flux estimates in the North Atlantic ocean. *J. Climate*, **4**, 819-836.

Iwasaka, N., and J. M. Wallace, 1995: Large scale air sea interaction in the Northern Hemisphere from a view point of variations of surface heat flux by SVD analysis. *J. Meteor. Soc. Japan*, **73**, 781-794.

Jones, A., and A. Slingo, 1996: Predicting cloud-droplet effective radius and indirect sulphate aerosol forcing using a general circulation model. *Quart. J. Roy. Meteor. Soc.*, **122**, 1573-1595.

———, D. L. Roberts, and A. Slingo, 1994: A climate model study of indirect radiative forcing by anthropogenic sulphate aerosols. *Nature*, **370**, 450-453.

Jones, P. A., and A. Henderson-Sellers, 1992: Historical records of cloudiness and sunshine in Australia. *J. Climate*, **5**, 260-267.

Jones, P. D., T. M. L. Wigley, C. K. Folland, and D. E. Parker, 1987: Spatial patterns in recent worldwide temperature trends. *Climate Monitor*, **16**, 175-185.

Kalnay, E. M. Kanamitsu, R. Kistler, W. Collins, D. Deaven, L. Gandin, M. Iredell, S. Saha, G. White, J. Woollen, Y. Zhu, M. Chelliah, W. Ebisuzaki, W. Higgins, J. Janowiak, K. C. Mo, C. Ropelewski, J. Wang, A. Leetmaa, R. Reynolds, R. Jenne, and D. Joseph, 1996: The NCEP/NCAR 40-year reanalysis project. *Bull. Amer.*

Meteor. Soc., **77**, 437-471.

Katsaros, K. B., 1990: Parameterization schemes and models for estimating the surface radiation budget. *Surface Waves and Fluxes*, Geernaert and Plant, Eds., Kluwer Academic Publishers, 672-701.

Kent, E. C., P. K. Taylor, B. S. Truscott, and J. S. Hopkins, 1993a: The accuracy of voluntary observing ships' meteorological observations – results of the VSOP-NA. *J. Atmos. Oceanic Technol.*, **10**, 591-608.

———, R. J. Tiddy, and P. K. Taylor, 1993b: Correction of marine air temperature observations for solar radiation effects. *J. Atmos. Oceanic Technol.*, **10**, 900-906.

Kiehl, J. T., and V. Ramanathan, 1990: Comparison of cloud forcing derived from the Earth Radiation Budget Experiment with that simulated by the NCAR Community Climate Model. *J. Geophys. Res.*, **95**, 11679-11698.

———, and D. L. Williamson, 1991: Dependence of cloud amount on horizontal resolution in the National Center for Atmospheric Research Community Climate Model. *J. Geophys. Res.*, **96**, 10955-10980.

———, J. J. Hack, and B. P. Briegleb, 1994: The simulated Earth radiation budget of the National Center for Atmospheric Research community climate model CCM2 and comparisons with the Earth Radiation Budget Experiment (ERBE). *J. Geophys. Res.*, **99**, 20815-20827.

Klein, S. A., 1994: Large-scale variations in boundary layer cloud cover and their relationships to meteorological parameters. Ph.D. Thesis, University of Washington, Seattle, 206 pp.

———, 1997: Synoptic variability of low cloud properties and meteorological parameters in the subtropical trade wind boundary layer. *J. Climate*, accepted.

———, and D. L. Hartmann, 1993a: Spurious changes in the ISCCP dataset. *Geophys. Res. Lett.*, **20**, 455-458.

———, and D. L. Hartmann, 1993b: The seasonal cycle of low stratiform clouds. *J. Climate*, **6**, 1587-1606.

———, D. L. Hartmann, and J. R. Norris, 1995: On the relationships among low-cloud structure, sea surface temperature, and atmospheric circulation in the summertime northeast Pacific. *J. Climate*, **8**, 1140-1155.

Kloesel, K. A., 1992: Marine stratocumulus cloud clearing episodes observed during FIRE. *Mon. Wea. Rev.*, **120**, 565-578.

Knutson, T. R., S. Manabe, and D. Gu, 1997: Simulated ENSO in a global ocean-atmosphere model: multidecadal amplitude modulation and CO_2 sensitivity. *J. Climate*, **10**, 138-161.

Koracin, D., and D. P. Rogers, 1990: Numerical simulations of the response of the marine atmosphere to ocean forcing. *J. Atmos. Sci.*, **47**, 592-611.

Kushnir, Y., 1994: Interdecadal variations in North Atlantic sea surface temperature and associated atmospheric conditions. *J. Climate*, **7**, 141-157.

———, and N.-C. Lau, 1992: The general circulation model response to a North Pacific SST anomaly: dependence on time scale and pattern polarity. *J. Climate*, **5**, 271-283.

———, and I. M. Held, 1996: Equilibrium atmospheric response to North Atlantic SST anomalies. *J. Climate*, **9**, 1208-1220.

Kutzbach, J. E., 1967: Empirical eigenvectors of sea-level pressure, surface temperature and precipitation complexes over North America. *J. Appl. Meteor.*, **6**, 791-802.

Lambert, S. J., 1996: Intense extratropical northern hemisphere winter cyclone events: 1899-1991. *J. Geophys. Res.*, **101**, 21319-21325.

Langner, J., H. Rodhe, P. J. Crutzen, and P. Zimmermann, 1992: Anthropogenic influence on the distribution of tropospheric sulphate aerosol. *Nature*, **359**, 712-716.

Laszlo, I., and R. Pinker, 1993: Shortwave cloud-radiative forcing at the top of the atmosphere at the surface and of the atmospheric column as determined from ISCCP C1 data. *J. Geophys. Res.*, **98**, 2703-2713.

Latif, M., and T. P. Barnett, 1994; Causes of decadal climate variability over the North Pacific and North America. *Science*, **266**, 634-637.

———, and ———, 1996: Decadal climate variability over the North Pacific and North America: dynamics and predictability. *J. Climate*, **9**, 2407-2423.

Lau, N.-C., 1988: Variability of the observed midlatitude storm tracks in relation to low-frequency changes in the circulation pattern. *J. Atmos. Sci.*, **45**, 2718-2743.

———, 1997: Interactions between global SST anomalies and the midlatitude atmospheric circulation. *Bull. Amer. Meteor. Soc.*, **78**, 21-33.

———, and M. J. Nath, 1990: A general circulation model study of the atmospheric response to extratropical SST anomalies observed in 1950-1979. *J. Climate*, **3**, 965-989.

———, and M. J. Nath, 1994: A modeling study of the relative roles of tropical and extratropical SST anomalies in the variability of the global atmosphere–ocean system. *J. Climate*, **7**, 1184-1207.

———, and M. W. Crane, 1995: A satellite view of the synoptic-scale organization of cloud cover in midlatitude and tropical circulation systems. *Mon. Wea. Rev.*, **123**, 1984-2006.

———, and M. W. Crane, 1997: Comparing satellite and surface observations of cloud patterns in synoptic-scale circulation systems. *Mon. Wea. Rev.*, accepted.

Leipper, D. F., 1994: Fog on the U.S. west coast: a review. *Bull. Amer. Meteor. Soc.*, **75**, 229-240.

Li, Z., and H. G. Leighton, 1993: Global climatologies of solar radiation budgets at the surface and in the atmosphere from 5 years of ERBE data. *J. Geophys. Res.*, **98**, 4919-4930.

———, L. Moreau, and A. Arking, 1997: On solar energy disposition: a perspective from observation and modeling. *Bull. Amer. Meteor. Soc.*, **78**, 53-70.

Lilly, D. K., 1968: Models of cloud-topped mixed layers under a strong inversion. *Quart. J. Roy. Meteor. Soc.*, **94**, 292-309.

Lind, R. J., and K. B. Katsaros, 1982: A model of longwave irradiance for use with surface observations. *J. Appl. Meteor.*, **21**, 1015-1023.

———, and K. B. Katsaros, 1986: Radiation measurements and model results from R/V *Oceanographer* during STREX 1980. *J. Geophys. Res.*, **91**, 13308-13314.

Lohmann, U., and J. Feichter, 1997: Impact of sulfate aerosols on albedo and lifetime of clouds: a sensitivity study with the ECHAM4 GCM. *J. Geophys. Res.*, submitted.

Luksch, U., 1996: Simulation of North Atlantic low-frequency SST variability. *J. Climate*, **9**, 2083-2092.

———, and H. von Storch, 1992: Modeling the low-frequency sea surface temperature variability in the North Pacific. *J. Climate*, **5**, 893-906.

Lumb, F. E., 1964: The influence of cloud on hourly amounts of total solar radiation at the sea surface. *Quart. J. Roy. Meteor. Soc*, **90**, 43-56.

Ma, C.-C., C. R. Mechoso, A. W. Robertson, and A. Arakawa, 1996: Peruvian stratus clouds and the tropical Pacific circulation: a coupled ocean–atmosphere GCM study. *J. Climate*, **9**, 1635-1645.

Mannoji, N., 1995: An explicit cloud predicting scheme implemented in the Florida State University Global Spectral Model and its impact. *J. Meteor. Soc. Japan*, **73**, 993-1009.

Martin, G. M., D. W. Johnson, D. P. Rogers, P. R. Jonas, P. Minnis, and D. A. Hegg, 1995: Observations of the interaction between cumulus clouds and warm stratocumulus clouds in the marine boundary layer during ASTEX. *J. Atmos. Sci.*, **52**, 2902-2922.

McGuffie, K., and A. Henderson-Sellers, 1988: Is Canadian cloudiness increasing? *Atmos.-Ocean*, **26**, 608-633.

Miller, R. L., 1997: Tropical thermostats and low cloud cover. *J. Climate*, **10**, 409-440.

Mitchell, J. F. B, and T. C. Johns, 1997: On modification of global warming by sulfate aerosols. *J. Climate*, **10**, 245-267.

Moeng, C.-H., 1986: Large-eddy simulation of a stratus-topped boundary layer. Part I:

structure and budgets. *J. Atmos. Sci.*, **43**, 2886-2899.

Nakajima, T., M. D. King, and J. Spinhirne, 1991: Determination of the optical thickness and effective particle radius of clouds from reflected solar radiation measurements. Part II: marine stratocumulus observations. *J. Atmos. Sci.*, **48**, 728-750.

Namias, J., and R. M. Born, 1970: Temporal coherence in North Pacific sea surface temperature patterns. *J. Geophys. Res.*, **75**, 5952-5955.

———, and R. M. Born, 1974: Further studies of temporal coherence in North Pacific sea surface temperatures. *J. Geophys. Res.*, **79**, 797-798.

———, X. Yuan, and D. R. Cayan, 1988: Persistence of North Pacific sea surface temperature and atmospheric flow patterns. *J. Climate*, **1**, 682-703.

National Climatic Data Center (NCDC), 1962: History of the international code, in *TDF-13 Reference Manual*, pp. 0.6-0.10 (Available from NCDC, Asheville, NC).

Newman, M. and P. D. Sardeshmukh, 1995: A caveat concerning singular value decomposition. *J. Climate*, **8**, 352-360.

Nicholls, S., 1984: The dynamics of stratocumulus: aircraft observations and comparisons with a mixed layer model. *Quart. J. Roy. Meteor. Soc.*, **110**, 783-820.

———, and J. Leighton, 1986: An observational study of the structure if stratiform cloud sheets. Part 1: structure. *Quart. J. Roy. Meteor. Soc.*, **112**, 431-460.

———, B. Brümmer, F. Fiedler, A. Grant, T. Hauf, G. Jenkins, C. Reading, and W. Shaw, 1983: The structure of the turbulent atmospheric boundary layer. *Philos. Trans. Roy. Soc. London*, **308**, 291-309.

Norris, J. R., 1997a: Low cloud type over the ocean from surface observations. Part I: relationship to surface meteorology and the vertical distribution of temperature and moisture. *J. Climate*, accepted.

———, 1997b: Low cloud type over the ocean from surface observations. Part II: geographical and seasonal variations. *J. Climate*, accepted.

———, 1997c: On trends in global-mean ocean cloud cover between 1930–1992. manuscript in preparation.

———, and C. B. Leovy, 1994: Interannual variability in stratiform cloudiness and sea surface temperature. *J. Climate*, **7**, 1915-1925.

———, J. R., and C. B. Leovy, 1995: Comments on “Trends in global marine cloudiness and anthropogenic sulphur”. *J. Climate*, **8**, 2109-2110.

———, Y. Zhang, and J. M. Wallace, 1997: Role of low clouds in summertime atmosphere–ocean interactions over the North Pacific. *J. Climate*, submitted.

North, G. R., T. L. Bell, R. F. Cahalan, and F. J. Moeng, 1982: Sampling errors in the

estimation of empirical orthogonal functions. *Mon. Wea. Rev.*, **110**, 699-706.

Novakov, T., C. Rivera-Carpio, J. E. Penner, and C. F. Rogers, 1994: The effect of anthropogenic sulphate aerosols on marine cloud droplet concentrations. *Tellus*, **46B**, 132-141.

Ohlmann, J. C., D. A. Siegel, and C. Gautier, 1996: Ocean mixed layer radiant heating and solar penetration: a global analysis. *J. Climate*, **9**, 2265-2280.

Oreopoulos L., and R. Davies, 1993: Statistical dependence of albedo and cloud cover on sea surface temperature for two tropical marine stratocumulus regions. *J. Climate*, **6**, 2434-2447.

Palmer, A. H., 1917: Fog along the California coast. *Mon. Wea. Rev.*, **45**, 496-499.

Palmer, T. N., and Z. Sun, 1985: A modelling and observational study of the relationship between sea surface temperature in the north-west Atlantic and the atmospheric general circulation. *Quart. J. Roy. Meteor. Soc.*, **111**, 947-975.

Paluch, I. R., D. H. Lenschow, S. Siems, S. McKeen, G. L. Kok, and R. D. Schillawski, 1994: Evolution of the subtropical marine boundary layer: comparison of soundings over the eastern Pacific from FIRE and HaRP. *J. Atmos. Sci.*, **51**, 1465-1479.

Parungo, F., J. F. Boatman, H. Sievering, S. W. Wilkison, and B. B. Hicks, 1994: Trends in global marine cloudiness and anthropogenic sulfur. *J. Climate*, **7**, 434-440.

Payne, R. E., 1972: Albedo of the sea surface. *J. Atmos. Sci.*, **29**, 959-970.

Peng, S., and J. Fyfe, 1996: The coupled patterns between sea level pressure and sea surface temperature in the midlatitude North Atlantic. *J. Climate*, **9**, 1824-1839.

———, W. A. Robinson, and M. P. Hoerling, 1997: The modeled atmospheric response to midlatitude SST anomalies and its dependence on background circulation states. *J. Climate*, **10**, 971.

Peterson, T. C., 1991: The relationships between sea surface temperature anomalies and clouds, water vapor and their radiative effects. Ph.D. Thesis, Colorado State University, Fort Collins, CO, 259 pp.

Petty, G. W., 1995: Frequencies and characteristics of global oceanic precipitation from shipboard present-weather reports. *Bull. Amer. Meteor. Soc.*, **76**, 1593-1616.

Philander, S. G. H., D. Gu, D. Halpern, G. Lambert, N.-C. Lau, T. Li, and R. C. Pacanowski, 1996: Why the ITCZ is mostly north of the Equator. *J. Climate*, **99**, 2958-2972.

Pierrehumbert, R. T., 1994: Thermostats, radiator fins and the local runaway greenhouse. *J. Atmos. Sci.*, **52**, 1784-1806.

Pilewskie, P., and F. P. J. Valero, 1995: Direct observations of excess solar absorption by clouds. *Science*, **267**, 1626-1629.

Pitcher, E. J., M. L. Blackmon, G. T. Bates, and S. Muñoz, 1988: The effect of North Pacific sea surface temperature anomalies on the January climate of a general circulation model. *J. Atmos. Sci.*, **45**, 173-188.

Plantico, M. S., T. R. Karl, G. Kukla, and J. Gavin, 1990: Is recent climate change across the United States related to rising levels of anthropogenic greenhouse gases? *J. Geophys. Res.*, **95**, 16617-1637.

Qiu, B., and K. A. Kelly, 1993: Upper-ocean heat balance in the Kuroshio Extension region. *J. Phys. Oceangr.*, **23**, 2027-2041.

Radke, L. F., J. A. Coakley, Jr., and M. D. King, 1989: Direct and remote sensing observations of the effect of ships on clouds. *Science*, 246, 1146-1149.

Ramage, C. S., 1987: Secular change in reported surface wind speeds over the ocean. *J. Climate Appl. Meteor.*, **26**, 525-528.

Ramanathan, V., R. D. Cess, E. F. Harrison, P. Minnis, B. R. Barkstrom, E. Ahmad, and D. Hartmann, 1989: Cloud-radiative forcing and climate: results from the Earth Radiation Budget Experiment. *Science*, **243**, 57-63.

———, B. Subasilar, G. J. Zhang, W. Conant, R. D. Cess, J. T. Kiehl, H. Grassl, and L. Shi, 1995: Warm pool heat budget and shortwave cloud forcing: a missing physics? *Science*, **267**, 499-503.

Randall, D. A., J. A. Abeles, and T. G. Corsetti, 1985: Seasonal simulations of the planetary boundary layer and boundary-layer stratocumulus clouds with a general circulation model. *J. Atmos. Sci.*, **42**, 641-675.

Rasmusson, E. M., and J. M. Wallace, 1983: Meteorological aspects of the El Niño / Southern Oscillation. *Science*, **222**, 1195-1202.

Reed, R. K., 1977: On estimating insolation over the ocean. *J. Phys. Oceanogr.*, 482-485.

Reiter, E. R., and D. R. Westhoff, 1982: Linear trends in Northern Hemisphere tropospheric geopotential height and temperature patterns. *J. Atmos. Sci.*, **39**, 528-541.

Rogers, D. P., 1989: The marine boundary-layer in the vicinity of an ocean front. *J. Atmos. Sci.*, **46**, 2044-2062.

Rogers, J. C., 1997: North Atlantic storm track variability and its association to the North Atlantic Oscillation and climate variability of northern Europe. *J. Climate*, **10**, 1635-1647.

Ronca, R. E., 1995: Processes controlling anomalous sea surface temperature and air-se energy exchange on intra-annual timescales in the northeastern subtropical Pacific. M.S. Thesis, University of Washington, Seattle, WA, 90 pp.

———, and D. S. Battisti, 1997: Anomalous sea surface temperatures and local air-sea

energy exchange on intraannual timescales in the northeastern subtropical Pacific. *J. Climate*, **10**, 102-117.

Rossow, W. B., and R. A. Schiffer, 1991: ISCCP cloud data products. *Bull. Amer. Meteor. Soc.*, **72**, 2-20.

Rozendaal, M. A., C. B. Leovy, and S. A. Klein, 1995: An observational study of diurnal variations of marine stratiform cloud. *J. Climate*, **8**, 1795-1809.

Russak, V., 1990: Trends of solar radiation, cloudiness, and atmospheric transparency during recent decades in Estonia. *Tellus*, **42B**, 206-210.

Schubert, W. H., J. S. Wakefield, E. J. Steiner, and S. K. Cox, 1979a: Marine stratocumulus convection. Part I: governing equations and horizontally homogeneous solutions. *J. Atmos. Sci.*, **36**, 1286-1307.

———, ———, ———, ———, 1979b: Marine stratocumulus convection. Part II: horizontally inhomogeneous solutions. *J. Atmos. Sci.*, **36**, 1308-1324.

Schwartz, S. E., 1988: Are global cloud albedo and climate controlled by marine phytoplankton? *Nature*, **336**, 441-445.

Seaver, W. L., and J. E. Lee, 1987: A statistical examination of sky cover changes in the contiguous United States.*J. Climate Appl. Meteor.,* **26**, 88-95.

Senior, C. A., and J. F. B. Mitchell, 1993: Carbon dioxide and climate: the impact of cloud parameterization. *J. Climate*, **6**, 393-418.

Serreze, M. C., F. Carse, R. G. Barry, and J. C. Rogers, 1997: Icelandic low cyclone activity: climatological features, linkages with the NAO, and relationships with recent changes in the Northern Hemisphere circulation. *J. Climate*, **10**, 453-464.

Shabbar, A., K. Higuchi, and J. L. Knox, 1990: Regional analysis of Northern Hemisphere 50 kPa geopotential heights from 1946 to 1985. *J. Climate*, **3**, 543-557.

Slingo, A., 1990: Sensitivity of the Earth's radiation budget to changes in low clouds. *Nature*, **343**, 49-51.

———, and H. M. Schrecker, 1982: On the shortwave radiative properties of stratiform water clouds. *Quart. J. Roy. Meteor. Soc.*, **108**, 407-426.

———, and J. M. Slingo, 1991: Response of the National Center for Atmospheric Research Community Climate Model to improvements in the representation of clouds. *J. Geophys. Res.*, **96**, 15341-15357.

Smith, I. N., M. Dix, and R. J. Allan, 1997: The effect of greenhouse SSTs on ENSO simulations with an AGCM. *J. Climate*, **10**, 342-352.

Smith, L. D., and T. H. Vonder Haar, 1991: Clouds–radiation interactions in a general circulation model: impact upon the planetary radiation balance. *J. Geophys. Res.*, **96**, 893-914.

Smith, S. D., 1988: Coefficients for sea surface wind stress, heat flux, and wind profiles as a function of wind speed and temperature. *J. Geophys. Res.*, **93**, 15467-15472.

Soden, B. J., 1992: Validation of cloud forcing simulated by the National Center for Atmospheric Research Community Climate Model using observations from the Earth Radiation Budget Experiment. *J. Geophys. Res.*, **97**, 18137-18159.

Somerville, R. C. J., and L. A. Remer, 1984: Cloud optical thickness feedbacks in the CO_2 climate problem. *J. Geophys. Res.*, **89**, 9668-9672.

Stephens, G. L., and T. J. Greenwald, 1991: The Earth's radiation budget and its relation to atmospheric hydrology, 2, Observations of cloud effects. *J. Geophys. Res.*, **96**, 15325-15340.

Strub, P. T., J. S. Allen, A. Huyer, and R. L. Smith, 1987: Large-scale structure of the spring transition in the coastal ocean off western North America. *J Geophys. Res.*, **92**, 1527-1544.

Stubenrauch, C. J., A. D. Del Genio, and W. B. Rossow, 1997: Implementation of subgrid cloud vertical structure inside a GCM and its effect on the radiation budget. *J. Climate*, **10**, 273-287.

Taylor, G. I., 1917: The formation of fog and mist. *Quart. J. Roy. Meteor. Soc.*, **43**, 250-257.

Teweles, S., 1970: A spurious diurnal variation in radiosonde humidity records. *Bull. Amer. Meteor. Soc.*, **51**, 836-840.

Tiedtke, M., 1993: Representation of clouds in large-scale models. *Mon. Wea. Rev.*, **121**, 3040-3061.

Trenberth, K. E., 1990: Recent observed interdecadal climate changes in the Northern Hemisphere. *Bull. Amer. Meteor. Soc.*, **71**, 988-993.

———, and D. A. Paolino, 1980: The Northern Hemisphere sea-level pressure data set: trends, errors, and discontinuities. *Mon. Wea. Rev.*, **108**, 855-872.

———, and J. W. Hurrell, 1994: Decadal atmosphere–ocean variations in the Pacific. *Climate Dyn.*, **9**, 303-319.

———, and T. J. Hoar, 1996: The 1990–1995 El Niño–Southern Oscillation event: longest on record. *Geophys. Res. Lett.*, **23**, 57-60.

———, W. G. Large, and J. G. Olson, 1990: The mean annual cycle in global ocean wind stress. *J. Phys. Oceangr.*, **20**, 1742-1760.

Tselioudis, G., W. B. Rossow, and D. Rind, 1992: Global patterns of cloud optical thickness variation with temperature. *J. Climate*, **5**, 1484-1495.

———, A. A. Lacis, D. Rind, and W. B. Rossow, 1993: Potential effects of cloud optical thickness on climate warming. *Nature*, **366**, 670-672.

Tsukuda, K., 1932: On the sea fog in the North Pacific ocean. *Geophys. Mag.*, **6**, 147-165.

Twohy, C. H., P. A. Durkee, B. J. Huebert, and R. J. Charlson, 1995: Effects of aerosol particles on the microphysics of coastal stratiform clouds. *J. Climate*, **8**, 773-783.

Twomey, S. A., M. Piepgrass, and T. L. Wolfe, 1984: An assessment of the impact of pollution on global cloud albedo. *Tellus*, **36B**, 356-366.

Wallace, J. M., and P. V. Hobbs, 1977: *Atmospheric Science: An introductory survey.* Academic Press, 467 pp.

———, and D. S. Gutzler, 1981: Teleconnections in the geopotential height field during Northern Hemisphere winter. *Mon. Wea. Rev.*, **109**, 784-812.

———, C. Smith, and Q. Jiang, 1990: Spatial patterns of atmosphere–ocean interaction in the northern winter. *J. Climate*, **3**, 990-998.

———, Y. Zhang, and K.-H. Lau, 1993: Structure and seasonality of interannual and interdecadal variability of the geopotential height and temperature fields in the Northern Hemisphere troposphere. *J. Climate*, **6**, 2063-2082.

Wang, J., and W. B. Rossow, 1995: Determination of cloud vertical structure from upper-air observations. *J. Appl. Meteor.*, **34**, 2243-2258.

Wang, W.-C., Q.-Y. Zhang, D. R. Easterling, and T. R. Karl, 1993: Beijing cloudiness since 1875. *J. Climate*, **6**, 1921-1927.

Ward, D. M., 1995: Comparison of the surface solar radiation budget derived from satellite data with that simulated by the NCAR CCM2. *J. Climate*, **8**, 2824-2842.

Ward, M. N., and B. J. Hoskins, 1996: Near-surface wind over the global ocean 1949-1988. *J. Climate*, **9**, 1877-1895.

Warren, S. G., C. J. Hahn, J. London, R. M. Chervin, and R. L. Jenne, 1988: *Global distribution of total cloud cover and cloud type amounts over the ocean.* NCAR/TN-317+STR, NCAR Boulder, CO, 42 pp. + 170 maps.

Weare, B. C., 1989: Uncertainties in estimates of surface heat fluxes derived from marine reports over the tropical and subtropical oceans. *Tellus*, **41A**, 357-370.

———, 1993: Multi-year statistics of selected variables from the ISCCP C2 data set. *J. Roy. Meteor. Soc.*, **119**, 795-808.

———, 1994: Interrelationships between cloud properties and sea surface temperatures on seasonal and interannual time scales. *J. Climate*, **7**, 248-260.

———, and P. T. Strub, 1981: The significance of sampling biases on calculated monthly mean ocean surface heat fluxes. *Tellus*, **33**, 211-234.

———, A. R. Navato, and R. E. Newell, 1976: Empirical orthogonal analysis of Pacific sea surface temperatures. *J. Phys. Oceangr.*, **6**, 671-678.

———, I. I. Mokhov, and Project Members, 1995: Evaluation of total cloudiness and its variability in the Atmospheric Model Intercomparison Project. *J. Climate*, **8**, 2224-2238.

———, and AMIP modeling groups, 1996: Evaluation of the vertical structure of zonally averaged cloudiness and its variability in the Atmospheric Model Intercomparison Project. *J. Climate*, **9**, 3419-3431.

Weaver, C. P., and V. Ramanathan, 1996: The link between summertime cloud radiative forcing and extratropical cyclones in the N. Pacific. *J. Climate*, **9**, 2093-2109.

Weng, F., N. C. Grody, R. Ferraro, A. Basist, and D. Forsyth, 1997: Cloud liquid water climatology from the Special Sensor Microwave/Imager. *J. Climate*, **10**, 1086-1098.

Whitlock, C. H., T. P. Charlock, W. F. Staylor, R. T. Pinker, I. Laszlo, A. Ohmura, H. Gilgen, T. Konzelman, R. C. DiPasquale, C. D. Moats, S. R. LeCroy, and N. A. Ritchey, 1995: First global WCRP shortwave surface radiation budget dataset. *Bull. Amer. Meteor. Soc.*, **76**, 905-922.

Woodruff, S. D., R. J. Slutz, R. L. Jenne, and P. M. Steurer, 1987: A comprehensive ocean-atmosphere data set. *Bull. Amer. Meteor. Soc.*, **68**, 1239-1250.

World Meteorological Organization (WMO), 1974: *Manual on Codes*. (WMO Pub. No. 306), WMO, Geneva.

World Meteorological Organization, 1975: *Manual on the Observation of Clouds and Other Meteors*. (WMO Pub. No. 407), WMO, Geneva.

Wright, P. B., 1986: Problems in the use of ship observations for the study of interdecadal climate changes. *Mon. Wea. Rev.*, **114**, 1028-1034.

Wyant, M. C., C. S. Bretherton, H. A. Rand, and D. E. Stevens, 1997: Numerical simulations and a conceptual model of the stratocumulus to trade cumulus transition. *J. Atmos. Sci.*, **54**, 168-192.

Zhang, R.-H., and S. Levitus, 1997: Structure and cycle of decadal variability of upper-ocean temperature in the North Pacific. *J. Climate*, **10**, 710-727.

Zhang, Y., 1996: An observational study of atmosphere–ocean interactions in the northern oceans on interannual and interdecadal time-scales. Ph.D. Thesis, University of Washington, Seattle, WA, 163 pp.

———, J. M. Wallace, and N. Iwasaka, 1996: Is climate variability over the North Pacific a linear response to ENSO? *J. Climate*, **9**, 1468-1478.

———, J. R. Norris, and J. M. Wallace, 1997: Seasonality of large scale atmosphere–ocean interaction over the North Pacific. *J Climate*, submitted.

Zhi, H., and Harshvardhan, 1993: A hybrid technique for computing the monthly mean net longwave surface radiation over ocean areas. *Theo. Appl. Climatol.*, **47**, 65-79.

Zuidema, P., and D. Hartmann, 1995: Satellite determination of stratus cloud microphysical properties. *J. Climate*, **8**, 1638-1657.

VITA

Joel Norris was born in West Covina, California, on August 26, 1967, to Judy and Roland Norris. He has one younger sister, Julie, presently a graduate student studying seismology at the California Institute of Technology. Joel attended Caltech himself and graduated in in 1990 with a degree in Planetary Science. After briefly working at the Jet Propulsion Laboratory examining interannual variability in water vapor in the Mars atmosphere (an intractable problem!), he moved to Seattle for graduate study at the University of Washington and began the work which is described in the present study. In October of 1997 Joel will move to Boulder, Colorado, to begin an Advanced Study Program postdoctoral fellowship at the National Center for Atmospheric Research.

Besides science, Joel Norris enjoys spending time with friends, listening to classical music, playing soccer, biking and hiking, and discussing politics, economics, and theology. However, the most important part of Joel's life is that he, by the grace of God, has salvation in Jesus Christ. For this reason he strives, albeit very imperfectly, to love God with all his heart, soul, mind, and strength, and to love his neighbor as himself.